



National Library
of Canada

Acquisitions and
Bibliographic Services Branch

395 Wellington Street
Ottawa, Ontario
K1A 0N4

Bibliothèque nationale
du Canada

Direction des acquisitions et
des services bibliographiques

395, rue Wellington
Ottawa (Ontario)
K1A 0N4

Your file Votre référence

Our file Notre référence

NOTICE

The quality of this microform is heavily dependent upon the quality of the original thesis submitted for microfilming. Every effort has been made to ensure the highest quality of reproduction possible.

If pages are missing, contact the university which granted the degree.

Some pages may have indistinct print especially if the original pages were typed with a poor typewriter ribbon or if the university sent us an inferior photocopy.

Reproduction in full or in part of this microform is governed by the Canadian Copyright Act, R.S.C. 1970, c. C-30, and subsequent amendments.

AVIS

La qualité de cette microforme dépend grandement de la qualité de la thèse soumise au microfilmage. Nous avons tout fait pour assurer une qualité supérieure de reproduction.

S'il manque des pages, veuillez communiquer avec l'université qui a conféré le grade.

La qualité d'impression de certaines pages peut laisser à désirer, surtout si les pages originales ont été dactylographiées à l'aide d'un ruban usé ou si l'université nous a fait parvenir une photocopie de qualité inférieure.

La reproduction, même partielle, de cette microforme est soumise à la Loi canadienne sur le droit d'auteur, SRC 1970, c. C-30, et ses amendements subséquents.

Canada

**RESERVOIR GEOLOGY OF UPPER DEVONIAN
LEDUC BUILDUPS, DEEP ALBERTA BASIN**

by

Xiomara M. Marquez C.

**Department of Earth and Planetary Sciences
McGill University
Montreal, Quebec, Canada**

July, 1994

**A thesis submitted to the Faculty of Graduate Studies and Research
in partial fulfilment of the requirements for the degree of
Doctor of Philosophy**

@ Xiomara M. Marquez C., 1994



National Library
of Canada

Acquisitions and
Bibliographic Services Branch

395 Wellington Street
Ottawa, Ontario
K1A 0N4

Bibliothèque nationale
du Canada

Direction des acquisitions et
des services bibliographiques

395, rue Wellington
Ottawa (Ontario)
K1A 0N4

Your file Votre référence

Our file Notre référence

THE AUTHOR HAS GRANTED AN
IRREVOCABLE NON-EXCLUSIVE
LICENCE ALLOWING THE NATIONAL
LIBRARY OF CANADA TO
REPRODUCE, LOAN, DISTRIBUTE OR
SELL COPIES OF HIS/HER THESIS BY
ANY MEANS AND IN ANY FORM OR
FORMAT, MAKING THIS THESIS
AVAILABLE TO INTERESTED
PERSONS.

L'AUTEUR A ACCORDE UNE LICENCE
IRREVOCABLE ET NON EXCLUSIVE
PERMETTANT A LA BIBLIOTHEQUE
NATIONALE DU CANADA DE
REPRODUIRE, PRETER, DISTRIBUER
OU VENDRE DES COPIES DE SA
THESE DE QUELQUE MANIERE ET
SOUS QUELQUE FORME QUE CE SOIT
POUR METTRE DES EXEMPLAIRES DE
CETTE THESE A LA DISPOSITION DES
PERSONNE INTERESSEES.

THE AUTHOR RETAINS OWNERSHIP
OF THE COPYRIGHT IN HIS/HER
THESIS. NEITHER THE THESIS NOR
SUBSTANTIAL EXTRACTS FROM IT
MAY BE PRINTED OR OTHERWISE
REPRODUCED WITHOUT HIS/HER
PERMISSION.

L'AUTEUR CONSERVE LA PROPRIETE
DU DROIT D'AUTEUR QUI PROTEGE
SA THESE. NI LA THESE NI DES
EXTRAITS SUBSTANTIELS DE CELLE-
CI NE DOIVENT ETRE IMPRIMES OU
AUTREMENT REPRODUITS SANS SON
AUTORISATION.

ISBN 0-612-00111-3

Canada

*To the women who have inspired my life
and have given me the support to keep going*

*Ruth , Ingrid, Gabi
and,
Carmen Ramona, in memoriam*

GUIDELINES CONCERNING THESIS PREPARATION

2/ Manuscripts and Authorship: Candidates have the option, **subject to approval of their department**, of including, as part of their thesis, copies of the text of a paper(s) submitted for publication, or the clearly-duplicated text of a published paper(s), provided that these copies are bound as integral part of the thesis.

- If this option is chosen, **connecting texts, providing logical bridges between the different papers, are mandatory.**

- The thesis must still conform to all other requirements of the "Guidelines Concerning Thesis Preparation" and should be in a literary form that is more than a mere collection of manuscripts published or to be published. **The thesis must include, as separate chapters or sections:** (1) a Table of Contents, (2) a general abstract in English and French, (3) a introduction which clearly states the rationale and objectives of the study, (4) a comprehensive general review of the background literature to the subject of the thesis, when this review is appropriate, and (5) a final overall conclusion and/or summary.

- Additional material (procedural and designed data, as well of description of equipment used) must be provided where appropriate and in sufficient detail (eg. in appendices) to allow a clear and precise judgement to be made of the importance and originality of the research reported in the thesis.

- In the case of manuscripts co-authored by the candidate and others, **the candidate is required to make and explicit statement in the thesis of who contributed to such work and to what extent;** supervisors must attest to the accuracy of such claims at the Ph.D. Oral Defense. Since the task of the examiners is made more difficult in these cases, it is in the candidate's interest to make perfectly clear the responsibilities of the different authors of co-authored papers.

GENERAL ABSTRACT

Upper Devonian (Frasnian) stromatoporoid and coral buildups in the Alberta Basin are among the most important hydrocarbon reservoirs in Western Canada. In the deep basin (>4000 m), Strachan, Ricinus West and adjacent buildups have similar depositional facies, but have experienced different diagenetic processes that affected their reservoir characteristics. The most important diagenetic alteration is dolomitization that partially to completely replaced the original limestone buildups. Replacement dolomitization occurred at shallow depths near 500 m, indicated by petrographic and geologic relationships. The dolomitizing fluid was probably modified Upper Devonian seawater, as suggested by trace element concentrations and $^{87}\text{Sr}/^{86}\text{Sr}$ ratios (0.7083 to 0.7092). These replacement dolomites have similar petrography and geochemical signatures as those in buildups along the Rimbey Meadowbrook reef trend. The presence of similar replacement dolomites over such a broad extent suggests that they formed from similar fluids during a regional to basin-wide event.

Distribution of pore types is controlled by depositional facies, whereas permeability is controlled by diagenetic processes, especially dolomitization. At depths > 4000 m dolostones have higher porosities and permeabilities than limestones because the dolostones are more resistant to pressure solution. Bitumen is observed to decrease permeability in the upper part of the reservoirs. Later thermal sulphate reduction (TSR) related products both increased and decreased porosity and permeability in the lower part of the reservoirs.

Major differences in diagenesis between the partially dolomitized Strachan buildup (hairline microfracturing) and the completely dolomitized Ricinus West and adjacent buildups likely resulted from the completely dolomitized buildups being connected to a regional fluid conduit system along the west margin of the Cooking Lake platform underlying the Rimbey Meadowbrook reef trend.

Hairline microfractures filled with bitumen are abundant in the Strachan buildup. Subhorizontally, randomly and radially oriented microfractures crosscut all sedimentary and diagenetic phases. Overpressuring caused by the thermal cracking of crude oil to gas during burial and Laramide compression best explains their origin and distribution.

SOMMAIRE

Les stromatopores et les récifs coraliens du dévonien supérieur (Frasnien) dans le bassin de l'Alberta sont parmi les plus importants réservoirs d'hydrocarbures de l'ouest du Canada. Dans le bassin profond, les récifs de Strachan, Ricinus ouest et les récifs adjacents ont des faciès et des environnements de déposition similaires, mais ils ont subi des processus diagénétiques différents, ce qui affecte les caractéristiques du réservoir. L'altération diagénétique la plus importante est la dolomitisation, pouvant remplacer partiellement ou complètement les récifs calcaires originaux. Les relations pétrographiques et géologiques indiquent que la dolomitisation se produit à une faible profondeur de 500m environ. La concentration des éléments traces et les rapports $^{87}\text{Sr}/^{86}\text{Sr}$ (0.7083 à 0.7092) suggèrent que le fluide responsable de la dolomitisation était de l'eau marine modifiée du dévonien supérieur. Ces dolomies de remplacement ont une signature pétrographique et géochimique semblable à celle de l'alignement de récifs de Rimbey Meadowbrook. Ces étroites similitudes indiquent que ces dolomies ont été formées par des fluides apparentés, lors d'un événement d'ampleur régionale, voir même de la taille du bassin.

La distribution des types de pores est contrôlée par les faciès de déposition alors que la perméabilité est contrôlée par des processus diagénétiques, en particulier la dolomitisation. De par leur plus grande résistance à la dissolution sous pression, les dolomies ont une porosité et une perméabilité supérieure à celle des calcaires à des profondeurs excédant 4000m. En présence de bitumineux on peut observer une diminution de la perméabilité. Des produits tardifs reliés à la RTS ont soit augmenté, soit diminué la porosité et la perméabilité dans la partie inférieure du réservoir.

Les principales différences diagénétiques entre les récifs partiellement dolomitisés (microfractures) de Strachan et ceux complètement dolomitisés (Ricinus ouest et les récifs adjacents) sont probablement dues au fait que ces derniers ont été connectés à des conduits régionaux de fluide le long de la marge ouest de la plateforme de Cooking Lake, sous les récifs de Rimbey Meadowbrook.

Des microfractures remplies de bitumineux sont abondantes dans le récif de Strachan. Ces microfractures subhorizontales, orientées de façon aléatoire ou radiaire recoupent toutes les phases sédimentaires ou diagénétiques. Leur origine et leur distribution s'explique par la surpression due au craquage thermique des huiles brutes en gaz lors de l'enfouissement.

RESUMEN

Los arrecifes de stromatoporoides y corales del Devonico Superior son unos de los yacimientos de hidrocarburos mas importantes en la cuenca de Alberta, Canada occidental. En la parte profunda de la cuenca, los arrecifes de Strachan, Ricinus West y arrecifes adyacentes se formaron en ambientes sedimentarios similares, sin embargo fueron sometidos a distintos procesos diageneticos. El proceso diagenetico mas importante fue la dolomitizacion parcial y total de las calizas originales. Las características petrograficas y geoquimicas de las dolomitas indican que la dolomitizacion ocurrio a profundidades de aproximadamente 500 m. Las concentraciones de los elementos traza y los isotopos de estroncio ($^{87}\text{Sr}/^{86}\text{Sr}$) sugieren que los fluidos para la dolomitizacion fueron probablemente aguas marinas modificadas del Devonico Superior. Estas dolomitas de reemplazo tienen a su vez características petrograficas y geoquimicas similares a las dolomitas de la cadena de arrecifes Rimbey-Meadowbrook. Esta similitud en las dolomitas de todos los arrecifes, sugiere que la dolomitizacion fue un proceso regional que ocurrio en toda la cuenca.

La distribucion de los poros en las rocas esta controlada por las facies sedimentarias, pero la permeabilidad esta controlada por la diagenesis, principalmente la dolomitizacion. A profundidades mayores de 4000 m, las dolomitas son mejores yacimientos que las calizas, por que son mas resistentes a la presion-solucion. En la parte superior de los arrecifes, la permeabilidad esta reducida por la presencia de bitumen. En la parte inferior de los mismos, los productos de la reduccion termal de sulfatos (RTS) aumentaron o redujeron la porosidad y permeabilidad.

Las diferencias en diagenesis entre los arrecifes de Strachan (parcialmente dolomitizado) y el arrecife de Ricinus West (completamente dolomitizado) pueden deberse a que los arrecifes dolomitizados, estaban conectados a un conducto de fluidos a lo largo del margen occidental de la plataforma Cooking Lake, que se encuentra por debajo de la cadena de arrecifes Rimbey-Meadowbrook.

En el arrecife Strachan, se observan abundantes microfracturas rellenas con bitumen. Estas microfracturas se encuentran orientadas subhorizontalmente, arbitrariamente o radialmente y se formaron tarde en la historia paragenetica. El origen y la distribucion de estas microfracturas se debe a sobrepresiones generadas por la alteracion termal del petroleo que se encontraba originalmente en los yacimientos durante la orogenesis de Laramide.

TABLE OF CONTENTS

GENERAL ABSTRACT	Page ii
SOMMAIRE	iii
RESUMEN	iv
Table of contents	v
List of figures	viii
List of tables	xi
List of plates	xii
List of appendices	xiii
GENERAL ACKNOWLEDGEMENTS	xiv
PREFACE	xvii
Thesis format	xvii
Original contributions to knowledge	xviii
Publications	xx
CHAPTER 1 GENERAL INTRODUCTION	
Rationale and objectives	1
Previous work	2
Study area	5
Geologic setting and stratigraphy	6
CHAPTER 2 DEPOSITIONAL FACIES AND DIAGENESIS OF THE LEDUC BUILDUPS (UPPER DEVONIAN) IN THE DEEP ALBERTA BASIN	
Abstract	12
Introduction	13
Methods.....	14
Depositional Facies	15
Strachan Gas Reservoir	15
Ricinus West and Adjacent Gas Reservoirs.....	26
Depositional environments.....	34
Diagenesis.....	40
Petrography	40
Paragenetic sequence	57
Distribution of replacement dolomites and later diagenetic features.....	64
Geochemistry	69
Major and minor elements	69
Carbon and oxygen isotopes	70
Strontium isotopes	73
Fluid inclusions	74
Discussion	77
Comparison with other dolostones	84
Discussion	85

Origin of dolomites	85
Origin of dolomite cements.....	89
Origin of later diagenetic features	92
Conclusions	98

CHAPTER 3 PORE SYSTEMS AND THE EFFECT OF DOLOMITIZATION ON RESERVOIR PROPERTIES, IN UPPER DEVONIAN LEDUC BUILDUPS, DEEP ALBERTA BASIN

Abstract	102
Introduction	103
Methods	104
Pore types and definitions.....	107
Limestones.....	108
Partly dolomitized limestones	111
Dolostones.....	111
Pore systems in dolostones.....	116
Distribution of pore systems (large scale).....	119
Porosity and permeability (medium scale).....	122
Porosity and permeability (small scale).....	130
Comparison with other reservoirs.....	130
Porosity and permeability distribution.....	134
Dolomitization and porosity.....	137
Dolomitization and permeability.....	140
Discussion	140
Depositional control	143
Diagenetic control	143
Effect of dolomitization.....	143
Effect of cementation and dissolution.....	144
Effects of reservoir bitumen.....	144
Porosity evolution in the Strachan and Ricinus buildups.....	146
Conclusions	150

CHAPTER 4 ORIGIN OF MICROFRACTURES IN UPPER DEVONIAN LEDUC STRACHAN RESERVOIR, DEEP ALBERTA BASIN

Abstract	152
Introduction	153
Methods	153
Strachan Gas Field	154
Reservoir rock	154
Underlying strata.....	161
Sealing shales and carbonates.....	162
Microfractures	167
Patterns	167
Distribution within the Strachan reservoir	170
Distribution in other buildups	170
Relative timing of microfracturing	180
Discussion	181
Origins of microfractures	181
Development of pore pressures	190
Microfracture orientations.....	195
Distribution of microfractures.....	196

Conclusions	197
CHAPTER 5. GENERAL CONCLUSIONS	199
Future Work	204
REFERENCES	205

LIST OF FIGURES

CHAPTER 1	Page
Figure 1.1: Study area located in downdip portion of Rimbey Meadowbrook reef trend.....	3
Figure 1.2: Regional distribution of Upper Devonian Leduc complexes in the Alberta basin.....	7
Figure 1.3: Subsurface Upper Devonian stratigraphy of central Alberta.....	10
 CHAPTER 2	
Figure 2.1: a) NW-SE cross section across the Strachan buildup.....	16
b) Net pay thickness map showing well locations.....	16
Figure 2.2: Depositional facies in the Strachan buildup	
a) Pool D3B.....	19
b) Pool D3A	21
Figure 2.3: a) NW-SE cross section across the Ricinus West buildup.....	27
b) Net pay thickness map showing well locations.....	27
Figure 2.4: Depositional facies in the Ricinus West buildup	
a) Buildup interior.....	30
b) Buildup margin.....	32
Figure 2.5: Paragenetic sequence of Strachan buildup rocks	
a) Limestones and partly dolomitized rocks.....	59
b) Dolostones.....	59
Figure 2.6: Paragenetic sequence of adjacent buildups	
a) Ricinus West buildup.....	61
b) Chedderville buildup.....	61
Figure 2.7: Plot of carbon and oxygen isotopes	
a) Marine cements, limestones matrices and dolomite patches.....	71
b) Replacement dolomites.....	71
c) Dolomite cements and late calcites.....	71
Figure 2.8: Strontium ratios vs. oxygen isotopes.....	75

Figure 2.9:	Histograms of aqueous liquid-vapour primary fluid inclusions a), b) Dolomite cements (C_1 , C_2).....	78
	c) Late calcite cements.....	78
Figure 2.10:	Histograms of aqueous liquid-vapour primary fluid inclusions a), b), c) Late calcites.....	80
Figure 2.11:	Burial - temperature plot for Leduc Formation.....	90

CHAPTER 3

Figure 3.1:	Distribution of porosity and permeability in the Ricinus West a) Large scale.....	120
	b) Medium scale.....	120
Figure 3.2:	Permeability zones in pore system I a) Moldic pores.....	123
	b) Fenestral-like pores.....	123
	c) Intercrystalline pores.....	123
Figure 3.3:	Permeability zones in pore system II a) Moldic (<u>Thamnopora</u> -like) pores.....	126
	b) Moldic (Stromatoporoid-like) pores.....	126
Figure 3.4:	Permeability zones in pore system III.....	128
Figure 3.5:	Porosity and permeability in Strachan well 10-31.....	135
Figure 3.6:	Porosity in skeletal wackestone facies.....	138
Figure 3.7:	Permeability in skeletal wackestone facies.....	141
Figure 3.8:	Pore evolution in studied reservoirs.....	147

CHAPTER 4

Figure 4.1:	Depositional facies in the Strachan buildup a) Pool D3B.....	155
	b) Pool D3A.....	157
Figure 4.2:	Microfracture patterns in the Strachan buildup.....	168
Figure 4.3:	Distribution of Leduc buildups in the deep Alberta basin showing discovery pressures.....	178
Figure 4.4:	Pressure-depth plot for reservoirs in the deep Alberta basin.....	182
Figure 4.5:	Burial - temperature plot for Leduc Formation.....	184

Figure 4.6:	a) Role of pore pressure in fracture initiation.....	188
	b) Stresses at principal points around a circular pore.....	188

LIST OF TABLES

CHAPTER 2	Page
Table 2-1: Distribution of dolostones and late diagenetic features in Leduc buildups, deep Alberta basin.....	68
Table 2-2: Summary of dolostone characteristics from different buildups along the Rimbey Meadowbrook trend	86
Table 2-3: Characteristics of late calcite cements	96
Table 2-4: Processes of crude oil alteration.	99
CHAPTER 3	
Table 3-1: Summary observations from cores	106
Table 3-2: Characteristics of pore types in limestones.....	109
Table 3-3: Characteristics of pore types in dolostones.....	110
Table 3-4: Porosity and permeability data in all depositional facies.....	113
Table 3-5: Porosity and permeability data in pore systems.....	118
Table 3-6: Comparison of porosity and permeability data in different buildups.....	132
Table 3-7: Effect of reservoir bitumen on porosity and permeability.....	133
CHAPTER 4	
Table 4-1: Characteristics of hairline microfractures.....	187

LIST OF PLATES

CHAPTER 2	Page
Plate 2.1: Depositional facies in the Strachan buildup.....	24
Plate 2.2: Depositional facies in the Ricinus West buildup interior.....	35
Plate 2.3: Depositional facies in the Ricinus West buildup margin.....	37
Plate 2.4: Early diagenetic products.....	41
Plate 2.5: Cathodoluminescence and fluorescence characteristics of calcite cements, replacement dolomite, and dolomite cements.....	45
Plate 2.6: Replacement dolomites.....	49
Plate 2.7: Replacement dolomites (continuation) and dolomite cements.....	52
Plate 2.8: Late diagenetic products.....	55
Plate 2.9: Dolomite distribution.....	65
 CHAPTER 3	
Plate 3.1: Pore types in the Strachan and Ricinus West buildups	114
 CHAPTER 4	
Plate 4.1: Characteristics of Ireton shales.....	163
Plate 4.2: Microfracture patterns in the Strachan reservoir.....	171
Plate 4.3: Microfracture patterns in the Strachan reservoir (continuation).....	173
Plate 4.4: Microfractures in other buildups in the Alberta basin.....	176
 APPENDIX D	
Plate D1: Optical textures in reservoir bitumens.....	242

LIST OF APPENDICES

	Page
A: List of wells studied.....	227
B: Depositional facies in the Strachan and Ricinus West buildups...	229
C: Diagenetic features potentially related to thermal sulphate reduction reactions.....	232
D: Characteristics of reservoir bitumens	237
E: Geochemistry data:.....	243
1) Major and trace elements, Strachan Reservoir Rocks and approximate concentrations of trace elements.....	244
2) C, O isotope data and temperature calculations from oxygen isotope data.....	247
3) Fluid Inclusion data.....	251
F: Gas compositions	254
G: Wells that penetrate the Cooking Lake Formation.....	258
H: Vertical permeability profiles of different depositional facies in the Ricinus West reservoir.....	260

GENERAL ACKNOWLEDGMENTS

This study was made possible by contributions from many individuals to whom I will always be thankful. In the early days of my research, when I had difficulties focusing and needed help to channel my ideas, the following individuals were always there. My principal advisor, Dr. Eric Mountjoy, who has been a thoughtful teacher and mentor that introduced and guided me through the world of carbonate diagenesis and dolomites. His understanding of my thought and my work processes has been a constant source of surprise and delight to me. His wife Anita, who has been, as well, a joy to socialize with over the years. Dr. J. Amthor and his wife Eva constantly encouraged me. Dr. J. Paquette greatly contributed to my focussing through countless discussions. Dr. C. Schreiber was and always will be an unforgettable role model. Dr. H. Vali and K. Sears were always there to encourage me when I was down. These people have my warmest appreciation and gratitude.

While in Calgary Dr. G. Davies and his wife Maureen made me feel at home away from home. I will always be thankful for their wonderful hospitality and friendship, no graduate student ever had this luck.

My search for information was greatly helped by the generosity of several individuals who shared their own work and knowledge with me and who led me to important sources : H. Machel and E. Dembick (Univ. of Alberta); F. Krause, B. McNamara, R. Shedd and N. Wardlaw (Univ. of Calgary); D. Beringer, B. Martindale, J. Reimer and M. Teare (Home Oil); A. Laflamme, B. Scott and B. Watt (Husky Oil); P. Fejer and B. Stain (Shell), B. Thornhill, A. Chow (Chevron), and J. and J.W. Keith.

I am specially indebted to my committee members, Drs. R. Hesse and J. Paquette for their critical review of the manuscript and valuable discussions and suggestions.

At the Seals and Traps Hedberg Conference in Crested Butte, Colorado (June 21-

23, 1993) I gained invaluable experience and was fortunate to discuss some aspects of my research with the following individuals: P. D'Onfro (Conoco Inc.); J. Ebanks (Arco Bali North Inc.); T. Engelder (Penn State Univ.); M. Grigg (Canadian Hunter Exploration); N. M. Jr. Hannon (Canadian Hydrodynamics Ltd); H. W. Reid (H.W. Reid & Associates); R. Sneider (R. M. Sneider Expl.); R. C. Surdam (Univ. of Wyoming), and many others.

Technical assistance was received from the following people: the staff of the ERCB core depository in Calgary; S. Salvi (cathodoluminoscope); R. Lamarche and C. Smith (fluorescence microscopy); A. Dolan-Laughlin (stable isotope analyses); S. Whittaker (strontium isotope analyses); T. Mulja and J. Mungall (SEM); G. Poirier (microprobe); W. Tan and S. Shata (XRD analyses), and D. Palmer, P. Kraniotis and B. Stefanini (fluid inclusions). A French translation of the abstract was kindly provided by Werner Halter.

I extend my thanks to Dr. V. Stasiuk (Geological Survey of Canada, ISPG) for providing me with detailed petrography of the reservoir bitumens from the Strachan and Ricinus West reservoirs.

In a work of this scope the criticism of experts in the various fields is indispensable. I benefited greatly from the generosity of many individuals who were willing to read and criticize parts of the manuscript which related to their particular expertise. My profound thanks go to P. Budkewitsch, E. Drivet, K. Sears, H. Vali, and G. Zhang. Special thanks must go to Steve Whittaker, whose patience and understanding I will always be grateful for.

I also extend my thanks to Dr. P. E. Gretener for reading Chapter 4 and helping me to clarify my ideas about rock mechanics from a geologists' point of view.

For the friendship during my study at McGill, I am indebted to my fellow students, especially S. Becker, H. Chouinard, E. Drivet, A. Frederiksen, S. Harris, G. Hartley, S. Khodabakhsh, M. Mallamo, K. Sears, S. Shata, W. Tan, and H. Qing.

This work was done in years of solitary living, and always, through these time,

despite the geographical distance between us, the love and support of my family, Ruth, Ingrid, Gabi, Nairo, Edgar and Manuel Alfredo has nurtured and sustained me.

My close friends: I. Azpirtxaga, O. Colmenares, I. Duran, L. Echeverria, D. Fuentes, C. Hernandez, S. Mederos and L. Picoli have given me love and friendship through the good times and the bad, hearing and sharing.

R. Canard and L. Mompart trusted and encouraged me to pursue my studies. They also helped me to obtain financial support from Maraven S.A. M. Adrianza and Z. Alarcon kindly provided me with all the information and support I needed from Maraven S.A.

Funding was provided by Natural Science and Engineering Research Council (NSERC) strategic grants to Drs. Mountjoy and Machel; an individual grant to Mountjoy; and, through financial and technical support from Imperial Oil, Home Oil, Mobil Oil, Norcen, Petro-Canada, Chevron and Shell, and a scholarship that I received from Maraven S.A., as well as financial aid from the American Association of Petroleum Geologists Grants-in-Aid program.

PREFACE

This research project was initiated in September of 1990 under the supervision of Dr. Eric Mountjoy who suggested a study of the Leduc Formation in the deep part of the central Alberta basin. December 1990 and the following two summers (1991-1992) were spent studying core at the Energy Resources Conservation Board (ERCB) core-storage facility in Calgary as well as gathering reservoir information from several oil companies. I also examined outcrops of equivalent strata in the Front Ranges for comparison purposes. This thesis includes my observations and interpretations of the Leduc Formation in the area between Townships 34 to 39 and Ranges 7 to 12 W5 in central Alberta. **Responsibility for the content of this thesis rests with the author**, except where indicated in the text. Dr. Mountjoy's name appears as junior author on the manuscripts contained within the thesis, having served as supervisor, having assisted in the description and data gathering, having provided ideas and as critic and editor.

Thesis Format

This thesis consists of five chapters and a general abstract. The abstract that precedes this preface contains general aspects from the three main chapters. Chapter 1 is the general introduction to the thesis. Chapter 2 is titled: Depositional facies and diagenesis of the Leduc buildups (Upper Devonian) in the deep Alberta basin. It includes observations and interpretations regarding the reservoir rocks, emphasizing their origin and diagenetic evolution. Chapter 3 is titled: Pore systems and the effect of dolomitization on reservoir properties, in Upper Devonian Leduc buildups, deep Alberta basin. Pore systems are defined, porosity and permeability trends are established, and reservoir quality is examined. Chapters 2 and 3 complement one another. Chapter 4 is titled: Origin of

microfractures in the Upper Devonian Leduc Strachan reservoir, deep Alberta basin. It provides information about reservoir bitumens and the characteristics and possible origins of late-stage microfractures present in the reservoir rocks.

Chapter 5 includes the general conclusions of the thesis derived from the more specific conclusions in chapters 2, 3, and 4. Chapters 2, 3 and 4 are written as manuscripts for journal publication, and some repetition is unavoidable. Figures are included with the appropriate chapter, and a general reference list is included at the beginning of the thesis. A complete reference list follows Chapter 5. Core descriptions, samples, photo negatives, and general reservoir data are on file in the Department of Earth and Planetary Sciences, McGill University, c/o Professor Eric W. Mountjoy.

Original contributions to knowledge

When this study commenced in 1990, only one paper (Hriskevich et. al., 1980) was published on the geology and preliminary reservoir characteristics of the Leduc buildups in the study area. Thus, almost the entire thesis contributes to original knowledge. These data and interpretations have immediate application in terms of the reservoir characterization and the diagenesis relative to other parts of the Western Canada Sedimentary Basin, and other sedimentary basins in the world. The following are considered particularly noteworthy:

- 1) The diagenetic paragenesis of the Leduc buildups in the deeper part of the Rimbey-Meadowbrook reef trend is established.

- 2) Four types of replacement dolomites are described (R_1 to R_4), including a fine-crystalline dolomite (R_1 , 30 to 62 μm) which is interpreted to be a replacement of lime mud. These replacement dolomites are similar to replacement dolomites in buildups along

the Rimbey Meadowbrook reef trend. The widespread distribution of replacement dolomites suggest that they formed from the same fluids during a regional to basin-wide event in the shallow to intermediate burial environment.

3) In the partly dolomitized Strachan buildup hairline microfractures are abundant and thermal sulphate reduction (TSR) products are rare. In the completely dolomitized buildups microfractures are rare and TSR products are abundant. These differences in diagenesis are best explained by completely dolomitized buildups being connected to a regional fluid conduit system along the Cooking Lake platform that underlies the Rimbey Meadowbrook reef trend. This conduit system provided the flow paths for fluids responsible for replacement dolomitization, secondary migration of hydrocarbons, H₂S and later diagenetic products.

4) At depths > 4000 m dolostones have higher porosities and permeabilities than limestones because the dolostones retain their porosity being more resistant to pressure solution. Bitumen decreases permeability in the upper part of the reservoirs. Later thermal sulphate reduction (TSR) products have both increased and decreased porosity and permeability in the lower part of the reservoirs. These results have important implications for both hydrocarbon exploration and development especially during enhanced recovery.

5) Hairline microfractures in the Strachan reservoir are described for the first time and their possible origins constrained. These hairline microfractures most likely formed in response to the development of high pore pressures caused by the thermal cracking of crude oil to gas, in conjunction with compression due to thrusting during the Late Cretaceous.

Publications

Prior to completion of this thesis, parts of this research have been published as abstracts, presented orally or as a poster display, or submitted for publication (Marquez and Mountjoy, in review). The information contained in these papers and abstracts is integrated into the body of the thesis.

Marquez, X., E.W., Mountjoy and J. Amthor, (1992), Microfracturing in an overpressured carbonate buildup: Upper Devonian Strachan reservoir, deep Alberta basin. American Association of Petroleum Geologists, Annual Convention Abstracts, Calgary, p. 81.

Marquez, X., E.W., Mountjoy and J. Amthor, (1992), Microfracturing in deeply buried carbonate buildups: Upper Devonian Strachan and Ricinus reservoirs. American Association of Petroleum Geologists, Annual Convention Abstracts, Calgary, (abs., core), p. 81.

Marquez, X, (1993), Sedimentological and Diagenetic controls on pore systems in a dolomitized reservoir. A case study: The Ricinus West gas field, Central Alberta. (abs.). American Association of Petroleum Geologists, 1993 Annual Convention Abstracts, New Orleans, Louisiana, p. 145.

Mountjoy, E. and X. Marquez, (1993), Microfracturing - Evidence of overpressuring in a sealed Devonian carbonate reservoir. (abs.). AAPG Hedberg Research Conference on "Seals & Traps: A multidisciplinary Approach. June 21-23, Crested Butte, Colorado.

Marquez, X. and E.W. Mountjoy, (1994), Origin of microfractures in the Upper Devonian Leduc, Strachan reservoir, Deep Alberta Basin. Submitted to AAPG Bulletin.

CHAPTER 1

GENERAL INTRODUCTION

Rationale and objectives

Mature hydrocarbon provinces such as the Central Alberta Basin, are likely to produce more oil and gas through enhanced oil recovery than may be discovered through new exploration. Current efforts to maximize oil and gas production from mature hydrocarbon basins are becoming increasingly dependent on geological reservoir studies because hydrocarbon reservoirs are more heterogeneous and compartmentalized than previously thought. Consequently, there is a need to determine the origin and distribution of heterogeneity within carbonate hydrocarbon reservoirs, especially in relatively deep (> 4000 m) reservoirs. The deep reservoirs are examined to help differentiate local versus regional as well as shallow versus deep-burial diagenetic effects on porosity and permeability.

Reservoir geology attempts to identify and quantify properties of the rock-pore system (heterogeneities) affecting hydrocarbon flow under specific conditions, and provides information that is important for reservoir evaluation, simulation, and prediction of ultimate recovery. The present thesis focusses on how sedimentary facies and diagenesis controls the rock-pore system in dolomitized Upper Devonian Leduc buildups from the deep Alberta Basin (Fig. 1.1), addresses the problem of reservoir heterogeneity, and explains the origin of late-stage hairline microfractures.

The objectives of Chapter 2 are to: 1) examine the diagenetic histories of the Upper Devonian (Frasnian) Strachan, Ricinus West, Ricinus East, Crimson and Chedderville buildups (Fig. 1.1) and establish their similarities and differences; 2) compare dolostones from this area with dolostones from the central parts of the Rimbey-Meadowbrook trend and, 3) investigate mechanisms governing the distribution and origin of dolomites and late

cements.

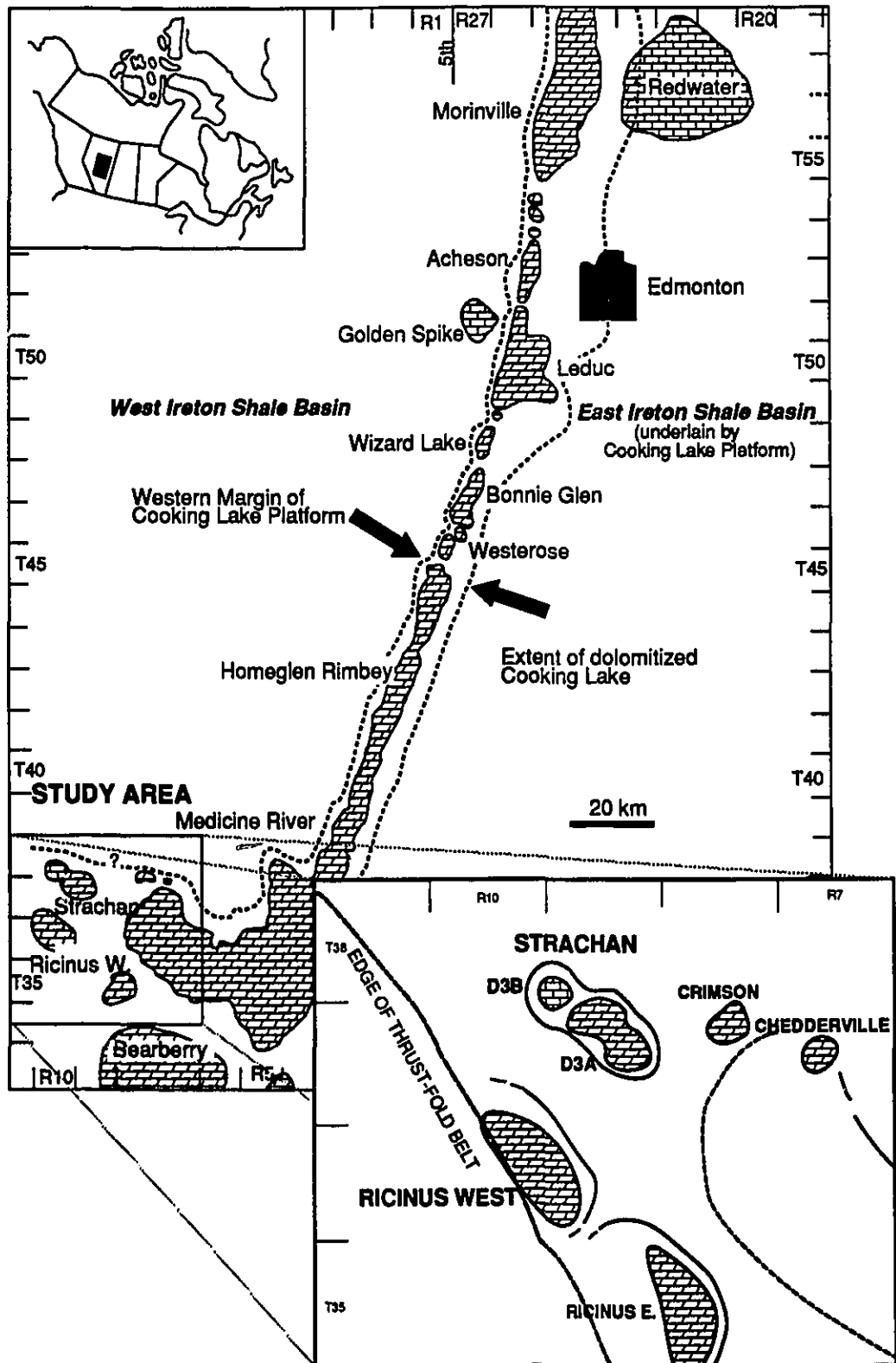
In Chapter 3, 1) the different pore systems in the Strachan and Ricinus West buildups are defined; 2) the effects of sedimentological and diagenetic controls on the pore systems are established; 3) porosity and permeability trends relative to the different phases of diagenesis are identified, and 4) the effects of dolomitization, cementation and reservoir bitumen on reservoir quality are examined. In Chapter 4 the characteristics of hairline microfractures associated with the pore systems in the Strachan reservoir are examined and their possible origins are assessed with respect to reservoir quality.

Previous work

There are several previous studies of subsurface limestone buildups along the Rimbey-Meadowbrook trend (e.g. Waring and Layer, 1950; Andrichuk, 1958a,b; Klován, 1964; McGillivray and Mountjoy, 1975; Walls, 1983); surface exposures, along Rocky Mountain thrust sheets, have also been examined (e.g. Mountjoy, 1965, 1987, 1989; Mattes and Mountjoy, 1980; Burrowes and Weihmann, 1982; McLean, 1992) and provide good exposures of equivalent strata with similar characteristics.

Most Leduc buildups have been extensively and pervasively dolomitized. However, except for the studies of Layer (1949), Illing (1959), Andrichuk (1958a), who reported the extensively dolomitized character of the Leduc and underlying Cooking Lake Formations in the subsurface, these dolomites have been little studied, especially their paragenetic relationships and relative timing. Mattes and Mountjoy (1980) identified 5 different types of dolomites and their paragenetic relationship in the outcropping Miette buildup. Machel and Mountjoy (1986, 1987) summarized the general constraints on extensive and pervasive dolomitization in the Western Alberta Basin. Recently, Amthor et. al. (1993) described and discussed the origin of the dolomites along the middle portion of the Rimbey-Meadowbrook reef trend. Dix (1993) studied the Leduc dolomites in the fringing-reef

Figure 1.1 **Distribution of Leduc buildups along the Rimbey-Meadowbrook reef trend and extent of dolomitization in the underlying Cooking Lake carbonate platform (modified from Amthor et. al., 1993). Buildups are dolomitized except for Golden Spike and Redwater in the updip part of the trend and the western D3B pool of Strachan in the downdip portion. Study area (inset) includes townships (T) 34 to 39 and Ranges (R) 7 to 12 west of the 5th meridian (116° W longitude).**



complex around the Peace River Arch.

Studies of reservoir characteristics in some Upper Devonian buildups in the Alberta basin showed that reservoir porosity and permeability are related to depositional facies and diagenesis, which varies markedly from one buildup to another (e.g. Langton and Chin, 1968; Reitzel and Callow, 1976; Jardine et. al. 1977; Barfoot and Rodgers, 1984; Walls and Burrowes, 1985; Barfoot and Ko, 1987; Burrowes and Krause, 1987; Hawlander and Machel, 1991). McNamara and Wardlaw (1991) are among the first to describe the reservoir character of the Leduc dolostones along the Rimbey Meadowbrook reef trend. They studied the stratigraphy and porosity and permeability variations within the Westerosé buildup. Drivet (1993) studied the dolomites and described the reservoir properties of buildups along the middle part of the Rimbey Meadowbrook trend, particularly the Homeglen Rimbey buildup. Drivet and Mountjoy (1993, 1994a,b) further discussed the timing and origins of secondary porosity. Amthor et. al. (1994) discussed the porosity and permeability trends in dolomites along the Rimbey Meadowbrook reef trend.

For the area studied, this study is the first to provide detailed descriptions and interpretations of the Leduc dolostones. Other than the preliminary study of the geology of Strachan and Ricinus gas fields by Hriskevich et. al. (1980), and the diagenetic study of the Leduc and Swan Hill dolomites in the Caroline area by Laflamme (1990), there are no published data concerning the relationships of sedimentology, diagenesis and petrophysics of the Leduc carbonates in the deeper part of the Rimbey-Meadowbrook reef trend.

Study area

The study area includes the Strachan, Ricinus West, Ricinus, Crimson and Chedderville buildups, located in the downdip portion of the NNE-SSW oriented Rimbey-Meadowbrook reef trend (Fig. 1.1), approximately 100 km northwest of Calgary, Alberta. It encompasses the area between townships 34 to 39 and ranges 7 to 12 W5 (Appendix A).

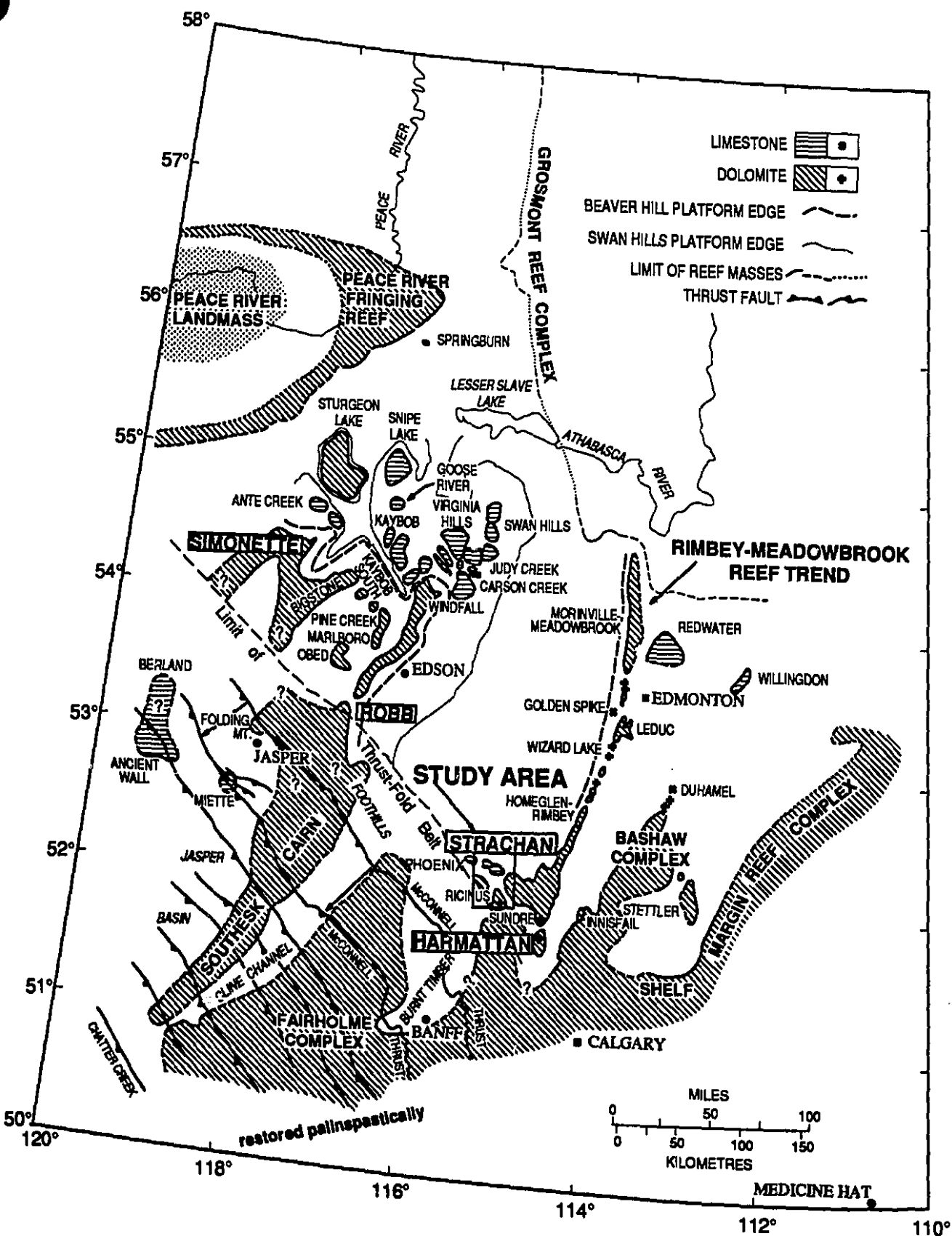
The Leduc Formation is completely dolomitized along the entire 320 km Rimbey-Meadowbrook reef trend, except for the limestone Golden Spike and Redwater buildups in the updip portion of the trend (e.g. Amthor et. al., 1993). In the downdip part of the trend, the Strachan buildup is partially to completely dolomitized and is isolated from this major reef trend. The Ricinus West and adjacent buildups are completely dolomitized representing an excellent area for studying and comparing the diagenetic relationships of both limestones and dolostones in the deeper part of the Alberta basin.

Geological setting and stratigraphy

The central Alberta basin is a shallow, protected seaway of the Western Canada Sedimentary Basin (Geldsetzer and Mountjoy, 1992; Geldsetzer and Mallamo, 1993). During the Late Devonian (Frasnian) an extensive reef domain developed in the central Alberta basin. The eastern and central parts of this reef domain occur today entirely in the subsurface (Fig. 1.2; Leduc Formation), and the western part is exposed in a series of thrust sheets (Cairn Formation and Peechee Member) that form mountains with more than 2000 m relief (e.g. Mountjoy, 1980; McLean, 1992; Geldsetzer and Mallamo, 1993).

During the early Frasnian time, the subsurface Rimbey-Meadowbrook trend developed on the western edge of the extensive, shallow-water Cooking Lake Formation platform (Andrichuk, 1958b; Stoakes, 1992; Chouinard, 1993). The Cooking Lake Formation represents an extensive cratonic carbonate shelf (Morrow and Geldsetzer, 1988) in tropical to sub-tropical epicratonic seas, within 30° north or 10° south of the Frasnian paleoequator (McLean, 1992). It rests on Beaverhill Lake strata which in turn rest unconformably on Upper and Middle Cambrian rocks. Off-reef basin strata conformably overlie the Cooking Lake platform (Fig.1.3). The lowermost Duvernay Formation is organic rich and is the source rock for the Leduc hydrocarbons (Deroo et. al., 1977; Stoakes and Creaney, 1984; Allan and Creaney, 1991; Creaney and Allan, 1992), whereas

Figure 1.2 Regional distribution of Upper Devonian Leduc and Upper and Middle Devonian Swan Hills reef complexes. The Rimbey-Meadowbrook reef trend is located in the center of the basin. Hairline microfractured reservoirs are shown by square boxes. Modified from Mountjoy (1980).



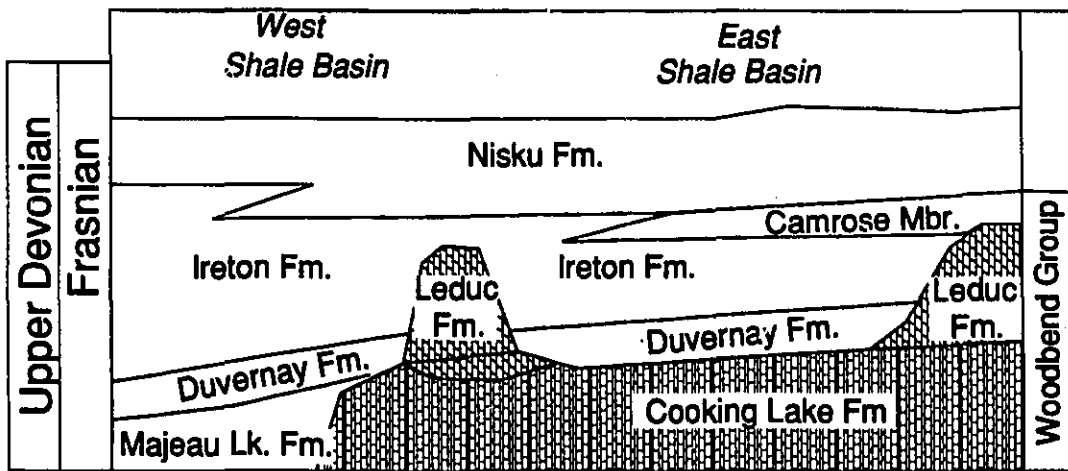
the overlying Ireton Formation includes calcareous shales and argillaceous limestones and completely encloses and seals the Leduc buildups (Fig. 1.3).

During the Late Frasnian, the Leduc buildups were buried by northerly-derived, terrigenous sediments (Ireton Formation; Stoakes, 1980). In latest Frasnian and Early/Middle Famennian widespread shallow-water carbonate deposition returned to the central Alberta Basin, which in turn was followed by the Upper Famennian black shales of the Exshaw Formation (e.g. Geldsetzer and Mallamo, 1993).

Generally, Upper Devonian sediments experienced nearly continuous burial during differential subsidence of the central Alberta Basin from Late Devonian to Mississippian time (McLean and Mountjoy, 1994). During the Permian and early Mesozoic, the Alberta Basin was progressively tilted westward (Porter et. al., 1982) causing uplift of the eastern part of the basin and extensive erosion and peneplanation of Paleozoic strata (e.g. Walls et. al., 1979; Krebs and Macqueen, 1984).

During Middle Jurassic through Paleocene time, accretion of oceanic terranes onto the western margin of the North American craton formed a foreland basin which was filled with over 4 km of a northeasterly thinning clastic wedge (Porter et. al., 1982). The clastic wedge formed during two orogenic episodes, the first during the Late Jurassic to Early Cretaceous, and the second during the Late Cretaceous to Early Tertiary, that resulted in the development of compressional mountains that shed sediments eastward (Porter et. al., 1982). Upper Devonian rocks in the Alberta Basin reached their maximum burial depth during the Late Cretaceous to Early Tertiary. Subsequently, there was gradual uplift and erosion of about 1000 m of the Tertiary strata in the study area.

Figure 1.3 **Subsurface Upper Devonian stratigraphy of central Alberta illustrating the relationships of the dolomitized Leduc buildups above the western dolomitized part of the Cooking Lake platform, and basin filling sediments (Duvernay Formation, black shales and limestones, and Ireton Formation enclosing shales). Modified from Stoakes (1980).**



CHAPTER 2

DEPOSITIONAL FACIES AND DIAGENESIS OF THE LEDUC BUILDUPS (UPPER DEVONIAN) IN THE DEEP ALBERTA BASIN

X. Marquez and E.W. Mountjoy
Dept. of Earth and Planetary Sciences, McGill University
Montreal, H3A 2A7, Canada

ABSTRACT

The Upper Devonian (Leduc) Strachan, Ricinus West and adjacent buildups in the deep Alberta basin are similar in terms of their facies and succession of interpreted depositional environments. However, diagenetic features differ. Replacement dolomitization took place during shallow burial at depths of about 500 m, based on crosscutting relationships with early submarine cements, relationships with stylolites, and its occurrence in the overlying Ireton Formation. Dolomitizing fluids were probably modified from Upper Devonian seawater based on trace element concentrations and $^{87}\text{Sr}/^{86}\text{Sr}$ ratios (0.7083 to 0.7092). These replacement dolomites are similar to replacement dolomites in buildups along the Rimbey Meadowbrook reef trend, and suggest that most replacement dolomites formed from the same fluids during a regional to basin-wide event.

In the Strachan buildup hairline microfractures are abundant and thermal sulphate reduction (TSR) products are rare. In the Ricinus West and adjacent buildups microfractures are rare and TSR products are abundant. These differences in diagenesis between the partially dolomitized Strachan buildup (hairline microfracturing) and the completely dolomitized Ricinus West and adjacent buildups are best explained by the completely dolomitized buildups being connected to a regional fluid conduit system along the Cooking Lake platform that underlies the Rimbey Meadowbrook reef trend.

INTRODUCTION

Leduc carbonate buildups extend for a distance of about 320 km along the Rimbey-Meadowbrook reef trend in the subsurface of central Alberta (Fig. 1.1) and have produced prolific amounts of oil and gas for more than 45 years (e.g. Podrusky, et. al., 1987). Despite their economic importance there are few published studies concerning the diagenesis, sedimentology, and petrophysical characteristics of these buildups, especially those that are dolomitized and that occur in the deep portion of the basin. In the updip portion of the reef trend (< 2,000 m burial), information about the limestone buildups (Golden Spike and Redwater) and the completely dolomitized buildups such as Leduc, have been published (e.g. Layer, 1949; Waring and Layer, 1950; Andrichuk, 1958 a,b; Illing, 1959; Klován, 1964; McGillivray and Mountjoy, 1975; Walls, 1977; Burrowes, 1977; Barfoot and Rogers, 1984; Barfoot and Ko, 1987; Machel and Mountjoy, 1987).

Recent work done in the central (Westerose, Homeglen-Rimbey) part of the reef trend (McNamara and Wardlaw, 1991; Amthor et. al., 1993; Drivet, 1993; Drivet and Mountjoy, 1994a,b) has for the first time documented the characteristics, possible origins, and reservoir properties of some of the dolomitized buildups. In the deeper part of the reef trend (> 4,000 m burial), there are no published data on the sedimentology and diagenesis of the buildups, other than the preliminary report on the geology of Strachan and Ricinus reservoirs by Hriskevich et. al. (1980) and the unpublished diagenetic study of the Leduc and Swan Hills dolomites in the Caroline area by Laflamme (1990).

This paper presents the sedimentology and diagenetic history of the Upper Devonian (Frasnian) Strachan, Ricinus West, Crimson, and Chedderville buildups in the deeper part of the Rimbey-Meadowbrook reef trend, located approximately 100 km northwest of Calgary, Alberta. The similarities and differences in the diagenesis especially between limestones and dolostones among the buildups are described, and the dolostone

buildups are compared with those in the central part of the reef trend. This research identifies factors that control the distribution of dolomites and the later diagenetic products in the deeper part of the trend, some of which are related to thermal sulphate reduction (TSR).

METHODS

All available cores were studied from the Strachan, Ricinus West, Crimson and Chedderville buildups in the Upper Devonian of central Alberta, Canada, between Townships 34 to 39 and Ranges 7 to 12 W5 (Fig. 1.1; Appendix A). Thin sections ($n=300$) were examined using a petrographic microscope with diffused light and a blue-light epifluorescence microscope (480 to 520 nm). Thin sections were stained with Alizarin-S and some were injected with blue and fluorescent epoxy to delineate porosity. Cathodoluminescence of selected samples was examined using a Nuclide Luminoscope, Model ELM-2. Cathodoluminescence petrography was carried out with a beam voltage of 16 KV and a beam current of 0.5 mA in a 40-50 mTorr vacuum under an air atmosphere.

Microsamples (0.05 g) of limestones, dolostones, and late calcite were obtained using a dental drill and analyzed for carbon ($\delta^{13}\text{C}$) and oxygen ($\delta^{18}\text{O}$) at the University of Michigan. Carbon and oxygen isotopic values are reported relative to the PDB scale and have a precision of $\pm 0.05\text{‰}$. Strontium isotope ratios were measured by S. Whittaker at L'Universite du Quebec a Montreal (UQAM). Strontium (Sr) was separated from samples by dissolving them in cold 1 N HCL and by elution with 3N HNO_3 and H_2O on columns containing 50 μl of Sr Spec resin. At UQAM, Sr was loaded on Re single filaments with a Ta emitter and analyzed on a multicollector in dynamic mode. Errors associated with these analyses are reported as 2σ values. $^{87}\text{Sr}/^{86}\text{Sr}$ ratios were normalized to 0.1194. Selected polished thin sections were studied using a Cameca Camebax microprobe. Operating

conditions for the microprobe were 15 KV accelerating voltage, 8 nA beam current, approximately 10 micron beam diameter, and maximum counting times of 25 seconds. Spots were analyzed for Ca, Mg, Fe, Mn, Sr, and Na. XRD analyses and insoluble residue determinations were performed for selected dolomite samples.

Fluid inclusions in dolomite cements (C_1 and C_2) and late calcite cements were analyzed by D. Palmer, P. Kranidiotis, and B. Stefanini using a fluid inclusion heating/freezing stage at McGill University based on a United States Geological Survey design (Werre et. al., 1979; Hollister et. al., 1981). The melting temperature of ice was converted to weight percent NaCl equivalent using equations in Oakes et. al. (1990).

DEPOSITIONAL FACIES

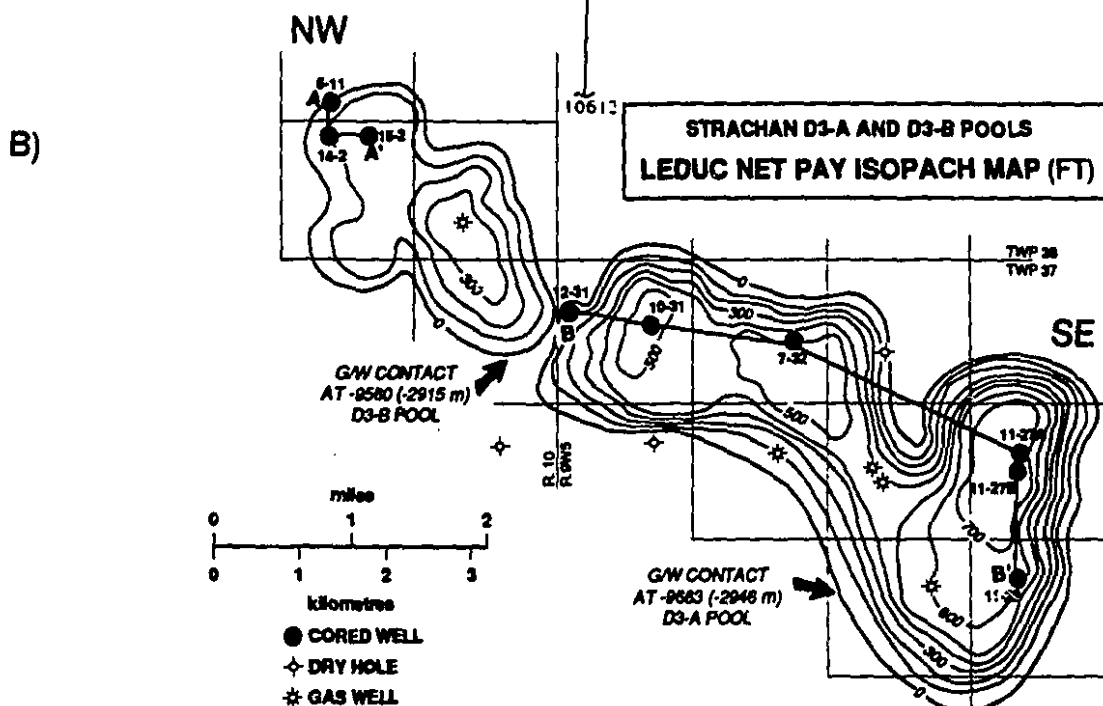
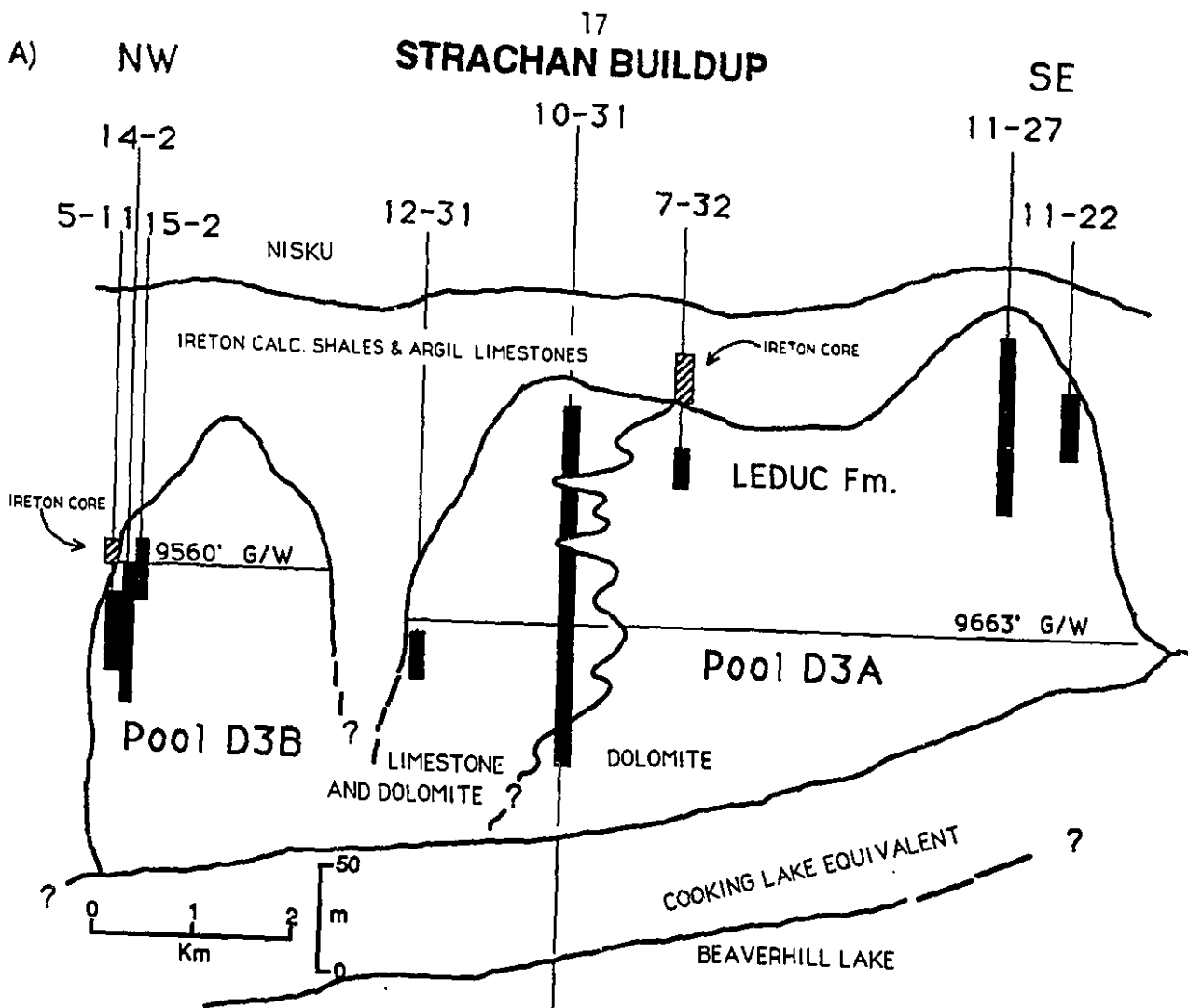
The sedimentological characteristics and depositional environments of the Strachan, Ricinus West and adjacents buildups are presented below.

Strachan Gas Reservoir

The Strachan gas field was discovered in 1967 (well 12-31, Fig. 2.1) and was the first commercial production from depths in excess of 4,000 m in this basin (Hriskevich, et. al., 1980). The reservoir consists of a carbonate buildup 11 x 4 km in area and 274 m thick. The net pay interval is 163 m having a maximum of 224 m in well 11-27. The Strachan field consists of a western pool, D3B, and an eastern pool, D3A (Fig. 2.1 A,B). Eight wells were cored, three of which (5-11, 15-2, 14-2) are from the western end of pool D3B (Fig. 2.1 A,B) and two from the western portion of pool D3A (12-31, 10-31). Three other cores are from the interior and eastern part of pool D3A (7-32, 11-27, 11-22). The D3B pool is partially dolomitized throughout and the D3A pool is almost completely dolomitized except for the western margin that is partially dolomitized. The relatively undolomitized to partially dolomitized character of these cores allows original sedimentary

Figure 2.1 **A) NW-SE cross section across the Strachan buildup showing general stratigraphy, dolomite distribution and location of cores (black bars).**

B) Map showing well locations (black dots) and net pay thickness (modified from Hriskevich et. al., 1980).



Modified from: Hristovitch et. al. (1980)

facies to be identified. However, complete dolomitization makes facies identification difficult.

Depositional facies are best recognized in pool D3B and were determined on the basis of texture (Dunham, 1962; and Embry and Klovan, 1971), diagnostic fauna, and location with respect to the buildup margin. Northwest-southeast cross sections illustrate the facies distribution in pool D3B and D3A (Fig. 2.2 A,B). Six depositional facies have been recognized: 1) coral rudstone; 2) tabular stromatoporoid boundstone; 3) stromatoporoid-coral rudstone; 4) domal stromatoporoid floatstone; 5) skeletal wackstones; and 6) skeletal packstones/grainstones.

The **coral rudstone** facies is composed of moderately sorted coral debris in a skeletal packstone matrix (Plate 2.1A). Coral components account for 10 to 40% of the rock and usually are larger than 2 cm. Thamnopora, a dendroid tabulate coral, and Alveolites are the most abundant genera, although locally large fragments of tabular corals are present. The thickness of the coral rudstone beds varies from 3 m in well 12-31 to 19 m in well 10-31. The matrix consists of poorly to moderately sorted fragments of corals, stromatoporoids, crinoids, brachiopods, gastropods and micritized grains. Locally minor growth cavities are completely filled by radiaxial calcite cement. Isopachous radiaxial calcite cement commonly surrounds the coral fragments. Coral rudstones are found closely associated with stromatoporoid-coral rudstones. The poor to moderate sorting of the matrix and the fragmentation of stromatoporoids suggest deposition in a shallow, high energy environment along the reef margin. This facies is similar to the detrital coral facies of McGillivray and Mountjoy (1975) and Walls (1977).

The **tabular-stromatoporoid boundstones** facies is observed in wells 15-2, 14-2 and 10-31 (Appendix B). It consists of laminar/tabular stromatoporoid (in situ?) in a skeletal matrix of crinoids, brachiopods, micritized packstone and less commonly grainstone. Abundant Renalcis often appears as encrustations on stromatoporoids and

Figure 2.2A Distribution of depositional facies in the Strachan D3B pool. See Fig. 2.1 for well locations. Datum is top of the Calmar Formation. Calculated arithmetic average porosity in percent and geometric average permeabilities in millidarcies are given in the right columns for each depositional facies. Porosity and permeability data are based on core analyses from ERCB.

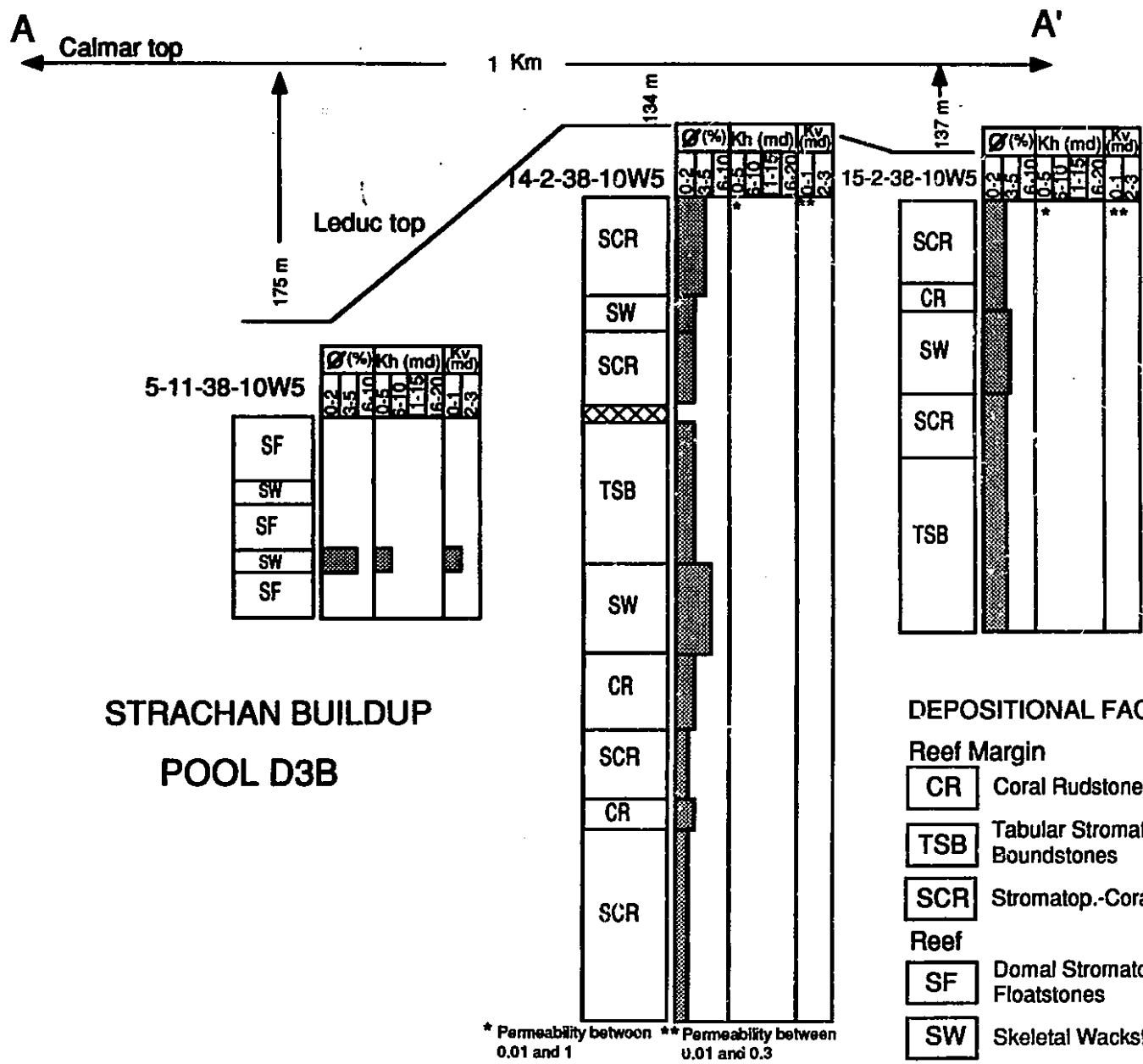


Figure 2.2B: Distribution of depositional facies in the Strachan D3A pool. See Fig. 2.1 for well locations. Datum is top of the Calmar Formation. Calculated arithmetic average porosity in percent and geometric average permeabilities in millidarcies are given in the right columns for each depositional facies. Porosity and permeability data are based on core analyses from ERCB.

DEPOSITIONAL FACIES

Reef Margin

CR Coral Rudstones

TSB Tabular Stromatoporoid Boundstones

SCR **Stromatop.-Coral Rudstones**

Reef

SF Domal Stromatoporoid Floatstones

SW Skeletal Wackestones

SP/G Skeletal Packstones/Grainstones

15 m

skeletal debris (Plate 2.1B). Shelter and growth cavities are filled with radial calcite cement (Plate 2.1C). Thickness varies from 10 to 34 m. This facies is similar to the tabular stromatoporoid facies recognized by McGillivray and Mountjoy (1975) and Walls (1977) in Golden Spike and Klován (1964) in the Redwater reef complexes.

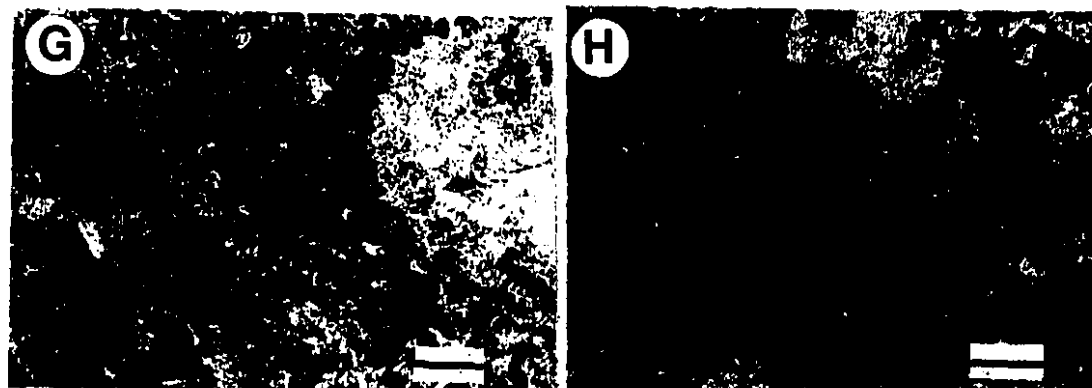
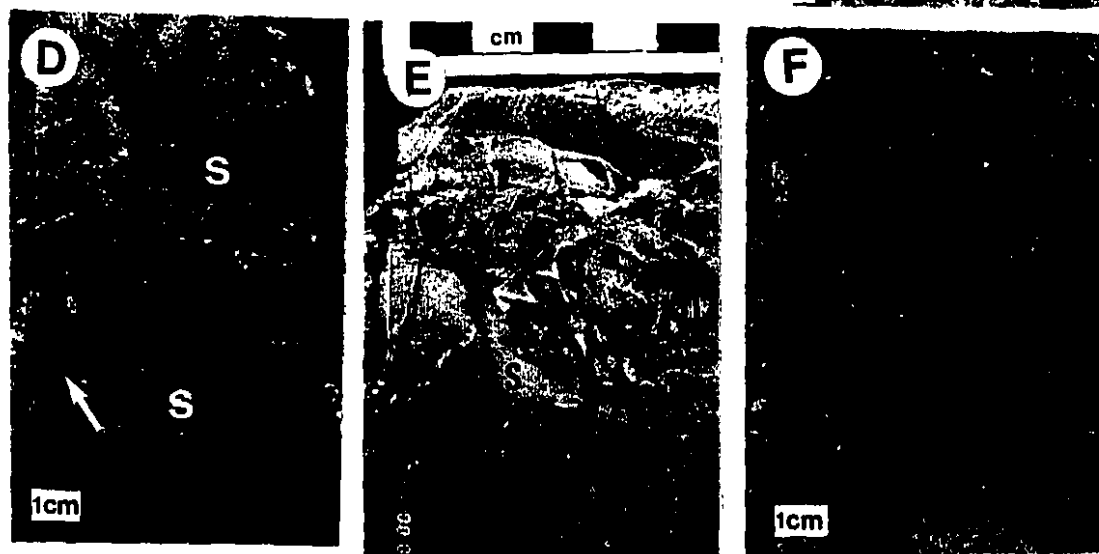
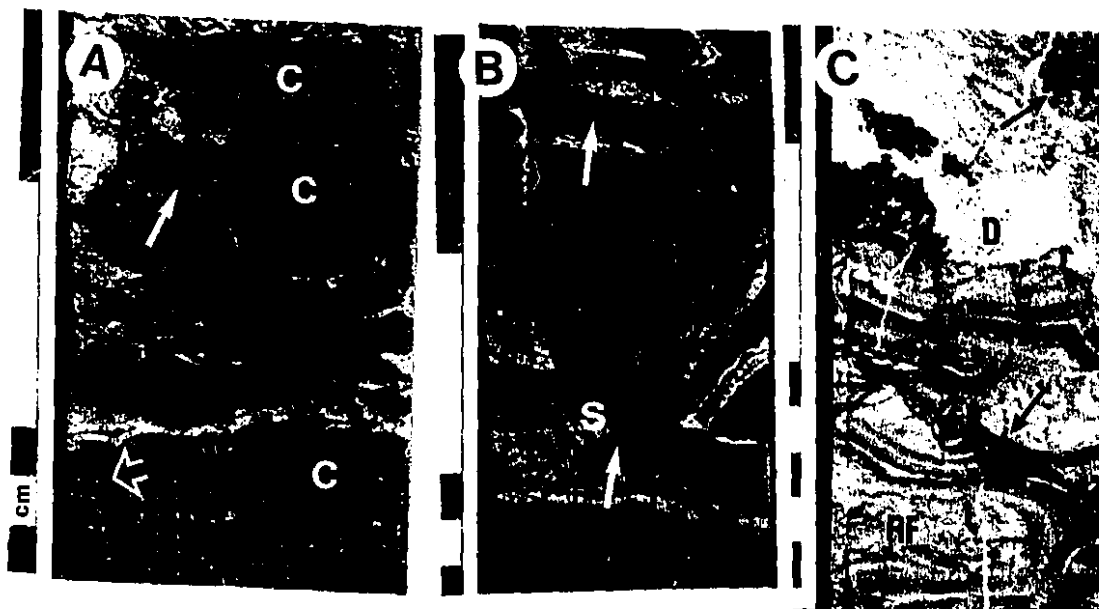
The **stromatoporoid-coral rudstone** facies is represented by thick accumulations of laminar (tabular) and domal stromatoporoids, locally branching Stachyodes, tabulate corals and crinoid rudstones (Plate 2.1D). The matrix consists of fragments of crinoids, brachiopods, mollusks and micritized grains with packstones and/or grainstone textures. Grains are bound together by syntaxial and blocky calcite cements. It reaches thicknesses up to 81 m in well 10-31. It is distinguished from tabular-stromatoporoid boundstones by the lack of in situ fossils and radial calcite cements. This facies probably represents reef-derived rubble deposited seaward of the buildup margin.

The **domal stromatoporoid floatstone** facies is composed of large, domal (2 to 7 cm) and bulbous stromatoporoids occurring in situ and as poorly sorted detrital components in a skeletal packstone matrix. Stachyodes are locally present (Plate 2.1E). Renalcis is rare to absent. This facies is generally 6 m thick but attains a thickness of 16 m in well 5-11. These rocks are interbedded with skeletal wackestones (well 5-11) and with stromatoporoid-coral rudstones in well 10-31.

The **skeletal wackestone** facies constitutes the most widespread facies, with thickness of 2 to 10 m, but reach a total of 93 m in well 10-31 (Appendix B). It consists of moderate-to-well-sorted, rounded grains in a lime mud matrix. Micritization of grains makes their identification difficult. However, some stromatoporoid, coral, mollusk, crinoid and algal fragments can be recognized (Plate 2.1F).

Plate 2.1: DEPOSITIONAL FACIES IN THE STRACHAN BUILDUP

- A) Coral rudstone: poorly to moderately sorted coral debris (C) in a skeletal packstone matrix. Hairline microfractures extend from intraskeletal pores in coral fragment (solid arrow). Intraskeletal porosity (open arrow) is partly filled with reservoir bitumen. 15-2-38-10W5, 4110 m.
- B) Tabular stromatoporoid boundstone: tabular stromatoporoid (S) in a matrix composed of crinoid, brachiopod and coral fragments. Renalcis (arrows) is abundant. Intercrystalline porosity in partly dolomitized matrix is filled with reservoir bitumen. 14-2-38-10W5, 4131.7 m.
- C) Several generations of radiaxial fibrous calcite cements (RF) in tabular stromatoporoid boundstone. Fine-grained internal sediments have been dolomitized (D). Hairline microfractures extend away from intercrystalline pores and previously formed subvertical fractures, which are filled with dolomite cement (arrows). 10-31-37-9W5, 4239.3 m.
- D) Stromatoporoid-coral rudstone: tabular stromatoporoid fragments (S) in a coarse grained, skeletal grainstone matrix. Hairline microfractures extend from intraskeletal pores in stromatoporoid fragment (arrow). 14-2-38-10W5, 4120.7 m.
- E) Stachyodes (ST) and stromatoporoid (S) debris locally deposited in the domal stromatoporoid floatstones. Dolomite rhombs and patches are present in the skeletal packstone matrix (arrows). 10-31-37-9W5, 4296 m.
- F) Skeletal wackestones with moderately sorted, rounded skeletal fragments (F). Dolomite rhombs and patches are abundant (arrows). Note lack of hairline microfractures. 10-31-37-9W5, 4295 m.
- G) Photomicrograph showing a skeletal grainstone matrix in tabular-stromatoporoid boundstone with cavity filled by radiaxial fibrous calcite cement (RF). Note lack of hairline microfractures. 15-2-38-10W5, 4135.3 m. Scale bar 250 μ m.
- H) Photomicrograph illustrating moderately sorted, micritized skeletal debris in skeletal grainstone/packstone matrices of rudstone facies. Note lack of hairline microfractures. 14-2-38-10W5, 4125 m. Scale bar 250 μ m.



Ricinus West and Adjacent Gas Reservoirs

The Ricinus West gas reservoir was discovered in 1969 in well 6-25 which encountered sour gas over a thick interval of completely dolomitized rocks (Hriskevich et.al., 1980). The reservoir consists of a dolomitized buildup 9.5 x 4 km in area and 259 m thick. The net pay reaches a maximum of 192 m in well 6-25. Presently there are eight gas producing wells in the D3A pool (Fig. 2.3 A,B)

Despite complete dolomitization of the Ricinus West buildup depositional facies can be recognized on the basis of: 1) the vertical and lateral arrangement of vuggy, moldic, fenestral-like and intercrystalline pores, and 2) relic primary textures observed in cores and under diffused light microscopy. In the reef interior, meter-scale shallowing upward facies broadly resemble depositional peritidal sequences described in outcrop equivalents of the Leduc Formation (McLean, 1992; Shields and Geldsetzer, 1992; McLean and Mountjoy, 1993 a,b).

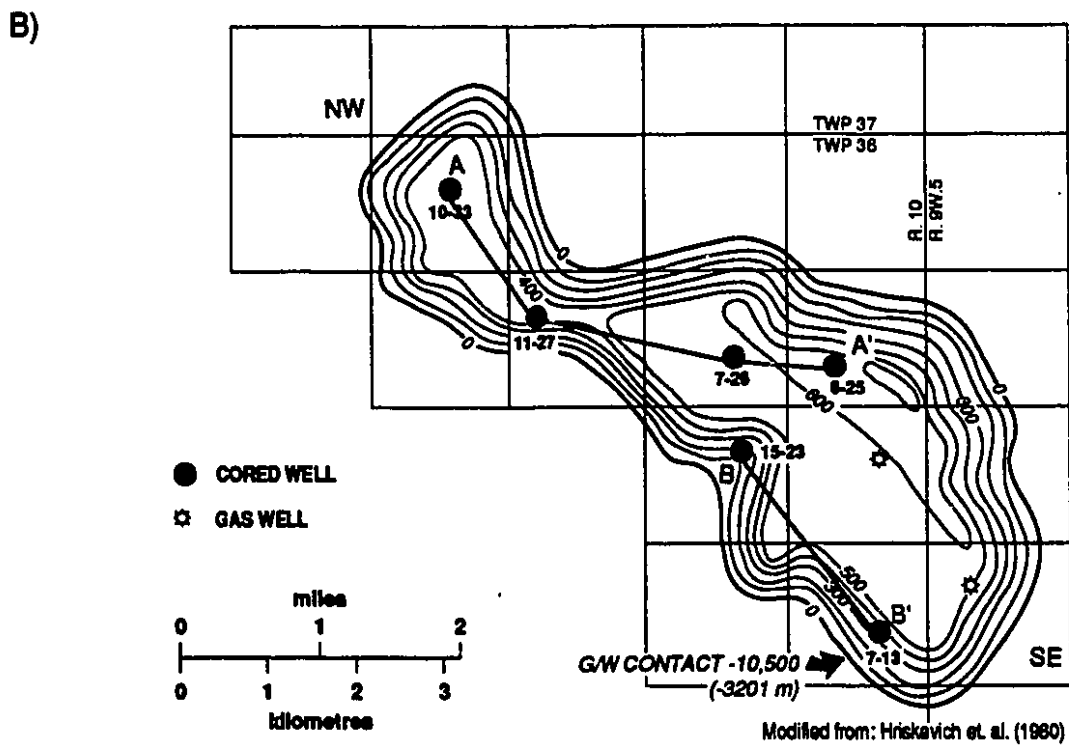
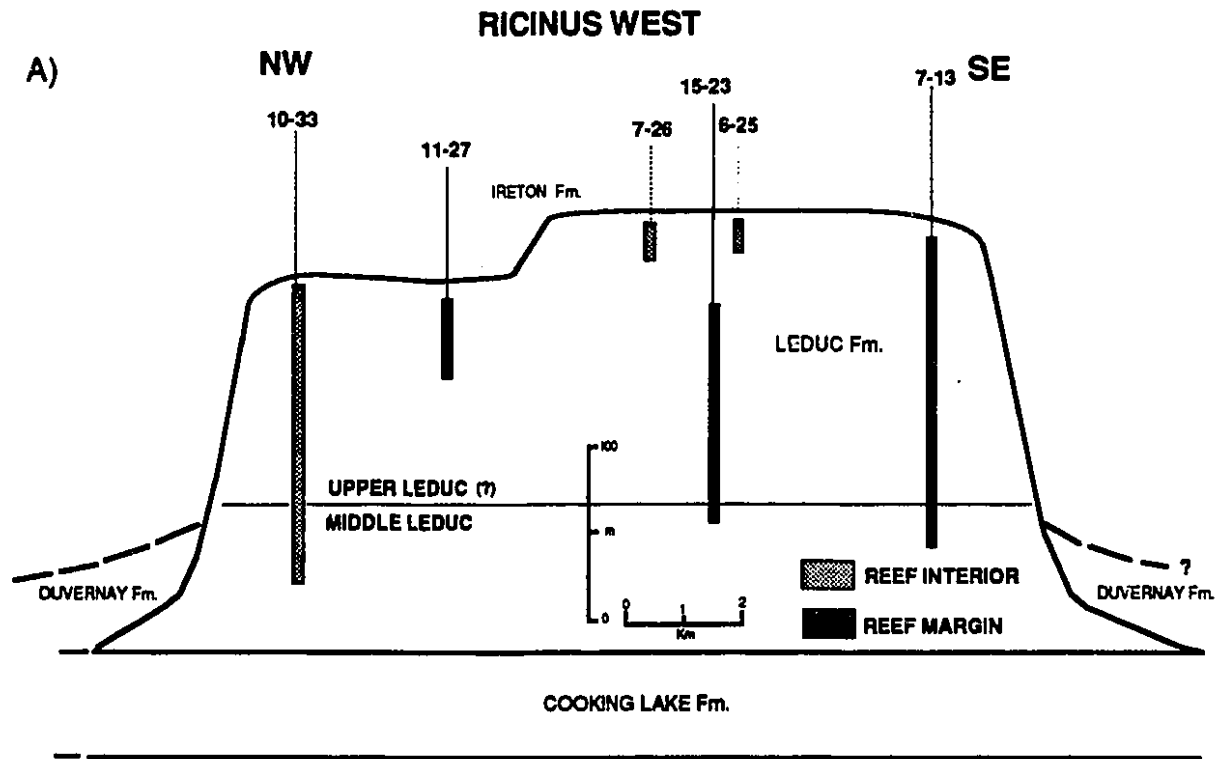
In the reef margin the tabular stromatoporoid boundstones, domal stromatoporoid floatstones, skeletal wackestones, and coral rudstones resemble depositional facies described in the adjacent partly dolomitized Strachan buildup. The facies and their distribution across the Ricinus West reservoir are described below and illustrated in a west-east cross section (Fig. 2.4 A,B; Appendix B).

Reef interior

The **stromatoporoid floatstone or rudstone** facies are generally thick (about 30 m) and are composed of domal (spherical) or bulbous-shaped molds and vugs that resemble stromatoporoids in a dense and/or porous matrix. Stromatoporoid floatstone or rudstone facies are most abundant in the lower 61 m of the reef interior and occur locally in the buildup margin (well 7-13). Most spherical-shaped molds are lined by thin (< 2 mm) coatings of reservoir bitumen and subsequently filled partly by late calcite cement cement (Plate 2.2G).

Figure 2.3: A) NW-SE cross section across the Ricinus West buildup showing stratigraphy, and location of cores (black bars).

 B) Map showing well locations (black dots). and net pay thickness (modified from Hriskevich et. al., 1980).



The **skeletal packstone or grainstone** facies consists of randomly oriented tubular molds (Amphipora-like) in a dense and/or porous matrix. Tubular molds range in size from 1 to 4 cm. Other pore types include tabular fenestral-like and locally spherical-shaped molds which presumably reflect the dissolution of stromatoporoids. The thickness of the skeletal packstone-grainstone facies varies from 3 to 15 m. High amplitude stylolites are present with stylocumulates of green shale up to 5 mm thick. Bitumen < 1 mm thick lines Amphipora-like molds.

The **skeletal wackestone** facies is characterized by thick, 3 to 18 m (maximum of 26 m, well 15-23; Appendix B) intervals of intercrystalline pores with minor, small (1 to 5 mm) vugs (Plate 2.2B,D). Partial to completely leached domal-shaped stromatoporoids are locally present. Despite dolomitization, some cores reveal that grains are mostly skeletal fragments (e.g. well 10-33, 4579.8 m). This facies is widely distributed within the Ricinus West buildup. It can be correlated across the entire buildup interior with a few beds extending to the buildup margin (Fig. 2.4B).

The **microbial laminite** facies is composed of thick beds of finely laminated dolomudstones with irregular, discontinuous, generally tabular vugs (fenestrae-like) parallel to the laminations. Other pore types present in this facies include small (1 cm) irregular vugs and intercrystalline pores. The thickness of microbial laminite facies varies from 5 to 10 m. High amplitude stylolites are abundant (e.g. well 7-26) with stylocumulates of green shale up to 3 mm thick (Plate 2.2I).

The **green shales** comprise intervals up to 30 cm thick that are interbedded with microbial laminite facies in the buildup interior (e.g. well 10-33, 4546 m). Green shales are also present as geopetal fillings in vugs and thin irregular layers along digital stylolites surfaces (e.g. well 7-26, 4395 m). These green shales are discontinuous and are more common in the upper part of the buildup.

Figure 2.4A: Distribution of depositional facies in the Ricinus West buildup interior wells 10-33, 11-27, 7-26 and 6-25. See Fig. 2.3 for well locations. Datum is top of the Calmar Formation. Calculated arithmetic average porosity in percent and geometric average permeabilities in millidarcies are given in the right columns for each depositional facies. Porosity and permeability data are based on core analyses from ERCB. The sequence indicated (arrow) in pore system I is outlined in more detail in Fig. 3.2 (see Chapter 3)

Figure 2.4B: Distribution of depositional facies and pore types in the Ricinus West buildup margin (wells 15-23 and 7-13). See Fig. 2.3 for well locations. Datum is top of the Calmar Formation. Calculated arithmetic average porosity in percent and geometric average permeabilities in millidarcies are given in the right columns for each depositional facies. Porosity and permeability data are based on core analyses from ERCB. Pore systems II and III are illustrated in Figs. 3.3 and 3.4 (see Chapter 3). See Table 3.3 for pore type symbols.

Reef margin

Tabular-stromatoporoid boundstones are present in one well (7-13; Appendix B) and consist of large irregular vugs in a tight or porous matrix. Non-mimetic replacement of radiaxial fibrous calcite cements is common only in this facies. These radiaxial fibrous calcite cements are interpreted to be marine in origin on the basis of their fibrous textures similar to those observed in the Strachan buildup. This facies is present in 5 to 25 m thick intervals, with some up to 34 m and is interbedded with skeletal grainstones. Brecciated intervals are common in this facies and are comprised of angular dolomite fragments in a highly porous dolomite matrix (Plate 2.3A, C).

The **coral rudstone** facies consists of randomly oriented tubular-shaped molds of corals (*Thamnopora*- like) and minor spherical-shaped molds of stromatoporoids. Irregular vugs about 4 cm in diameter, resulting from the dissolution of stromatoporoids, are common. The thickness of the coral rudstone facies ranges from 4 to 19 m (Plate 2.3D).

Depositional Environments

Depositional environments for the Upper Devonian Leduc Formation in the Strachan and Ricinus West fields are interpreted on the basis of vertical and lateral correlations of depositional facies and by comparison with limestones of the Golden Spike buildup. Depositional environments are used to subdivide the reservoirs into depositional units. Each depositional facies is characterized by different pore types.

The depositional history of the Strachan, Ricinus West, Crimson, and Chedderville buildups is similar in many aspects to other Leduc buildups (e.g. Golden Spike), however, information about these buildups is available only from the top of the middle and the upper Leduc.

At the top of the middle Leduc, depositional facies consist of domal stromatoporoid floatstones and/or rudstones (e.g. Ricinus West; well 10-33; Fig. 2.4A,B), coral

Plate 2.2: DEPOSITIONAL FACIES AND ASSOCIATED PORE TYPE IN THE RICINUS WEST BUILDUP INTERIOR

- A) Skeletal packstone facies: moldic pores after leaching of Amphipora debris with a packstone framework in a tight matrix. 10-33-36-10W5, 4601.5 m.
- B) Skeletal wackestone facies: isolated tubular, moldic pores (arrows) after leaching of Amphipora debris in a tight mudstone matrix. 10-33-36-10W5, 4603.4 m.
- C) Skeletal wackestone facies: Intercrystalline pores partly filled with reservoir bitumen (black staining) and isolated moldic pores (arrows) and vugs. 10-33-36-10W5, 4576 m.
- D) Skeletal wackestone facies: patches (P) of polyhedral intercrystalline pores partly filled with bitumen in an otherwise tight matrix. Stromatoporoid fragment with solution enlarged, tabular intraskeletal pores (S). Note subvertical fracture (F) partly filled with late calcite cement. 10-33-36-10W5, 4579.2 m.
- E) Microbial laminite facies: finely laminated mudstones with elongated, irregular, fenestral-like pores. 10-33-36-10W5, 4608.5 m.
- F) Stylolitic contact between microbial laminite facies and mudstones with geopetal-like pores filled with green shales. 10-33-36-10W5, 4596.2 m.
- G) Domal stromatoporoid floatstone facies: partly leached domal stromatoporoid (DS) with intraskeletal pores partly filled by reservoir bitumen (black). Late calcites (Ca) completely fill the remaining pore space. 10-33-36-10W5, 4627.4 m.
- H) Domal stromatoporoid rudstones: partly leached stromatoporoid (S) and coral (arrow) fragments in a dolomudstone matrix. 10-33-36-10W5, 4652 m.
- I) Green shaly laminations (arrow) and associated stylolites. Note tight dolomudstone with vug completely filled with anhydrite (lower portion). 10-33-36-10W5, 4632.6 m.

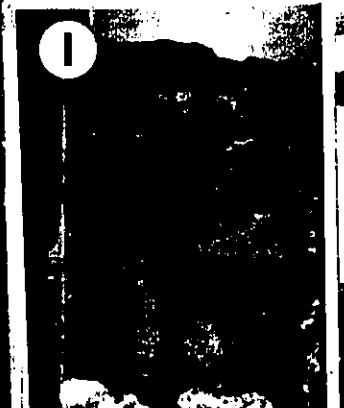
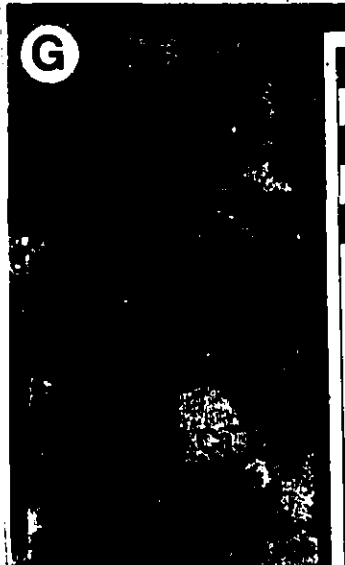
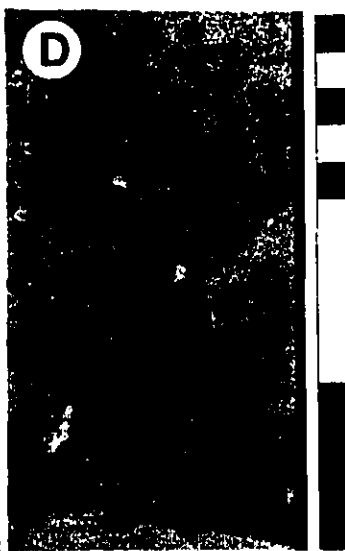
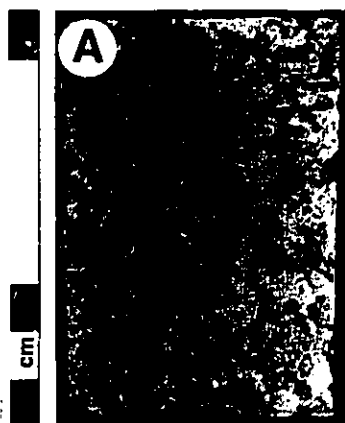
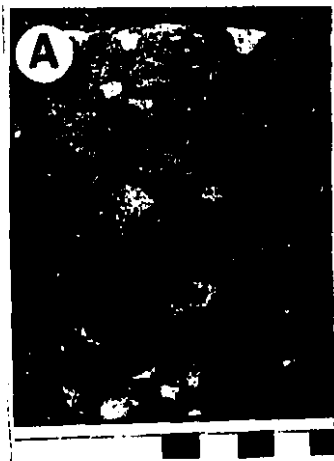


**Plate 2.3: DEPOSITIONAL FACIES IN THE RICINUS WEST BUILDUP
MARGIN**

- A) Tabular stromatoporoid boundstone facies: Tabular stromatoporoids with solution enlarged intraskeletal pores (arrows) lined with reservoir bitumen. Note vugs filled with calcitized anhydrite. 7-13-36-10W5, 4421.3 m.
- B) Several generations of radiaxial fibrous calcite cements (RF) completely dolomitized in tabular stromatoporoid boundstone. 7-13-36-10W5, 4438 m.
- C) Growth cavity filled by several generations of radiaxial fibrous calcite cements (RF) in tabular stromatoporoid boundstones. Note mosaic breccia (B) with intercrystalline pores lined with reservoir bitumen in the matrix portion. 7-13-36-10W5, 4432 m.
- D) Coral rudstone facies: tubular molds after leaching of probable Thamnopora coral fragments (C) in a tight packstone matrix. 7-13-36-10W5, 4514 m.
- E) Mosaic breccia: Angular clasts in a porous matrix with intercrystalline pores lined with reservoir bitumen. 7-13-36-10W5, 4393.5 m.



rudstones, and skeletal grainstones that suggest deposition in a shallow, probably lagoonal reef interior.

The upper Leduc consists of reef margin and reef interior environments. The reef margin environment includes the vertical and lateral association of coral rudstones, tabular stromatoporoid boundstones, and stromatoporoid-coral rudstones facies that indicate deposition in shallow, high energy environments. The reef interior environment is characterized by the vertical and lateral association of skeletal packstones/grainstones, skeletal wackestones, microbial laminites, and locally green shales that suggest shallowing upward, peritidal conditions.

In the interior of the Ricinus West buildup, vertical and lateral correlation of depositional facies allows recognition of two depositional units, upper and lower. The upper unit is 131 m thick and consists of six shallowing upward successions generally 8 m thick but up to 27 m thick (Fig. 2.4A). The shallowing-upward successions are represented by the vertical association of subtidal, meter-scale Amphipora-rich grainstones or packstones with or without small domal stromatoporoids. They are conformably overlain by skeletal wackestones, and by more peritidal microbial laminites (Plate 2.2). Locally one of the three facies is missing or poorly developed. These successions are two to three times as thick as those reported from the Cairn Formation in outcrop equivalents (McLean and Mountjoy, 1993b). This may be a result of 1) obliteration or amalgamation of some facies by dolomitization, or 2) continuous deposition of different facies without obvious breaks. Drivet (1993) observed similar sequences (parasequences) in both the interior and margins of the dolomitized Homeglen-Rimbey reservoir. The lower 61 m of the Ricinus West buildup interior are characterized predominantly by the association of domal, stromatoproidal floatstones, skeletal wackestones, and coral rudstones facies.

In the reef margin, depositional facies like those reported in the dolomitized Homeglen-Rimbey buildup (Drivet, 1993) and in Redwater and Golden Spike limestone

buildups (Stoakes, 1992), were not observed. This may be due to 1) obliteration of some facies by dolomitization, or 2) non-cyclic deposition, since accumulation on the reef margin may have kept pace with a rising sea level and consequently deposited fewer distinct cycles than the reef interior (Wendte, 1992).

Available data do not allow the recognition of the stacking pattern of the sequences. They are probably backstepping in style similar to cycles in the limestones buildups (Wendte, 1992; Stoakes, 1992) and the dolomitized Homeglen-Rimbey buildup (Drivet, 1993) and in outcrop (Mountjoy, 1965; 1989).

DIAGENESIS

The Strachan, Ricinus West and adjacent buildups have undergone a complex history of diagenetic alteration. Petrographic observations of the diagenetic features in limestones, partly dolomitized rocks and dolostones and their paragenetic relationships are presented below. Geochemical information of the diagenetic features is integrated with their petrographic characteristics and the distribution of dolomites and late diagenetic features are also discussed.

Petrography

Micrite envelopes form thin micrite rims (50 μm) around most coral, stromatoporoid, and brachiopod fragments (Plate 2.4A). Many grains are also completely micritized.

Calcite cementation is represented by: 1) **radial fibrous cements**, and 2) **syntaxial overgrowths**. **Radial fibrous cements** (Bathurst, 1975) are common particularly along the reef margin. They are characterized by prismatic crystals (600 x 200 μm) with curved twin lamellae, irregular boundaries, converging optic axis, and contain diverging subcrystals (Plate 2.4C). Marine internal sedimentation occurred concurrently with precipitation of radial fibrous calcite cements (Plate 2.4 D) indicating a marine

Plate 2.4: EARLY DIAGENETIC PRODUCTS

- A) Photomicrograph showing micrite envelopes (E) surrounding a coral fragment. Primary cavity lined by isopachous rim of radiaxial fibrous calcite cement (RF) and subsequently filled by internal sediments (IS) and blocky calcite cement (BCa). Note dolomite rhombs (D) partly replacing the internal sediments. Plane light. 14-2-38-10W5, 4116.4 m. Scale bar 100 μ m

- B) Photomicrograph illustrating syntaxial cementation (Sy) around crinoids fragments. 5-11-38-10W5, 4226 m. Scale bar 100 μ m . Plane light.

- C) Photomicrograph in polarized light of radiaxial fibrous calcite cements (RF). The crystals characteristically have curved twins, convergent optic axis and contain diverging subcrystals. Note internal sediments replaced by dolomite. Cavity is subsequently filled with blocky calcite (Bca) cement. Plane light. 10-31-37-9W5, 4177.1 m. Scale bar 200 μ m

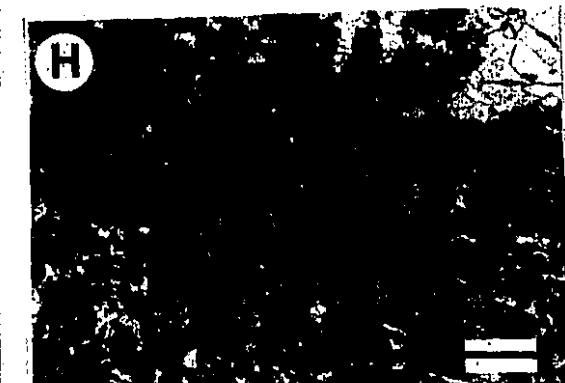
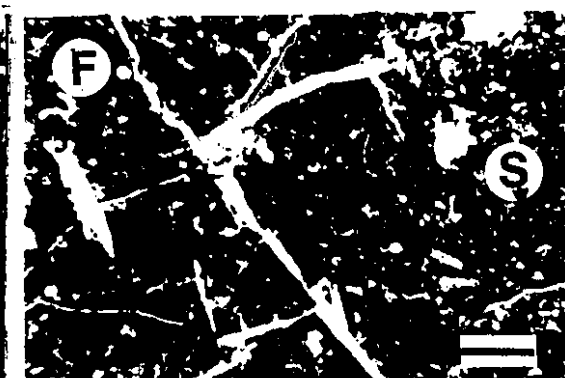
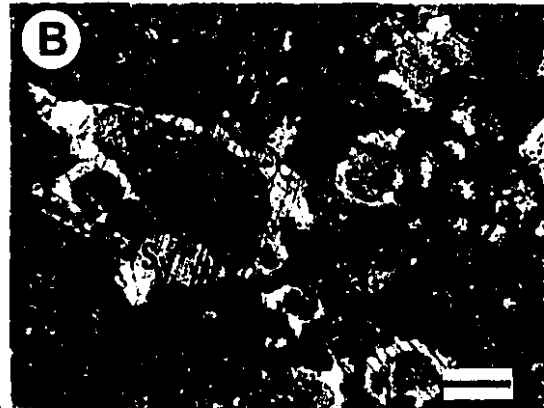
- D) Detail of box in photomicrograph C showing dolomite crystal (D) within radiaxial fibrous calcite crystals. 10-31-37-9W5, 4177.1 m. Plane light. Scale bar 100 μ m

- E) Photomicrograph showing radiaxial fibrous calcite cement (RF) partly replaced by fibrous quartz (Si). 5-11-38-10W5, 4126 m. Scale bar 100 μ m

- F) Fractures filled with late calcite cement. Note stylolite surface (S) crosscut by fractures. 5-11-38-10W5, 4239 m. Scale bar 250 μ m. Plane light.

- G) Stylolites as result of chemical compaction. Note dolomite rhombs with corroded boundaries in contact with stylolite surfaces (arrow). Dolomite in the lime mud matrix are not corroded. 5-11-38-10W5, 4126 m. Scale bar 250 μ m Plane light.

- H) Stylolite surface filled with reservoir bitumen. Note that dolomite rhombs seem to grow out of or along the stylolite surface (arrow). Some hairline microfractures extend away from the stylolite. Plane light. 14-2-38-10W5, 4125 m. Scale bar 250 μ m



environment of deposition for these cements. Some small (10 μm) crystals of dolomite are associated with dissolution surfaces (Plate 2.4 D) suggesting that most radiaxial fibrous cements were originally composed of magnesian calcites. These cements fill shelter, growth framework and irregular cavities (Plate 2.1C) and were deposited in several generations as indicated by white and pale brown bands. Radiaxial fibrous calcite cements also occur as isopachous crusts on coarse skeletal fragments and line cavities associated with clusters of Renalcis.

Syntaxial overgrowth cements are common in skeletal grainstones and packstones containing echinoderm fragments. They occur as large calcite crystals in optical continuity with the host echinoderm fragment (Plate 2.4B). The cement occupies primary pore space indicating precipitation of cements prior to any mechanical compaction.

Minor fibrous quartz replaces some thin-shelled brachiopod and crinoid fragments. Quartz fibres radiate from a single point and resemble lutecite quartz (Hesse, 1990). Fibrous quartz also occurs as spherulitic replacements (chalcedony) of radiaxial fibrous calcite cements (Plate 2.4E). The timing of this quartz replacement is uncertain.

Blocky calcite occurs as equant, anhedral to subhedral crystals (about 100 μm) filling intra- and interskeletal pores. Most voids affected by this type of cement were completely occluded. Two types of blocky calcite were observed under cathodoluminescence. The first contains non-luminescent and bright yellow luminescent zoning (BC_1) and the later is non-luminescent (BC_2 , Plate 2.5A). Similar blocky calcite cements have been reported in the Golden Spike and Nevis buildups (Walls, 1977; Walls and Burrowes, 1985; Carpenter and Lohmann, 1989). In these buildups, zoned blocky calcite cement (BC_1) has been interpreted as having precipitated from early meteoric waters that entered the buildups based on their association with vadose zone features and the presence of bright yellow luminescent zones, since surface meteoric waters are more Mn

rich than subsurface waters (Walls, 1977; Walls and Burrowes, 1985). However, Mn can be precipitated in marine cements as a result of redox dynamics. Non-luminescent blocky calcite cement (BC_2) has been interpreted as a shallow burial cement based on its occurrence along stylolites and early fractures. Although BC_1 and BC_2 postdate near seafloor radiaxial fibrous cements, the lack of vadose diagenetic features and absence of BC_2 cements along stylolites preclude an accurate determination of their timing and environments of precipitation.

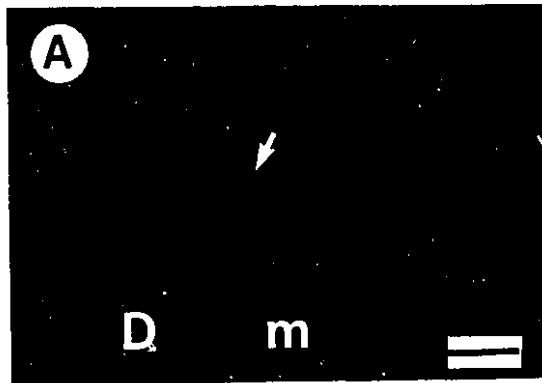
Stylolites show average amplitudes ranging from 1 to 5 mm. These stylolites have relatively sharp boundaries in limestone intervals (Plate 2.8A), but are somewhat more diffuse in the dolomitized parts of the buildups (Plate 2.8B). This indicates that dolostones are more resistant to pressure solution. In the Ricinus West buildup stylolites are closely associated with green shale laminations. Stylolites may have started to develop in limestones at burial depths between 500 and 700 m (Dunnington, 1967). A recent study of a continuous limestone core from the Ontong Java Plateau by Lind (1993) indicates that stylolites first appear at 470m and become common below 830 m. Thus stylolites can be used to indicate the onset of intermediate chemical diagenesis and in this study are inferred to have begun at burial depths of about 500 m.

Subvertical, extensional fractures truncate radiaxial fibrous calcite cements (Plate 2.1C), dolomite rhombs, and low amplitude stylolites (Plate 2.4F). They have irregular surfaces that suggest dissolution and are partly filled with dolomite cement (C_2 , Plate 2.7E), reservoir bitumen and late calcite cements (Plate 2.4F).

Dolostones of the Strachan, Ricinus West and adjacent buildups are characterized by four texturally different replacement dolomites (R_1 to R_4) and two dolomite cements (C_1 and C_2 ; following Amthor et. al. (1993) and Drivet (1993)). Planar-euhedral, isolated dolomite rhombs are abundant in the fine-grained, lime matrix of skeletal packstones

Plate 2.5: CATHODOLUMINESCENCE AND FLUORESCENCE
CHARACTERISTICS OF CALCITE CEMENTS, REPLACEMENT
DOLOMITES AND DOLOMITE CEMENTS

- A) Partly dolomitized packstone matrix (m) in tabular stromatoporoid facies. Note dull, red luminescent dolomite rhombs and patches (D) and yellow bright-dark zoning in blocky calcite cement (arrow). 15-2-38-10W5, 4143.9 m. Scale bar 330 μm .
- B) Dull red luminescence of replacement dolomite R_3 . Note thin, bright luminescent rims of dolomite cement C_1 (arrows). Vug partly filled with late calcite cement (Ca). 10-31-37-9W5, 4300 m. Scale bar 330 μm .
- C), D) Paired plane-polarized and fluorescence views of replacement dolomite R_2 . Intercrystalline pores are partly filled with droplets of reservoir bitumen (arrows). Note dark green cores, greenish-yellow zone (gy) and dark green outer rims. Microbial laminite facies. 10-33-36-10W5, 4522.8 m. Scale bar 75 μm .
- E), F) Paired plane-polarized and fluorescence views of replacement dolomite R_2 with clear rim of dolomite cement C_1 . Note the absence of fluorescence. 6-24-34-8W5, 4384.9 m. Scale bar 75 μm .



and wackestones (Plate 2.6A) creating an idiotopic-P texture (porphyrotopic; Gregg and Sibley, 1984). In skeletal grainstones matrices, dolomite rhombs are present only in micritized skeletal components. Individual dolomite rhombs are 60 to 225 μm across, but most are around 110 μm in size. Crystals are clear and limpid with straight extinction. They do not show cloudy cores. Under SEM, most rhombs show straight boundaries and sharp contacts with the fine-grained lime matrix. Dolomite rhombs and patches are closely associated with stylolites. In some places near stylolites, the dolomite rhombs have corroded boundaries indicating dissolution during stylolitization (Plate 2.4G). In other places the dolomite rhombs seem to grow out of or along the stylolite surfaces (Plate 2.4H) becoming abundant to the point of forming patches of planar-subhedral dolomite (similar to replacement dolomites R_1 and R_2).

In one sample (well: 10-31, 4300 m) next to a fracture partly filled with coarse crystalline dolomite cement (C_2), the dolomite rhombs are very coarse (350 μm) and non-planar, and exhibit sweeping extinction similar to dolomite cement (C_2). This suggests that there has been additional crystal growth and minor replacement of the lime matrix during later stages of dolomite cementation (C_2) (Plate 2.6B).

Replacement dolomite textures

R_1 : Fine-crystalline, planar euhedral to subhedral

Dense and porous mosaics of fine-crystalline (30 - 62 μm), planar euhedral to subhedral crystals are characteristic of this type (Plate 2.6C-E). Luminescence is homogeneously dull red and does not fluoresce. Nonmimetic replacement of skeletal components in which the coral and stromatoporoid or crinoid rudstone/packstone texture can be recognized (wells 15-23, 11-27 and 7-32) is common. In partially dolomitized rocks (e.g. well 14-2, 4145 m) the matrix of skeletal packstones and rudstones has been dolomitized by this fine crystalline dolomite. This dolomite is the second most abundant

type.

R₂ : Medium-crystalline, planar euhedral to subhedral

This dolomite is the most common and volumetrically most important textural type, comprising up to 90% in some wells (e.g. 10-31 and 10-24). It is type 1 of Amthor et. al. (1993). It comprises dense and porous mosaics of medium-crystalline (62 to 250 μm), planar euhedral to subhedral crystals (Plate 2.6F-H). This dolomite is characterized by a dull red luminescence. Some zoning is evident under fluorescence (Plate 2.5C,D); dark green cores followed by greenish-yellow thin (10 μm) rim and a dark green outer rim (e.g. well 10-33; 4523 m). Ghosts of primary textures are rarely observed. In porous mosaics there is commonly an increase in crystal size to the boundaries of vugs and moldic pores. In partially dolomitized rocks (e.g. well 12-31, 4296 m) isolated rhombs and dolomite patches have similar characteristics to R₂ dolomites.

R₃: Coarse-crystalline, planar euhedral to subhedral

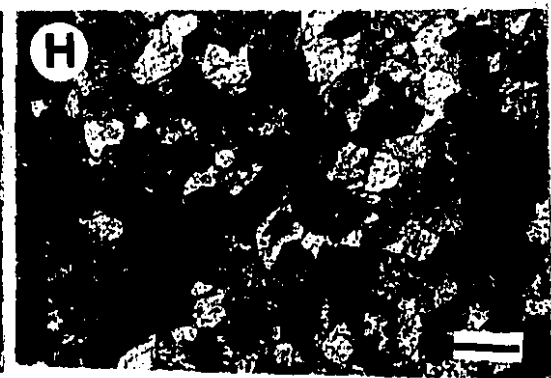
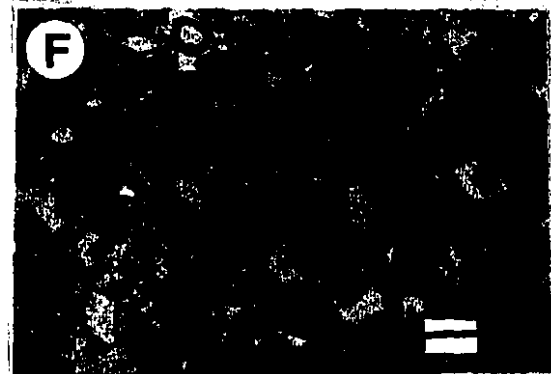
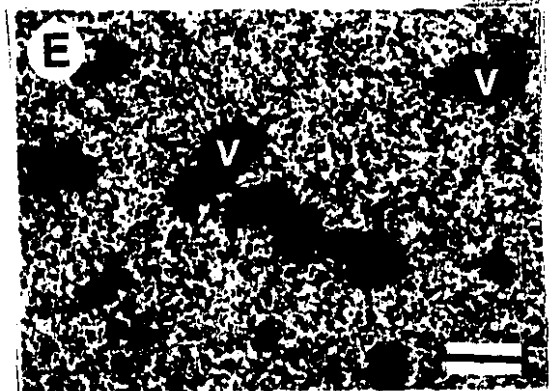
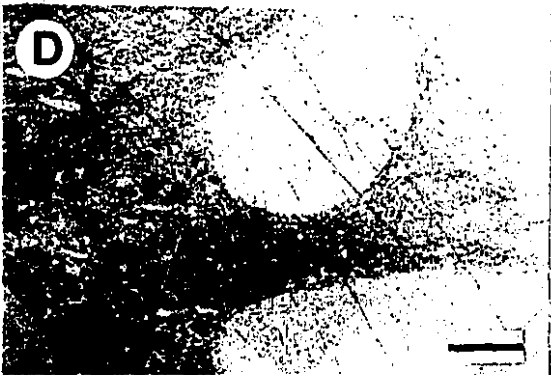
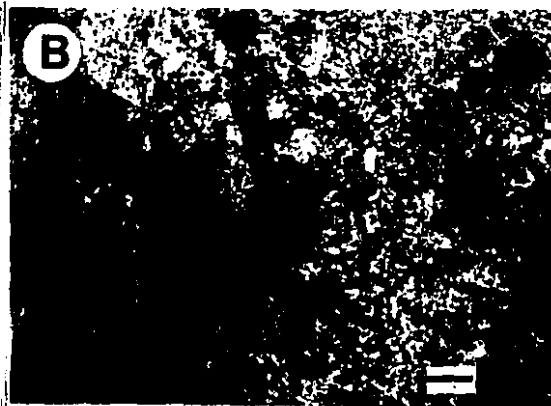
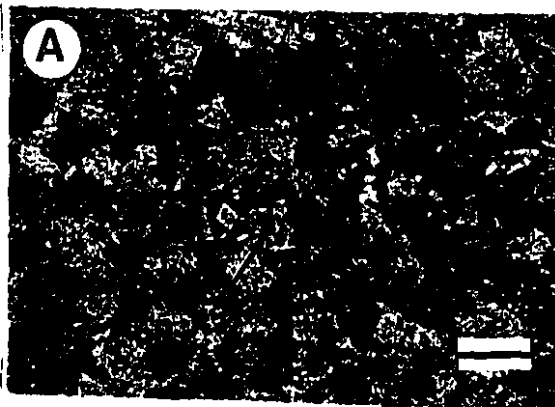
Dense, unimodal mosaics of subhedral crystals (250 to 600 μm) and porous mosaics of planar euhedral to subhedral crystals are characteristic of this type (Plate 2.7A). The luminescence is a homogeneously dull red with outer rims exhibiting a brighter red luminescence. It is not fluorescent. This type is less common, but locally abundant (e.g. well 11-27). This dolomite is type 2 of Amthor et.al. (1993).

R₄: Medium-crystalline non-planar anhedral dolomite

Medium crystalline (300 μm) crystals with irregular and serrated crystal boundaries, sweeping extinction and red CL colour make up this type (Plate 2.7B). This texture always lines pores filled with internal sediments in wells of the buildup margin (eg. Well 11-27, 4490 m). It represents a replacement of radiaxial calcite cements. This dolomite is minor accounting for less than 1% overall. Similar replacement of radiaxial calcite cements have been reported by Laflamme (1990; Well: 8-19-34-7W5), Amthor et.

Plate 2.6: PHOTOMICROGRAPHS OF REPLACEMENT DOLOMITE TEXTURES

- A) Partly dolomitized limestone matrix with euhedral rhombs (arrow) and patches of dolomite (D) creating an idiotopic-P texture. 12-31-37-9W5, 4295.7 m. Scale bar 250 μm
- B) Very coarse, non-planar dolomite rhombs (D) replacing lime matrix in skeletal packstones. 10-31-37-9W5, 4300.9 m. Scale bar 50 μm
- C) Dense, fine crystalline (30-62 μm), planar euhedral to subhedral replacement dolomite R_1 . Non-mimetic replacement of skeletal debris shows a packstone texture. 15-23-36-10W5, 4545.4 m. Scale bar 250 μm
- D) Dolomite R_1 in C under diffuse light showing fine grained skeletal matrix. 15-23-36-10W5, 4545.4 m. Scale bar 250 μm
- E) Dense matrix of replacement dolomite R_1 with solution enlarged pores (V) probably after coral fragments. 15-23-36-10W5, 4592.9 m. Scale bar 250 μm
- F) Porous, medium crystalline (62 to 250 μm) planar euhedral replacement dolomite R_2 . Inter-crystalline pores are lined by thin coats of reservoir bitumen (black). 10-31-37-9W5, 4287.8 m. Scale bar 50 μm
- G) Dense matrix of replacement dolomite R_2 with irregular vugs (V). Stylolites (arrows) provide a connection between vugs since they are filled with reservoir bitumen (black). Late calcite cement (Ca) partly filling a vug. 10-33-36-10W5, 4601.5 m. Scale bar 200 μm
- H) Dense mosaic of subhedral, medium crystalline, planar replacement dolomite R_2 . 10-24-37-9W5, 4032.3 m. Scale bar 100 μm



al. (1993; type 4 dolomite) and Drivet (1993).

Dolomite Cements

C₁: Medium crystalline, planar dolomite cement.

This type occurs as medium (100 to 250 μm), euhedral to subhedral planar crystals, either clear (e.g. well 10-31, 4288 m), or with cloudy cores and clear rims (e.g. well 10-31, 4318.2 m) that commonly line intercrystalline vugs and fracture pores (Plate 2.7C,D). All crystals exhibit sharp extinction and contain fluid inclusions. Under cathodoluminescence the clear rims have a slightly bright red to dull red zoning that does not fluoresce (Plate 2.5B,E,F). It accounts for less than 1% of the dolomites.

C₂: Coarse to very coarse-crystalline, non-planar dolomite cement.

Clear crystals, coarse to very coarse (100 μm to 5 mm) that line vugs and fractures and completely fill moldic pores (e.g. well 10-31, 4308 m) comprise this type (Plate 2.7E-F). This dolomite cement has curved crystal faces and sweeping extinction that is characteristic of saddle dolomites (Radke and Mathis, 1980). This is dolomite type 5 of Amthor et. al. (1993). Under cathodoluminescence they are homogeneously dark red to purplish. This dolomite does not fluoresce and accounts for a maximum of only about 1% of all dolomites (e.g. well 6-24). Some crystals show corroded boundaries suggesting that dissolution occurred before the emplacement of reservoir bitumen.

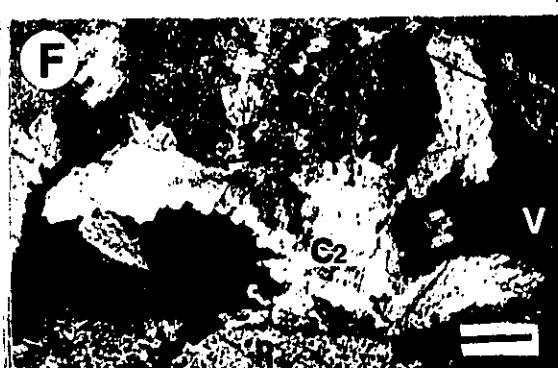
Anhydrite fills pores and is a minor replacement of carbonates (Plate 2.8D). In all dolomitized buildups, milky white anhydrite cement is volumetrically important occluding vugs, molds, textures resembling geopetal fabrics, and fracture related porosity. Anhydrites are minor in dolomitized pool D3A of the Strachan buildup, and rare in partly dolomitized pool D3B. Anhydrites occur commonly as coarsely crystalline (250 μm), fibrous crystals that overlie dolomite cement (C₁) and are coated by reservoir bitumen (well 10-33, 4652.7 m). Some crystals occur as fine to coarse granular (200 μm) aggregates

**Plate 2.7: PHOTOMICROGRAPHS OF REPLACEMENT DOLOMITE
TEXTURES AND DOLOMITE CEMENTS**

- A) Porous, coarse crystalline (250 - 600 μm), planar euhedral replacement dolomite R_3 showing lighter rims around the crystals (arrows). Reservoir bitumen (black) lines and/or completely fills intercrystalline pores. 10-31-37-9W5, 4289 m. Scale bar 100 μm
- B) Replacement of radiaxial fibrous calcite by dolomite R_4 . The coarse fibrous crystals radiate out from a pore filled with internal sediments which in turn are replaced by dolomite R_1 . 11-27-36-10W5, 4490.8 m. Scale bar 250 μm

Dolomite Cements

- C) Clear rims (100 μm) of planar dolomite cement C_1 (arrow) partly filling a vug (V) in replacement dolomite R_2 . 10-31-37-9W5, 4318.2 m. Scale bar 200 μm
- D) Dolomite cement C_1 as a fracture filling (arrow) overlain by reservoir bitumen (black). In replacement dolomite (R_2). 11-27-36-10W5, 4500.6 m. Scale bar 100 μm
- E) Coarse crystalline, non-planar dolomite cement C_2 (arrow) filling a fracture in partly dolomitized coral (C) rudstones. Late calcite cement (Ca) completely fills the fracture. Pool D3B Strachan reservoir. 5-11-38-10W5, 4226 m. Scale bar 200 μm
- F) Very coarse crystalline dolomite cement C_2 partly filling a vug (V) in replacement dolomite R_1 . Ricinus West reservoir. 15-23-36-10W5, 4586.8 m. Scale bar 250 μm



(well 15-23, 4464.6 m). Locally, angular clasts of the dolostone host rock and pyrite float in the anhydrite. In wells from the Strachan buildup (e.g. well 10-31, 4258.5 m, D3A pool) anhydrite fills large vugs up to 8 cm long. Minor anhydrite replacement of dolomite type R₂ is observed in the proximity of moldic pores that are partly filled by coarsely crystalline, bladed anhydrite (well 11-22, 3956 m).

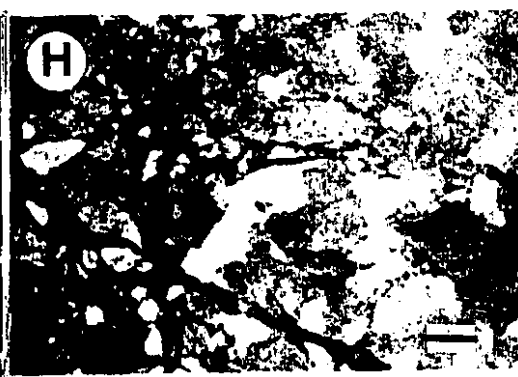
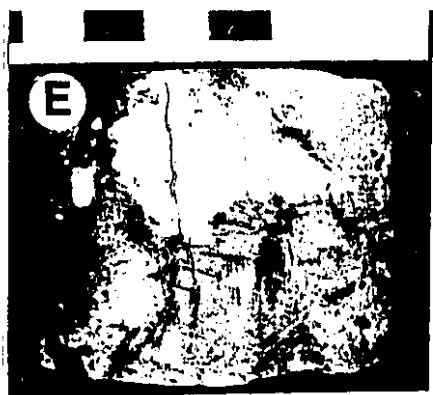
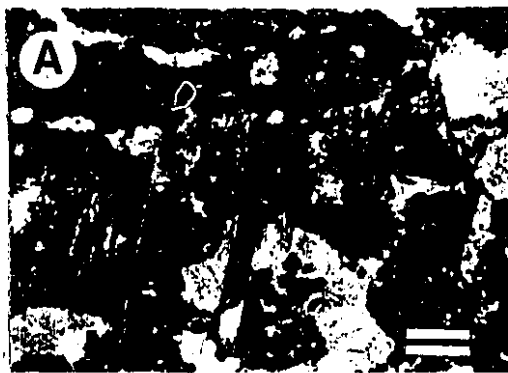
Sulphides, pyrite and sphalerite, are volumetrically minor and postdate anhydrite cements, although locally (well 10-20, 3541.1 m) minor pyrite cubes float in anhydrite cements (see Appendix C). Native sulphur partly to completely fills vugs and moldic pores.

Reservoir bitumen is a black precipitate that lines and fills pore spaces. Reservoir bitumen (Rogers et. al., 1974) is used as a descriptive term to avoid genetic implications and confusion with source rock bitumen and in situ kerogen. In pool D3B of the Strachan buildup it occurs as dull, black, continuous to discontinuous thin coatings on both primary (intraskelatal) and secondary pores (microfractures). In pool D3A and dolomitized Ricinus West and adjacent buildups reservoir bitumen is dull to bright black, sometimes vitreous, and occurs in three morphotypes: droplets, carpets, and peanut brittle (Lomando, 1992). Droplets are rounded individual particles scattered or clotted mostly on intercrystalline pore walls. Carpets are continuous coatings with a smooth surface lining vug walls. Peanut brittle ranges from continuous to discontinuous thin coatings with random rounded lumps in intercrystalline pores, vugs and microfractures. Optical textures in these bitumens (Appendix D) indicate that they are anisotropic, with minor amounts of isotropic bitumens. (Also see Chapter 4 for a discussion on the significance of those textures).

Hairline microfractures are most abundant in the Strachan buildup and minor in all other buildups of the study area (see Chapter 4). Microfractures are always filled with reservoir bitumen and crosscut most sedimentary and diagenetic phases. They occur in three different patterns depending on the pore type. In decreasing abundance these patterns

Plate 2.8: LATE DIAGENETIC FEATURES

- A) High amplitude stylolites in limestones crosscutting blocky calcite cements. Insoluble residue consists of clays and minor bitumen (black material). 12-31-37-9W5, 4284.1 m. Scale bar 200 μm
- B) Low amplitude stylolites crosscutting dolomite rhombs in partly dolomitized skeletal wackestones. 10-31-37-9W5, 4314.9 m. Scale bar 100 μm
- C) Vug occluded by late calcite cement after dolomite C_1 (arrows) in replacement dolomite R_2 . 10-31-37-9W5, 4318.2 m. Scale bar 50 μm
- D) Vug filled with anhydrite (An) . Note coarse crystalline dolomite rhomb replaced by anhydrite. Replacement dolomite R_2 . 10-24-37-9W5, 4040.5 m. Scale bar 250 μm
- E) Vug filled with milky white anhydrite and subsequently crosscut by hairline microfractures filled with reservoir bitumen. Scale in cm.
- F) Pyrite precipitation (arrows) after dissolution of replacement dolomite R_2 and subsequent precipitation of late calcite cement (Ca). 15-23-36-10W5, 4495.7 m. Scale bar 50 μm
- G) Vug in replacement dolomite R_1 partly filled with coarse crystalline dolomite cement C_2 (saddle dolomite) and prismatic quartz crystals (arrow). 15-23-36-10W5, 4592.9 m. Scale bar 100 μm
- H) Clast in a mosaic breccia texture by dissolution of replacement dolomite R_2 . 10-31-37-9W5, 4314.9 m. Scale bar 100 μm



are: 1) subhorizontal, extending from intraskeletal pores and perpendicular to subvertical fractures, 2) radial, extending from intraskeletal pores and irregular vugs, and 3) random, extending away from intraskeletal and intercrystalline pores. Their origins are discussed in detail in Chapter 4.

Minor **quartz** occurs as both replacement of dolomite R_1 (see replacement dolomites) and as clusters of euhedral, prismatic crystals partly filling vugs in the Ricinus West buildup (well 15-23, 4592.9 m). In well 11-28-37-8W5 (3700 m) from the Crimson field, euhedral, prismatic, up to 15 mm long crystals of quartz precipitated on dolomite cement (C_2) and partly fill a vug. The time of quartz emplacement can not be determined accurately, but based on the presence of hydrocarbon-bearing fluid inclusions in these large quartz crystals, quartz emplacement occurred late, during or after the migration of hydrocarbons, possibly at about the same time as the precipitation of late calcite cements.

Late calcite cements postdate all diagenetic features, are minor, occur as medium to very coarse (> 1 cm) equant crystals filling intraskeletal pores, fractures, and partially filling molds and vugs (Plate 2.8C,F). Calcite crystals have abundant fluid inclusions. Two phases of calcite cementation are indicated on the basis of carbon isotopes and fluid inclusion data (see discussion). Locally calcite replaces anhydrite (e.g. well 10-33, 4630 m).

Paragenetic sequence

Diagenesis in the Leduc Strachan, Ricinus West and adjacent buildups is complex and occurred in three general environments, nearsurface seafloor, shallow burial, and intermediate to deep burial (Figs. 2.5, 2.6). The onset of stylolitization (> 500 m according to Dunnington, 1967; Lind, 1993) designates the beginning of intermediate burial. Shallow burial is pre-incipient stylolitization and corresponds to depths of < 500 m. The maturation

of organic matter is used to designate deep burial.

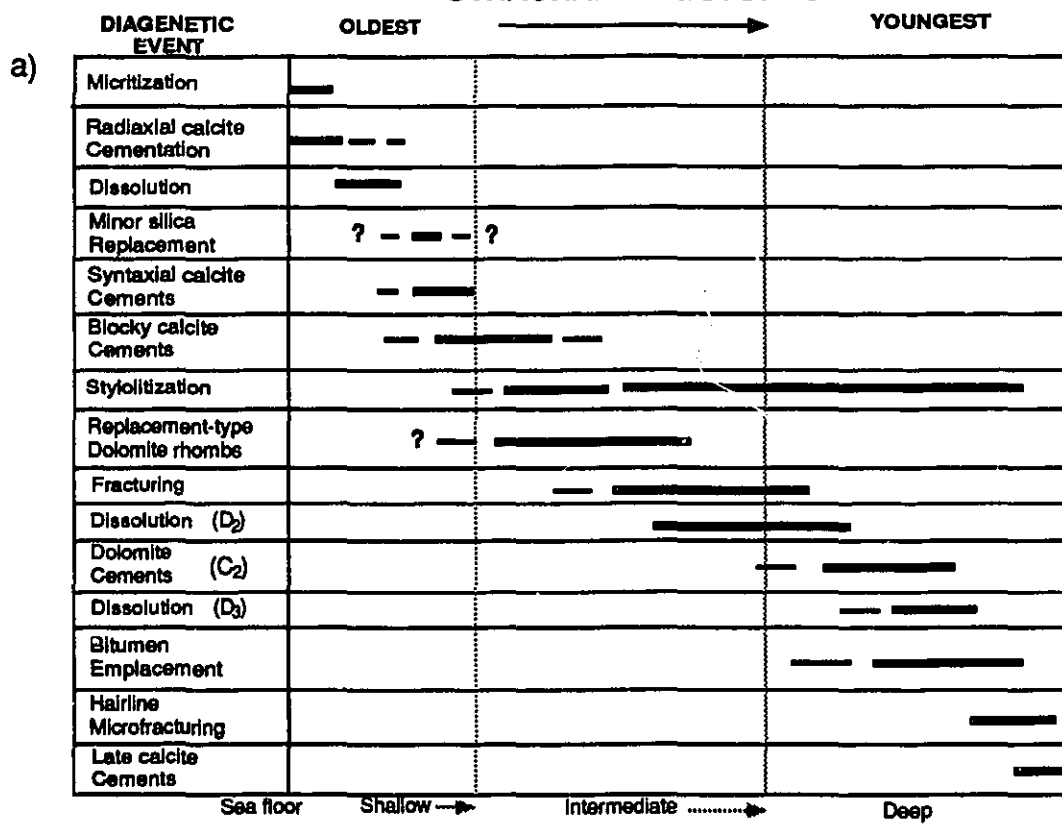
Radiaxial fibrous calcites are the earliest cement phase in the reef margin because: 1) they occur as the first cement in primary pores (intergranular, shelter and growth framework cavities), and 2) locally are interstratified with marine internal sediments. They are analogous to other occurrences observed in many Devonian buildups (e.g. Golden Spike, Walls et. al., 1979; Mountjoy and Walls, 1977) and modern reefs (e.g. James and Ginsburg, 1979). Syntaxial overgrowths are rarely seen in conjunction with other cements thus precluding an accurate determination of their time of precipitation, but based on studies of modern sediments probably represent an early cement that formed at or just below the seafloor (e.g. James and Choquette, 1990). This is also indicated by their occurrence in primary pores that lack mechanical compaction. Widespread blocky calcite cements in intra- and interskeletal pores postdate the radiaxial calcite cements. These cement types predate significant compaction since they are crosscut by stylolites.

Major diagenetic changes occurred during shallow to intermediate burial with the onset of chemical compaction (low-amplitude stylolite development) and precipitation of replacement dolomites. Replacement dolomite rhombs and patches postdate early diagenetic features such as micritization, radiaxial fibrous, syntaxial and blocky calcite cementation. This dolomitization is closely related to stylolites, however, its relative timing is difficult to establish. In some cases stylolite seams cut dolomite rhombs, suggesting that some dolomitization predated pressure solution. Commonly, isolated rhombs are abundant near stylolites forming patches. This occurs where the adjacent strata lack dolomite rhombs suggesting that stylolites may have served as a conduit for dolomitizing fluids.

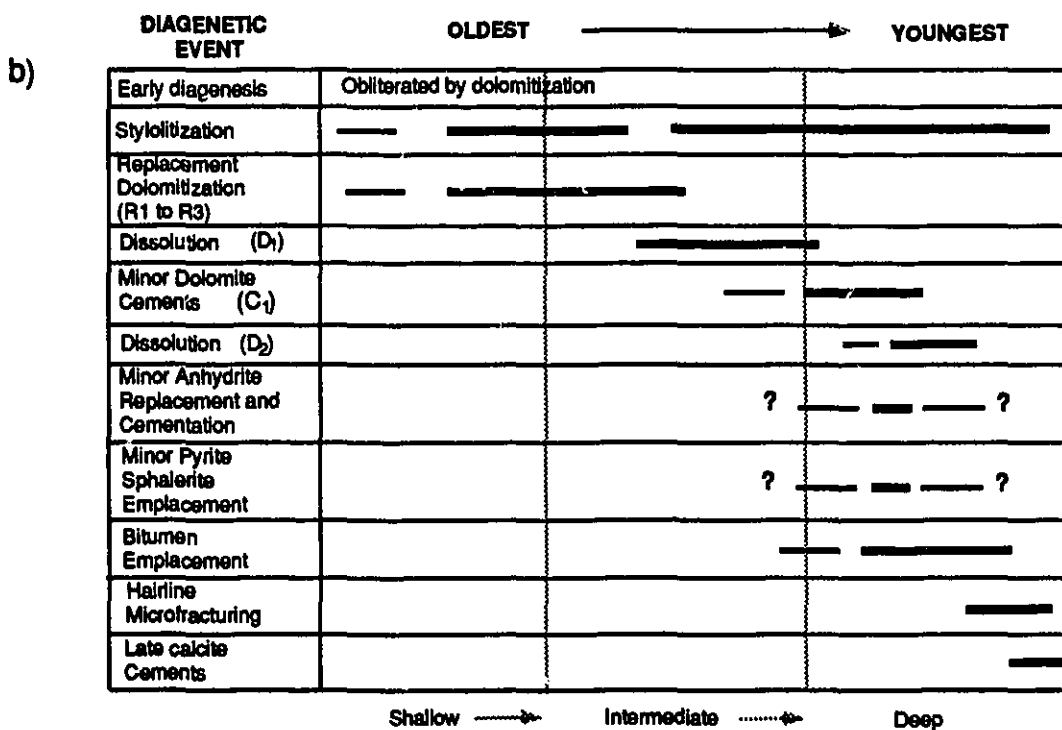
Some fractures truncate dolomite rhombs and low-amplitude stylolites. Dissolution occurred along both fractures and stylolite surfaces as indicated by the irregular enlargement of their boundaries. Dissolution of the lime matrix and skeletal components is rarely observed in limestones. Partly leached stromatoporoid fragments and moldic and

Figure 2.5: a) Paragenetic sequence of the limestone portion of the Strachan buildup.
b) Paragenetic sequence of the dolostones of the Strachan buildup.
The onset of stylolitization (> 500 m according to Dunnington, 1967; Lind, 1993, see text) designates the beginning of intermediate burial. Shallow burial is pre-incipient stylolitization and corresponds to depths of < 500 m. The maturation of organic matter is used to designate deep burial.

STRACHAN LIMESTONES



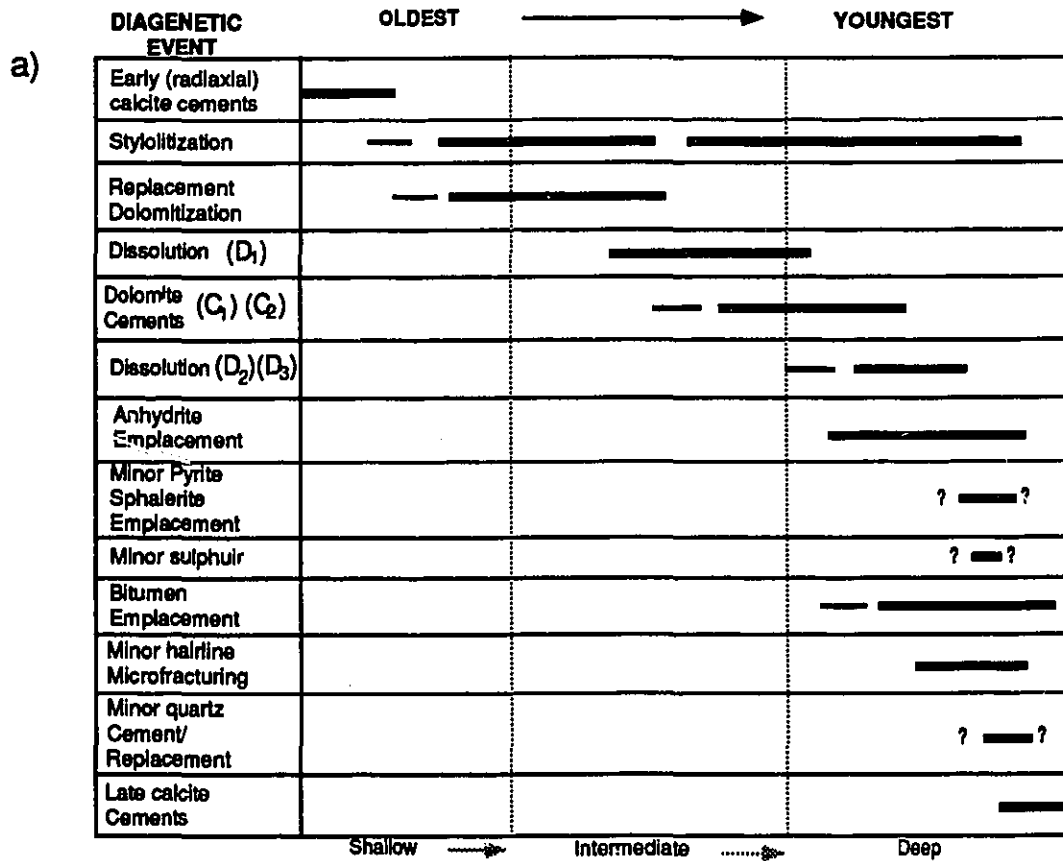
STRACHAN DOLOSTONES



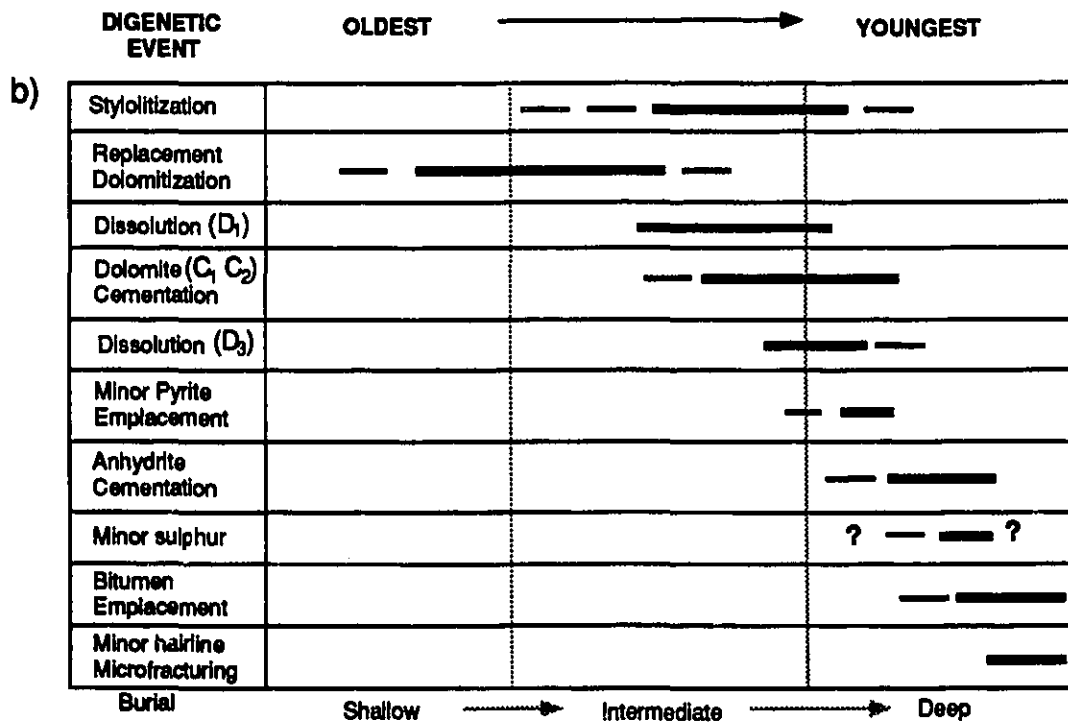
- Figure 2.6: a) Paragenetic sequence of Ricinus West dolostones.
b) Paragenetic sequence of Chedderville dolostones.

The onset of stylolitization (> 500 m according to Dunnington, 1967; Lind, 1993, see text) designates the beginning of intermediate burial. Shallow burial is pre-incipient stylolitization and corresponds to depths of < 500 m. The maturation of organic matter is used to designate deep burial. The sequence is similar to Strachan dolostones except for the addition of dolomite cement C_2 and minor quartz replacement and cementation.

RICINUS WEST DOLOSTONES



CHEDDERVILLE DOLOSTONES



vuggy porosity are evidence of calcite dissolution (D_1). Calcite dissolution (D_1) was contemporaneous with, or postdated, replacement dolomitization. This suggests a direct relationship between dolomitization and dissolution (Plate 2.9). Similar relationships have been reported by Amthor et al. (1993) in the central part and by Drivet and Mountjoy (1994a) for the southern part of the Rimbey Meadowbrook reef trend, Machel and Anderson (1989) for the Nisku Formation in the West Pembina reefs, and Kaufman et al. (1991) for the Swan Hills buildups.

Minor dolomite cement (C_1) postdates calcite dissolution (D_1) as this cement commonly lines secondary pores (vugs) in dolostones. Corroded boundaries of dolomite cement (C_1), rubble breccias (e.g. well 10-31, 4315 m), and enlargements of stylolite surfaces in dolostones are evidence for a second phase of dolomite dissolution (D_2). Leaching along the walls of fractures occurred before dolomite cement (C_2). Some dolomite (C_2) crystals have corroded boundaries, suggesting that a third phase of dissolution (D_3) took place.

Anhydrite cementation postdates dolomite cements C_1 and C_2 and precedes sulphide precipitation. Replacement of dolomite (R_2) by anhydrite may have overlapped with anhydrite cementation. The relative timing between anhydrite and native sulphur could not be resolved since the two were not observed together, but both postdate dolomite cements C_1 and C_2 .

Intermediate to deep burial is characterized by the migration of hydrocarbons (Late Cretaceous to Early Tertiary; Deroo et al., 1977) and emplacement of reservoir bitumen which postdates replacement dolomites, dolomite cements (C_1 , C_2), and anhydrite cements. Hairline microfracturing crosscuts most diagenetic features, with the exception of late calcite cements, and probably was contemporaneous with some bitumen emplacement

(see Chapter 4). Minor amounts of calcite cements postdate microfracturing and bitumen emplacement as these calcites overlie thin bitumen coatings in vugs and intercrystalline pores and are not crosscut by microfractures. Two phases of calcite cementation occurred based on isotope and fluid inclusion data. The heavier carbon isotope calcites in the Strachan buildup probably represents an earlier phase as compared to the lighter carbon isotope, and higher temperature calcites from the Ricinus West buildup.

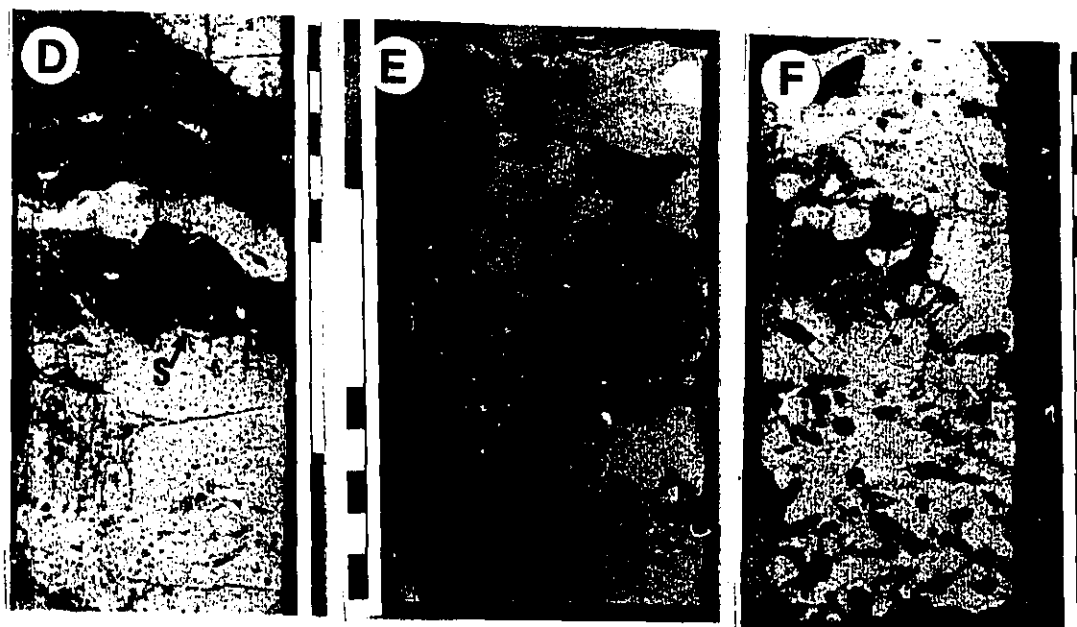
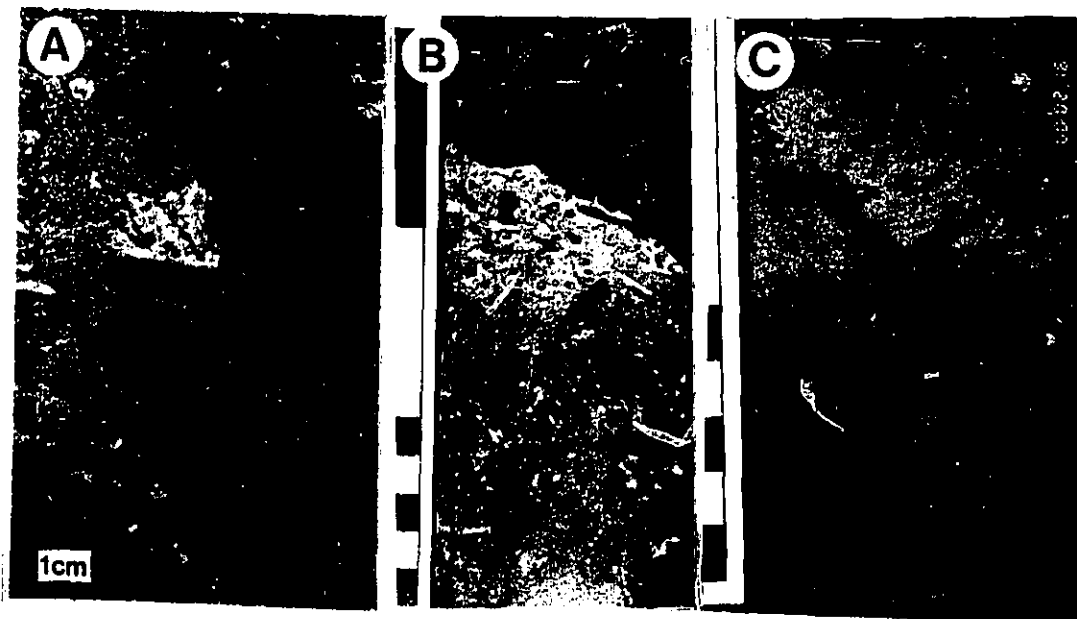
Distribution of replacement dolomites and later-diagenetic products

The extent of dolomitization in these buildups ranges from isolated rhombs to patches of dolomite in pool D3B of the Strachan reservoir to complete fabric destruction in all other buildups. In all wells of pool D3B isolated dolomite rhombs in the limestone matrix (Plate 2.9A) become most abundant near stylolites where they form patches of planar-subhedral dolomite similar to those in the completely dolomitized intervals. Even within individual wells, such as 10-31 of pool D3A, a complete range from partial to total replacive dolomitization is observed. Contacts between dolostone and limestone are both gradational and sharp. Dolomitization is fabric selective and preferentially replaces the finer matrix (Plate 2.9 B,D), although some skeletal fragments and some marine cements are also dolomitized. Where dolomitization is partial, the matrix is completely replaced and the majority of skeletal fragments and marine cements are preserved as calcite (Plate 2.9C). The interior and eastern margin of pool D3A in Strachan and all other buildups in the study area are characterized by fabric-destructive dolomitization. Here skeletal debris are partially to completely dissolved (Plate 2.9 E,F) forming vuggy and moldic porosity.

Dolomite R₁ occurs mostly in wells of the reef interior (e.g. 11-27, 7-26 and 15-23 in Ricinus West and 7-32 in Strachan). Dolomite R₂ is widespread throughout the

Plate 2.9 DOLOMITE DISTRIBUTION IN THE STRACHAN BUILDUP

- A) Selective replacement of lime mud matrix by isolated, rhombs (110 μm) and patches (arrows) of dolomites in stromatoporoid (S) and coral (C) rudstones facies. 10-31-37-9W5, 4281 m.
- B) Selective replacement of matrix and initiation of dolomite mosaics. Compare with sample (F) only 0.5 m apart. Stromatoporoid (S) and coral rudstones facies. 10-31-37-9W5, 4279.8 m.
- C) Complete replacement of matrix, marine cements (mc) and skeletal fragments are still calcite. Stromatoporoid and coral rudstones facies. 10-31-37-9W5, 4181.4 m.
- D) Complete replacement of matrix. Intraskkeletal pores in stromatoporoid fragment (S) are partly filled with reservoir bitumen. Note vugs in the dolomitized matrix. Stromatoporoid and coral rudstones facies. 10-31-37-9W5, 4265 m.
- E) Complete replacement of the matrix resulting in a tight mosaic of dolomite crystals with some vugs. Partly leached domal stromatoporoid fragments. Stromatoporoid and coral rudstones facies. 12-31-37-9W5, 4287.5 m.
- F) Dissolution of skeletal fragments resulting in molds, solution enlarged molds and vugs. Note pores lined by reservoir bitumen. Stromatoporoid and coral rudstones facies. 10-31-37-9W5, 4279.2 m.



buildups, replacing all sedimentary facies (Table 2-1). Dolomite R₃ is most abundant in wackestones and mudstones of the reef interior (e.g. well 11-27 in Strachan). Dolomite R₄ replaces radiaxial fibrous calcite cements and it is restricted to the margins of the Ricinus West buildup. The reason for differences in crystal size between R₁, R₂, and R₃ is not evident, however, it appears to be related to original grain sizes and permeability differences between grainstone, packstone and wackestone matrices. While there are some exceptions, R₁ and R₂ dolomites occur mainly in sediment types which initially possessed high permeability, such as grainstones and packstones. Modern packstone textures have permeabilities between 1840 and 30800 md. In contrast, sediments that make up the precursor of R₃ dolomites were probably wackestones and mudstones since they are most abundant in buildup interiors. Modern analogue textures have high porosities (68%) but low permeabilities (228 to 0.87 md; Enos and Sawatsky, 1981). Therefore, initial low permeabilities in wackestone and mudstone matrices may have restricted the flow of the dolomitizing fluids through these rocks, thereby affecting the nucleation and growth kinetics and consequently producing coarser crystalline, euhedral dolomites (e.g. Dawans and Swart, 1988). The high initial permeability of R₁ and R₂ precursors may have allowed greater and faster dolomitization producing small crystals and non-mimetic replacements (e.g. Dawans and Swart, 1988). This distribution of dolomite textures suggests that their occurrence is in part related to primary textures and structures in the original limestones, despite fabric destructive dolomitization.

The general distribution and relative abundance of later diagenetic features is shown in Table 2-1. Dolomite cements, sulphides, native sulphur and quartz occur in minor amounts ($\leq 2\%$). Of all the pore-occluding phases, reservoir bitumen and anhydrite are volumetrically important. Calcite cements are locally common. Several important observations are evident from Table 2-1: 1) In partly dolomitized rocks of Strachan D3B

TABLE 2 - 1 Distribution of late diagenetic features in Leduc buildups, in the deep Alberta basin

DIAGENETIC FEATURE	STRACHAN		RICINUS WEST	RICINUS EAST	CRIMSON	CHEDDERVILLE
	D3B POOL	D3A POOL				
Replacement dolomites	Rhombs, patches	R ₁ R ₂ R ₃	R ₁ R ₂ R ₃ R ₄	R ₂ R ₃	R ₂	R ₂ R ₃
Dolomite cements	C ₂	C ₁	C ₁ C ₂	C ₂	C ₂	C ₁ C ₂
Anhydrite	absent	rare	common	common	common	common
Sulphides	absent	Sphalerite Pyrite	Sphalerite Pyrite	Pyrite	Pyrite	Pyrite
Native sulphur	absent	rare	rare	common	rare	common
Reservoir bitumen	abundant	abundant	abundant	common	common	common
Hairline microfractures	abundant	abundant	Locally common	absent	rare	rare
Quartz	absent	absent	rare	absent	common	absent
Calcite cements	rare	common	common	rare	rare	rare

GAS COMPOSITION

CH ₄	90%	80%	60%	NA	NA	83%
H ₂ S	4.8%	8%	33%	NA	9.9%	8%
CO ₂	1.8%	2.2%	6.6%	NA	NA	1.2%

Total volume percent, based on visual estimation in cores
 abundant = 5 - 8% common = 2 - 4% rare = ≤1%

NA = Not Available

Gas composition from ERCB files

pool anhydrite, sulphides and native sulfur are absent and the amount of H_2S is low (4.8%). In dolostones of the D3A pool and all other dolomitized buildups anhydrite, sulphide and native sulphur cements are common and H_2S concentrations are high (up to 33%), 2) Dolomite cement C_1 is associated with the presence of anhydrite cements, 3) dolomite cement C_2 is minor in all buildups, and 4) hairline microfractures are abundant only in the partially dolomitized Strachan buildup. This indicates that major differences in diagenesis occurred in partly dolomitized Strachan buildup compared to completely dolomitized buildups.

GEOCHEMISTRY

To further document the different dolomite types and the late diagenetic products, several geochemical analyses were undertaken. The results are summarized below.

Major and minor elements

Microprobe analyses (5 samples) and XRD analyses (10 samples) indicate that replacement dolomites (R_2 , R_3) are nearly stoichiometric (48.7 to 50.9 mole% $CaCO_3$) and well ordered, with low Mn (173 to 320 ppm) and Sr (20 to 227 ppm) concentrations, and higher Fe concentrations (555 to 1385 ppm) (Appendix E1). These Mn and Fe concentrations are much higher than a hypothetical marine dolomite (Amthor et. al., 1993; Table 4) which has concentrations of Mn: 1 ppm and Fe: 3 to 50 ppm.

Dolomite cements (C_1 , C_2) (3 samples) from the Strachan buildup are nearly stoichiometric (49.6 to 50.1 mole% $CaCO_3$) with higher Fe concentrations (1620 ppm) and lower Sr concentrations (20 to 40 ppm) with respect to replacement dolomites. The Mn concentration is similar to that of replacement dolomites (140 to 310 ppm). Microprobe traverses across individual rhombs 600 μm in size of dolomite cement C_2 (e.g. well 10-31, 4300 m) show no systematic variations in Ca, Mg, Mn and Fe contents (Appendix E1).

Carbon and oxygen isotopes

Oxygen and carbon isotopes were measured on early calcite cements, limestone matrix and coral fragments, dolomite patches, replacement dolomites, dolomite cements and late calcite cements from the Strachan, Ricinus West and adjacent buildups (Appendix E2). Radial fibrous calcite cements have oxygen and carbon isotopic values ranging from $\delta^{13}\text{C} = 1.55$ to 2.43‰ PDB and $\delta^{18}\text{O} = -7.59$ to -5.51‰ PDB ($n = 12$). One sample of isopachous radial cement gave values of $\delta^{13}\text{C} = 1.90\text{‰}$ PDB and $\delta^{18}\text{O} = -8.78\text{‰}$ PDB. These values are almost the same as marine cements from the Golden Spike buildup ($\delta^{13}\text{C} = 1.6$ to 3.1‰ PDB, $\delta^{18}\text{O} = -7.4$ to -5.8‰ PDB, Walls et. al., 1979).

Limestone packstone matrices range from $\delta^{13}\text{C} = 1.71$ to 3.73‰ PDB and $\delta^{18}\text{O} = -6.65$ to -5.46‰ PDB ($n = 4$), showing a slight enrichment (1‰) in ^{13}C relative to calcite cements (Fig. 2.7A). Isotopic values from skeletal components (corals) are slightly lighter in oxygen, ranging from $\delta^{18}\text{O} = -8.67$ to -6.22‰ PDB and $\delta^{13}\text{C} = 1.89$ to 3.44‰ PDB ($n = 5$). Isotopic compositions of early calcite cements, limestone matrix and coral fragments overlap with Upper Devonian marine calcite values reported by Amthor et. al. (1993; $\delta^{13}\text{C} = 1.5$ to 3.5‰ PDB, $\delta^{18}\text{O} = -6.0$ to -4.0‰ PDB), some values are up to 3‰ lighter in oxygen (Fig. 2.7A), suggesting that the host material have been modified and/or reequilibrated or neomorphosed under increasing temperature during burial.

Dolomite patches which may have small amounts of calcite, range from $\delta^{13}\text{C} = 2.51$ to 3.40‰ PDB and $\delta^{18}\text{O} = -8.53$ to -7.45‰ PDB ($n = 5$; Fig 2.7 B). Replacement dolomites (R_1 , R_2 , R_3) from the Strachan reservoir range from $\delta^{13}\text{C} = 1.94$ to 3.57‰ PDB and $\delta^{18}\text{O} = -6.58$ to -4.23‰ PDB ($n = 10$). Replacement dolomites (R_1 , R_2 , R_3) from Ricinus West and adjacent buildups range from $\delta^{13}\text{C} = 1.35$ to 2.58‰ PDB and $\delta^{18}\text{O} = -7.19$ to -3.67‰ PDB ($n = 20$). Isotopic composition of these dolomites overlap

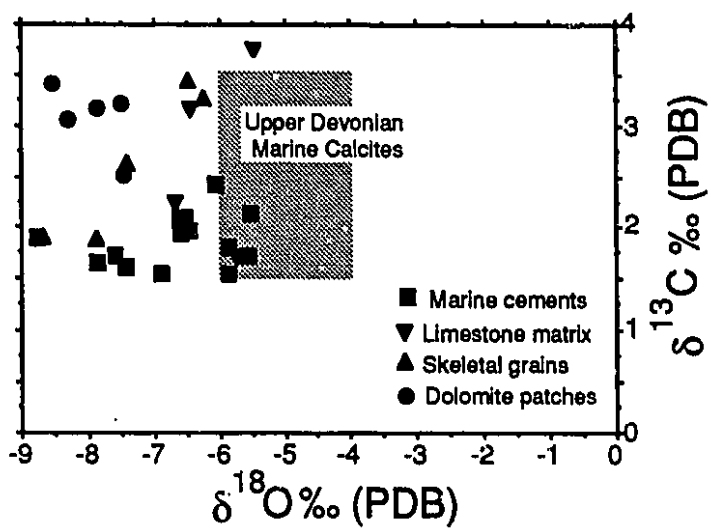
Figure 2.7 Plot of $\delta^{13}\text{C}$ versus $\delta^{18}\text{O}$ isotope values for

A) marine cements, limestone matrix and skeletal components, and dolomite patches. Upper Devonian marine calcite box from Amthor et. al. (1993).

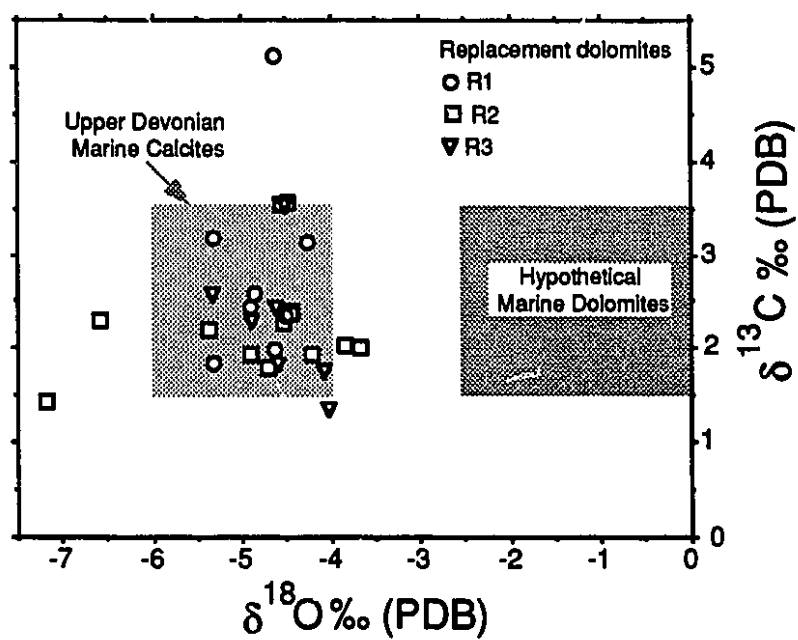
B) replacement dolomites (R_1 to R_3) from Strachan, Ricinus West and adjacent buildups. Hypothetical marine dolomites from Amthor et. al. (1993).

C) dolomite cements (C_2) from Crimson and Ricinus West. Late calcites from Strachan and Ricinus West buildups.

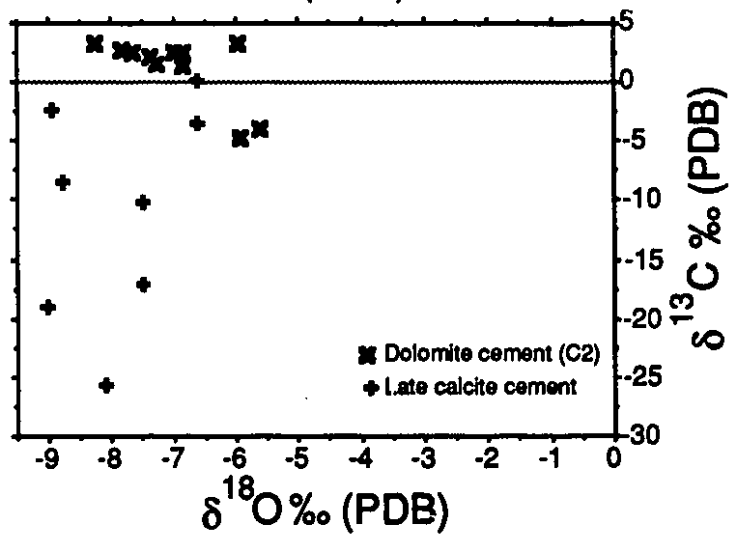
a)



b)



c)



and are about 2 to 4‰ depleted in $\delta^{18}\text{O}$ relative to hypothetical Upper Devonian marine dolomite ($\delta^{18}\text{O} = 0$ to -2.4 ‰ PDB; Amthor et. al., 1993) that is up to 3‰ heavier than limestones and dolomite patches (Fig. 2.7B). Interestingly almost all of these dolomites fall within the marine calcite field suggesting that they have largely retained the isotopic signature of the precursor limestones.

Dolomite cements (C2) from Strachan (Fig. 2.7C) show values that range from $\delta^{13}\text{C} = 2.47$ to 3.31 ‰ PDB and $\delta^{18}\text{O} = -8.28$ to -5.97 ‰ PDB and from Ricinus West and adjacent buildups exhibit values ranging from $\delta^{13}\text{C} = -4.83$ to 2.79 ‰ and $\delta^{18}\text{O} = -7.84$ to -5.63 ‰. The lighter carbon values are from the Crimson buildup (well 11-28-37-8W5, 3700 m) and probably resulted from thermal sulphate reduction reactions (TSR).

Late calcite cements (Fig. 2.7C) show the most negative carbon and oxygen isotope values ranging from $\delta^{13}\text{C} = -10.29$ to 0.08 ‰ PDB and $\delta^{18}\text{O} = -7.49$ to -6.60 ‰ PDB in Strachan and from $\delta^{13}\text{C} = -25.7$ to -2.49 ‰ and $\delta^{18}\text{O} = -9.01$ to -7.48 ‰ in the other buildups. These light carbon calcites are usually associated with other TSR features such as anhydrite cements, native sulphur, and high H_2S (Appendix C), suggesting that they may have resulted from TSR reactions.

Strontium isotopes

Strontium isotopes were measured from one sample of limestone matrix in the Phoenix area (well 5-13-37-12W5, 5067.4 m) and selected samples from dolomite patches, replacement dolomites (R_2), dolomite cements (C2) and late calcite cements (Appendix E). The limestone matrix has a $^{87}\text{Sr}/^{86}\text{Sr}$ ratio of 0.7083. This value is similar to Upper Devonian seawater ($^{87}\text{Sr}/^{86}\text{Sr} = 0.7080$ to 0.7083 , Mountjoy et. al., 1992). Dolomite patches have $^{87}\text{Sr}/^{86}\text{Sr}$ ratios that range from 0.7082 to 0.7086 (mean: 0.7084). Replacement dolomites (R_2) from the Strachan buildup yield $^{87}\text{Sr}/^{86}\text{Sr}$ ratios of 0.7082 and

0.7096. $^{87}\text{Sr}/^{86}\text{Sr}$ ratios of replacement dolomites (R_1 , R_2 , R_3) from Ricinus West and adjacent buildups range from 0.7083 to 0.7100 (mean: 0.7087). The $^{87}\text{Sr}/^{86}\text{Sr}$ ratio of dolomite patches and replacement dolomites are close to, but slightly higher than Upper Devonian seawater (Fig. 2.8), indicating that the dolomitizing fluids were probably slightly more radiogenic than Upper Devonian seawater.

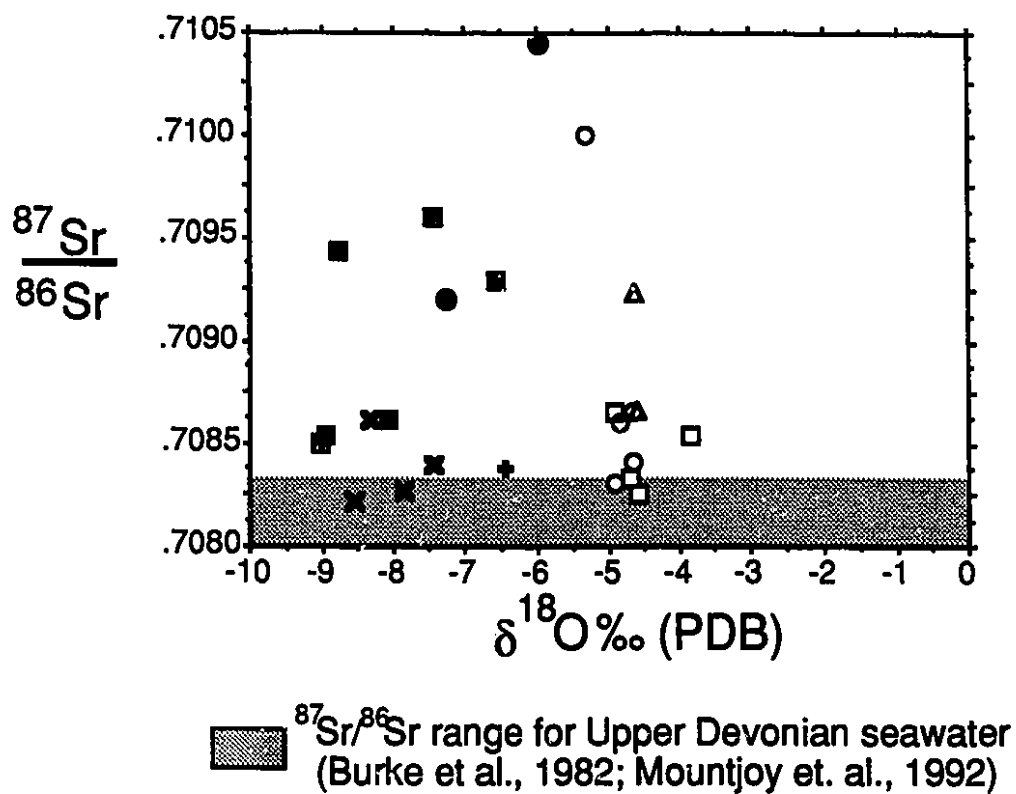
Dolomite cement (C_2) from Ricinus West and adjacent buildups have $^{87}\text{Sr}/^{86}\text{Sr}$ ratios ranging from 0.7088 to 0.7104 (mean: 0.7095) and are clearly more radiogenic than Devonian seawater. Late calcite cements from all buildups have $^{87}\text{Sr}/^{86}\text{Sr}$ ratios that range from 0.7085 to 0.7094 (mean: 0.7090). Dolomite and late calcite cements are generally more radiogenic than Devonian seawater and probably precipitated from formation waters during intermediate or deeper burial. No correlation is found between $^{87}\text{Sr}/^{86}\text{Sr}$ ratios, stable isotopes and dolomite types (Fig. 2.8), except that the cements are generally lighter and more radiogenic.

Fluid inclusions

Fluid inclusion data have been obtained from selected samples of dolomite cements (C_1 and C_2), and late calcite cements (Figs. 2.9, 2.10, Appendix E3). These inclusions are interpreted to be primary because they are commonly isolated, and when clustered they are randomly oriented and distributed along crystal growth zones.

Seven primary liquid-vapor fluid inclusions within dolomite cement (C_1) crystals were analyzed. The inclusions are 10 to 20 μm in length, about 3 μm in width, and contain an aqueous liquid and a small vapor bubble (about 1 μm in diameter). Homogenization temperatures from these inclusions range from 86 to 153°C (mean= 130.6°C; Fig. 2.9A). Ice melting temperatures from only two inclusions (-10.7 and -11.2°C) indicate salinities of about 14.8 wt% NaCl eq.

Figure 2.8: Cross plot of $^{87}\text{Sr}/^{86}\text{Sr}$ and $\delta^{18}\text{O}$ for lime matrix, dolomite patches, replacement dolomites (R_1 to R_3), dolomite cement (C_2) and late calcite cement from all buildups. No clear trend is observed. In general dolomite cement (C_2) and late calcite cements have lighter $\delta^{18}\text{O}$ and higher $^{87}\text{Sr}/^{86}\text{Sr}$ ratios than the replacement dolomites.



- + Lime matrix
- ✕ Dolomite patches
- Dolomite-R1
- Dolomite-R2
- △ Dolomite-R3
- Dolomite-C2
- Late calcite

Twenty primary liquid-vapor fluid inclusions in saddle dolomite cement (C_2) have been measured from one sample in the Crimson field. These inclusions are 5 to 18 μm in length and 1 to 10 μm in width with an aqueous liquid and a small vapor bubble (2 to 3 μm in diameter). They have homogenization temperatures between 113 and 162°C (mean = 149.6°C) that are generally higher than temperatures in dolomite cement C_1 (Fig. 2.9B). Initial and final melting temperatures in dolomite cements are difficult to determine accurately due to the small size of the inclusions.

In late calcite cements from Strachan buildup twenty two fluid inclusions were analyzed. A relatively narrow range of homogenization temperatures from 146 to 148°C (mean = 147°C, Fig. 2.10B,C) is present in calcites from partially dolomitized strata in pool D3B (well 5-11, 4228 m; Appendix E3). Calcites from dolomitized strata in pool D3A (well 10-31, 4300 m) show slightly higher homogenization temperatures (mean = 153°C). Twenty four primary liquid-vapor fluid inclusions in late calcite cements from the Ricinus West and adjacent reservoirs were analyzed (Fig. 2.10A). These inclusions are larger than inclusions in the dolomites (up to 50 μm in length and 5 μm in width). Homogenization temperatures obtained range from 132 to 168°C (mean = 150°C, and salinities are between 17.4 and 19.1 wt% NaCl equivalent (mean = 18.1). These late-stage saddle dolomite and calcite cements have average homogenization temperatures (147 to 153°C) that are about 20°C higher than the dolomite cements (C_1).

Discussion

Our understanding of trace elements in dolomites is severely limited by the fact that dolomites have not been precipitated in the laboratory at room temperatures. For this reason, the distribution coefficients for various trace elements (D_{me}) in dolomites are not well constrained (e.g. Vahrenkamp and Swart, 1990). A dolomite precipitating in

Figure 2.9 Histograms of aqueous liquid-vapour primary fluid inclusions showing homogenization temperatures (T_h), and corresponding salinities in weight percent NaCl equivalent for

- A) dolomite cements (C_1) from the Ricinus West buildup.
- B) dolomite cement (C_2) from the Crimson buildup.
- C) for late calcites from Ricinus West and Strachan buildups

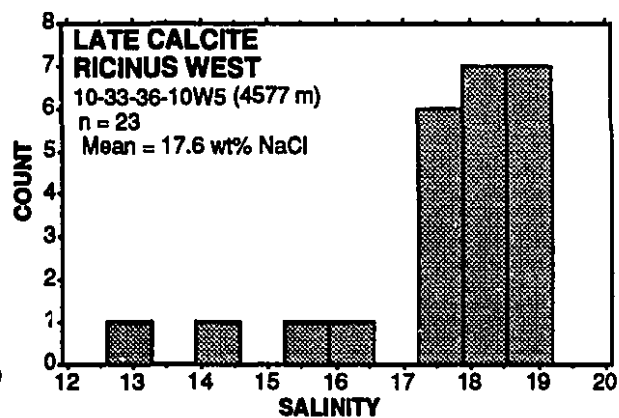
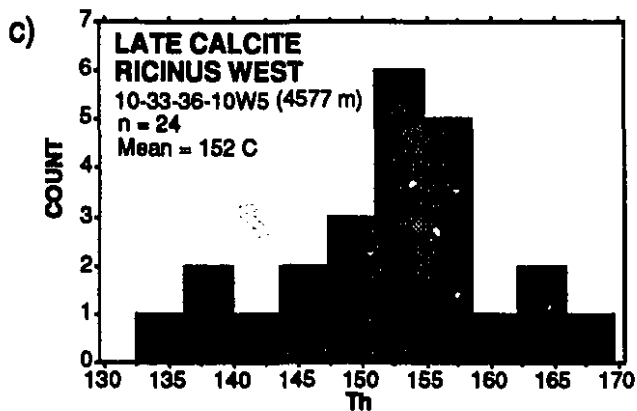
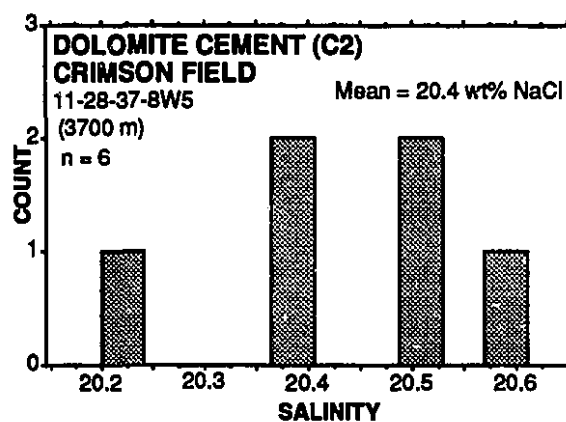
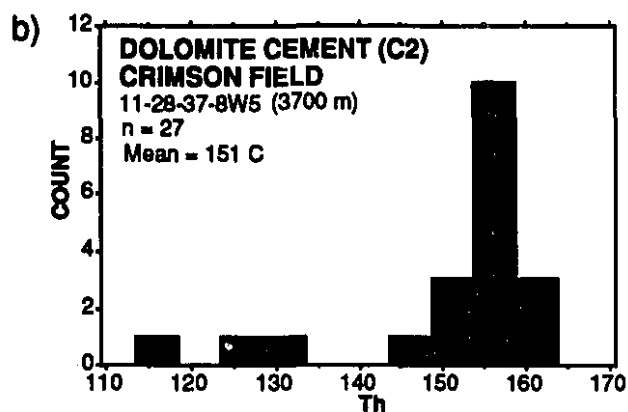
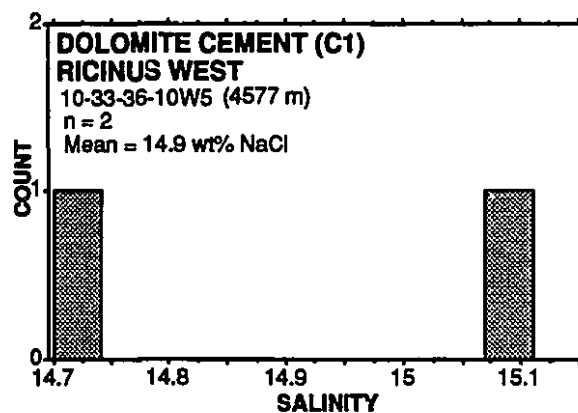
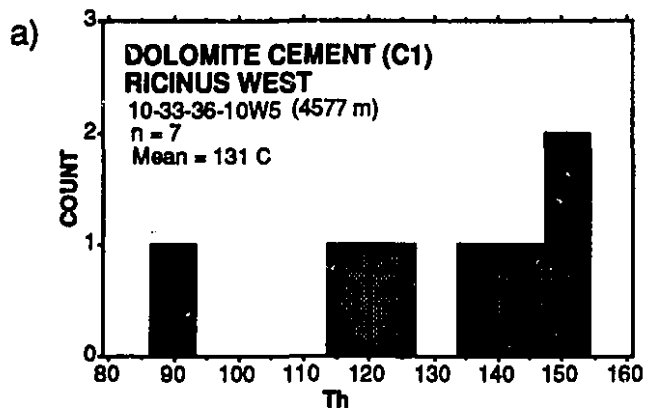
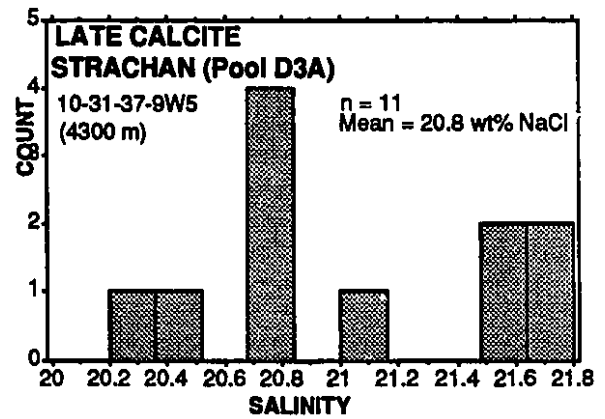
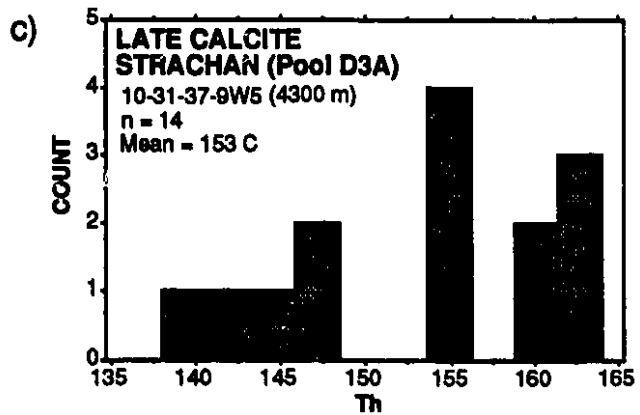
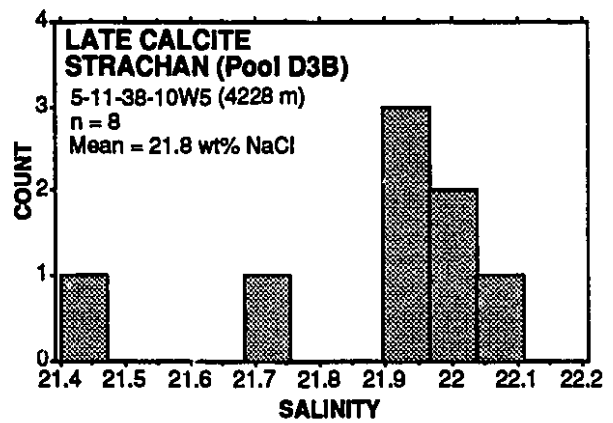
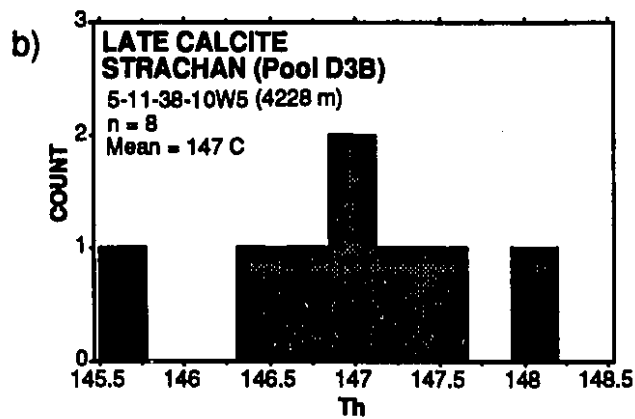
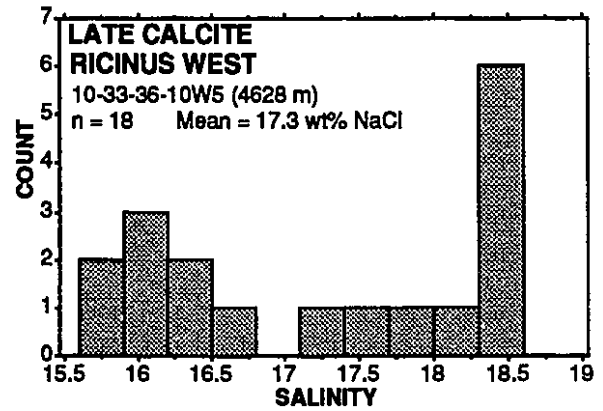
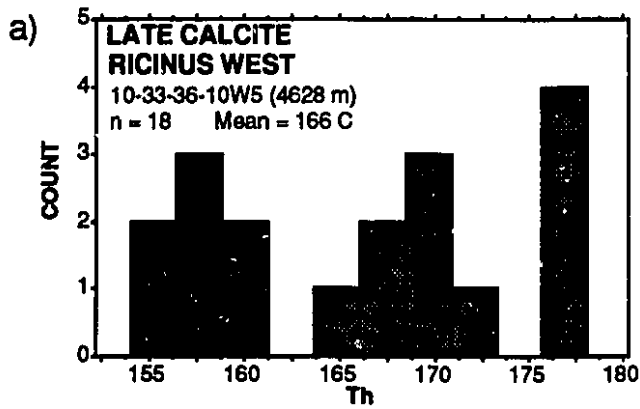


Figure 2.10 Histograms of aqueous liquid-vapour primary fluid inclusions showing homogenization temperatures (T_h), and corresponding salinities in weight percent NaCl equivalent for
A) late calcites from the Ricinus West buildup.
B), C) late calcites from the Strachan buildups



equilibrium with seawater should have trace element concentrations of Fe (3 - 50 ppm), Mn (1 ppm), and Sr (470 - 550 ppm) using the distribution coefficients recommended by Veizer (1983) (see Appendix E1). However, if the distribution coefficient for strontium ($D_{Sr}^{Dolomite}$) reported by Vahrenkamp and Swart (1990) is used, the concentration of strontium is lowered considerably (50 - 70 ppm). Therefore, the hypothetical composition for Upper Devonian marine dolomites reported by Amthor et. al. (1993) is used. Replacement dolomites in Strachan are nearly stoichiometric with trace elements concentrations that deviate from hypothetical Upper Devonian marine dolomites, suggesting that 1) trace elements concentrations of the dolomitizing fluids were modified from those of seawater, or 2) that dolomites neomorphosed after dolomitization by diagenetic fluids having trace element compositions somewhat different from seawater.

Information on ancient seawater can be obtained from $\delta^{13}C$ and $\delta^{18}O$ values since inorganically-precipitated high-Mg calcite cements are almost in isotopic equilibrium with ambient seawater (Gonzalez and Lohmann, 1985). According to Carpenter and Lohmann (1989) clear radiaxial fibrous calcite cements from the Golden Spike and Nevis Leduc buildups preserve original marine $\delta^{13}C$ and $\delta^{18}O$ values, whereas cloudy or inclusion-rich radiaxial fibrous calcite cements show evidence of diagenetic alteration. Texturally similar radiaxial fibrous calcite cements from Strachan buildup have $\delta^{13}C$ and $\delta^{18}O$ values (Fig. 2.7A) that overlap with Carpenter and Lohmann's cloudy or inclusion-rich radiaxial fibrous calcite. This isotopic composition is more variable, up to 3‰ lighter, than clear radiaxial cements and can be considered to be the result of alteration by later diagenetic fluids. Original marine $\delta^{13}C$ and $\delta^{18}O$ values are not present in radiaxial fibrous calcite cements analyzed from the Strachan buildup.

The isotopic composition of Upper Devonian marine calcites ranges from $\delta^{13}C = 1.5$ to 3.5 ‰ PDB and $\delta^{18}O = -6$ to -4 ‰ PDB based on data from Carpenter and

Lohmann (1989). Dolomite that precipitates in isotopic equilibrium with seawater should be about 2 to 4‰ heavier than coexisting calcites (Land, 1980, 1983, 1985). In this study, the oxygen isotopic values of replacement dolomites do not show this difference suggesting that replacement dolomites formed from the precursor limestone and modified seawater.

$^{87}\text{Sr}/^{86}\text{Sr}$ of marine carbonate minerals are assumed to be identical to those of seawater at the time of precipitation, since isotopic fractionation of Sr during carbonate precipitation is negligible (Veizer, 1983). Analysis of marine carbonates indicates that the $^{87}\text{Sr}/^{86}\text{Sr}$ of oceans has varied systematically throughout Phanerozoic time, but apparently has been constant in the open ocean at any given time (Burke et.al., 1982). Thus, marine carbonates precipitated during Upper Devonian time should have $^{87}\text{Sr}/^{86}\text{Sr}$ between 0.7080 to 0.7083 (Burke et.al., 1982, Mountjoy et. al., 1992). In this study, $^{87}\text{Sr}/^{86}\text{Sr}$ ratios from dolomite patches and replacement dolomites suggest that dolomitizing fluids were probably slightly more radiogenic than Upper Devonian seawater.

The present day basin fluids in the Edmonton area of Western Canada Sedimentary Basin display three distinct zones in terms of $^{87}\text{Sr}/^{86}\text{Sr}$ ratios (Connolly et. al., 1990a,b). Fluids in Upper Cretaceous strata have low $^{87}\text{Sr}/^{86}\text{Sr}$ ratios (e.g. 0.7058) and fluids in Lower Cretaceous to Jurassic strata have intermediate values. The fluids in the deeper Paleozoic interval are the most radiogenic (and vary from 0.7076 to 0.7129) with most fluids being more radiogenic than 0.7095 (Connolly et. al., 1990b). Apparently the topographically driven fluids, which passed through the Mesozoic and Early Tertiary clastic wedge mostly during the Cretaceous and early Tertiary, have not lowered the radiogenic Sr in the fluids of the Paleozoic section of the basin because several shale intervals acted as permeability barriers (Mountjoy et. al., 1992). Therefore, the increase of $^{87}\text{Sr}/^{86}\text{Sr}$ ratios in formation waters with depth suggest, that sources of radiogenic Sr are from the lower parts of the stratigraphic succession. The two most likely sources of radiogenic Sr are in the

underlying Precambrian crystalline and metamorphic basement or from clastic sequences downdip in the Lower Cambrian Gog Group and the feldspathic grits of the Late Proterozoic Windermere Supergroup (Mountjoy et. al.,1992).

This information suggests that replacement dolomites formed from the precursor limestone and modified seawater and that dolomite and late calcite cements precipitated from formation waters during intermediate or deeper burial.

COMPARISON OF DOLOSTONES

Isolated dolomite rhombs and patches have luminescence and fluorescence characteristics similar to replacement dolomites. Uniformity of fabric, composition and geochemistry indicates that dolomite rhombs, patches and replacement dolomites formed during the same dolomitizing event in the Strachan buildup.

Replacement dolomites have similar petrographic and geochemical characteristics in Strachan, Ricinus West and adjacent buildups (Table 2.2). The absence of replacement dolomite (R₄) is the most distinctive difference between Strachan and Ricinus West and adjacent buildups dolomites. They probably represent replacement of submarine cements in the buildup margins. Similar cements, that are still preserved as calcite are common in the partly dolomitized Strachan buildup.

Replacement dolomite (R₂) in Strachan has comparable Fe concentration (about 1015 ppm) but lower Mn concentration (199 ppm) with respect to dolomite Type 1 of Amthor et. al. (1993; 984 and 502 ppm respectively). Replacement dolomites (R₂, R₃) are slightly heavier in oxygen isotopes and lighter in carbon than type 1 and 2 dolomites of Amthor et. al. (1993). Replacement dolomites (R₃) in Ricinus show similar Fe but lower Mn concentration when compared with dolomite type 2 of Amthor et. al. (1993). Replacement dolomites (R₁, R₂) in the studied buildups are similar in texture,

cathodoluminescence and fluorescence character to replacement dolomites in Bearberry (Table 2.2). The higher $^{87}\text{Sr}/^{86}\text{Sr}$ ratio (0.7090) is the most distinctive difference between these dolomites. Replacement dolomites are similar in textures and geochemical characteristics in adjacent buildups (Ricinus West, Ricinus East, Crimson, Chedderville and Bearberry) and in buildups along the Rimbey Meadowbrook reef trend. This suggests that replacement dolomites formed from the same fluids during a regional to basin wide event.

DISCUSSION

Origin of dolomites

Based on textural, crosscutting relationships and geochemical information dolomitization of the Leduc Formation in the study area took place in two episodes as a major replacement event (R_1 to R_4) and minor cementation (C_1 and C_2). The possible origin of these two episodes is discussed below.

Replacement dolomites

The spectrum of dolomite textures in the Strachan buildup from idiopathic-P texture in partly dolomitized rocks of D3B pool to coarse-crystalline, planar euhedral to subhedral mosaics (R_3) in the D3A pool suggests progressive replacement of the buildup. In skeletal packstones and wackestones the finer-grained matrix was preferentially replaced by isolated dolomite rhombs (idiopathic-P texture). With increasing dolomitization, isolated rhombs become abundant until the crystals meet, form patches, and subsequently result in a unimodal, planar euhedral to subhedral dolomite mosaic with calcite fossils. If dolomitization continues, the matrix would result in a dense mosaic of unimodal, planar subhedral dolomite. Subsequent complete replacement of skeletal components would form non-mimetic dolomite mosaics (e.g. dense, replacement dolomite R_1). Alternatively, if any

TABLE 2 - 2: Petrographic and geochemical characteristics of replacement dolomites in Upper Devonian buildups, Alberta basin

	Strachan, Ricinus West and adjacent buildups		Intermediate Rimbey Meadowbrook reef trend *	Bearberry ***
CHARACTERISTIC	Rhomb patches	Replacement dolomites	Replacement dolomites	Replacement dolomites
PETROGRAPHY				
CRYSTAL SIZE	110 µm	R ₁ 30-62 µm R ₂ 62-250 µm R ₃ 250-600 µm R ₄ 300 µm	R ₁ 35-60 µm ** Type 1 62-250 µm Type 2 250-600 µm Type 4 250 µm – 1 mm	35-60 µm 100-140 µm 200-250 µm
TEXTURE	Euhedral Planar	Euhedral Subhedral Planar R ₄ Non-planar	Euhedral Subhedral Planar Type 4 Non-planar	Subhedral Anhedral Planar Non-planar
CL	Homogeneous	Homogeneous	Homogeneous	Homogeneous
FLUORESCENCE	Dull red	Dull red	Orange-red	red
	Not fluorescent	R ₂ Green - yellow	Green - yellow **	Green - yellow
GEOCHEMISTRY				
$\delta^{13}\text{C}:\bar{X}$	2.95 ‰	2.35 ‰	3.09 ‰	1.77 ‰
$\delta^{18}\text{O}:\bar{X}$	-7.99 ‰	-5.4 ‰	-5.98 ‰	-4.1 ‰
$^{87}\text{Sr}/^{86}\text{Sr}:\bar{X}$	0.7084	0.7090	0.7085 **	0.7082
$\text{MgCO}_3:\bar{X}$	NA	50.2 mole%	50.0 mole%	50.1 mole%
TRACE ELEMENTS				
$\text{Fe}:\bar{X}$		970 ppm	1182 ppm	1531 ppm
$\text{Mn}:\bar{X}$		246 ppm	409 ppm	104 ppm
$\text{Sr}:\bar{X}$		123 ppm		84 ppm
$\text{Na}:\bar{X}$				441 ppm

Data from: * Amthor et. al. (1993)

** Drivet (1993)

*** Laflamme (1990)

NA: Not available

undolomitized matrix and fossils are dissolved, the resultant dolomite would be an unimodal, planar euhedral to subhedral dolomite with intercrystalline and moldic porosity (porous, replacement dolomites R₁, R₂). The differences in texture and distribution appears to be in part related to primary textures and structures in the original limestones, despite fabric destructive dolomitization.

The textural characteristics of 1) increasing crystal size with an increase in non-planar crystal boundaries, and 2) homogeneous and blotchy cathodoluminescence, as well as the geochemical features such as 1) increase in stoichiometry and ordering of crystals, and 2) changes in oxygen and strontium isotopes and trace element compositions (e.g. Sr; Gregg and Sibley, 1984, Kupecz et. al., 1992, Mazzullo, 1992) are not observed. This suggest that replacement dolomite is not a neomorphic modification of earlier dolomites. Dolomite rhombs and patches in pool D3B indicate that dolomitization clearly replaces limestones.

Dense mosaics of fine crystalline (< 25 µm) planar-s dolomite are typical of dolomites formed under nearsurface, low temperature, saline to hypersaline conditions (eg. Gregg and Sibley, 1984; Machel and Mountjoy, 1987; Gregg and Shelton, 1990). The general lack of fine-crystalline dolomite in partially to completely dolomitized rocks of Strachan and other buildups along the Rimbey Meadowbrook trend and especially in limestone buildups (e.g. Golden Spike and Redwater buildups) suggests that early seafloor or nearsurface hypersaline dolomitization did not occur in these buildups. Partly dolomitized debris-flows in some buildup slopes have limestone clasts indicating that replacement dolomitization postdated deposition (Drivet, 1993).

Replacement dolomitization crosscuts early cements (e.g. Plate 2.9C, Fig. 2.5) and is closely related to the onset of stylolites. It also crosscuts depositional boundaries and extends into underlying strata (Cooking Lake platform; Chouinard, 1993) and adjacent and overlying limestones and shales (Duvernay Formation; Andrichuk, 1958b). Stylolites form

in limestones at depth between 500 and 1000 m (Dunnington, 1967, Lind, 1993) suggesting that replacement dolomites probably formed at depths greater than about 500 m. This information indicates that replacement dolomitization formed after deposition, probably at shallow to intermediate burial depths. Despite some reequilibration that may have occurred with burial, they have undergone no neomorphism. Similar relationships have been reported by Amthor et. al. (1993) in the central part and by Drivet and Mountjoy (1994a) for the southern part of the Rimbey Meadowbrook reef trend.

Carbon and oxygen isotopes also supports this interpretation of replacement dolomite textures. Oxygen values of replacement dolomites overlap with oxygen values of Upper Devonian marine calcites and do not show the expected enrichment (2 to 4‰; Land, 1980, 1983, 1985) in oxygen for dolomites that should precipitate in isotopic equilibrium with Upper Devonian seawater. This supports the textural observation of direct replacement of limestones. $^{87}\text{Sr}/^{86}\text{Sr}$ ratios from dolomite patches and replacement dolomites suggest that dolomitizing fluids were probably slightly more radiogenic than Upper Devonian seawater.

Amthor et. al. (1993) estimated a range of approximately 50° to 60°C for the temperature of formation of the Leduc replacement dolomites (assuming isotopic composition of dolomitizing fluids similar to Late Devonian seawater) and reported that these temperatures could have been reached at burial depths of about 600 to 1200 m towards the end of the Late Devonian to Early Mississippian. Similar results were reported by Drivet (1993). Following Amthor et. al. (1993) and using oxygen isotopic composition of replacement dolomites (R_1) similar paleotemperatures were obtained (55°C, Appendix E). Textural and isotopic composition suggest that replacement dolomites in the studied buildups are similar to dolomites along the Rimbey Meadowbrook reef trend and formed from the same fluids during a regional to basin wide event. This dolomitizing event most

likely occurred in the shallow burial environment (> 500 m) during the Late Devonian to Early Mississippian.

Origin of dolomite cements

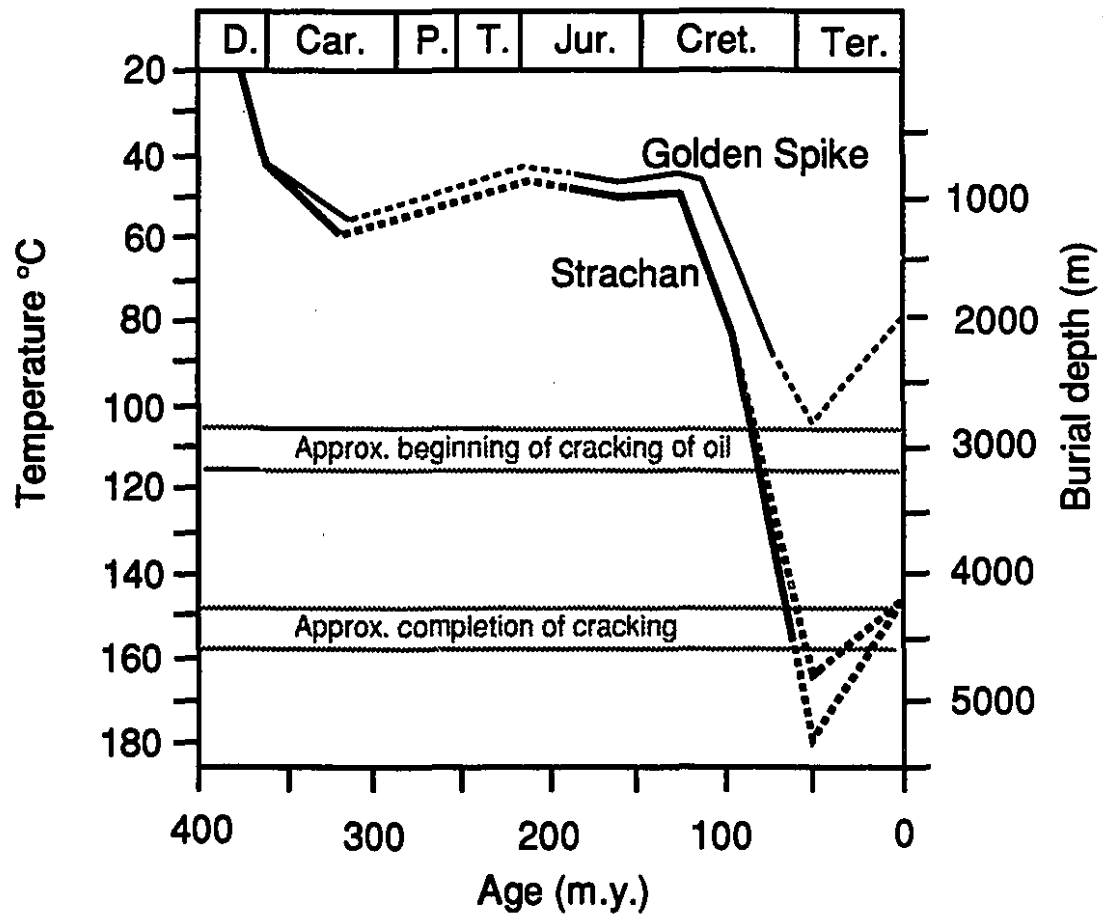
Two textural types of dolomite cements are present, medium crystalline planar C_1 and very coarse nonplanar C_2 (saddle dolomite). Both cements postdate all replacement dolomite textures. Dolomite C_1 postdates calcite dissolution (D_1) as it commonly lines secondary pores in dolostones and predates anhydrite cementation and bitumen emplacement. Measurements from fluid inclusions indicate that dolomite C_1 precipitated at temperatures of about 130°C (Fig. 2.9A) from fluids with salinities higher than seawater (14.9 wt% NaCl equi.). Using a surface paleotemperature of 20°C and a paleogeothermal gradient of 30°C/km (Fig. 2.11) this temperature corresponds to burial depths of about 3500 m during the Late Cretaceous. However, generation and migration of hydrocarbons occurred at depths between 2000 and 3000 m (Deroo et. al., 1977; Allan and Creaney, 1991; Creaney and Allan, 1992) and inferred temperatures of 80° to 110°C indicating that dolomite C_1 , based on crosscutting relationships, would have been precipitated at shallower depths. This suggest that dolomite cement C_1 precipitated from fluids hotter than expected from normal paleogeothermal gradient (inferred 30°C/km). Another possibility is that dolomite cement C_1 precipitated during conditions of higher paleogeothermal gradient (Drivet, 1993; Drivet and Mountjoy, 1994a). Based on the relationship between dolomite C_1 and stylolites Drivet (1993) concluded that the dolomite cement formed under intermediate to deep burial conditions (2000 to 2800 m) during the Cretaceous.

Dolomite C_2 cements postdated dolomite cement C_1 and dissolution D_2 and predate bitumen emplacement. Dolomite C_2 cements have an oxygen isotopic composition slightly

Figure 2.11 Burial-temperature plot for the Leduc Formation in the Strachan buildup, constructed assuming a geothermal gradient of $30^{\circ}\text{C}/\text{km}$ and a surface temperature of 20°C . The burial plot for the Golden Spike buildup (in the updip portion of the Rimbey-Meadowbrook trend; Walls et. al., 1979) is shown for comparison. The inferred burial depths, temperatures, and relative timing of thermal cracking of oil are also plotted.

BURIAL PLOTS

Top of Leduc
30o C/Km geothermal gradient



more negative than replacement dolomites (-8.28 to -5.63 PDB) probably as a result of increasing temperature during progressive burial. Amthor et. al. (1993) reported that similar cements (their Type 5) probably formed at temperatures of about 75°C and related them to pressure solution of earlier replacement dolomites. Machel (1987a) also related dolomite cements C₂ (saddle dolomite) to pressure solution, as does Dix (1993) who shows stylolites filled with dolomite. Measurements from fluid inclusions in one sample from the Crimson buildup (Fig. 2.9B) indicate that dolomite C₂ precipitated at temperatures of about 151°C. This corresponds to burial depths of 4500 m during the last stages of thermal cracking of crude oil (Fig. 2.11; see Chapter 4). Dolomite C₂ cements from the Crimson buildup have light carbon isotopic compositions (-5 PDB, Fig. 2.7C) and are associated with thermal sulphate reduction products (TSR, minor sulphides and native sulphur, Table 2.1, Appendix C) suggesting that they may be related to TSR reactions (this is discussed in the following section). This indicates that some organically derived carbonate was available in addition to carbonate from pressure solution as indicated by Amthor et. al. (1993).

Origin of late diagenetic features

Post-oil diagenetic processes in the Leduc are highly variable and heterogeneous across the study area. For the most part they occur in minor amounts except for the local filling of vugs by anhydrite. Hairline microfractures occur in partly dolomitized, isolated buildups where anhydrite is rare. Other features such as high H₂S content and native sulphur occur only in anhydrite-bearing dolostone buildups.

Following the generation and migration of oil into the Leduc buildups in the study area (probably during the Late Cretaceous, Fig. 2.11) at depths between 2 to 3 km, the reservoirs were subjected to rapid burial and temperature increases. Under these conditions

oil pooled in the reservoirs is thermodynamically metastable and susceptible to alteration (Tissot and Welte, 1984; p.459). This alteration (thermal cracking) is mainly controlled by increasing temperatures (see Chapter 4 for details about thermal cracking). Thermal cracking proceeds by oils becoming lighter until converted to gas (Hunt, 1979). This conversion of oil to gas involves a redistribution of hydrogen (Barker, 1979), in which process the overall effect is to form methane and carbon.

Most crude oils, however, contain small amounts of sulphur, oxygen and nitrogen (Hunt, 1979), which may also remove some hydrogen as H_2S and H_2O during thermal cracking, with nitrogen being removed as nitrogen gas (Barker, 1990). In particular the role of sulphur is quite important since it can strip large quantities of hydrogen from crude oil to form hydrogen sulfide (H_2S). For example, Barker (1990) indicated that for an average CH_4/H_2S volume ratio of 2:1, about 20% of the hydrogen from the oil would be consumed to form H_2S . Hydrogen sulphide is present in all reservoirs of the study area, suggesting that sulphur was present during cracking of the oil either as a part of the initial crude oil or as dissolved sulphate in the formation waters. The concentration of H_2S varies significantly between the Strachan and Ricinus West fields (Appendix F). In the Strachan reservoir the H_2S concentration is low (4.8%) in partly dolomitized strata of pool D3B (well 14-2) and is up to 8% in wells of the dolomitized pool D3A (Appendix F). This together with the rare abundance of anhydrite cements, sulphides and lack of native sulphur suggests that sulphur and/or dissolved sulphate was minor in the Strachan reservoir at the time of thermal cracking. In the Ricinus West reservoir, however, H_2S concentrations are up to 33%, anhydrite cements are abundant, sulphides are common, and native sulphur is rare but locally common (Table 2-2). This suggests that significant amounts of sulphur were available allowing the production of H_2S during the cracking of crude oil. Therefore, cracking of crude oil in the Strachan and Ricinus West reservoirs may have followed

reactions (see equation 3; Barker, 1990) in which some hydrogen was removed as H₂S.

H₂S and thermal sulphate reactions (TSR)

The amount of H₂S that may be generated by thermal cracking of oil is important since according to Orr (1974), thermal cracking of crude oil forms up to 3% H₂S, with 1 to 1.5% H₂S being a more realistic amount (Machel, 1985). Thermal cracking of oil may have generated some H₂S, however, a process other than thermal cracking must be considered to explain the high percentages of H₂S. As experimentally demonstrated by Toland (1960) and simplified by Orr (1974), the mechanism of thermal sulphate reduction (TSR) involves the reaction of hydrogen sulphide and dissolved sulphate to produce native sulphur and polysulphides, which in turn, react to generate more hydrogen sulphide. Many reactions have been proposed for this process (e.g. Machel, 1987b). As stated above, thermal cracking of initially pooled crude oil results in the formation of methane, minor ethane, and a few per cent hydrogen sulphide. The resulting H₂S acts as a catalyst in the following reactions as reported by Machel (1987b):



via:



Native sulphur is a product of subreactions 2 and 3 that rapidly oxidize hydrocarbons (e.g. -CH₂-) shown in reaction 1 to generate more H₂S. Some native sulphur will be present at the reaction site if it is not totally consumed (equation 2, 3). This will happen if, for example, reactive hydrocarbons are not supplied fast enough (Machel, 1987b). Evidence that TSR took place following the reactions in equations 2 and 3 has been reported from the adjacent Burnt Timber and Limestones fields by Eliuk (1984) and

Krouse et.al. (1988). Sulphur isotopic compositions from anhydrites, H_2S and native sulphur in the Burnt Timber and Limestone fields showed that H_2S is 7‰ lighter than the anhydrites with native sulphur having a ^{34}S value intermediate between the H_2S and anhydrites (Krouse et.al., 1988). Native sulphur in the studied reservoirs is rare but locally common (e.g. Chedderville reservoir, Table 2-2) suggesting that TSR may have taken place via equations 2 and/or 3.

Reaction products of equation 1 are hydrogen sulphide (H_2S) and bicarbonate (HCO_3^-). Hydrogen sulphide will evolve as a separate gas phase and/or will induce the precipitation of minerals such as pyrite, galena, and sphalerite if transition or base metals are present (e.g. Anderson, 1983). Some pyrite and sphalerite in the Strachan and Ricinus West reservoirs suggest that minor amounts of Fe and Zn were available, however, most H_2S occurs as a gas phase.

Bicarbonate (HCO_3^-) will increase carbonate alkalinity causing concomitant carbonate precipitation, where base and transition metals are scarce or absent (Machel, 1987a). Any carbonate precipitated will show a negative carbon isotopic composition as a result of its organic (oxidated hydrocarbons) source (e.g. Krouse et.al., 1988). Late calcite cements in the studied reservoirs show carbon isotopic compositions ranging from -25.7 to 0‰ PDB (Fig. 2.7C, Table 2.3). Late calcite cements from partially dolomitized D3B pool in the Strachan reservoir show the heaviest values ($\delta^{13}\text{C} = 0.08\text{‰ PDB}$). Calcite cements from the dolomitized D3A pool are slightly lighter ($\delta^{13}\text{C} = -6.97\text{‰ PDB}$) with the lightest values ($\delta^{13}\text{C} = -25.77\text{‰ PDB}$) being from the dolomitized Ricinus West reservoir. Thus isotopically light carbon generated by TSR was more abundant in the dolomite reservoirs. The heaviest calcites may be the result of a different and earlier phase of calcite cementation. Dolomite cements (C_2) in the dolomitized Crimson reservoir, which are

TABLE 2-3 Characteristics of late calcite cements

	STRACHAN		RICINUS WEST	
	Pool D3B	Pool D3A		
Well	5-11-38-10W5	10-31-37-9W5	10-33-36-10W5	
Depth (m)	4228	4301	4577	4628
$\delta^{13}\text{C}_{\text{‰PDB}}$	0.08		-2.49	-25.77
$\delta^{18}\text{O}_{\text{‰PDB}}$	-6.60		-8.95	-8.07
Th (°C)	147	140.3	152	166

associated with anhydrite and quartz cements, have light carbon values (-4.8‰ PDB) suggesting they formed in response to TSR reactions.

If methane is the only gaseous hydrocarbon available with dissolved sulphate, a common situation in sour gas provinces (Orr, 1974), bitumen would not form since all the carbon will be incorporated in the resultant bicarbonate and/or carbon dioxide (CO_2) and carbon monoxide (CO) (Toland, 1960; Orr, 1974; Machel, 1987b). The carbon dioxide (CO_2) produced may then induce carbonate dissolution. In the Strachan reservoir minor amounts of ethane gas and isotropic bitumens from a non-graphitizing (NSO) source suggest that light hydrocarbons other than methane may have been present at the time of TSR. Consequently, generation of CO_2 may have been minor. The present amounts of CO_2 are low in the Strachan reservoir, ranging from 1.8% in pool D3B to 2.2% in pool D3A, and slightly higher in the Ricinus West up to 6.6% where ethane gas is rare ($<0.6\%$). This suggests that the generation of CO_2 in the dolostone reservoirs may have been significant, and probably responsible for dissolution of some replacement dolomites.

Reactions 1, 2, and 3 were performed (e.g. Toland, 1960) at elevated temperatures (greater than 300°C). However, they can also take place at temperatures lower than 200°C when light hydrocarbons are the reducing agents (Krouse et. al., 1988). Homogenization temperatures, from isotopically light calcite cements, which are believed to have formed as a result of TSR in the Ricinus West reservoir, range between 152 and 166°C (Table 2.3). The highest homogenization temperature (166°C) is from the isotopically lightest calcite cement ($\delta^{13}\text{C} = -25.77\text{‰}$ PDB)

The association of hydrogen sulfide, native sulphur, isotropic reservoir bitumen, anhydrite, minor dolomite and calcite cements with isotopically light ^{13}C in the D3A pool of Strachan, Ricinus West and adjacent buildups indicate that thermochemical sulphate

reduction (TSR) occurred during thermal alteration of the reservoired oil (Table 2.4). This has also been reported for other carbonate buildups in the deep Alberta basin (e.g. Krouse, et. al., 1988, Viau, et.al., 1994). In partly dolomitized rocks of Strachan D3B pool anhydrite, sulphides and native sulfur are absent and the amount of H_2S is low (4.8%). Hairline microfractures are abundant only in the partially dolomitized Strachan buildup. These major differences in diagenesis, that took place in the partially dolomitized Strachan buildup compared to completely dolomitized buildups, are best explained if the completely dolomitized buildups were connected, probably since the time of dolomitization, to a regional fluid conduit system along the Cooking Lake platform that underlies the Rimbey Meadowbrook reef trend. This conduit system provided the flow paths for replacement dolomitization, secondary migration of hydrocarbons and later diagenetic products. On the other hand, the Strachan buildup being somewhat isolated from this conduit system explains its rather unique characteristics of, partial dolomitization, different diagenesis, thermal cracking of crude oil, overpressuring, and hairline microfractures (see Chapter 4). Restriction of fluid flow to the Strachan buildup appears to be related to the underlying Cooking Lake platform being more argillaceous and thinner beneath this buildup.

CONCLUSIONS

1) The upper Leduc Formation in the Strachan, Ricinus West and adjacent buildups represents shallow-marine carbonates. High energy, reef margin facies include coral, tabular stromatoporoid and stromatoporoid-coral rudstones. The reef interior is characterized by skeletal packstones/grainstones, skeletal wackestones and microbial laminite facies that indicate shallowing upward peritidal conditions.

2) Textures and compositions of isolated dolomite rhombs and patches in pool D3B of the partially dolomitized Strachan buildup are similar to replacement dolomites in

Table 2-4 Processes of crude oil alteration

Thermal process	Inferred depth (m)	Inferred temperature (°C)	Evidences
Generation and migration of crude oil	2000 - 3000	80 to 110	From: Deroo et.al. (1977) Allan and Creaney (1991) Creaney and Allan (1992)
Thermal cracking of crude oil	3000 - 4000	110 - 150	Dry gas composition Anisotropic bitumen with fine and coarse deformed lamellar textures Carbon isotopes analyses (e.g. James, 1990)
Thermal sulphate reduction	3000 - 4000	110 - 150	High H ₂ S content (> 2 %) Native sulphur Sulphides Calcite and minor dolomite (saddle) cements with isotopically light carbon

the completely dolomitized pool D3A. Textural, crosscutting relationships and geochemical information indicate that the replacement dolomitization of the Leduc Formation in the study area took place as a major event (R_1 to R_4). This dolomitizing event occurred in the shallow burial environment at depths of about 500 m based on their crosscutting relationships with early submarine cements, relationship to stylolites, and their occurrence in the overlying Ireton Formation. Dolomitizing fluids were probably modified from Devonian seawater as shown by slight deviations in trace element concentrations and higher $^{87}\text{Sr}/^{86}\text{Sr}$ ratios (0.7083 to 0.7092) than corresponding hypothetical Devonian seawater. These replacement dolomites are similar to replacement dolomites in adjacent buildups (Ricinus West, Ricinus East, Crimson and Chedderville) and in buildups along the Rimbey Meadowbrook reef trend. This suggests that replacement dolomites formed from the same fluids during a regional to basin-wide event.

3) Migration of crude oil into the reservoir from the adjacent Duvernay Formation took place during the Late Cretaceous (Fig. 2.11). Thermal cracking of crude oil was initiated during rapid burial and increasing temperature at about 125°C and depths most likely between 3000 and 4000 m. Cracking resulted in the formation of gas-condensates and reservoir bitumens. Some of the gas generated dissolved in the crude oil and caused minor deasphalting. However, the presence of abundant methane together with dissolved sulphate facilitated the onset of thermochemical sulphate reduction (TSR), producing minor amounts of H_2S . Accelerated by exothermic heat from TSR reactions thermal cracking and thermochemical sulfate reduction occurred over a long period of geologic time during increasing burial at temperatures in the 110-150°C range.

4) In partly dolomitized rocks of the Strachan D3B pool, anhydrite, sulphides and native sulfur are absent and the amount of H_2S is low (3.2%). In dolostones of the D3A pool and adjacent dolomitized buildups these cements are common and H_2S concentrations

are high (up to 33%). Hairline microfractures are abundant only in the partially dolomitized Strachan buildup. This can be explained by major differences in diagenesis that took place in the partially dolomitized Strachan buildup compared to completely dolomitized buildups. These differences are best explained if the completely dolomitized buildups were connected, probably since the time of replacement dolomitization, to a regional fluid conduit system along the Cooking Lake platform that underlies the Rimbey Meadowbrook reef trend.

5) The Cooking Lake conduit system provided the flow paths for replacement dolomitization, secondary migration of hydrocarbons and later diagenetic products. On the other hand, the rather unique characteristics of the Strachan buildup (partial dolomitization, different diagenesis, thermal cracking of crude oil, overpressuring and, hairline microfractures) are explained if it was somewhat isolated from this conduit system. Restriction of fluid flow to the Strachan buildup appears to be related to the underlying Cooking Lake platform being more argillaceous and thinner beneath this buildup.

CHAPTER 3

PORE SYSTEMS AND THE EFFECT OF DOLOMITIZATION ON RESERVOIR PROPERTIES, IN UPPER DEVONIAN LEDUC BUILDUPS, DEEP ALBERTA BASIN

X. Marquez and E. W. Mountjoy
Dept. of Earth and Planetary Sciences, McGill University
Montreal, H3A 2A7

ABSTRACT

Completely dolomitized Upper Devonian Leduc buildups at depths greater than 4000 m have higher porosities and permeabilities than limestones because the dolostones being more resistant to pressure solution retain their porosity. The distribution of pore types is controlled by depositional facies whereas distribution of permeability is controlled by diagenetic processes, especially dolomitization. In pool D3A of the Strachan reservoir, porosities and permeabilities are highest in the interior of the buildup where the strata are completely dolomitized compared to limestone margins. In the reef margin, porous and permeable dolomitized zones are interbedded with nonporous and nonpermeable limestone units. The presence of porous and permeable zones are closely related to the degree of dolomitization, with the greatest porosity and permeability occurring in completely dolomitized rocks.

Three pore systems that closely follow depositional units were identified in the Ricinus West buildup, despite complete dolomitization. At the reservoir-scale porosity and permeability are similar throughout. At the medium scale meter to 10's meters, the upper 131 m of the reservoir are characterized by pore system I in which 1 to 2 m thick, permeable, and laterally continuous, reef interior (lagoonal) zones are present. Pore system II predominates in the lower 61 m of the reef interior, and consists of laterally discontinuous permeable zones. Pore system III is restricted to the 259 m thick reef margin where vertical permeability is controlled by fractures and interconnected vugs. At the small

mm-scale porosity and permeability are controlled by diagenetic processes. Late cementation and dissolution processes have both increased and decreased porosity and permeability in the lower part of the reservoirs. Bitumen plugging decreased porosity and permeability in the upper part of the reservoirs.

INTRODUCTION

The Leduc buildups (Upper Devonian, Frasnian) along the 320 km long Rimbey Meadowbrook reef trend in central Alberta are prolific oil and gas producers, and their reservoir characteristics have been partly documented in the shallow (< 2000 m) and intermediate (2000 to about 3500 m) portion of the trend (e.g. Reitzel and Callow, 1976; Barfoot and Rogers, 1984; Barfoot and Ko, 1987; McNamara and Wardlaw, 1991; Drivet, 1993; Drivet and Mountjoy, 1994b; Amthor et. al., 1994). In the deeper (> 4000 m) part of the Rimbey Meadowbrook reef trend, however, other than the preliminary report on the geology and reservoir characteristics of the Strachan and Ricinus West gas reservoirs by Hriskevich et.al., (1980), there are no published data on reservoir properties and their variability within the Leduc buildups. Consequently, little is known about porosity and permeability variations within these reservoirs.

The partly dolomitized Strachan and completely dolomitized Ricinus West buildups represent excellent areas for studying and comparing reservoir characteristics of limestone and dolostone buildups in the deep basin.

Based on regional-scale relationships of porosity and permeability, limestones and dolostones at shallow depth (< 2000 m) have comparable values and distributions of porosity (Amthor, et. al., 1994). At these depths dolomitization resulted in redistribution of porosity and increased permeability slightly (Amthor, et. al., 1994). At deeper burial (> 2000 m), however, dolostones are significantly more porous and permeable than limestones. Dolostones tend to have better retained their porosity whereas limestones have

lost considerable porosity and permeability by means of pressure solution (Drivet and Mountjoy, 1994; Amthor et. al., 1994).

This paper addresses porosity and permeability variability in the deep basin and shows how depositional facies and diagenesis ultimately control the pore systems. This analysis is done at different scales; from the entire reservoir, to individual pore types (following Weber, 1986). The objectives are: 1) to identify different pore types and define pore systems, and to determine their distribution within the Leduc gas reservoirs, 2) to determine reservoir continuity and variability, and the porosity and permeability trends relative to different depositional facies and diagenetic phases, 3) to compare reservoir characteristics of limestone and dolostone reservoirs in the deep basin, and 4) to determine how dolomitization, cementation and reservoir bitumen have effected the reservoir character.

METHODS

All available cores from the Strachan and Ricinus West buildups in the Upper Devonian of central Alberta, Canada, between Townships 34 to 39 and Ranges 7 to 12 W5 (Fig. 1.1; Appendix A) were logged and sampled from depths generally greater than 4000 m. Core parameters were determined systematically (Table 3-1).

In this study, core-derived horizontal (K_h) and vertical permeabilities (K_v) and porosities were provided by the Energy Resources Conservation Board (ERCB, Calgary). Permeability and porosity data from the gas-producing zone were obtained from whole-core (full-diameter 8 cm) samples of 0.3 m.

To compare porosity among different facies an arithmetic mean of the core measurements is used because porosity is closely related to depositional facies and generally follows a layer-cake arrangement. Permeability, however, is strongly modified by diagenesis resulting in a more random distribution of values so that a geometric mean,

or mean of the logarithmic distribution of values, is more representative of differences among facies (Wardlaw, 1990, 1992). McNamara and Wardlaw (1991) reported that the geometric mean of core-measured permeability provided the best correspondence with permeability estimated from a pressure buildup-test in the Westrose reservoir. Permeability and porosity profiles within dolostones were obtained by plotting porosity, K_h and K_v values for each sample depth (Appendix H).

In this study emphasis have been placed on information from core observations and their correlation with porosity and permeability data. No correlation with well logs have been done because many of the logs are of poor quality and due to difficulties of determining the parameters needed for calculating porosity. Maddox (1984) determined the correlation between core porosity and log porosity from digitized neutron-density and sonic logs over the cored interval in the Ricinus West reservoir. Core analyses yielded similar to slightly higher porosities compared to those calculated from logs. Comparisons of porosities from cores and logs of Leduc dolomites along the Rimbey-Meadowbrook reef trend made by McNamara et. al. (1991) and Drivet (1993) indicate that core porosities are generally comparable to porosities calculated from logs when suitable logs are available. Further, McNamara et. al. (1991) indicated that when a core contains pores larger than the core diameter of 8 cm the value measured directly from cores underestimated the porosity by about 3% or more. Thus, core analyses measurements can be considered reliable for the recognition of porosity and permeability trends, but they will tend to underestimate porosity in coarse vuggy carbonates.

Measurements of permeability at simulated reservoir conditions are an order of magnitude lower than similar measurements at ambient pressure (Vavra et. al., 1991), so that measured values represent maximum permeability. Porosity values measured during conventional core analyses do not require adjustment to reflect porosity at reservoir conditions.

Table 3-1 Systematic observations made from core

1) Core number, Box, Depth, Recovery (%)	6) Pore Association Connection Matrix (intercrystalline) Fractures Touching vugs/molds
2) Lithology a) Limestones Texture, fossils, contacts Depositional facies Degree of dolomitization b) Dolostones *Crystal Size Fine: 30-62 μ m Medium: 62-250 μ m Very Coarse: >600 μ m	7) Cements Type: Dolomite Anhydrite Sulphides Sulphur Quartz Reservoir bitumen Calcite Pore Type Degree of Filling Open Partly filled Filled
3) Pore Type Intraskkeletal Fossil Type Intercrystalline Moldic <u>Amphipora</u> <u>Thamnopora-like</u> Vug Fracture Breccia	8) Fractures Orientation Subvertical Subhorizontal Intensity Width, Length Filling
4) Pore Size Very large: >1.0 cm Large: 0.5-1.0 cm Medium: 1.0-5.0 mm Small: 0.1-1.0 mm Very Small: <0.1 mm	9) Breccias Crackle Mosaic Rubble
5) Pore Shape Spherical Tubular Tabular Irregular Polyhedral	

PORE TYPES AND DEFINITIONS

Strachan and Ricinus West are stromatoporoid-coral buildups of Upper Devonian age with generally similar distributions of depositional facies, but different diagenetic overprints (see Chapter 2). These reservoirs behave as somewhat "closed" systems (weak water drive) and thus experienced rapid pressure decline during production. Pressure maintenance in reservoirs is dependent on enhanced recovery methods that are very sensitive to pore structure and arrangement. The following sections focus on the pore types and resulting porosity network within each of these reservoirs, Strachan being partly dolomitized and Ricinus West being completely dolomitized.

The depositional facies and diagenetic processes observed within these buildups were outlined and described in Chapter 2. The primary depositional porosity and permeability have been greatly modified by several processes (see paragenetic sequences in Chapter 2, Figs. 2.5, 2.6) including pressure solution, dolomitization, cementation, dissolution and bitumen plugging. Replacement dolomitization, where present, has created intercrystalline and vuggy porosity. Cementation and dissolution have modified porosity and permeability mostly in the lower part of the reservoirs. Bitumen plugging has decreased porosity and significantly modified permeability in the upper part of the reservoirs. Dolomite content in each depositional facies ranges from 0 to 100%. The depositional facies were grouped into limestones (< 50 volume% dolomite), partly dolomitized limestones (50 to 75 vol% dolomite) and dolostones (> 75 vol.% dolomite, most of which are 100% dolomite).

Pores types are characterized by shape, size, orientation and interconnection (Tables 3.2, 3.3), and are grouped into pore systems using their abundance, association with other pore types and distribution within the buildup. Terminology for the different pore types is taken from Choquette and Pray (1970). Intercrystalline porosity in the matrix is defined as

the spaces between dolomite crystals, except where evidence of dissolution is present and the term vug is appropriate (equivalent to "pinpoint" porosity of McNamara and Wardlaw, 1991). Dense matrix refers to compact crystalline texture (after Archie, 1952). Fracture porosity is described as unfilled, partly filled and filled, since apparently filled fractures may have some permeability when applying a hand-permeameter (Wardlaw 1992, per. com.). Interconnection between pores is described as being fracture-connected, as interconnected vugs/molds, and as matrix intercrystalline porosity (after McNamara and Wardlaw, 1991).




Pore types in limestones

Limestones are present in pool D3B of the Strachan reservoir (wells 5-11, 14-2, 15-4; Fig. 2.1). The facies distribution across pool D3B is illustrated in cross section A-A', constructed using the top of the Calmar Formation as a datum (Fig. 2.2A). Porosity and permeability charts have been included with the facies distribution to show the relation between these reservoir parameters and the depositional facies. Skeletal wackestone facies have the highest porosity values (3.6%, Table 3.4). Average horizontal and vertical permeabilities are very low overall (0.8 and 0.4 md).





The most common pore types in these limestones are, in decreasing abundance, intraskeletal (50-100%), subvertical fractures (5-15%), and vugs (5%, Table 3.2). Intraskeletal pores have spherical shapes in corals (Plate 3.1A), and tabular shapes in stromatoporoid fragments, and are always lined with reservoir bitumen. Interconnection is provided by the intraskeletal framework. Vugs are irregular in shape, small and isolated. Minor subvertical fractures, with irregular surfaces that suggest dissolution, are filled with dolomite cement C₂ (saddle dolomite), bitumen and late-stage calcite (Plate 2.7C).

TABLE 3-2 Pore types in limestone and partly dolomitized strata

LIMESTONES

	PORE TYPE	SYMBOL	SHAPE	SIZE	ORIENTATION	CONNECTION	* DEGREE OF FILLING	CEMENT
FABRIC SELECTIVE	Intraskkeletal		Spherical	50 -100 µm	Parallel to growth structure	connected pores within skeletal fragments	Partly filled	Bitumen
	Corals Stromatoporoids		Tabular				Partly filled	Bitumen
NOT FABRIC SELECTIVE	Vug		Irregular	1 -10 mm	Random	intercrystalline pores in matrix fractures	Partly filled	Bitumen Calcite
	Fracture		Tabular	20-100 mm long	Subvertical	fractures	Partly filled Filled	Dolomite C ₂ Bitumen Calcite

PARTLY DOLOMITIZED

NOT FABRIC SELECTIVE	Intraskkeletal Stromatoporoids		Tabular	50 -100 µm	Parallel to growth structure	connected pores within skeletal fragments	Partly filled	Bitumen
	Intercrystalline		Polyhedral	100 µm	Random	intercrystalline pores in matrix	Partly filled	Bitumen
NOT FABRIC SELECTIVE	Vug		Irregular	5 - 20 mm	Random	intercrystalline pores in matrix fractures	Partly filled	Bitumen Calcite
	Fracture		Tabular	10 - 60 mm long	Subvertical	fractures	Partly filled Filled	Bitumen Calcite



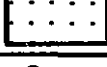






PORE SIZE

Very small < 1 mm
Small: 1 - 5 mm
Medium: 6 - 10 mm
Large: 11 mm - 3 cm
Very large: > 3 cm

*** DEGREE OF PORE FILLING**

Filled: Pore completely filled with cements
Open: No cement present
Partly filled: Some cement present

TABLE 3-3 Pore types in dolostones

	PORE TYPE	SYMBOL	SHAPE	SIZE	ORIENTATION	CONNECTION	* DEGREE OF FILLING	CEMENT
FABRIC SELECTIVE	Intraskelatal		Tabular	50 -100 μ m	Parallel to growth structure	connected pores in skel. fragments	Partly filled	Bitumen
	Fenestral-like		Tabular	2 to 20 mm	Parallel to laminations	intercrystalline pores in matrix	Partly filled	Bitumen
	Intercrystalline		Polyhedra	110 to 250 μ m	Random	fractures	Partly filled	Bitumen
	Moldic: <i>Amphipora</i> -like		Tubular	10 to 20 mm	Random to bedding parallel	touching molds	Open	
	<i>Stromatoporoid</i> -like		Spherical	30 to 60 mm	Random	touching molds intercrystalline	Partly filled	Anhydrite Bitumen
	<i>Thamnopora</i> -like		Tubular	20 to 40 mm	Random	touching molds	Partly filled	Anhydrite Bitumen
NOT FABRIC SELECTIVE	Vug		Irregular	1 to 70 mm	Random	touching vugs fractures	Partly filled	Calcite Anhydrite Quartz
	Fracture		Tabular	40 to 80 mm long	Subvertical	fractures	Partly filled Filled	Bitumen
	Breccia		Irregular	10 to 30 mm	Random	intercrystalline fractures	Partly filled	Bitumen

PORE SIZE

Very small < 1 mm
Small: 1 - 5 mm
Medium: 6 - 10 mm
Large: 11 mm - 3 cm
Very large: > 3 cm

*** DEGREE OF PORE FILLING**

Filled: Pore completely filled with cements
Open: No cement present
Partly filled: Some cement present

Pore types in partly dolomitized limestones

Partly dolomitized limestones are present in pool D3A of the Strachan reservoir (wells 12-31 and 10-31; Fig. 2.1). Facies distribution and relation to porosity and permeability are illustrated in cross section B-B' (Fig. 2.2B). With 50 to 75 vol.% dolomite, all lime matrix is replaced resulting in matrices with variable porosity ranging from porous intercrystalline to dense. Most skeletal fragments and marine cements remain as calcite (Plate 2.9 C). In partly dolomitized limestones porosity is higher than in limestones (Table 3.4). Stromatoporoid-coral rudstone and skeletal wackestone facies have the highest porosity values, 7.7 and 4.9% respectively. Average horizontal and vertical permeabilities are slightly higher than in limestones (1 and 0.1 md).

Pore types include intraskeletal (40-80%), intercrystalline (5-20%), vugs (5%) and subvertical fractures (5-15%). Intraskeletal pores are restricted to stromatoporoid fragments (Table 3.2). Intercrystalline pores are polyhedral in shape and very small (about 100 μm). Small to medium, irregular vugs are common in the dolomitized matrix of all facies (Plate 2.9 D).

Pore types in dolostones

Dolostones are present in pool D3A of the Strachan reef interior (wells 7-32, 11-27, 11-22; Fig. 2.2B), and the Ricinus West buildup. The facies distribution and porosity and permeability values across the Ricinus West reservoir are illustrated in cross sections A-A' and B-B' (Fig. 2.4 A, B). With greater than 75 vol.% dolomite, most of the lime matrix is replaced resulting in a dense dolomite mosaic. Most skeletal grains have been dissolved forming slightly enlarged molds and irregular vugs indicating a genetic relationship between the amount of dolomite and the moldic and vuggy pores (Plate 2.9). These pores likely result from the dissolution of calcite during or after replacement dolomitization. Porosity (up to 8.4% average) and permeability are greater than in limestones and partly

dolomitized limestones (Table 3.4).

These dolostones contain varying amounts of vugs (40-100%), molds (10-60%), fenestral-like (10-30%), intercrystalline (5-15%), fractures and breccias (5 to 10%), and minor (< 1%) solution-enlarged intraskeletal pores (Table 3.3). Vugs show a gradation from solution-enlarged molds to very large (3 to 7 cm) irregular pores that do not show any indication as to their precursor fabric (Plate 3.1F). The most common moldic pores are those produced by selective dissolution of tubular Amphipora fragments (e.g. well 7-32, 4110.6 m; Plate 2.2A,B) in the upper part of the reef interior, referred to as Amphipora-like molds. In the lower part of the buildup interior, molds are commonly after dissolution of domal (spherical) stromatoporoids and tubular Thamnopora fragments (Stromatoporoid-like and Thamnopora-like respectively, Plates 2.3D). Molds after Amphipora and Thamnopora fragments are distinguished on the basis of their size, association with other pore types, and location within the buildup. Smaller pores that are tabular and aligned parallel to laminations (fenestral-like) are considered molds related to microbial laminite facies (Plate 2.2E).

Intercrystalline pores in fine-crystalline dolomite-R₁ (see replacement dolomite textures, Chapter 2), are rare and very small (10 µm; e.g. Ricinus West, well 10-33, 4633.8 m). In contrast, intercrystalline pores in more coarsely crystalline, and more abundant dolomite-R₂ are larger (250 µm; e.g. Ricinus West, well 10-33, 4535 m). Thus, these dolostones show a positive relationship between pore size and crystal size, as has been reported elsewhere for other dolomites (e.g. Lucia, 1983; Choquette, et. al., 1992).

Natural fractures are commonly oriented in a subvertical direction and are partly to completely filled by dolomite cement C1 and reservoir bitumen. Fracture width varies between 1 and 5 mm, and length ranges between 10 and 60 mm. Dissolution along the fractures is indicated by associated solution-enlarged intercrystalline and vuggy porosity

**TABLE 3-4 Porosity and Permeability Values in Limestones,
Partly Dolomitized Rocks and Dolostones**

Depositional Facies	Porosity			Kh (md)			Kv (md)			N
	Ar	Min	Max	Geo	Min	Max	Geo	Min	Max	
LIMESTONES										
STRACHAN BUILDUP MARGIN										
Stromatoporoid Floatstone	N/A			N/A			N/A			
Skeletal Wackestones	3.6	0.5	7.1	0.8	0.01	16.2	0.4	0.01	6.4	82
Tabular Stromatoporoid Boundstone	2.3	0.3	8.6	0.1	0.01	360	0.02	0.01	6.5	92
Stromatoporoid Coral Rudstone	2.6	0.3	15.4	0.1	0.01	2.1	0.01	0.01	74	179
Coral Rudstone	3.0	0.4	29.0	0.3	0.01	247	0.01	0.02	55	95
PARTLY DOLOMITIZED										
STRACHAN BUILDUP MARGIN										
Stromatoporoid Floatstone	N/A			N/A			N/A			
Skeletal Wackestones	4.91	2.0	8.0	0.21	0.01	20.7	0.02	0.01	11.5	8
Tabular Stromatoporoid Boundstone	3.5	0.3	9.2	1.1	0.01	7	0.1	0.01	9.8	74
Stromatoporoid Coral Rudstone	7.7	0.1	16.8	N/A	0.01	N/A	0.1	0.01	6.6	26
Coral Rudstone	4.5	0.5	9.9	2.2	0.03	82	1.0	0.01	147	41
DOLOSTONES										
STRACHAN BUILDUP INTERIOR										
Skeletal Wackestones	8.4	0.5	26	7.0	0.1	370	1.0	0.12	19	143
Skeletal Packstones/Grainstones	7.1	4.8	12.6	15.0	1.2	396	5.1	0.43	367	13
RICINUS WEST MARGIN										
Tabular Stromatoporoid Boundstone	6.3	1.6	12.4	16.7	0.2	384	3.7	0.01	129	195
Skeletal Wackestones	7.1	2.0	15.1	15.8	0.9	725	2.5	0.01	65	134
Stromatoporoid Floatstone	7.7	2.0	15.3	27.9	1.9	501	2.4	0.2	38	89
Coral Rudstone	6.6	3.0	12.4	18.5	2.3	262	2.0	0.2	28.4	30
Breccias	6.5	3.3	12.0	21.1	1.7	525	1.5	0.2	9.6	19
RICINUS WEST INTERIOR (UPPER PORTION)										
Microbial Laminites	6.2	0.9	13.8	15.6	0.7	900	2.8	0.01	96	154
Skeletal Wackestones	7.9	1.5	20.7	11.1	0.1	947	1.5	0.01	221	184
Skeletal Packstones/Grainstones	6.1	1.3	15.0	9.5	0.06	753	1.9	0.01	142	313
RICINUS WEST INTERIOR (LOWER PORTION)										
Stromatoporoid Floatstone	6.0	0.6	15.5	12.7	0.1	764	1.7	0.01	100	228
Coral Rudstone	5.6	1.0	15.2	11.9	1.6	418	1.5	0.01	41	70

Limestones = <50 Vol% Dolomite
Partly Dolomitized = 50-75 Vol% Dolomite
Dolostone = >75 Vol% Dolomite

Ar = Arithmetic Mean
Geo = Geometric Mean
Kh = Horizontal Permeability (in millidarcies)
Kv = Vertical Permeability (in millidarcies)
Max = Maximum
Min = Minimum
N = Number of Values

Plate 3.1 PORE TYPES IN THE STRACHAN AND RICINUS WEST
RESERVOIR

- A) Spherical intraskeletal pores in a coral fragment. 15-2-38-10W5, 4113.4 m.
- B) Polyhedral intercrystalline pores in replacement dolomite R₂. Note lining by reservoir bitumen (black). Plane light. 15-23-36-10W5, 4488.4 m. Scale bar 50 μ m.
- C) Tabular stromatoporoid boundstone facies: Tabular stromatoporoids with solution enlarged intraskeletal pores (arrows) lined with reservoir bitumen. Note vugs filled with calcitized anhydrite. 7-13-36-10W5, 4621.3 m.
- D) Microbial laminite dolostones with irregular vugs in a tight matrix. Note lining by reservoir bitumen (black). Plane light. 11-27-36-10W5, 4490.8 m. Scale bar 250 μ m.
- E) Tubular moldic pores probably after Thamnopora fragments in a tight matrix. Some fractures (arrow) connect the molds.
- F) Large irregular vugs in replacement dolomite R₂. 12-31-37-9W5, 4295 m.
- G) Intercrystalline porosity closely related to partly filled subvertical fracture. 10-33-36-10W5, 4621.6 m.

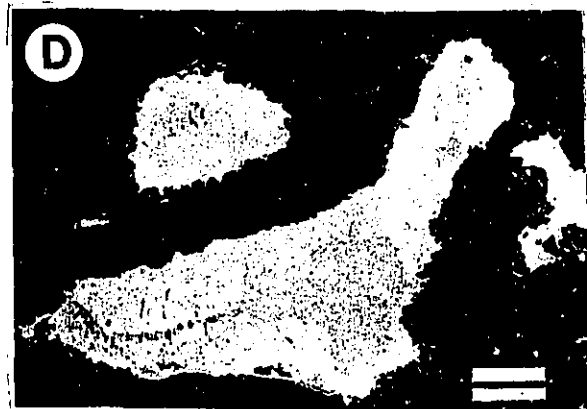
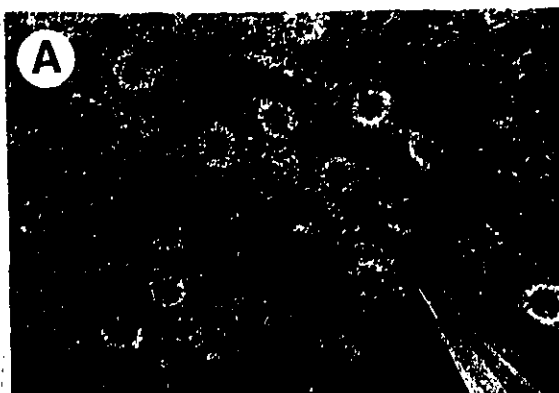


(Plate 3.1G). Brecciated intervals range from isolated occurrences to zones several meters thick in the Ricinus West margin (e.g. well: 7-13). Breccias are characterized by cm-sized dolomite clasts with crackle, moldic and rubble textures that are likely the result of solution collapse. Matrices in the moldic breccias have intercrystalline porosity (Plate 2.3). Similar pore types are recognized in dolomitized buildups (e.g. Westrose, Homeglen-Rimbey) along the Rimbey-Meadowbrook reef trend (McNamara and Wardlaw, 1991; Drivet, 1993).

PORE SYSTEMS IN DOLOSTONES

To evaluate the reservoir characteristics of dolostone buildups in the deeper part of the Alberta basin, the different pore types in the completely dolomitized Ricinus West buildup were grouped into pore systems in order to determine their relationship to depositional facies. A pore system is an arrangement of pores that may or may not be interconnected in a regularly repetitive fashion (Ghosh and Friedman, 1989). In order to characterize a pore system, it is necessary to determine the sizes and shapes of the pores, their interconnectivity, and the roughness of pore surfaces which are directly observable from the rocks. Other properties, such as porosity and permeability, pore/throat size ratios, and the number of throats per pore, must be measured in the laboratory (see methods in Ghosh and Friedman, 1989). In this study the pore systems are defined according to pore size and shape, orientation, interconnection, association with other pore types, relationship to depositional facies, distribution within the buildup and core porosity and permeability. Three major pore systems are present in Ricinus West: I) moldic/intercrystalline, II) connected molds, and III) random vugs/breccias.

Pore system I: moldic/intercrystalline

Three basic pore types constitute this system: 1) moldic (Amphipora-like) 2) intercrystalline, and 3) fenestral-like pores (Plates 2.2, 2.3). Moldic (Amphipora-like)

pores are tubular, large to very large (Table 3.3), and randomly oriented in a dense matrix. Effective communication is provided by interconnected molds. Intercrystalline pores are small and polyhedral in shape and are well-connected. They are commonly lined by thin (1 to 4 μm) coats of reservoir bitumen. Fenestral-like pores are small, tabular in shape and oriented parallel to laminations. These pores are interconnected through intercrystalline pores in the matrix. Pore system I occurs in the upper part of the Ricinus West interior (Fig. 2.4B). Total porosity of pore system I ranges from 0.9 to 20.7% (mean: 6.3%). Horizontal permeability varies between 0.06 and 2000 md (geometric mean: 12.7 md), and vertical permeability ranges from 0.01 and 861 md (geometric mean: 1.2 md, Table 3.5).

Pore system II: connected molds

Three basic pore types also form this pore network: 1) moldic (stromatoporoid-like), 2) intercrystalline, and 3) moldic (Thamnopora-like). It differs from pore system I in that it contains larger and more abundant molds of skeletal fragments. Moldic (stromatoporoid-like) pores are very large, spherical and randomly oriented in a dense matrix. These pores have the form, and appear to be related to the dissolution, of domal and bulbous stromatoporoids. Interconnectivity is provided by touching molds. Intercrystalline pores are similar to those of pore system I. Very large, randomly oriented tubular pores, probably dissolved corals (Thamnopora-like), are common in a dense matrix. Pore system II occurs in the lower and interior part of the buildup. Total porosity of pore system II varies between 0.6 and 19.1% (mean: 6.1%). Horizontal permeability ranges from 0.1 to 1400 md (geometric mean: 13.1 md), and vertical permeability from 0.01 to 843 md (geometric mean: 1.8, Table 3.5).

Pore system III: random vugs and breccias

Vugs, breccias, and intercrystalline porosity (in decreasing abundance) form the porosity network in pore system III. Interconnection is commonly provided by fractures

TABLE 3-5 Pore Systems in the Ricinus West Buildup

Pore System	Pore Types	Porosity (%)			Kh (md)			Kv (md)			N	Thickness (m)	Distribution Within Buildup
		Ar	Min	Max	Geo	Min	Max	Geo	Min	Max			
I. Moldic Intercrystalline	Moldic Amphipora-like Intercrystalline Fenestral like	6.3	0.9	20.7	12.7	0.06	2000	1.2	0.01	861	751	131	Upper Buildup Interior
II. Moldic Skeletal Framework	Moldic Pores (Stromatoporoid-like) Intercrystalline Moldic (Thamnopora-like)	6.1	0.6	19.1	13.1	0.1	1400	1.8	0.01	834	294	61	Lower Buildup Interior
III. Random Vugs/Breccias	Irregular Vugs Breccias Intercrystalline	6.9	1.6	15.3	19.4	0.2	2100	2.8	0.01	141	448	259	Reef Margin

Ar = Arithmetic Mean
Geo = Geometric Mean
Kh = Horizontal Permeability (in millidarcies)
Kv = Vertical Permeability (in millidarcies)
Max = Maximum
Min = Minimum
N = Number of Values

and some interconnected vugs. Pore system III is only present along the margin of the Ricinus West buildup (well 7-13). Total porosity ranges from 1.6 to 15.3% (mean: 6.9%). Horizontal permeability ranges from 0.2 to 2100 md (geometric mean: 15.3 md), and vertical permeability from 0.01 to 141 md (geometric mean: 2.8 md).

Distribution of pore systems: Large scale (tens of meters to kilometre)

The relationship between facies, pore types, porosity and permeability and pore systems are shown in cross-sections A-A' and B-B' (Figs. 2.4A,B, see Chapter 2). There is a good correspondence between pore systems and depositional units. Over the entire Ricinus West reservoir (tens of meters to kilometres), the distribution of these pore systems subdivide the Ricinus West buildup into three different porosity and permeability zones closely related to the depositional units (Fig. 3.1A). Pore system I dominates in the upper 131 m of the reef interior, whereas reservoir traits of the lower 61 m of the reef interior are influenced mainly by pore system II. Pore system III occurs along the 259 m thick margin of the reservoir. Porosity and permeability data from each of these pore systems within the Ricinus West reservoir indicates the lack of large-scale variability in these parameters since the average porosity is 6% in all pore systems with permeabilities being slightly higher in the reef margin versus the reef interior (see Table 3.5).

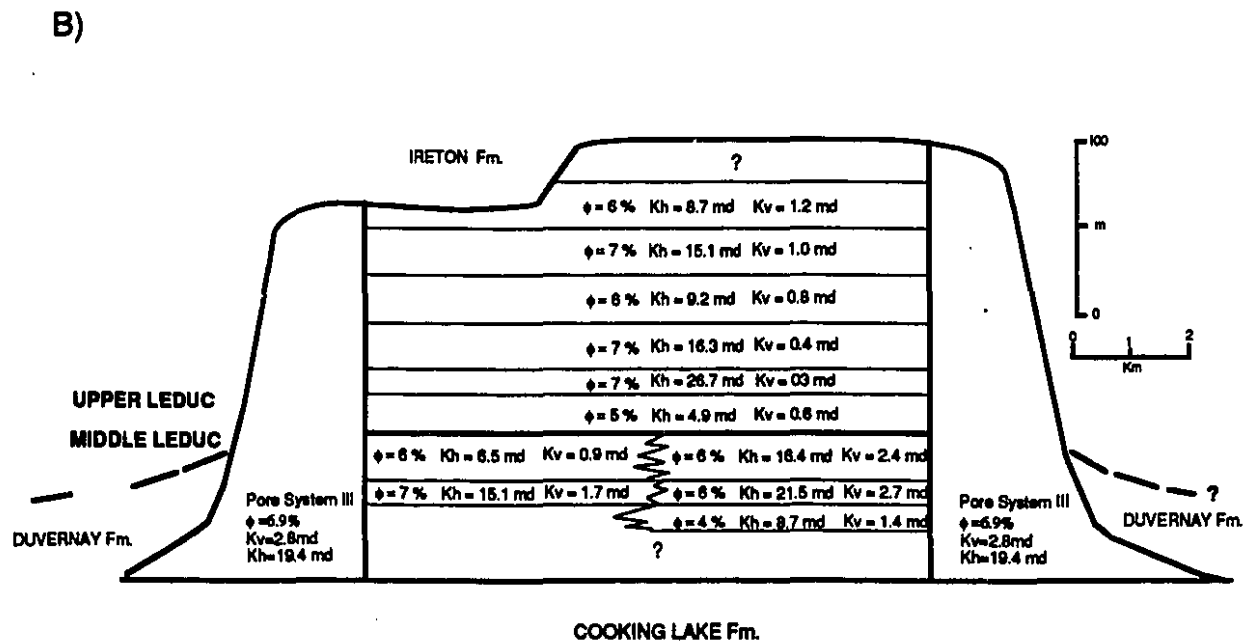
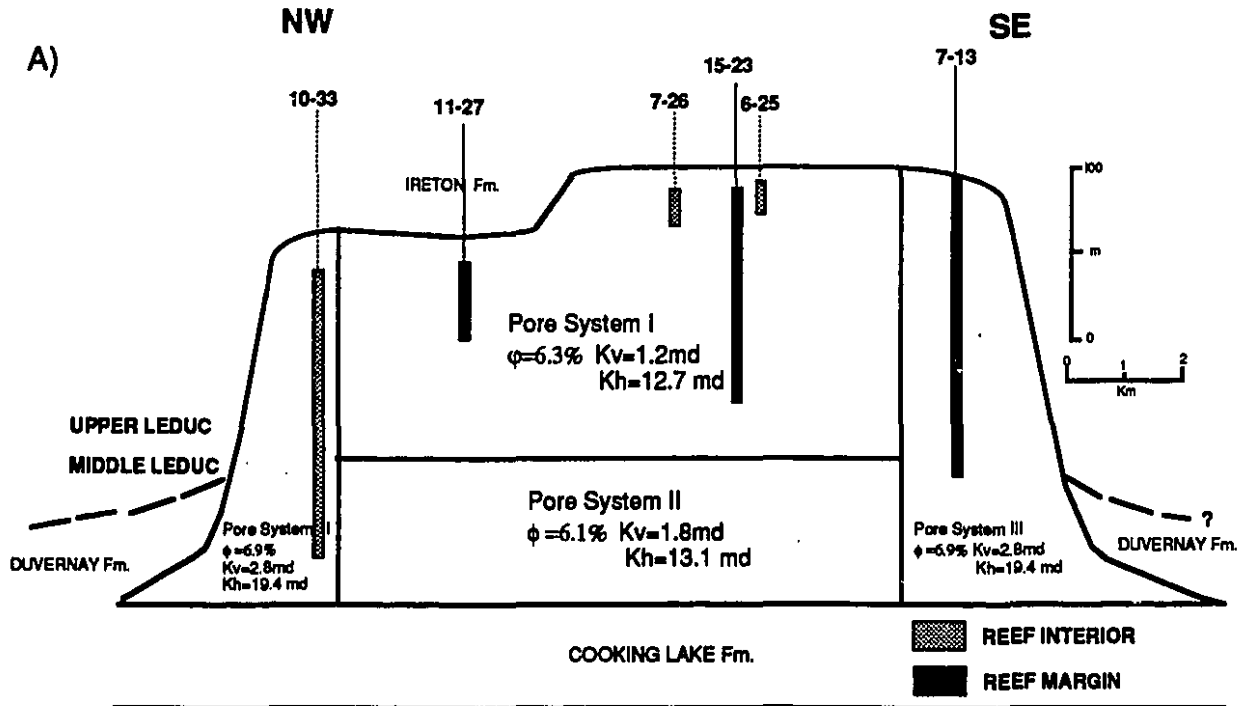
Hydrocarbon flow, however, will be different in each pore system since pore types and their arrangement are different thus affecting the petrophysical properties of the reservoir. This is discussed at the medium scale of meters to tens of meters in which the vertical and lateral arrangement of the dominant pore types vary considerably within a pore system and thus have a significant control on reservoir character.

Figure 3.1: Subdivisions of the Ricinus West buildup according to

A) Pore systems I, II and III. Average porosity (6%) distribution at this scale is similar throughout the entire reservoir. Horizontal and vertical permeabilities are slightly higher in pore system III.

B) Pore types, depositional facies and porosity and permeability. Pore type I is subdivided into 6 zones ranging in thickness between 8 and 27 m. Horizontal permeability in each zone is high but vertical permeabilities are low. See Fig. 2.4A for details of pore types and depositional facies. Pore system II is porous and permeable but laterally discontinuous. Pore system III is thick and has greater vertical permeability but is restricted to the buildup margin.

RICINUS WEST



Porosity and permeability variability within pore systems: Medium scale (meters to tens of meters)

Reservoir interconnection is the most important parameter in reservoir studies (e.g. Van de Graff and Ealey, 1989). Reservoir interconnection is related to the presence and distribution of internal vertical and horizontal changes in permeability. These changes in permeability are plotted in vertical profiles for each pore system (Figs. 3.2, 3.3 and 3.4). Horizontal permeability data have a wide range of values and therefore have arbitrarily been grouped into high (> 200 md), medium (10 and 200 md) and low (<10 md). Vertical permeabilities greater than 10 md are considered high.

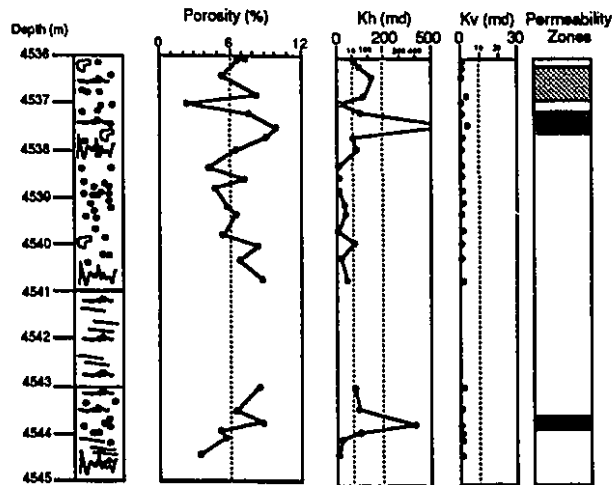
In pore system I the vertical succession of Amphipora-like molds, fenestral-like and intercrystalline pores resemble the shallowing upward depositional sequences developed in the upper reef interior (see Chapter 2). These sequences range in thickness between 8 and 27 m (see well 10-33 in Fig. 2.4A). The vertical permeability profiles in Figure 3.2 show that in a 27 m thick sequence containing Amphipora-like (Fig. 3.2A), fenestral-like (Fig. 3.2B), and intercrystalline pores (Fig. 3.2C, see Fig. 2.4A in Chapter 2 for location of this sequence), thin (1 to 2 m), high horizontal permeability zones, are separated by thicker intervals (2 to 5 m) of lower permeability. This indicates that within each sequence vertical interconnection is poor and that horizontal interconnection is provided by relatively thin zones. Slightly thicker permeability zones occur where the intercrystalline pore type is dominant. Based on cross sections A-A' and B-B' (Figs. 2.4A, B), depositional models for limestone buildups (e.g. McGillivray and Mountjoy, 1975) and outcrop studies of equivalent strata (e.g. McLean, 1992), these depositional sequences are extensive and laterally continuous. Pore system I is characterized by 6 sequences 8 to 27 m thick of different pore types that closely follow the depositional sequences, with poor vertical interconnection and thin, laterally continuous, highly permeable horizontal zones.

- Figure 3.2:** Examples of permeability zones in a 27 m thick sequence with dominant pore types in pore system I, upper Ricinus West buildup interior (well 10-33, see Fig. 2.4A for location of sequence). Thin, high permeability zones are separated by thicker zones with lower permeability.
- A) Moldic (Amphipora-like) pores in skeletal packstone and grainstone facies.**
 - B) Fenestral-like pores in microbial laminite facies**
 - C) Intercrystalline pores in skeletal wackestone facies**

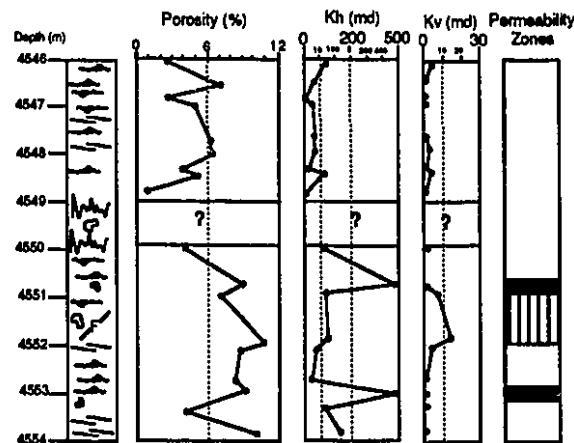
Pore System I

Well: 10-33

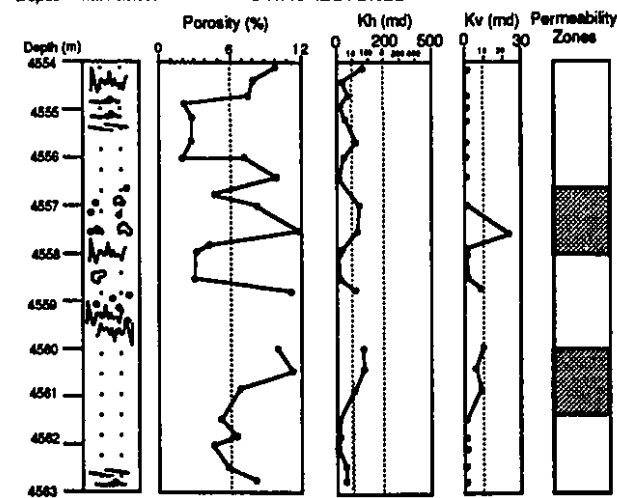
a) Depositional Facies: SKELETAL PACKSTONES/GRAINSTONES



b) Depositional Facies: LAMINITES



c) Depositional Facies: SKELETAL WACKESTONES



In pore system II vertical permeability is slightly higher (Fig. 3.3A,B). Horizontal permeability zones are slightly thicker where Thamnopora-like molds dominate (Fig. 3.3B) with connectivity provided by touching molds. From previous studies (e.g. McGillivray and Mountjoy, 1975, McLean, 1992) facies associated with stromatoporoid and coral molds are known to be laterally discontinuous. Pore system II consists of thin laterally discontinuous porous and permeable zones.

In pore system III vertical permeability is common and associated with subvertical fractures (e.g. Fig. 3.4, 4423 m) and touching vugs (e.g. Fig. 3.4, 4439 m). Horizontal permeability zones are thin (< 1 m) and laterally discontinuous. Brecciated intervals are common in the reef margin that contribute to reservoir interconnection (see cross section B-B', Fig. 2.4B). Thus, pore system III is characterized by thick intervals where vertical permeability predominates. This is similar for the Homeglen-Rimbey buildup margin (Drivet, 1993).

At the scale of meters to tens of meters each pore system within the Ricinus West reservoir shows several high to medium permeability intervals separated by lower permeability zones (Figs. 3.2, 3.3, 3.4 and Appendix H). Laterally continuous, and slightly thicker high horizontal permeability zones are associated with intercrystalline pore types in pore system I. In pore system II, higher permeability zones are related to Thamnopora-like pores that are laterally discontinuous. Vertical permeability zones are common in pore type III. Vertical permeability profiles indicate that the Ricinus West reservoir can be further subdivided into thinner facies and porosity-permeability slices as indicated in Figure 3.1B. In the reef interior, a lower sequence with laterally discontinuous permeable zones is overlain by a stacked sequence of thin laterally continuous permeable zones with poor vertical interconnection. In the reef margin thick, laterally discontinuous zones are characterized by higher vertical permeability.

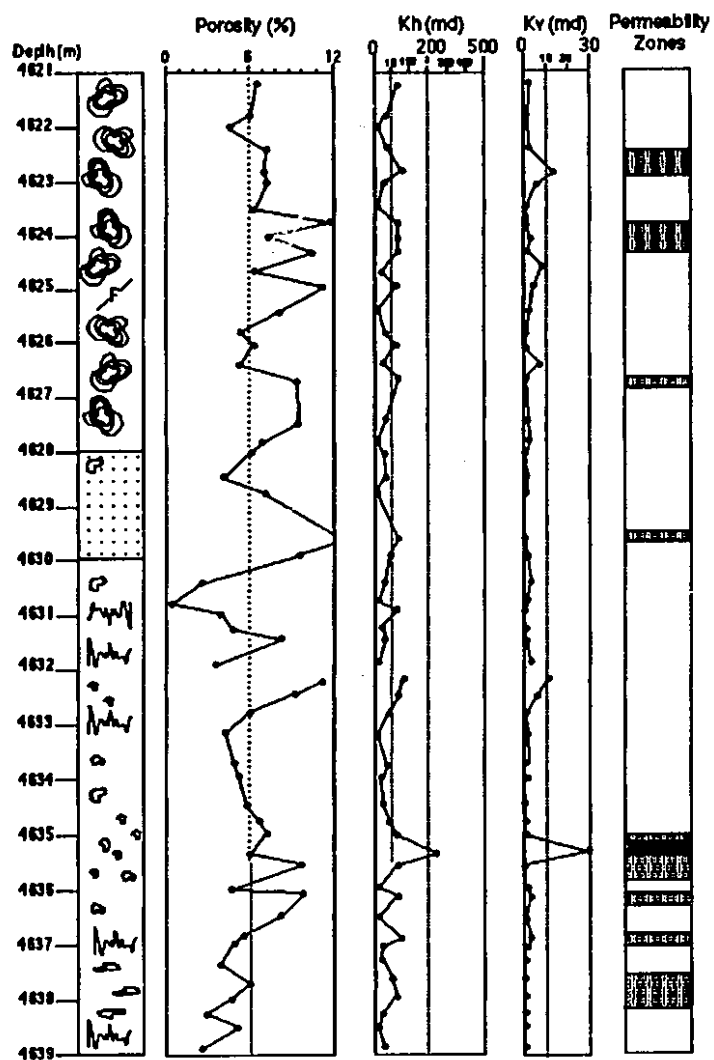
- Figure 3.3: Examples of permeability zones in pore system II, lower Ricinus West buildup interior (well 10-33, see Fig. 2.4A for location of sequence). Higher permeability zones are thicker in coral rudstone facies with abundant Thamnopora-like pores.
- A) Stromatoporoid-like molds in stromatoporoid floatstones/rudstone
 - B) Thamnopora-like molds in coral rudstone facies

Pore System II

Dominant Pore Type: Stromatoporoid-like molds

Well 10-33

a) Depositional Facies: STROMATOPOROID FLOATSTONES/RUDSTONES



Dominant Pore Type: Thamnopora-like molds

Well 10-33

b) Depositional facies: CORAL RUDSTONES

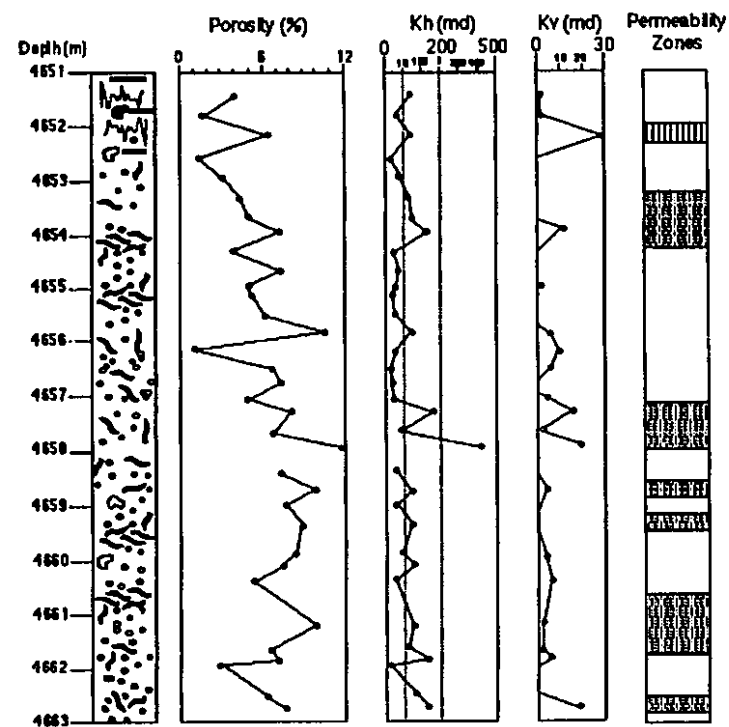
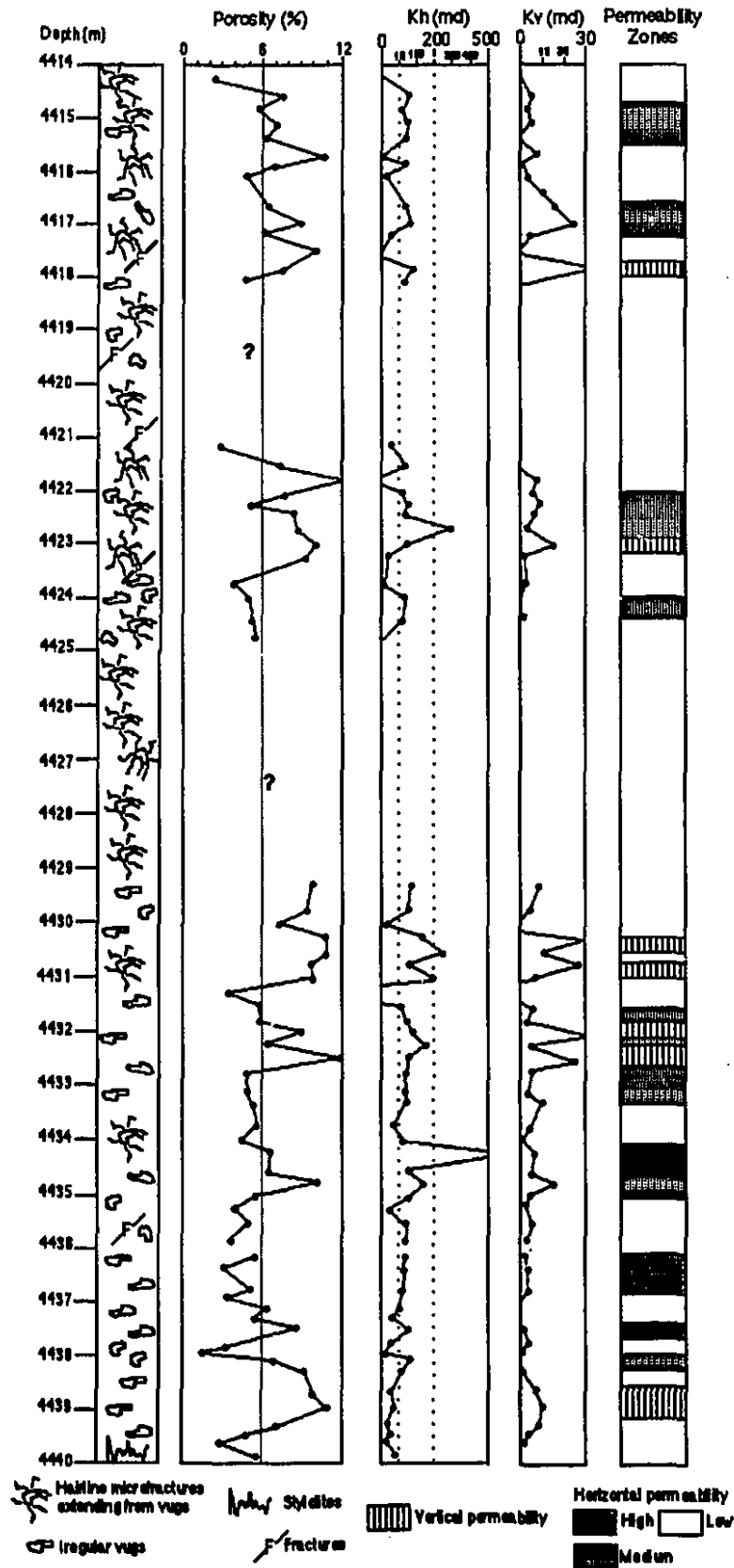


Figure 3.4: Examples of permeability zones in pore system III, Ricinus West buildup margin (well 7-13, see Fig. 2.4B for location of sequence). In the lower 11 m vertical permeability is provided by touching vugs and some fractures. In the upper 15 m vertical permeability is dominated by partly open subvertical fractures.

Pore System III

Dominant Pore Type: Vugs/Breccias
Well 7-13

Depositional Facies: TABULAR STROMATOPOROID BOUNDSTONES



Porosity and permeability variability related to pore types: Small scale (m to mm)

At this small scale, permeability is largely dependent on diagenetic controls. In intercrystalline pores (Fig. 3.2C) of pore type I the presence of 10 to 15% reservoir bitumen (Table 3.7) sufficiently lines most pore throats and thus greatly reduces the porosity and permeability. In stromatoporoid-like and Thamnopora-like molds of pore system II (Fig. 3.3) bitumen is less abundant (about 2%) and permeability is controlled by the presence of minor dolomite, anhydrite and calcite cements. In vugs of pore system III bitumen-filled hairline microfractures (see Chapter 4) are abundant in the upper part of the reservoir and therefore porosity and permeability is mainly controlled by the presence of subvertical fractures and vugs. In the lower part touching vugs with minor bitumen and cements and some fractures provide vertical permeability. The effects of reservoir bitumen, cementation and dissolution are discussed later.

COMPARISON WITH OTHER RESERVOIRS

In pool D3A of the Strachan reservoir, porosities and permeabilities are higher in the interior of the buildup, where the strata are completely dolomitized. In the reef margin porous and permeable dolostones are interbedded with non-porous, non-permeable limestone facies. The presence of porous and permeable facies are related to the degree of dolomitization, with the highest porosity and permeability values occurring in the completely dolomitized facies. Limestones in pool D3B have much lower average porosities (mean 2.9%) and permeabilities compared to dolostones. Also equivalent limestone facies in the Golden Spike buildup (1600 m present depth) have much higher porosities and permeabilities (Table 3.6). This dramatic decrease of porosity and permeability in the limestone buildup (Strachan) is primarily the result of pressure solution during an additional 2 km of burial, together with late stage cements.

The entire Ricinus West reservoir has similar average porosities and permeabilities

throughout, irrespective of pore systems. The reef margin has the most favourable vertical permeability due to the presence of thick intervals of connected vugs, and fractured and brecciated dolomites. The upper reef interior has lower vertical permeability, but the best laterally continuous horizontal permeability intervals, up to 2 m thick. The lower reef interior has the least favourable lateral continuity. This distribution of porous and permeable zones within the dolomitized Ricinus West buildup is different from that of the Westerosé buildup in the central part of the Rimbey-Meadowbrook reef trend (McNamara and Wardlaw, 1991) where the highest porosity and permeability rocks occur in the lower portion of the reef interior. This appears to be due to differences in the primary facies distribution in the Westerosé buildup since it is small (1.6 km by 5.5 km and 214 m thick) compared to the Ricinus West (9.5 by 4 km and 259 m thick). However, the main differences may be related to differences in the approach used to group the porosity and permeability data. In Ricinus West distribution of pore types closely follows depositional sequences (Fig. 2.4A, B) and subdivides the reservoir into three main zones. The upper reef interior, is characterized by porous and permeable, laterally continuous slices that range in thickness between 8 and 27 m indicating that arbitrary subdivision into layers of equal thickness as was done in the analysis of Westerosé are not realistic. The lower reef interior consists of laterally discontinuous, porous and permeable slices that range between 15 and 30 m thick and indicates that layers can not be considered laterally continuous throughout the reservoir. The reef margin is thick, laterally discontinuous with porous and permeable zones controlled by fractures and brecciated intervals.

Therefore, although porosity and permeability are related to depositional and diagenetic patterns, these patterns vary from reef to reef depending on their depositional and diagenetic history. The approach used for characterizing reservoir properties and for classification of porosity and permeability and pore systems is also critical. The approach used is often one of broad-scale lumping of horizontal slices and blocks having similar

Table 3.6: Porosity and Permeability in limestone buildups along the Rimbey Meadowbrook reef trend

	*GOLDEN SPIKE (< 2000 m)		STRACHAN (Pool D3B) (> 4000 m)		
	Depositional facies	Porosity Mean (%)	Permeability (kh = md)	Porosity Mean (%)	Permeability (kh = md) Permeability (kv = md)
Reef Margin	Coral Rudstones	4	1	3	0.3 0.01
	Tabular stromatoporoid Boundstones	5.5	10	2.3	0.1 0.02
	Stromatoporoid Coral Rudstones	10	100	2.6	0.1 0.01

*From: Walls and Burrowes (1985)

**TABLE 3-7 Effect of reservoir bitumen on porosity and permeability
in dolomitized skeletal wackestone facies, Ricinus West reservoir**

Well: 10-33-36-10W5

Dominant pore types	Depth (m)	Sample length (m)	ϕ^{**} (%)	Kh ^{**} (md)	Kv ^{**} (md)	Reservoir [*] bitumen (%)	Pre-Bitumen ϕ (%)	ϕ Reduction (%)	Comments
Intercrystalline (10 to 250 μ m)	4532.6	0.18	7.7	25.7	5.1	10	17.7	56.4	optical textures see Appendix C
	4561.5	0.30	5.2	2.1	0.1	15	20.2	74.2	Some larger vugs (2 cm)
Small vugs (1 to 5 mm)	4601.0	0.18	2.9	1.6	0.1	10	12.9	77.5	Interbedded with microbial laminites
	4601.5	0.34	6.5	12.1	0.4	10	16.5	60.6	Pores oriented parallel to laminations
Some fractures (Filled with bitumen)	4601.6	0.42	6.9	4.4	0.1	10	16.9	59.1	Interbedded with microbial laminites
	4628.9	0.36	7.8	9.6	1.5	2	9.2	15.2	Interbedded with domal stromatoporoid floatstones

Well: 11-27-36-10W5

Intercrystalline (10 to 250 μ m)	4478.0	0.30	8.3	5.8	1.1	10	18.3	54.6	
	4478.3	0.25	11.3	45.8	24.8	1	12.3	8.1	1% bitumen in a patch in center of sample
Small vugs (1 to 5 mm)	4478.5	0.24	7.7	3.1	0.6	10	17.7	56.4	
	4478.8	0.16	7.5	3.7	0.1	10	17.5	57.1	
Some fractures (Filled with bitumen)	4478.9	0.18	8.3	2.9	0.1	10	18.3	54.6	

* Visual estimation

** ϕ Kh Kv data from ERCB files

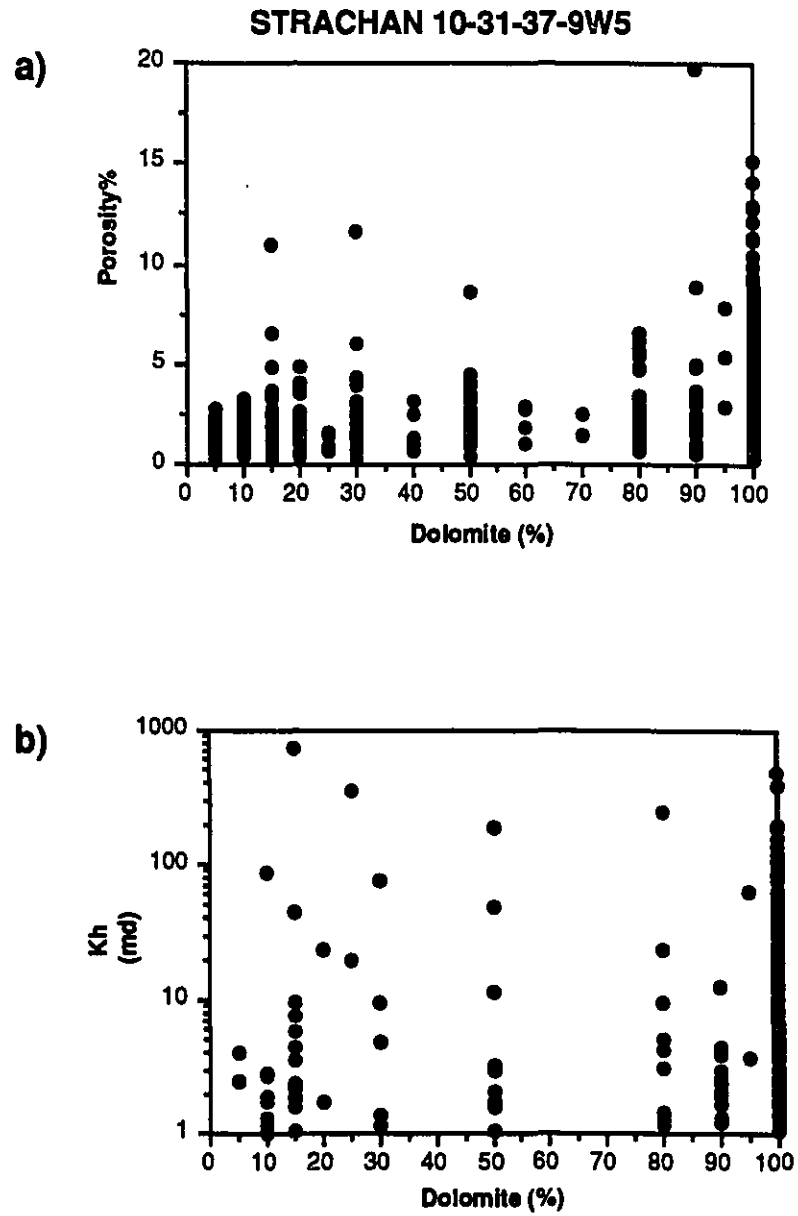
porosities. A reservoir description that closely follows the geology of the reservoir, as the one used here for the Ricinus West buildup, provides a much more realistic and accurate subdivision of the reservoir properties. This can not be performed unless the dolomitized facies and pore types are thoroughly documented by means of careful core observations.

POROSITY AND PERMEABILITY DISTRIBUTION

Based on statistical analysis of porosity data, Devonian limestone buildups of Western Canada have similar or higher porosities than their dolomitized counterparts, in the shallower part of the basin (Walls and Burrowes, 1985, 1989). Anthor et. al. (1994) considered the effect of burial on porosity and permeability in the Leduc buildups along the Rimbey Meadowbrook reef trend (partly based on data from this study), and determined that at shallow burial depths (< 2000 m) dolostones are generally less porous than limestones, but in the deeper part of the basin (> 4000 m) most dolostones are more porous than limestones at similar depths. Data presented here from the deeper buried Strachan and Ricinus West buildups also indicate that dolostones are more porous and permeable than limestones at equivalent depths, and show in more detail the complex factors that control porosity and permeability in these deep reservoirs.

In the Strachan buildup, porosity and permeability data (Table 3.4) show that dolostones have higher porosity and permeability than limestones irrespective of the depositional facies. The effects of increasing amounts of dolomite, ranging from 5 to 100%, on the porosity and permeability of the different depositional facies in well 10-31 located in the partly dolomitized margin of the Strachan reservoir are shown in Figure 3.5. Although there is no obvious trend between amounts of dolomite and porosity, higher porosity values are observed in the 90 to 100% dolomite. This is at variance with the results of some previous studies (e.g. Powers, 1962) which show a marked increase of porosity above 50 to 80% dolomite followed by a sharp decrease above 85% dolomite.

Figure 3.5: Porosity (a) and permeability (b) versus dolomite content in all depositional facies of the Strachan well 10-31 (pool D3A, see Fig. 2.2B for location and facies distribution)

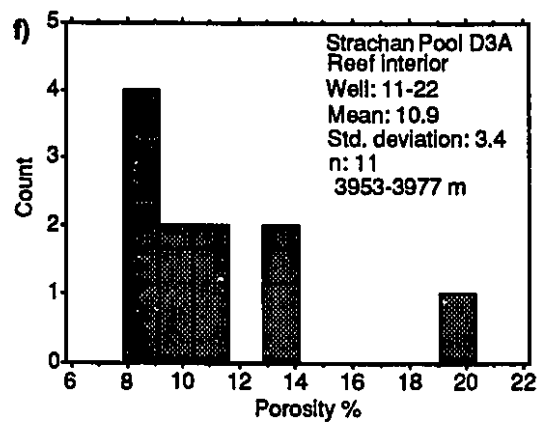
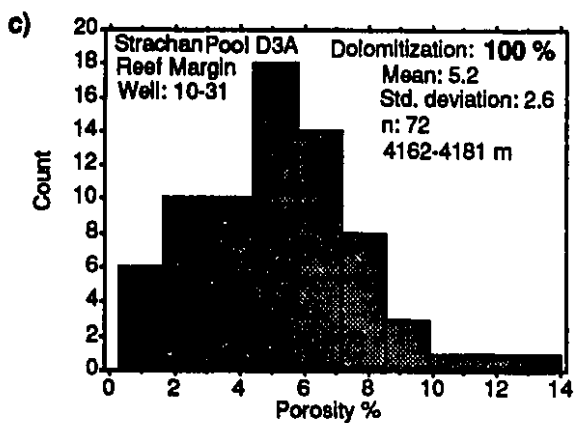
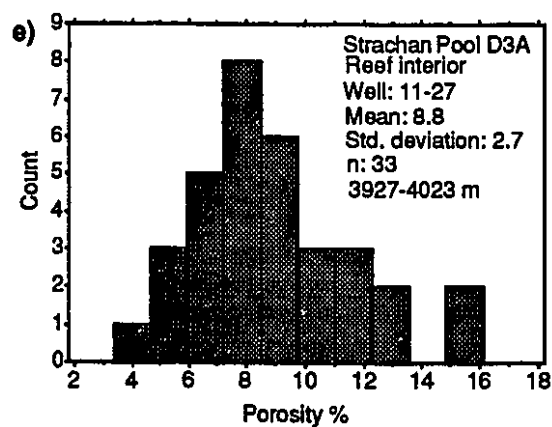
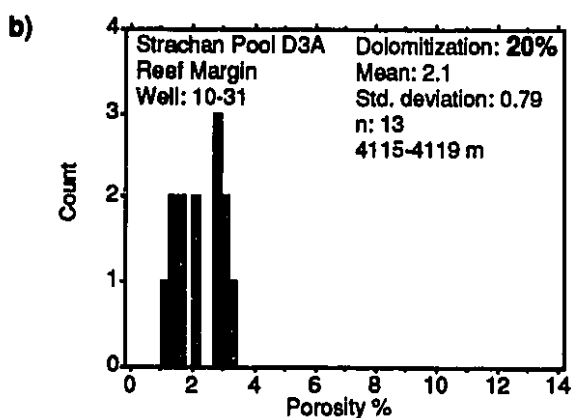
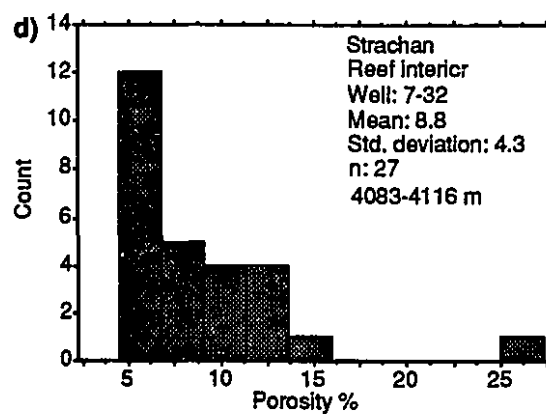
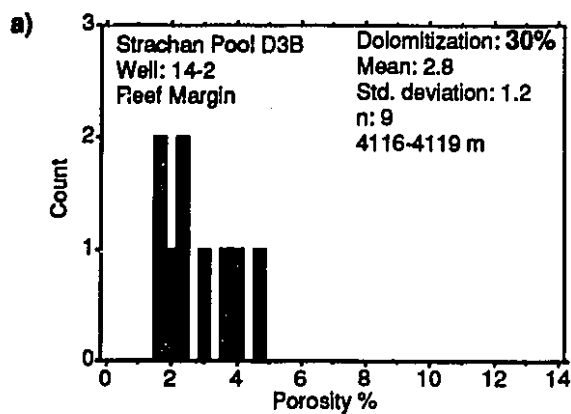


Post dolomitization diagenesis, such as dissolution, late-stage cementation or bitumen emplacement, will modify the relationship between the extent of dolomitization and porosity and, therefore, the complex relationships between dolomite and porosity cannot be determined with certainty in such complexly modified reservoir rocks. These late-stage features occurred after dolomitization and thus the porosities of these completely dolomitized rocks would be even higher.

Dolomitization and porosity

The degree of dolomitization in skeletal wackestones facies was investigated (Fig. 3.6) to examine the effects of dolomitization on porosity, and minimize other diagenetic effects. Skeletal wackestones are chosen as they have the most homogeneous depositional texture and are the most widespread facies throughout the buildups. In addition, except for the presence of about 10% reservoir bitumen, other late-stage diagenetic products such as dissolution vugs and late calcite are minor in these wackestones. Skeletal wackestones with less than 50 vol.% dolomite have porosities ranging from 1 to 5% (mean: 2.4%, Fig. 3.6A, B). Completely dolomitized skeletal wackestones range in porosity from 0.5 to 14% (mean: 5.2%, Fig. 3.6C). Thus porosity increases, on average, by about 50% in completely dolomitized facies. Completely dolomitized skeletal wackestones in the reef interior of pool D3A (Fig. 3.6 D-F) have the highest porosities in the entire buildup ranging from 3.4 to 20% (mean: 9.8%). This appears to be the result of dissolution (D_1) of calcitic skeletal fragments that was either associated with dolomitization or occurred later. The increased abundance of molds, solution-enlarged molds and irregular vugs and porosity may not necessarily be related to dolomitization itself, but may in part be due to later solution events (see paragenetic sequence in Chapter 2).

Figure 3.6: Histograms of porosity data in skeletal wackestone facies in the Strachan buildup showing variability of porosity in:
A), B), Limestones (< 50 vol.% dolomite content) in the reef margin (pools D3B and D3A).
C) Dolostones (> 75 vol.% dolomite content) in the reef margin (pool D3A)
D), e), f), Dolostones in the reef interior (pool D3A).
See Fig. 2.2A, B for locations.



Dolomitization and permeability

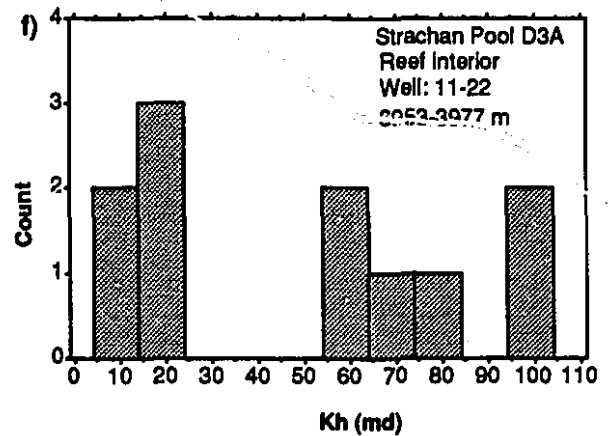
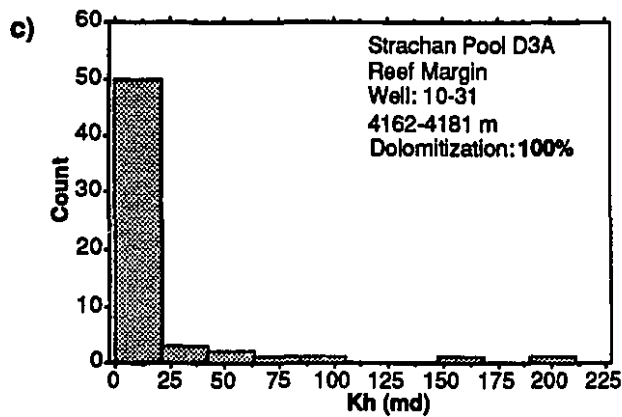
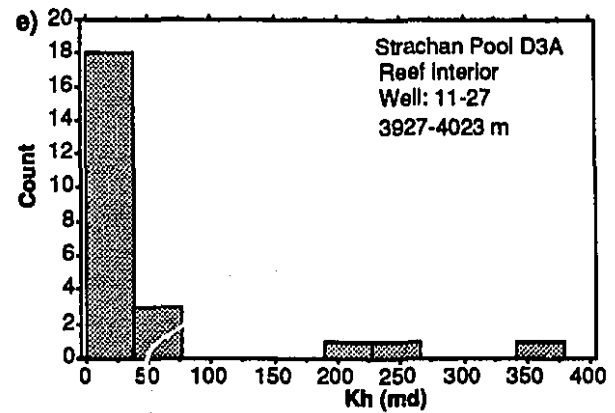
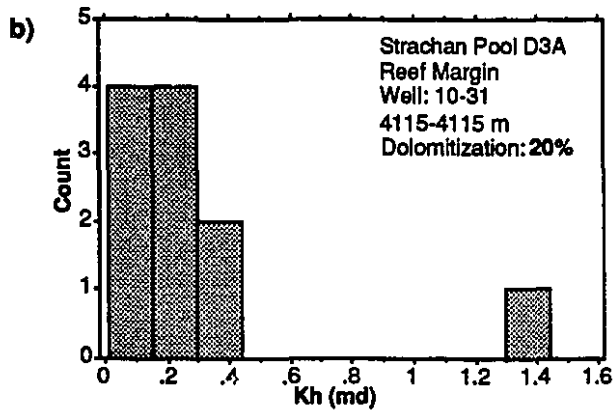
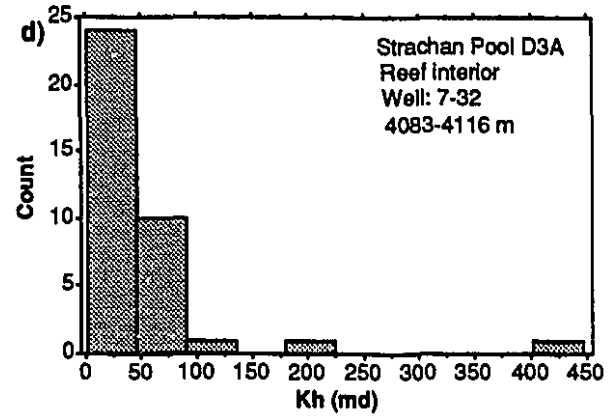
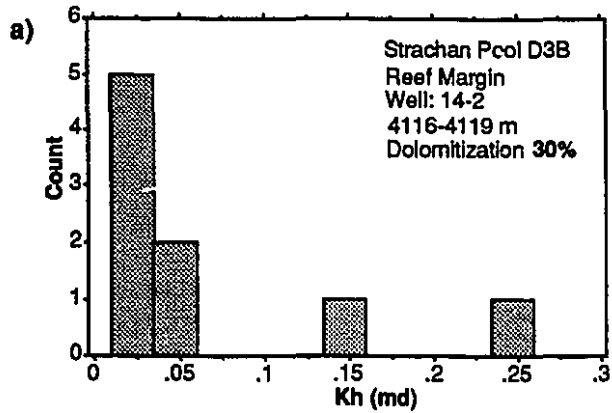
The effect of dolomitization on permeability, the most important reservoir parameter, is relatively straightforward (Table 3.4); as the amount of dolomite increases, permeabilities increase (Fig. 3.5B), although there is considerable scatter in the data. Dolostones have the highest absolute and average horizontal (geometric mean k_h : 27.9 md) and vertical (geometric mean k_v : 5.1 md, Table 3.4) permeability values. Skeletal wackestones with less than 50 vol.% dolomite content have low horizontal permeabilities between 0.01 and 0.4 md (Fig. 3.7A, B). Completely dolomitized skeletal wackestones in the reef margin have higher horizontal permeabilities, ranging from 0.01 to 200 md (Fig. 3.7C). Completely dolomitized skeletal wackestones in the Strachan buildup interior have the highest permeabilities between 0.01 and 450 md (Fig. 3.7 D-F).

Thus, although all depositional facies have been modified by several diagenetic processes, such as early cementation, chemical compaction and later dissolution and cementation (see Chapter 2), replacement dolomitization and associated dissolution exerts the most pronounced effect on reservoir properties (Figs. 3.6, 3.7). This effect is two fold, it results in significantly higher porosities and, more importantly, a significant increase in permeabilities.

DISCUSSION

Porosity and permeability variations in the Strachan and Ricinus West buildups are controlled by a series of complex interactions involving depositional environments and different diagenetic environments and processes during progressive burial, thermal maturation, overpressuring and TSR (see Chapter 2). Unlike clastic reservoirs where particular depositional facies generally remain permeable and others non-permeable, in carbonate reservoirs such as the Leduc buildups, any depositional facies can be permeable or nonpermeable depending on the type and extent of diagenesis.

Figure 3.7: Histograms of permeability data in skeletal wackestone facies in the Strachan buildup showing variability of permeability in:
A), B), Limestones (< 50 vol.% dolomite content) in the reef margin (pools D3B and D3A).
C) Dolostones (> 75 vol.% dolomite content) in the reef margin (pool D3A)
D), e), f), Dolostones in the reef interior (pool D3A).
See Fig. 2.2A, B for locations.



Depositional controls on pore systems

The distribution of the pore systems is closely related to the distribution of the depositional units. The vertical succession of Amphipora-like molds, fenestral-like and intercrystalline pores in pore system I are representative of the shallowing upward depositional sequences developed in the upper reef interior. Based on cross sections A-A' and B-B', depositional models for limestones buildups (e.g. McGillivray and Mountjoy, 1975), and outcrop studies of equivalent strata (e.g. McLean, 1992), these depositional sequences are extensive and laterally continuous. Pore system I is the most laterally continuous and the most volumetric of the Ricinus West reservoir. Pore system II correlates with laterally discontinuous stromatoporoid floatstone and coral rudstones facies in the lower reef interior. Pore system III is thick and porous, but is laterally limited as it is restricted to the reef margin. This indicates that depositional facies not only control the type and distribution of pore types but also the lateral continuity of the porous and permeable zones.

Diagenetic control on pore systems

Dolomitization, cementation, dissolution and bitumen plugging affected the pore systems and the relationship between porosity and permeability differently.

Effect of replacement dolomitization

Replacement dolomitization is the most important diagenetic process to have affected the Leduc buildups in the deep Alberta basin. Determining its effect on porosity and permeability is often difficult, because dolomitization may preserve, increase or decrease pre-existing porosity (see Chilingarian et. al., 1992; Weyl, 1960; Lippmann, 1973; Machel and Mountjoy, 1986).

In the Strachan buildup, dolomitization is inferred to have occurred at about 500 m, probably at the time of the onset of chemical compaction (see Chapter 2, Amthor et.al.,

1993, Drivet and Mountjoy, 1994). Therefore, the original porosity of the limestone had already been reduced considerably, owing mostly to near seafloor and early burial calcite cementation, and mechanical compaction. Initially during dolomitization, porosity was reduced by chemical compaction of the surrounding calcites until the crystals of dolomite gradually formed a supporting-framework. At around 40 to 70% replacement (Weyl, 1960; p.89) once the dolomite framework is in place, chemical compaction is greatly reduced for dolostones which are more resistant than limestones to dissolution and chemical compaction (e.g. Railsback, 1993). Limestones with less than about 40% dolomite, however, still will be subjected to continued chemical compaction and porosity reduction.

Effect of cementation and dissolution

In the Ricinus West cementation occurred at more than one stage (see paragenetic sequence in Chapter 2, Fig. 2.6). The net effect of cementation is not only to reduce pore size but to reduce or completely plug pore throats (e.g. Wardlaw, 1980). Such processes increase the pore/throat ratio resulting in a drastic reduction of permeability. Anhydrite cementation is volumetrically important in the lower part of the reservoir. At least three dissolution events modified the Ricinus West reservoir rock. Dissolution I (D₁) affected calcite skeletal fragments during or after replacement dolomitization resulting in molds, solution-enlarged molds and vugs in the entire reservoir. Dissolution II (D₂) minor dissolution III (D₃) of matrix dolomite resulted in vugs and brecciated intervals that are more abundant in the reef margin.

Effect of reservoir bitumen on porosity and permeability

Reservoir bitumen has been reported as a common porosity-occluding phase in some reservoirs (e.g. McCaffery, 1977; Lomando, 1992). The precipitation of reservoir bitumen can cause wettability characteristics (the relationship between hydrocarbon-rock

contact angles) to change from water-wet to mixed or strongly oil-wet (Lomando, 1992). For example, McCaffery (1977) reported that pore-lining bitumen in the Devonian Windfall D-3 pool made the rock intermediately wet for gas/water systems. Wettability strongly influences reservoir behaviour and ultimate hydrocarbon recovery (Wardlaw, 1992). Therefore the type, amount and distribution of reservoir bitumen needs to be carefully evaluated.

In the Strachan and Ricinus West buildups depositional facies with different pore types have different amounts of reservoir bitumen with homogeneous to heterogeneous distribution. Skeletal wackestones have the highest percentages (15%) of reservoir bitumen and are characterized by abundant intercrystalline pores (Plate 2.6F), some small vugs, and locally fractures. All pore types are lined to partly filled with reservoir bitumen as thin (1 to 4 μm) coats and droplets (up to 10 μm). The pre-bitumen porosity and present (core-measured) porosity for this facies are shown in Table 3-7. In well 10-33 skeletal wackestones interbedded with microbial laminites in the upper reef interior of the Ricinus West reservoir have pre-bitumen porosity of 12.9% that has been reduced to 2.9% after the emplacement of an average bitumen content of 10% (at 4601 m). A similar porosity reduction occurs at 4561.5 m. In the lower reef interior skeletal wackestones are interbedded with domal stromatoporoid facies and have a relative low bitumen content (2%, 4628.9 m) which reduced porosity by 22%. Similar results are present for well 11-27 (Table 3.7). Thus the precipitation of reservoir bitumen in the Ricinus West reservoir notably reduces porosity by 22% to more than 70%.

The greatest significance of reservoir bitumen precipitation on reservoir character, however, is its reduction of permeability and thereby increasing reservoir heterogeneity. Comparison of core permeability in a continuous, 1 m thick, interval of skeletal wackestone facies (well: 11-27, 4478 m; Table 3-7) illustrates the effect of bitumen plugging on permeability. With 10% reservoir bitumen, horizontal permeability averages 3.4 md and

vertical permeability averages 0.4 md, compared to 45.8 md and 24.8 md respectively in dolostones with 1% bitumen. This reduction in permeability results because thin coats or droplets of bitumen restrict or completely block the pore throats. This late-stage deep burial event (see Chapter 2 and Appendix D) imparts a component of reservoir heterogeneity that is unrelated to depositional facies or pre-bitumen diagenesis.

Porosity evolution in the Strachan and Ricinus West buildups

Evolution of the pore systems occurred in four major stages (Fig. 3.8) that represent important changes in porosity and permeability of the reservoirs.

Stage 1: Deposition (Facies controlled original porosity)

The paleogeographic setting originally controlled depositional environments and ultimately the original porosity and permeability. Skeletal boundstones and rudstones with packstone matrices and submarine cements were deposited at the reef margins. Skeletal rudstones, grainstones, packstones, wackestones and mudstones were deposited in the reef interiors. Initial porosities were probably high and differed among the different facies. For example, modern packstones and grainstones have permeabilities between 1840 and 30800 md, whereas wackestones and mudstones have higher porosities (68%) but lower permeabilities (228 to 0.87 md, Enos and Sawatsky, 1981). Thus depositional environments strongly control initial porosity and permeability. This porosity was reduced by near seafloor and early burial calcite cementation especially along the buildup margins (see paragenetic sequence in Chapter 2, Fig. 2.5). During the initial phases of burial the sediments were subjected to mechanical compaction, whereas at burial depth greater than about 500 m, chemical compaction began to reduce porosity especially in limestones (e.g. Lind, 1993).

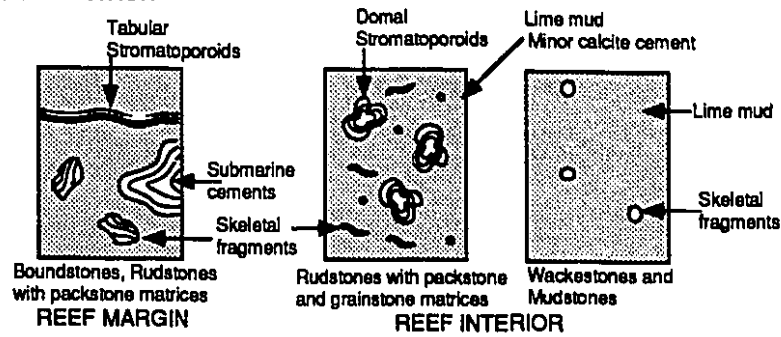
Stage 2: Replacement dolomitization (Early burial, porosity reduction)

a) During the early stages of replacement dolomitization in the Strachan buildup

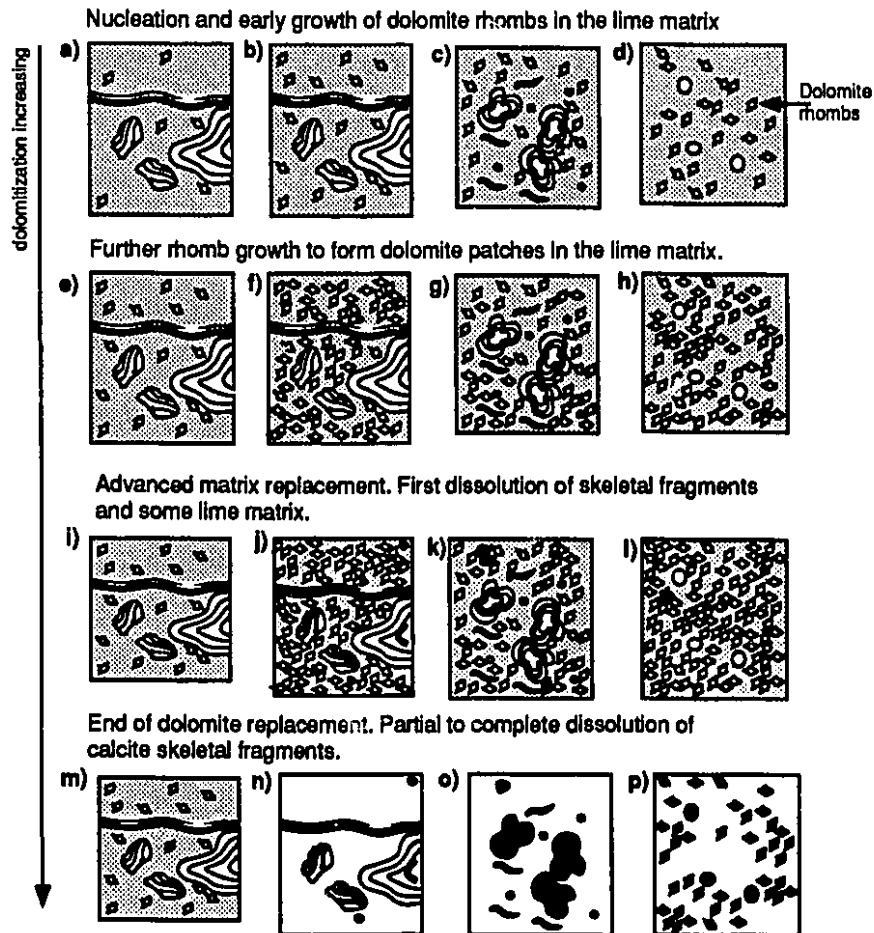
Figure 3.8: Porosity evolution in inferred steps of the conversion of Leduc limestones to dolostones with accompanying changes and modification of pore types.

- Stage 1:** deposition and early porosity reduction
- Stage 2:** dolomitization
- Stages 3 and 4:** Cementation, dissolution and bitumen plugging

Stage 1: DEPOSITION



Stage 2: DOLOMITIZATION



Stage 3 and 4: CEMENTATION, DISSOLUTION AND BITUMEN PLUGGING



(Late Devonian or younger), isolated dolomite rhombs nucleated and grew in lime mud of all depositional facies (Phases a to d, Fig. 3.8). As dolomitization progressed, dolomite rhombs grew to form dolomite patches in the lime mud matrix (Phases f to h) of rocks in the D3A pool and began filling some porosity. Less dolomite formed in the D3B pool (Phase e). Advanced matrix dolomitization formed a self supporting framework in rocks of the D3A pool that probably made these rocks resistant to chemical compaction (Phases j to l). Conversely limestones in pool D3B, were subjected to continuing pressure solution and porosity reduction. Once dolomite forms a self supporting framework, remnant lime matrix can potentially be dissolved to leave an open network (intercrystalline porosity) of dolomite crystals.

During additional burial the dolostone may remain essentially unaltered, having a porous matrix with calcite skeletal fragments and marine cements, or continue to be changed. Dissolution (D_1) may form vugs resulting in a porosity increase. Alternatively dolomite cement may precipitate reducing porosity and permeability. Low porosity in completely dolomitized rocks may be due to dolomite crystals progressively increasing in size, and may ultimately result in a dense anhedral mosaic with little or no porosity.

Stages 3 and 4: Cementation, dissolution and reservoir bitumen emplacement
(Reduction/enhancement of porosity and permeability)

The next stage began with the dissolution of skeletal (CaCO_3) grains and enhancement of porosity (D_1). Either toward the end of fossil dissolution or afterward, precipitation of dolomite cement (C_1) took place decreasing in part the pore space. Dolomite cement C_2 , anhydrite and minor sulphides partly filled pores mostly in the lower part of the reservoirs (see Chapter 2). The emplacement of reservoir bitumen, Late Cretaceous (see Chapters 2 and 4), notably reduced porosity and more importantly permeability in the upper part of the reservoir.

CONCLUSIONS

The association and distribution of pore types and permeability within the Leduc Strachan and Ricinus West gas reservoirs in the deep Alberta basin indicate:

1) Depositional facies ultimately controlled the distribution of the different pore types, whereas permeability is mainly controlled by diagenetic processes, especially dolomitization.

2) Completely dolomitized Upper Devonian Leduc buildups at depths greater than 4000 m have higher porosities and permeabilities than limestones because dolostones are more resistant to pressure solution.

3) The relationships between the proportion of dolomite and porosity are complex, but a slight increase in porosity with increasing dolomitization occurs, which becomes more pronounced above 80% dolomite. In general porosity and permeability increase with increasing dolomitization, with the highest porosity and permeability occurring in completely dolomitized facies. The highest porosities and permeabilities occur in the completely dolomitized interior of the Strachan buildup. At the reef margin, porous and permeable dolostones are interbedded with nonporous and nonpermeable limestones. These trends are modified by later cements, dissolution and bitumen emplacement.

4) Pore types are grouped into pore systems that closely follow depositional units, despite complete dolomitization in the Ricinus West buildup. At the reservoir scale porosity and permeability are similar throughout. At the next smaller meter scale, pore system I in the upper 131 m of the reservoir is characterized by 1 to 2 m thick, permeable, and laterally continuous, reef interior (lagoonal) zones. Pore system II in the lower 61 m of the reef interior have laterally discontinuous permeable zones. Pore system III is restricted to the 259 m thick reef margin where intervals of fractures and connected vugs provide vertical permeability. The best lateral permeability is related to laterally continuous skeletal wackestone facies that have been dolomitized to a rock with good intercrystalline porosity

in pore system I. The best vertical interconnections are provided by connected vugs and subvertical fractures in pore system III.

5) At the even smaller pore and mm scale porosity and permeability are controlled by diagenetic processes. Post-dolomitization processes, such as cementation, dissolution and bitumen plugging, modified porosity and permeability. Anhydrite cementation, minor dolomite, calcite and native sulphur cementation reduced porosity and, more significantly, permeability, producing a high degree of heterogeneity in the lower part of the reservoirs.

6) Reservoir bitumen reduces porosity and permeability by decreasing pore and pore throat sizes mainly in the upper part of the Ricinus West reservoir. Bitumen coating may cause wettability to change from water wet to intermediate in water/gas systems. Bitumen can only be determined by logging core, petrographic analysis, and core porosity measurements. Errors in reservoir volumetric calculations from well logs can arise because of the lack of significant density contrast between crude oil and bitumen making reservoir bitumen indistinguishable from oil-filled porosity.

Reconstruction of the depositional and diagenetic history from detailed studies of cores is essential for making realistic reservoir models. Differences in approach in grouping porosity and permeability data in reservoir characterization can lead to major differences in modeling and assessment of the reservoir. Critical to a realistic assessment is to describe the reservoir (depositional facies and sequences) as geologically faithfully as possible, rather than by means of arbitrary slices or blocks. As shown above, such studies demonstrate that carbonate reservoirs are extremely heterogeneous and that discontinuous relatively nonporous and low permeability zones impede fluid flow and greatly affect reservoir performance and production. These models are essential for understanding reservoir production and for predictions of reservoir performance and ultimate recovery by enhancement techniques. Only after putting together such realistic reservoir models can the more detailed petrophysical information be incorporated in them and assessed.

CHAPTER 4

ORIGIN OF MICROFRACTURES IN THE UPPER DEVONIAN LEDUC STRACHAN RESERVOIR, DEEP ALBERTA BASIN

X. Marquez and E.W. Mountjoy
Dept. of Earth and Planetary Sciences, McGill University
Montreal, H3A 2A7, Canada

ABSTRACT

Hairline microfractures (< 1 mm in width) occur in the upper 200 m of the partially to completely dolomitized Upper Devonian (Leduc Formation) Strachan buildup in the deep Alberta basin. Microfractures are filled with reservoir bitumen and crosscut all sedimentary and diagenetic phases and therefore are late-stage (depths of 3000 to 4000 m). They occur in three different patterns: 1) subhorizontal, extending from intraskeletal pores and perpendicular to subvertical fractures, 2) radial around vugs and molds, and 3) random, away from intercrystalline and intraskeletal pores, the most abundant being subhorizontal.

Overpressuring caused by thermal cracking of crude oil to gas during burial explains most of the characteristics of these microfractures; their association with all pore types, bitumen fillings, and timing. Hairline microfractures are restricted to isolated buildups in the deeper parts of the Alberta Basin, below depths of 3800 m. The lack of microfractures in adjacent gas-bearing and updip buildups along the Rimbey-Meadowbrook reef trend, appears to be because these buildups never developed sufficient pressures to form hairline microfractures since they are connected to the regional conduit system in the underlying Cooking Lake platform. Thermal cracking of crude oil to gas during burial is also shown by optical textures, such as fine and coarse deformed lamellar textures, in the reservoir bitumens that fill the microfractures. Thus thermal cracking of oil in conjunction with tectonic compression was responsible for the development of overpressures that created the hairline microfractures in those buildups that were isolated and effectively sealed.

INTRODUCTION

Microfractures have great economic significance since they may enhance or, if filled, obstruct permeability within any rock in which they occur. In either case microfractures can create highly anisotropic permeability in a reservoir. Therefore knowledge of their presence, characteristics and distribution are invaluable in reservoir characterization and evaluation.

Despite their occurrence, comprehensive studies of microfractures in the downdip portion of the Alberta basin have not been published. Keith (1971) observed "hairline" fractures at Strachan (well 10-24), many of which radiate from vugs and suggested that they may have been caused by increased pressures. In this study, hairline microfractures are shown to occur in both overpressured limestones and dolostones at depths of 3 to 5 km. This is based on 1) the occurrence of hairline microfractures in different pore types in both limestones and dolostones, 2) hairline microfractures crosscut late diagenetic products, 3) microfractures are filled with reservoir bitumen with textural characteristics indicating high temperatures, and 4) microfractures are restricted to isolated, well-sealed buildups. Their characteristics and possible origins are examined and discussed.

METHODS

All available cores from the Strachan and adjacent buildups in the Upper Devonian of central Alberta, Canada, were studied (Appendix A), encompassing the area between Townships 34 to 39 and Ranges 7 to 12 W5 (Fig. 1.1). Two cores from the Harmattan field also were examined: 13-9-33-4W5 and 4-15-32-4W5. In other areas of the Alberta basin wells examined include 5-5-58-24W5 from Colt, 8-4-59-23W5 from Berland River, 10-14-50-22W5 from Robb, and 16-16-63-25W5 and 9-3-63-25W5 from the Simonette reef trend, all of which contain evidence of microfracturing (Fig. 1.2).

Thin sections impregnated with fluorescence epoxy were examined by standard

petrographic, cathodoluminescence and fluorescence microscopy. Chips of microfractured rocks were studied using SEM. Optical textures and quantitative reflectance microscopy of reservoir bitumen were performed by V. Stasiuk on 22 samples from the Strachan buildup at the Institute of Sedimentary and Petroleum Geology, Calgary. Gas compositions were provided by the Energy Resources Conservation Board (ERCB), Calgary.

STRACHAN GAS FIELD

The isolated Strachan gas field is located approximately 100 km northwest of Calgary, Alberta (Fig. 1.1). Its discovery in 1967 (well: 12-31) marked the first commercial production from depths in excess of 4,000 m in this area (Hriskevich, et. al., 1980). The reservoir consists of a carbonate buildup 11 x 4 km in area and 274 m thick. The net pay interval is 163 m having a maximum of 224 m in well 11-27. The Strachan field consists of a western pool, D3B, and an eastern pool, D3A (Fig. 2.1). These pools have several significant differences. Whereas the D3B pool is partially dolomitized and allows the recognition of the original sedimentary facies, the D3A pool is partially to completely dolomitized making facies identification difficult. The following sections include descriptions of the reservoir rocks (both limestone facies and dolostones), the underlying rocks, and the sealing shales and carbonates in an attempt to determine their role in the origin of the hairline microfractures.

Reservoir Rock

Depositional facies are best recognized in pool D3B and are based on texture (Dunham, 1962; and Embry and Klovan, 1971), diagnostic fauna and location with respect to the buildup margin. Northwest-southeast cross sections illustrate the facies distribution in pool D3B and D3A (Fig. 4.1 A,B).

Figure 4.1A Distribution of depositional facies (Leduc Formation) in the Strachan D3B pool. See Fig. 2.1 for well locations. Datum is top of the Calmar Formation. Black, thin bar indicates the presence of reservoir bitumen. Patterns in thicker bar show the relative abundance of hairline microfractures.

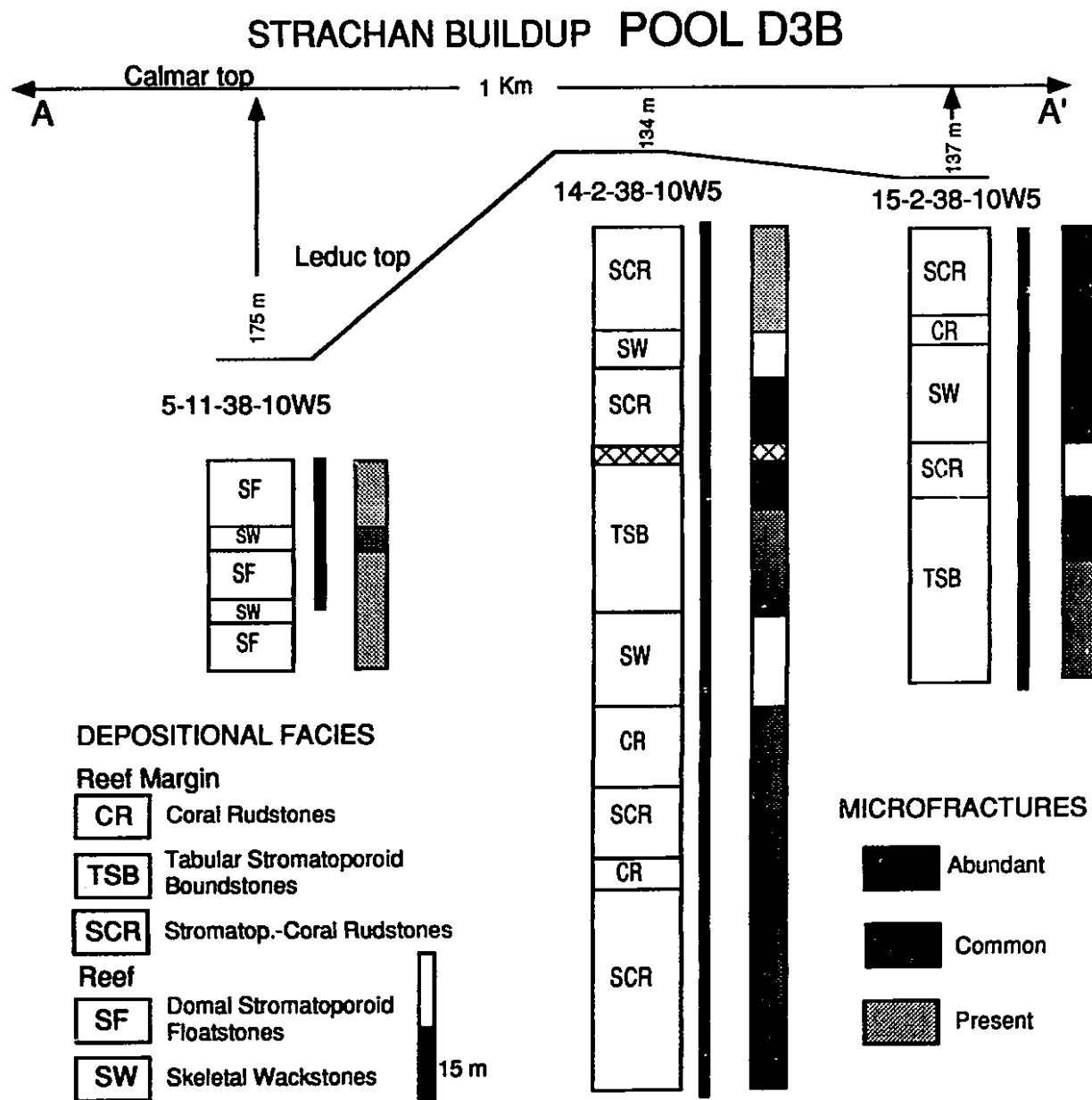
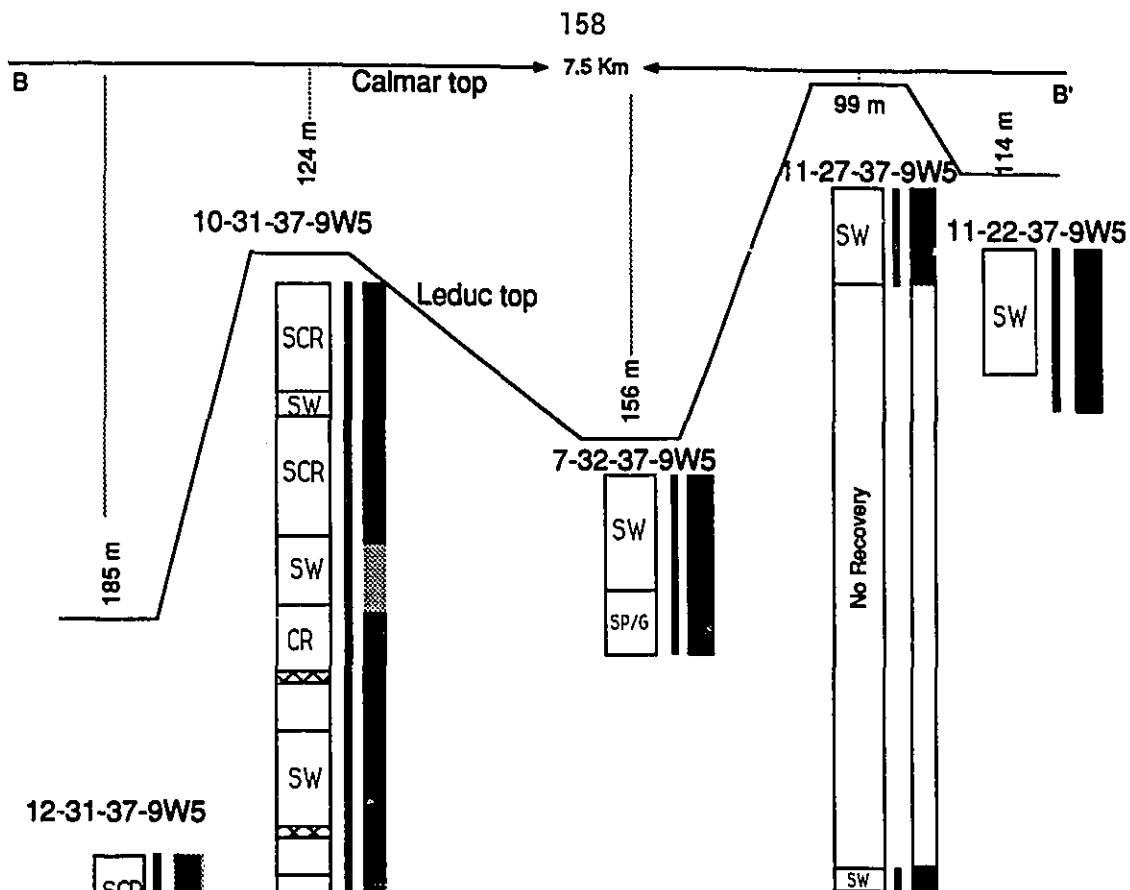


Figure 4.1B Distribution of depositional facies in the Strachan D3A pool. See Fig. 2.1 for well locations. Datum is top of the Calmar Formation. Black, thin bar indicates the presence of reservoir bitumen. Patterns in thicker bar show the relative abundance of hairline microfractures.



STRACHAN BUILDUP POOL D3A

DEPOSITIONAL FACIES

Reef Margin

- CR** Coral Rudstones
- TSB** Tabular Stromatoporoid Boundstones
- SCR** Stromatop.-Coral Rudstones

Reef

- SF** Domal Stromatoporoid Floatstones
- SW** Skeletal Wackstones
- SP/G** Skeletal packstones/grainstones

MICROFRACTURES

- Abundant**
- Common**
- Present**

RESERVOIR BITUMEN

15 m

Limestones

Five depositional facies of reservoir rocks have been recognized: 1) coral rudstone; 2) tabular stromatoporoid boundstone; 3) stromatoporoid-coral rudstone; 4) domal stromatoporoid floatstone; and 5) skeletal wackestones (Appendix B).

The **coral rudstone** facies is composed of moderately sorted coral debris in a skeletal packstone matrix (Plate 2.1 A). The matrix consists of poorly to moderately sorted fragments of corals, stromatoporoids, crinoids, brachiopods, gastropods and micritized grains. The thickness of coral rudstone beds varies from 3 m in well 12-31 to 19 m in well 10-31. The poor to moderate sorting of the matrix and fragmentation of stromatoporoids suggests deposition in a shallow, high energy environment along the reef margin. Pore types in this facies include, in decreasing abundance, tubular molds (1 to 2 cm), irregular vugs (0.5 to 6 cm), spherical intraskeletal and minor polyhedral intercrystalline pores.

The **tabular-stromatoporoid boundstones** facies is observed in wells 15-2, 14-2 and 10-31 (Appendix B). It consists of laminar/tabular stromatoporoid boundstones (in situ?) in a packstone or grainstone matrix of crinoids, brachiopods, and micritized grains. Shelter and growth cavities are filled with radiaxial fibrous calcite cement (Plate 2.1 C). Thickness of the boundstones varies from 10 to 34 m. Vugs (0.5 to 1 cm) make up 10 to 60% of all pores. Molds (5 to 20%), intercrystalline pores (10 to 50%), and subvertical fracture (5 to 10%) are also present.

The **stromatoporoid-coral rudstone** constitute the most abundant facies, and are represented by thick accumulations of laminar (tabular) and domal stromatoporoids, locally branching Stachyodes, tabulate corals and crinoid rudstones (Plate 2.1 D). The matrix consists of fragments of crinoids, brachiopods, mollusks and micritized grains with packstone and/or grainstone textures. It reaches thicknesses up to 81 m in well 10-31. It is distinguished from tabulate-stromatoporoid boundstones by the lack of in situ fossils and radiaxial calcite cements. This facies probably represents reef-derived rubble deposited

seaward of the buildup margin. Pore types in this facies include tabular and spherical intraskeletal pores (90%), subvertical fractures (10%), and irregular vugs (0.5 to 2 cm) 1%.

The **domal stromatoporoid floatstone** facies is composed of large, domal (2 to 7 cm) and bulbous stromatoporoids occurring in situ and as poorly sorted detrital components in a skeletal packstone matrix. Stachyodes are locally present (Plate 2.1 E). This facies is generally 6 m thick but attains a thickness of 16 m in well 5-11. These rocks are interbedded with skeletal wackestones (well 5-11) and stromatoporoid-coral rudstones in well (10-31). Pore types include tabular intraskeletal pores (80%), partly filled fractures (10%), vugs (1 to 2 cm; 5%), and minor intercrystal pores (2%).

The **skeletal wackestone** facies is present in almost all limestone wells, however, they are most abundant in well 10-31 reaching a thickness of 93 m (Appendix B). They consist of moderate to well-sorted, rounded grains in a lime mud matrix and locally cemented by calcite. Micritization of grains makes their identification difficult, however some mollusk, crinoid, and algal fragments can be recognized (Plate 2.1 F,H). The dominant pores are intercrystalline (90%), minor vug (0.5 to 2 cm; about 5%) and locally partly filled fractures (5%).

Dolostones

The extent of dolomitization in these depositional facies ranges from a few isolated rhombs in pool D3B, to complete fabric destructive dolomitization in the eastern portion of pool D3A (see Chapter 2). Within individual wells, such as 10-31 of pool D3A a complete range of replacive dolomitization is observed from total, to partial, to the original limestone being largely unaffected. Dolomitization is fabric selective and preferentially replaces the matrix (Plate 2.9). The interior and eastern margin of pool D3A are characterized by fabric destructive dolomitization. Here skeletal debris are partially to completely dissolved (Plate

2.9 E,F) forming vuggy and moldic porosity. Overall, dolostones are characterized by three textural types of replacement dolomite (R_1 to R_3) and two types of dolomite cement (C_1 and C_2), similar to the dolomites of Amthor et al. (1993).

Replacement dolomites (R_1 to R_3) consist of dense and porous mosaics of fine (30 - 62 μm) to coarse (250 - 600 μm) crystals. The crystals are planar euhedral to subhedral crystals and have homogeneous dull red luminescence color (Plate 2.6). Nonmimetic replacement of skeletal components in R_1 , where coral and stromatoporoid rudstone/packstone textures can be recognized, is common in well 7-32. Coarser-crystalline dolomites (R_3) are abundant in well 11-27. **Dolomite cement C_1** is euhedral to subhedral and medium crystalline (100 - 250 μm). The crystals have clear rims, and commonly line intercrystalline, vugs and fracture pores (Plate 2.7 C). **Dolomite cement C_2** is coarse to very coarse (100 μm to 1 mm), and lines vugs and fractures (Plate 2.7 E) and completely fills moldic pores (e.g. well: 10-31, 4308 m). This dolomite cement has curved crystal faces and sweeping extinction that is characteristic of saddle dolomites (Radke and Mathis, 1980).

Underlying strata

The widespread Cooking Lake carbonate platform that underlies the Strachan Leduc buildup (Fig. 1.3) is about 100 m thick in east-central Alberta (possibly thicker) and consists of 11 sedimentary facies that indicate sedimentation varied from deep water (25 m) to shallow intertidal and supratidal environments (Wendte, 1992;). Along the Rimbey-Meadowbrook reef trend the Cooking Lake platform is about 76 m thick (Amthor et. al., 1993; Chouinard, 1993). In the deeper part of the basin, information about the Cooking Lake platform is limited, but it is thinner (18 to 63 m; Appendix G) and more argillaceous in the study area.

There are no cores available from the Cooking Lake Formation underlying the Strachan buildup. However, in well 7-9-37-10W5, located 6 km southwest of Strachan between the Strachan and Ricinus West buildups, a 63 m thick interval of Cooking Lake Formation consists of dark grey, brachiopod-crinoidal, argillaceous wackestones, packstones and grainstones with some bulbous stromatoporoids interbedded with black lime mudstones (Plate 4.1 D,E). Some intervals of dark grey nodular lime mudstones are also present. Deposition of these facies is ascribed to an open marine, relatively deep-water environment. The matrices of these strata are selectively dolomitized, and overall, dolomitization of the Cooking Lake Formation is similar to that of the overlying buildups. Total porosity of partly dolomitized Cooking Lake strata in well 7-39 is 4.5%, and horizontal and vertical permeabilities are 36 and 0.69 md respectively.

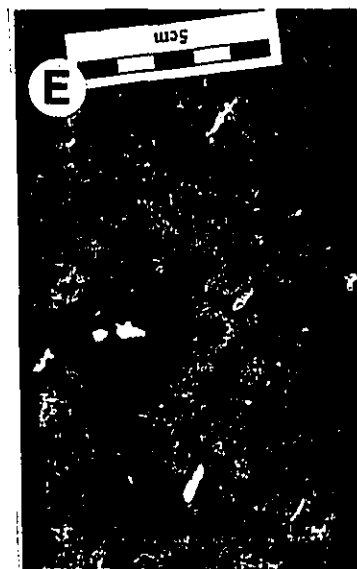
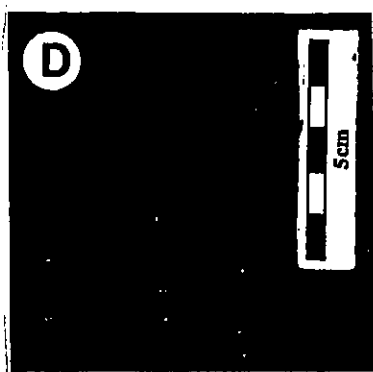
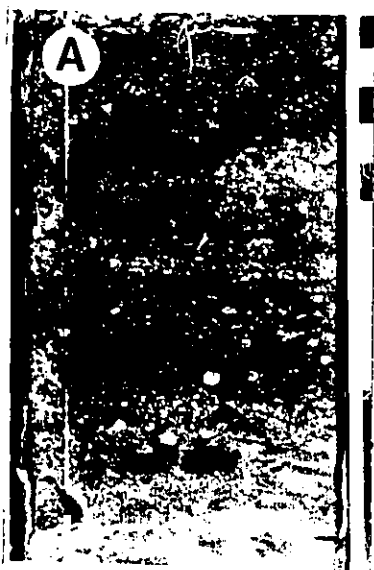
In well 7-19-37-8W5 located 3 km southeast of the Strachan buildup, 36 m of the Cooking Lake Formation are completely dolomitized. Total porosity is 4.7%, horizontal and vertical permeabilities are 21 and 1.3 md respectively. In well 5-4-39-11W5 (Phoenix area) 9 km northwest of the Strachan buildup, 24 m of the Cooking Lake are more argillaceous and less dolomitized. Although the limited porosity and permeability data suggest that the Cooking Lake Formation is porous and permeable, its more argillaceous nature combined with different degrees of dolomitization and variable thicknesses probably restricted fluid flow in this area. This would explain 1) the different degrees of dolomitization in buildups located northwest of pool D3A of the Strachan buildup (e.g. Phoenix area), 2) the present weak water drive in the Strachan reservoir, and 3) the major differences in diagenesis between Strachan and adjacent buildups (see Chapter 2).

Sealing shales and carbonates

Shales generally restrict fluid flow as their permeability decreases with depth (e.g. Gretener and Feng, 1985). In the Strachan area, greenish grey argillaceous and calcareous

**Plate 4-1 CHARACTERISTICS OF SEALING IRETON STRATA AND
UNDERLYING COOKING LAKE STRATA**

- A) Crinoid and brachiopods packstone with green shaly matrix. Ireton Formation. 5-11-38-10W5, 4127 m.
- B) Photomicrographs of well sorted crinoid fragments in a shaly, lime mud matrix. Note lack of hairline microfractures. Ireton Formation. 7-32-37-9W5, 4076.5 m. Scale bar 250 μ m
- C) Photomicrographs of argillaceous mudstones of the Ireton Formation. Subhorizontal fracture filled by late calcite cement and pyrite. 7-32-37-9W5, 4077 m. Scale bar 250 μ m
- D) Crinoid and brachiopod, grainstone of the Cooking Lake Formation with partly dolomitized matrix. 7-9-37-10W5, 4699.3 m.
- E) Domal Stromatoporoid in a skeletal and argillaceous rudstones matrix of the Cooking Lake Formation. Matrix is partly dolomitized. 7-9-37-10W5, 4714.6 m.



shales of the Ireton Formation occur adjacent to and overlie the Leduc buildups providing a seal (Fig. 1.3).

This formation is divided into lower, middle and upper units. The lower Ireton consists of interbedded calcareous shale and dense limestones, the middle Ireton consists of a monotonous sequence of slightly calcareous green shales, and the upper Ireton consists of interbedded calcareous shales and fossiliferous, often nodular, argillaceous limestones (McCrossan, 1961). The composition of the Ireton shales is essentially variable with calcite, dolomite, illite and fine-grained quartz (Stoakes, 1980). There are only two cores from the Ireton in the entire Strachan area, 17 m from well 7-32-37-9W5 and 2 m from well 5-11-38-10W5 (Fig. 2.1). In these cores, only the upper Ireton is present and consists of dark grey, crinoid-brachiopod packstone with green shaly matrix and minor pyrite. Mudstone beds up to 20 cm are also present (Plate 4.1 A-C). Thicknesses of the Ireton Formation based on gamma-ray log varies from 155 m in the offreef areas to 25 m above the buildups. No hairline microfractures were observed in the two Ireton Formation cores available (Plate 4.1 A-C). This suggests that the Ireton strata may have served as a membrane seal (a seal that fails by capillary leakage) for hydrocarbons in the Strachan reservoir. In membrane seals the trapping mechanism is the capillary properties of the rock which in turn are governed by the rock permeability (see Watts, 1987). Permeability would have to be in the range of 10^{-21} to 10^{-24} m² (Deming, 1994, Fig. 2) for a shale layer to effectively seal hydrocarbons for about 1 m.y. This range is several orders of magnitude lower than average shale permeabilities (10^{-16} to 10^{-20} m², Freeze and Cherry, 1979). Thus, for the Ireton shale to have served as an effective seal, permeability would have had to be low enough to limit pressure loss in comparison to rate of pressure generation, although considerable leakage may have occurred.

Studies of the compaction history of the Woodbend shales (Hugo, 1990), which

includes the Ireton Formation in the central Alberta basin, indicates that these shales were compacted faster than other shale sequences cited in the literature (e.g. Hinch, 1980). They were also subjected to submarine and early burial cementation (Stoakes, 1980). Despite their rapid compaction, no information is available about overpressures in the Ireton shales. The sonic logs from the two wells mentioned above do not show the reversal in sonic travel time that would be expected when shales are overpressured (eg. Surdam et. al., 1991). Conversely, rapid compaction resulted in lowering the permeability of the shales so that they form an aquiclude around the buildups channelling flow along the Rimbey Meadowbrook reef trend (Hugo, 1990).

Evaluating the paleo-sealing capacity of the Ireton shales that surround the Strachan buildup is difficult, since data about entry capillary pressure, densities of water and hydrocarbons phases are not available. However, assuming that the abundant and uniform distribution of reservoir bitumen in the buildup is an indication of the hydrocarbon (oil ?) saturated zone, it is possible to estimate the hydrocarbon column height that the Ireton shales were able to trap. Reservoir bitumen is distributed from the top of the reservoir (4092.2 m) to about 4313 m (well 10-31; Fig. 4.1 A,B; Appendix D) suggesting that the paleo oil/water contact was around 4313 m depth and therefore the maximum height of the hydrocarbon column held by the Ireton shales appears to be about 200 m. According to the classification of Sneider (1987; Sneider et. al., 1991) the Ireton shales overlying the Strachan buildup would have served as a good membrane seal (probably his type B ?). This information suggests that the Strachan reservoir was probably well-sealed by the overlying Ireton shales.

Information presented above indicates that the Strachan reservoir rock consists of skeletal limestones and dolostones with different pore types. The reservoir became well-sealed during compaction of adjacent and overlying Ireton shales. Some barriers to flow appear to have been present in the underlying Cooking Lake platform, probably since the

time of dolomitization.

MICROFRACTURES

Microfracturing in the Strachan field is ubiquitous and complex. These microfractures are < 1 mm in width and up to 6 cm in length and are herein termed **hairline microfractures**. Examination of microfractures in all cores indicate they are extension fractures, having little or no slip or displacement perpendicular to and away from the microfracture plane (Nelson, 1985). Microfractures always extend from the pores into the matrix, and none have been observed to be completely restricted to the matrix. They are always filled with reservoir bitumen (see Appendix D for information about the thermal history of the bitumens).

Microfracture patterns

Hairline microfracturing occurs in three different patterns depending on the pore type. In decreasing abundance these patterns are subhorizontal, radial, and random (Fig. 4.2).

Hairline microfractures extend subhorizontally away from intraskeletal pores in stromatoporoid and coral fragments, and previously formed subvertical fractures. In skeletal fragments, most microfractures extend from small (<100 μm), elongated intraskeletal pores and commonly stop at grain boundaries (Plate 4.2 A,B). Some, extend across both matrix and early calcite cements reaching up to 6 cm in length (Plate 4.2 D). Subhorizontal microfractures extend from previously formed subvertical fractures and occur in both limestone and partly dolomitized rocks (Plate 4.2 E).

Radially oriented hairline microfractures are always associated with spherical intraskeletal pores in coral fragments (Plate 4.3 A), moldic (Amphipora-like) pores, and irregular vugs (5 mm to 1 cm) in dolostones (Plate 4.2 G). Spherical intraskeletal pores are

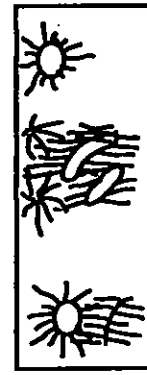
Figure 4.2 Hairline microfracture patterns in limestones, partly dolomitized rocks and dolostones in the Strachan reservoir.



a) Limestone



b) Partly dolomitized



c) Dolostone

- a) Subhorizontal, random and minor radial pattern extending from intraskeletal pores
- b) Subhorizontal extending from intraskeletal pores and subvertical fractures
- c) Subhorizontal, random and radial patterns extending from moldic, vugs, and intercrystalline pores

small (50-100 μm), and hairline microfractures that extend perpendicular away from them are up to 6 mm long. Pores and microfractures are always filled with reservoir bitumen. Some pores were subsequently filled by late-stage calcite cement.

Hairline microfractures have no preferred orientation, termed random pattern (Plate 4.3 B) in some stromatoporoid and coral rudstones and packstones (wells 14-2, 15-2), and occur where there are abundant irregular, elongated intraskeletal pores.

Hairline microfracture distribution - Strachan reservoir

The relative amounts of microfractures are classified as follows: 1) abundant when 75 to 100% of the pores have microfractures extending from them, 2) common when 25 to 75% of the pores have microfractures, 3) rare when less than 25% of the pores have microfractures, and 4) absent.

Hairline microfracturing is most abundant in the upper 200 m of the Strachan reservoir. Well 10-31 penetrated almost the entire Leduc buildup in pool D3A (Fig. 2.1 B; 4.1 B) and shows the absence of microfracturing 215 m below the top of the buildup (below 4313 m). However, the majority of the studied wells penetrate only the upper part of the Leduc Formation. Microfracturing is present in both limestones and dolostones. In limestones the microfractures are more abundant in skeletal boundstones and rudstones that contain abundant intraskeletal pores. Partly dolomitized skeletal grainstones, with intergranular and intercrystalline porosity, are completely impregnated with reservoir bitumen and do not show hairline microfractures (Plate 4.3 C,D). In dolostones microfractures are common and extend away from intercrystalline, moldic and irregular vugs.

Hairline microfracture distribution - other buildups

Hairline microfracturing similar to that in the Strachan buildup is rare to abundant in Ricinus West, Chedderville, Harmattan (Fig. 4.3), and other buildups in the deepest part of

Plate 4.2 HAIRLINE MICROFRACTURE PATTERNS IN THE STRACHAN BUILDUP

- A) Subhorizontal fractures extending from intraskeletal pores in skeletal debris (arrows). Note lack of microfractures in the matrix portion of the skeletal rudstones. 10-31-37-9W5, 4206 m.
- B) Photomicrographs showing a coral fragment with subhorizontal fractures (arrow) extending from intraskeletal pores. Microfractures stop at the boundary between fragment and radiaxial fibrous calcite cement (c). 15-2-38-10W5, 4121.3 m. Scale bar 250 μm
- C) Photomicrographs showing a close up of coral fragment with subhorizontal microfractures extending from intraskeletal pores. The pore is later filled with calcite cement (Ca). 15-2-38-10W5, 4113.4 m. Scale bar 100 μm
- D) Subhorizontal pattern extending from intraskeletal pores in the stromatoporoid fragment through the well cemented grainstone matrix. Some radially extending microfractures seem to crosscut the subhorizontal microfractures (arrow). 10-31-37-9W5, 4135 m.
- E) Subhorizontal pattern extending from previously formed subvertical fractures. 10-31-37-9W5, 4115.8 m. Scale bar 250 μm
- F) Radial pattern around a coral fragment (arrow). Note subhorizontal pattern extending from intraskeletal pores in stromatoporoid fragments (S). 10-31-37-9W5, 4150.9 m
- G) Radial pattern extending away from spherical mold (arrow). Note subhorizontal pattern extending from intercrystalline pores and vugs. 10-31-37-9W5, 4182 m.

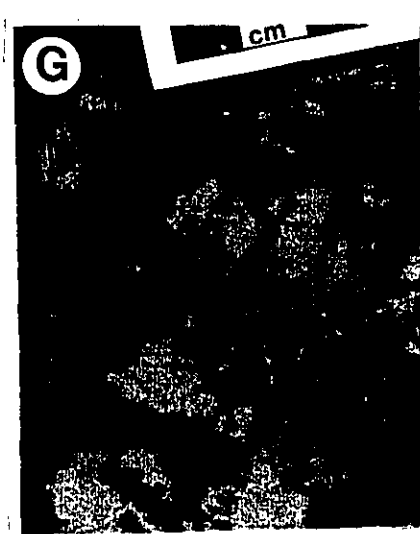
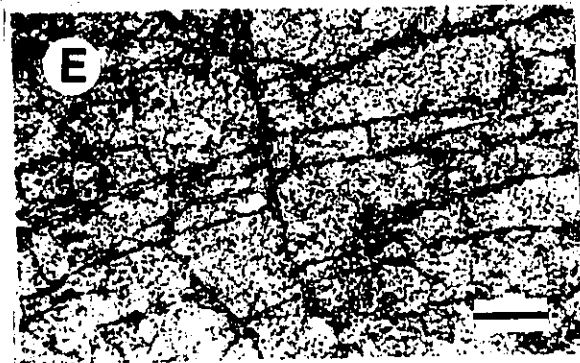
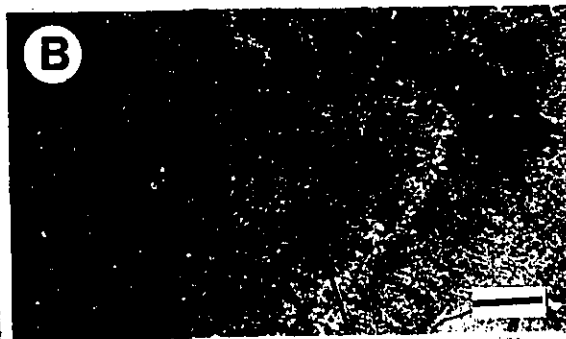
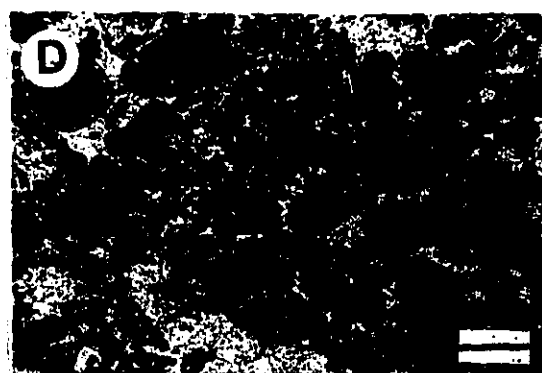
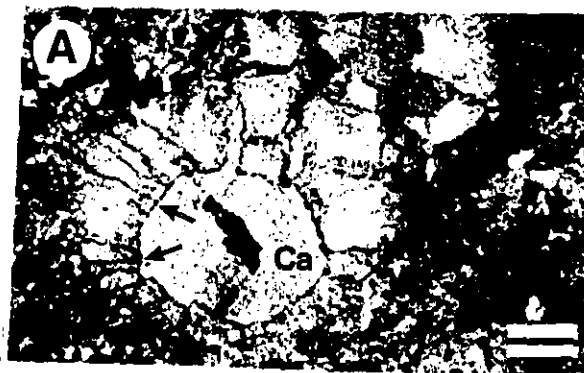


Plate 4.3 HAIRLINE MICROFRACTURE PATTERNS IN THE STRACHAN BUILDUP

- A) Coral fragment with hairline microfractures extending perpendicularly from intraskeletal, spherical pore (arrows). Pore is later filled with calcite cement (Ca). 14-2-38-10W5, 4110 m. Scale bar 100 μm
- B) Hairline microfractures oriented in a random pattern. Some subhorizontal microfractures extend from intercrystalline pores in partly dolomitized matrix (arrow). 10-31-37-9W5, 4110.3 m.
- C) Skeletal grainstones/packstones with moderately sorted, rounded skeletal fragments (F). Dolomite rhombs and patches are abundant (arrows). Note lack of hairline microfractures. 10-31-37-9W5, 4295 m.
- D) Photomicrographs showing micritized skeletal fragments with a grainstone texture. Note lack of hairline microfractures. 14-2-38-10W5, 4339.6 m. Scale bar 250 μm



the Alberta basin (Fig. 1.2). In the completely dolomitized Ricinus West buildup microfractures are rare throughout the 174 m cored interval of well 7-13, however, they become common in the upper 120 m of the buildup. In Ricinus West microfractures extend radially from moldic pores and subvertical fractures (Plate 4.4 A).

Hairline microfracturing is also present throughout 3 m of core in the small Chedderville buildup, in which dolostones have radial microfractures extending from irregular vugs (Plate 4.4 B). In the Harmattan buildup hairline microfractures are abundant, but their distribution throughout the 85 m cored interval in well 13-9 is not continuous. Microfractured intervals are separated either by brecciated intervals (3403-3410 m) or by non-fractured (3383-3388 m) intervals. All three microfracture patterns are present in the Harmattan buildups. Microfractures are also filled with reservoir bitumen and are crosscut by later fractures that exhibit dissolution along their walls and were subsequently filled with anhydrite (Plate 4.4 C)

In other Upper Devonian buildups in the Alberta basin (Fig. 1.2), such as the Simonette reef trend, hairline microfractures are rare. In limestones of the Colt buildup (well 5-5) very few microfractures extend from intraskeletal pores in stromatoporoid-coral boundstones (Plate 4.4 D). In dolostones of the Berland River (well 8-4) and Robb (well 10-14) buildups, hairline microfractures are mostly associated with subvertical fractures (Plate 4.4 E,F). In well 16-16 of the Simonette reef trend hairline microfractures are absent. Bitumen filled "microfractures" always perpendicular to stylolites surfaces are believed to be tension gashes, following the observations of Nelson (1985). Microfractures in the fringing-reef complex around the Peace River Arch (see Dix, 1993) are matrix-stress extensional fractures using definitions of Gretener (1983).

No hairline microfractures have been reported from Leduc buildups along the Rimbey-Meadowbrook reef trend (Fig. 4.3; Amthor et. al., 1993; Drivet, 1993). The Rimbey-Meadowbrook reef trend currently comprises a major conduit system in the

Plate 4-4 HAIRLINE MICROFRACTURE PATTERNS IN OTHER BUILDUPS
IN THE ALBERTA BASIN

- A) Hairline microfractures extending from moldic pores (arrows) and sub vertical fractures in skeletal packstones/grainstones facies in the interior of the Ricinus West buildup. 10-33-36-10W5, 4513.7 m.
- B) Microfractures extending from irregular vugs in the Chedderville buildup. 6-30-37-7W5, 3533 m.
- C) Hairline microfractures extending radially from moldic pores (Amphipora -like, arrows) in the Harmattan buildup. Note some molds are later filled with milky white anhydrite (An). 13-9-33-4W5, 3399.6 m.
- D) Minor microfractures extending from vugs in radiaxial fibrous calcite cements (arrow) in limestones of the Colt buildup. 5-5-58-24W5, 3872 m.
- E) In dolostones of the Berland River the microfractures commonly extend from subvertical fractures and intercrystalline pores. Some extend radially from spherical vugs (arrow). 8-4-59-23W5, 3687.1 m.
- F) In the dolostones of the Robb buildup microfractures extend from subvertical fractures (arrow). 10-14-50-22W5, 4592.3 m.

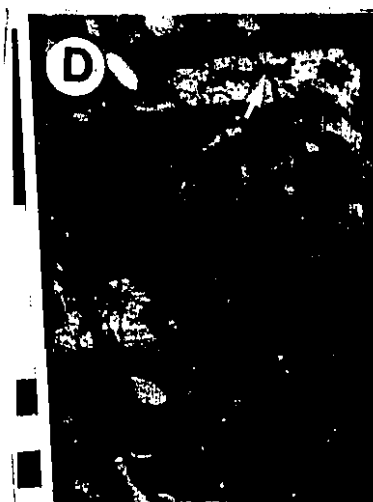
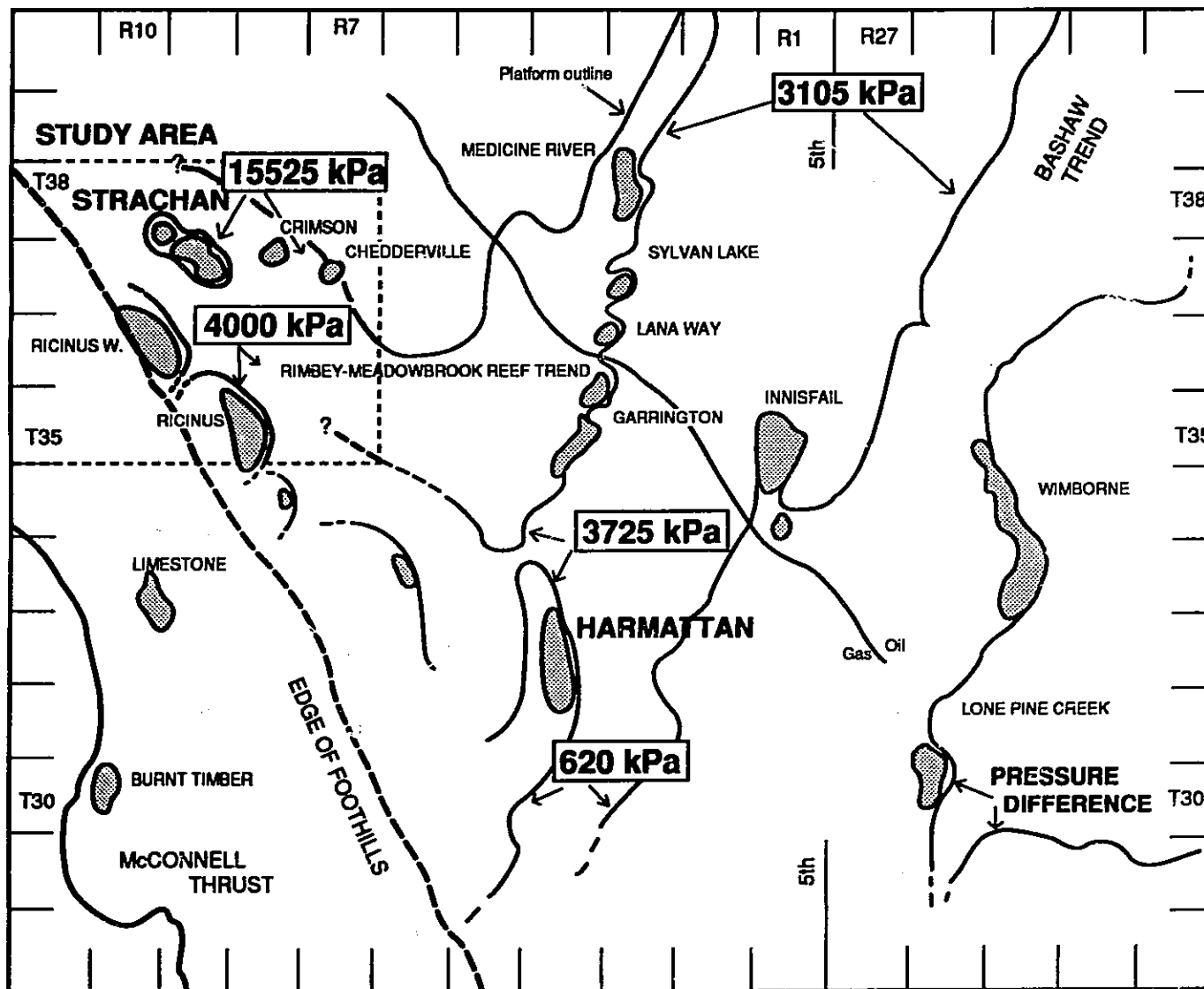


Figure 4.3 Distribution of Leduc buildups in the deep Alberta basin showing discovery pressures. Note the pressure differences (15525 kPa) between the Strachan buildup and the Rimbey Meadowbrook reef trend.



 Oil/Gas Field

 900 kPa Pressure Difference

subsurface (e.g. Amthor et. al., 1993). This unit is normally pressured and subject to regional gravity-driven flow, with recharge in the southwest (Rocky Mountains foothills) and discharge in the northeast (Hugo, 1990; Paul, 1994). Present day reservoir pressures indicate that NNE fluid flow occurs within the Leduc and Cooking Lake formations with flow velocities of 18 cm/year (Paul, 1994).

The Strachan, Ricinus West, Chedderville and Harmattan buildups with hairline microfractures are not presently connected to the main aquifer, as indicated by their anomalously high initial pressures. Pressure-depth plots (Fig. 4.4) clearly show that initial pressure data from Strachan (46644 kPa) and Ricinus West (39991 kPa) lie on different hydrostatic gradients and therefore these buildups are considered to be hydraulically restricted from the main Rimbey-Meadowbrook reef trend. This indicates that some barriers to fluid flow exist between the main Rimbey-Meadowbrook reef trend and the Strachan and adjacent buildups. All of what appear to be hydrologically isolated, overpressured buildups contain hairline microfractures.

Relative timing of hairline microfracturing

Hairline microfractures may have formed at any time during the history of burial and/or uplift of the Strachan buildup. Determining the approximate timing of the formation of the microfractures provides information about the relative depth, temperatures, pressures and stress systems at the time of their formation (see below).

The generation and migration of hydrocarbons occurred during intermediate to deep burial during Cretaceous to Early Tertiary time (Deroo et. al., 1977; Creaney and Allan, 1992) at depths of about 2 to 3 km, perhaps 2800 km (Walls, et. al., 1979). Hydrocarbon migration postdates both replacement dolomitization and dolomite cements. Diagenetic phases that postdate hydrocarbon migration in the Strachan buildup include hairline microfracturing and calcite cements (see paragenetic sequence in Chapter 2, Fig. 2.5).

Thus, microfracturing occurred late in the paragenetic sequence after hydrocarbon generation, probably close to or during deepest burial. Carbon and oxygen isotope and fluid inclusions from calcite cements that postdate microfracturing (see Chapter 2) indicate that calcite cementation occurred at temperatures of about 147°C (an estimate of the minimum temperature at which the fluids were trapped in the calcite cements). Using a paleogeothermal gradient of 30 °C/km and a paleosurface temperature of 20°C this temperature would have been reached at about 4000 m depth of burial during the Late Cretaceous (Fig. 4.5). This brackets the generation of hairline microfracturing to between 2000 and 4000 m burial depth, during the Late Cretaceous when the Strachan buildup was subjected to rapid burial.

The possible mechanisms responsible for the formation of hairline microfractures in the Strachan reservoir are discussed in the following section .

DISCUSSION

The hairline microfractures in the Strachan reservoir are extension fractures that occur in different pore types both in limestones and dolostones (Table 4-1). The microfractures are always filled with reservoir bitumen and formed late in the deep burial environment. Their presence is restricted to well sealed, isolated, overpressured reservoirs. Origin and propagation of extension fractures have been explained in classical papers by Hubbert and Rubey (1959), Secor (1965, 1969), Jaeger (1963), and others (eg. Jaeger and Cook, 1979; Meissner, 1985) by means of the so called law of effective stresses. This concept theoretically establishes that the total stresses (σ_1 , σ_2 , σ_3) across any plane in a fluid saturated rock can be resolved by the equations:

$$(1) \sigma_1 = \sigma_1' + p \quad (2) \sigma_2 = \sigma_2' + p \quad (3) \sigma_3 = \sigma_3' + p$$

where σ_1' , σ_2' , and σ_3' are maximum, intermediate and minimum effective stresses and

Figure 4.4 Pressure-depth plot for Leduc Formation pools in the downdip portion of the Rimbey-Meadowbrook reef trend showing different discovery pressures and present burial depths of the Strachan and Ricinus West buildups. A water density of 9.94 kP/m is used for the hydrostatic pressure gradient. Discovery pressure gradients for Strachan and Ricinus West were obtained from N. Hannon (Canadian Hydrodynamics Ltd.)

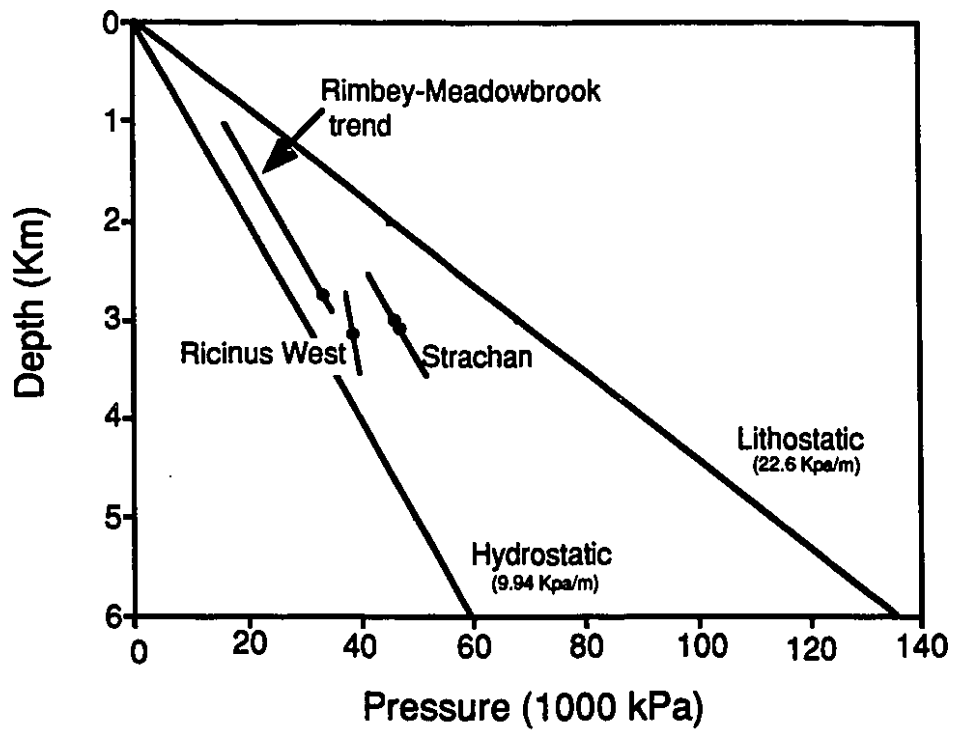
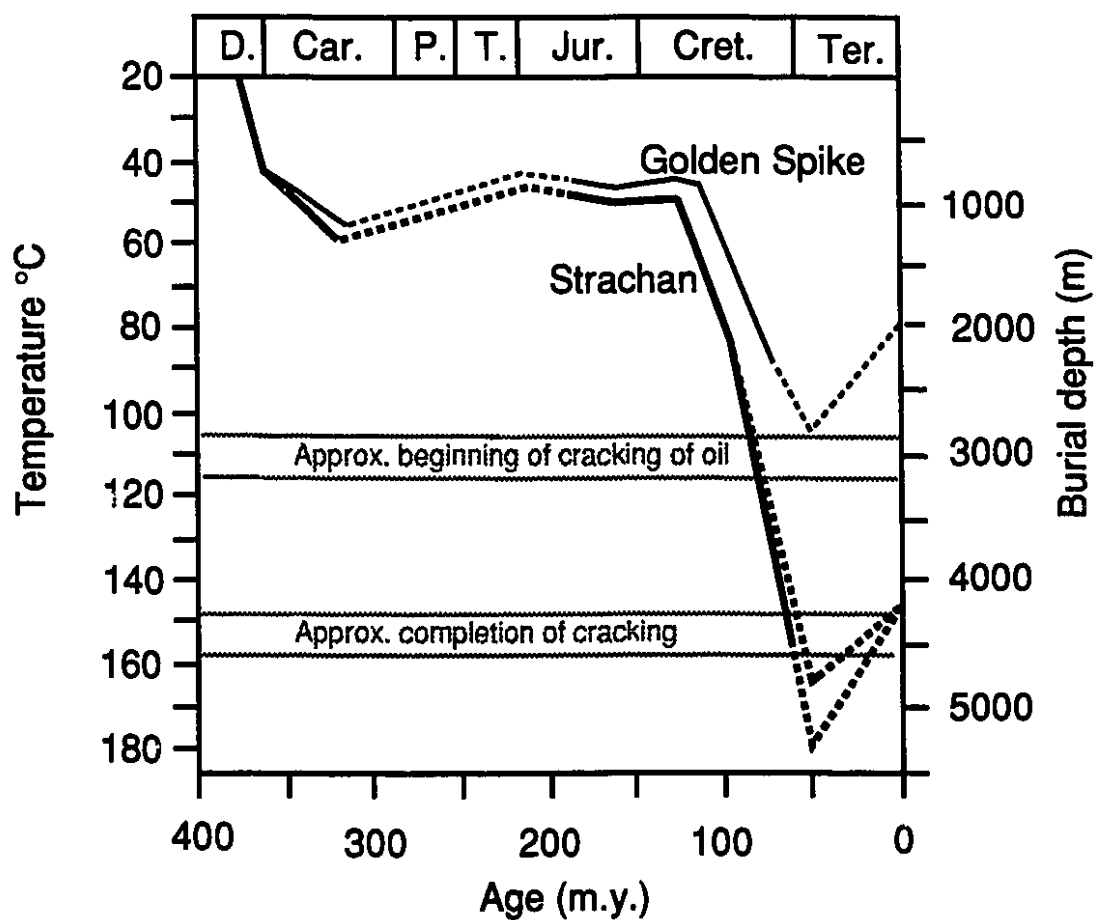


Figure 4.5 Burial-temperature plot for the Leduc Formation in the Strachan buildup, constructed assuming a geothermal gradient of 30°C/km and a surface temperature of 20°C . The burial plot for the Golden Spike buildup (in the updip portion of the Rimbey-Meadowbrook trend; Walls et. al., 1979) is shown for comparison. The inferred burial depths, temperatures, and relative timing of thermal cracking of oil are also plotted.

BURIAL PLOTS

Top of Leduc
30o C/Km geothermal gradient



p is the internal pore pressure (Hubbert and Rubey, 1959). Equations 1, 2 and 3 suggest that the total stress (e.g. total overburden weight) applied to a particular system is partly supported by the pore pressure and the matrix (effective) stress. Thus any increase or decrease (Δp) of the pore pressure will affect the effective stress. Experiments (e.g. Jaeger, 1963, Handin et. al., 1963) confirmed the theoretical prediction that fracturing is controlled by critical effective stresses.

The effect of an increase in pore pressure ($+\Delta p$), using the Mohr circles representation, is illustrated in Figure 4.6A. A positive Δp shifts the stress circle to the left, where σ_3' assumes a very small, yet still positive, value (Gretener, personal comm. 1994). In this region the ratio σ_1' / σ_3' becomes very large and high compressive as well as tensile wall stresses (σ_θ) occur in all pores. The distribution of wall stresses (σ_θ) around a circular pore are illustrated in Figure 4.6B. At points 1 and 2 the wall stresses assume a maximum value ($\sigma_{\theta \max}$) and at points 3 and 4 a minimum value ($\sigma_{\theta \min}$). The magnitude of these maximum and minimum pore wall stresses is related to the effective stresses as follows (Gretener, personal comm. 1994):

$$(4) \sigma_{\theta \max} = 3 \sigma_1' - \sigma_3' \quad (5) \sigma_{\theta \min} = 3 \sigma_3' - \sigma_1'$$

Under certain conditions, such as $\sigma_1' > 3 \sigma_3'$ the minimum pore wall stress ($\sigma_{\theta \min}$) become tensile:

$$(6) \sigma_{\theta \min} < 0 \quad \text{and} \quad (7) \sigma_{\theta \max} = 8 \sigma_3'$$

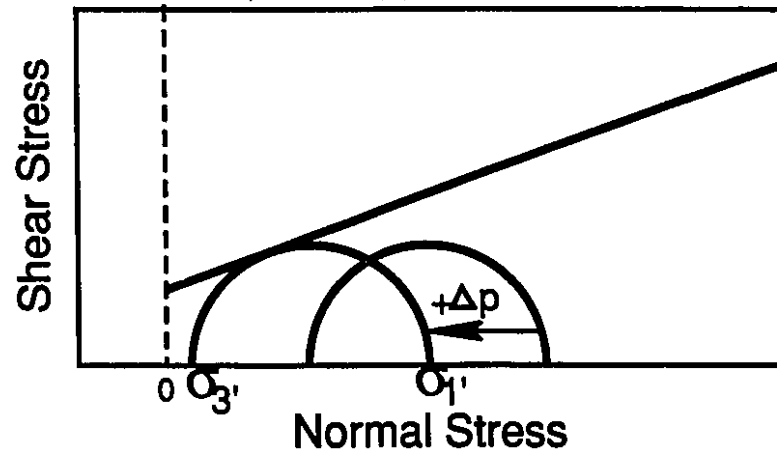
and tension fractures form in a compressive stress environment. The minimum tangential stress become tensile with a condition of high pore pressure ($+\Delta p$) and eventually lead to failure by hydraulic fracturing (Gretener, 1983, 1986; 1988). Fractures will propagate preferentially in the horizontal direction if the maximum compressive stress is horizontal,

TABLE 4-1 Characteristics of hairline microfractures in Strachan reservoir

- a. Formed by extension
 - b. Always extend from primary and secondary pores
 - c. Occur in three patterns: subhorizontal, radial and random
 - d. Occur in limestones (skeletal rudstones, packstones) and dolostones
 - e. Absent in skeletal grainstones
 - f. Abundant in the upper part of the reservoir
 - g. Always filled with reservoir bitumen
 - h. Formed late in the paragenetic sequence, after generation and migration of oil
 - i. Restricted to isolated, well sealed reservoirs
 - j. Occur in the deeper part of the basin below 3800 m
-

- Figure 4.6**
- a) Role of pore pressure in fracture initiation. An increase in pore pressure (p) shifts the Mohr half circle to the left where it may touch the failure envelope and initiate fracturing.
 - b) Stresses at principal points around a circular pore. At points 1 and 2 the tangential stresses assume a maximum value ($\sigma_{\theta\max}$) and at points 3 and 4 a minimum value ($\sigma_{\theta\min}$).

A) Tension (-), Compression (+)



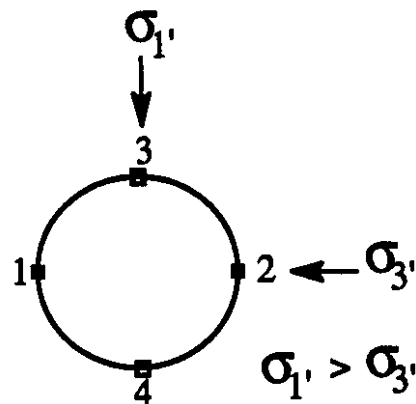
Effective stresses

$$\sigma_3' = \sigma_3 - p$$

$$\sigma_1' = \sigma_1 - p$$

σ_1, σ_3 = Total stresses
 p = Pore pressure

B)



$$\sigma_{\theta \min} = 3 \sigma_3' - \sigma_1' \quad \sigma_{\theta \max} = 3 \sigma_1' - \sigma_3'$$

and vertically if the maximum compressive stress is vertical (Kunlander et. al., 1979). Hubbert and Willis (1957) have shown that most hydraulic fractures are oriented vertically since commonly the maximum compressive stress (σ_1) is oriented vertically. However, under a tectonic condition of lateral compression (type A, Gretener, personal comm. 1994) leading to thrusting the maximum compressive stress is horizontal, with the following stress configuration (Kulander et al., 1990):

$\sigma_H > \sigma_h > \sigma_v$ where σ_H is the maximum stress (σ_1'), σ_h is the intermediate stress (σ_2') also oriented horizontally, and σ_v is the minimum stress (σ_3') oriented vertically. Thus, fractures will be oriented horizontally.

The preceding review of basic fracture theory, suggests that the type of extension microfractures present in the Strachan reservoir can be initiated under certain conditions during an increase in pore pressure. The following sections show how increasing pore pressure probably formed these microfractures, and attempt to explain the different patterns of the microfractures.

Development of Pore Pressures

Critical fluid overpressures leading to fracture can be caused by a number of processes (eg. Gretener, 1976). The most commonly cited processes are: 1) disequilibrium compaction, 2) tectonic stress, 3) hydrocarbon generation, 4) thermal expansion of pore fluids, and 5) thermal cracking of crude oil. The first three processes are outlined briefly and for various reasons are ruled out as suitable mechanisms for forming hairline microfractures. Thermal expansion of pore fluids together with thermal cracking of oil are discussed at greater length because they would have increased pore pressure to the point where microfracturing could take place late, after the migration of hydrocarbons into the Strachan reservoir.

Disequilibrium compaction - Disequilibrium compaction by rapid loading of rock or sediments by accelerated sediment deposition leads to a rate of loading that exceeds the rate of pore fluid escape during subsequent compaction (see, for example, Bradley, 1975; Magara, 1971; Mudford, 1990; Palciauskas and Domenico, 1980). In central Alberta, the Woodbend shales, including the sealing Ireton shales, underwent rapid compaction during their first 500 m of burial, largely during the Late Devonian, and no overpressures developed (see Hugo, 1990). The relative timing of the microfractures suggest that they most likely formed between 3000 and 4000 m of burial during the Late Cretaceous, as noted above. Although the Strachan reservoir underwent rapid burial, disequilibrium compaction cannot account for increases in pore pressures during the latest stages of burial because mechanical compaction of the strata had already taken place.

Tectonic stress - lateral tectonic stress generated by mountain building processes and commonly accompanied by thrust sheet loading and shearing (e.g. Shi and Wang, 1988) can be effective 100's of km cratonward in front of an advancing fold belt (i.e. Lorenz et al. 1991), and can modify significantly the horizontal stress orientations and magnitudes. These lateral tectonic stresses likely altered the stress magnitudes at the time of microfracturing in the Strachan reservoir.

Kerogen transformation - Du Rouchet (1981); Meissner (1980); Spencer (1987) and Surdam et. al. (1991) among others have pointed out that the kerogen to hydrocarbon transformation creates excess fluid pressures in source rocks. Hairline microfractures in the Strachan reservoir originated after the generation and migration of hydrocarbons, excluding this process from the generation of high pore pressures in the Strachan buildup.

Thermal processes - Thermal processes such as the expansion of pore fluids in rocks of very low permeability (e.g. aquathermal pressuring; Barker, 1972; Magara 1975), and cracking of oil (Barker, 1988, 1990) can lead to high pore pressures, provided that the

rates of pressure production were larger than rates of pressure dissipation (Domenico and Schwartz, 1990). These two processes most likely would cause overpressuring in deeply buried reservoirs and would take place together in the deep, isolated Strachan buildup. The potential of thermal cracking of oil for developing pressures considerably higher than hydrostatic pressure was demonstrated by Barker (1990). The conversion of oil to gas involves a redistribution of hydrogen (Barker, 1979). The overall effect of this process when it proceeds to completion is to form methane as the hydrogen-rich material and carbon. Barker (1990) modeled a system in which gas is generated by the thermal cracking of oil and illustrated the hydrogen redistribution according to variations in the composition of the oil (see equation 3, Barker, 1990).

Using this hydrogen redistribution, Barker (1990) calculated the volume of gas that can be produced by cracking a barrel of crude oil and indicated that in the presence of sulphur (see Chapter 2), 1 bbl of oil (0.16 m^3) will produce 69 m^3 of gas. Thus, a volume increase of about 430 times should be expected for a specific type of crude oil. If the system is effectively isolated so that the pore volume remains constant, then the pressure that develops in the gas may be much higher than hydrostatic pressure for a given depth. The response to a significant increase in pore pressure in an isolated reservoir is fracturing with partial loss of gas (e.g. Secor, 1965; Price, 1974).

The importance of thermal alteration in affecting the hydrocarbons in the deeper part of the Alberta basin has been discussed by several researchers (e.g. Rogers et.al., 1974; James, 1990). Significant oil generation would have been initiated in the Duvernay source beds at burial depths of between about 2 to 3 km during the Late Cretaceous (Fig. 4.5). During and following migration of oil into the Leduc buildups in the study area the Strachan reservoir was subjected to rapid burial and temperature increases. Under these conditions oil pooled in the reservoir becomes thermodynamically metastable and is altered by cracking to dry gas (CH_4) and carbonaceous material (Tissot and Welte, 1984; p. 459).

Methane (CH_4 ; 85%) and ethane (C_2H_6 ; 2.9%) are the most volumetrically abundant hydrocarbons in the Strachan reservoir (Appendix F). Common non-hydrocarbon gases include hydrogen sulphide (H_2S ; 7.1%) and minor carbon dioxide (CO_2 ; 2.1%). This gas composition, H_2S plus dry gas (CH_4) is typical of gases generated in the deep subsurface predominantly by the thermal degradation of oils (Evans and Staplin, 1971; Hunt, 1979, p. 151). Methane formed by thermal cracking have been shown by Stahl (1974) to have $\delta^{13}\text{C}$ values in the range of -35 to -40‰ PBD. No information on the carbon isotopic composition of gases in the Strachan reservoir is available in this study, however, James (1990) reported the carbon isotopic composition for methane in the adjacent Ricinus West reservoir to be $\delta^{13}\text{C} = -39.84$ ‰ PBD, and for ethane $\delta^{13}\text{C} = -17.77$ ‰ PBD, which are heavier than $\delta^{13}\text{C}$ for gases along the Rimbey Meadowbrook reef trend (-44.3 and -31.9‰ PBD, respectively). This means that gases in the Ricinus West and adjacent reservoirs (e.g. Strachan) have undergone thermal degradation (James, 1990).

The most compelling evidence for thermal cracking of liquid oil in the Strachan reservoir, however, comes from the reservoir bitumens (see Appendix D). Two types of reservoir bitumens, isotropic and anisotropic are present in the Strachan reservoir (Stasiuk, 1994). Isotropic bitumens are minor and suggest a non-graphitizing source (NSO compounds). Anisotropic bitumens are widespread in the upper 200 m of the reservoir and are characterized by fine deformed (fibrous and lamellar) and coarse deformed lamellar textures that indicate nucleation, growth and percolation of gas bubbles during the cracking of a graphitizing (petroleum-like) material (Stasiuk, 1994). This cracking may have started immediately after the emplacement of liquid hydrocarbons between about 2000 to 3000 m of burial and temperatures between 80 and 110°C, assuming a paleogeothermal gradient of 30°C/km and a surface temperature of 20°C (Fig. 4.5). However, it probably became

increasingly important at higher temperatures ($>125^{\circ}\text{C}$; Hunt, 1979). Completion of cracking commonly occurs near the floor of the oil window at about 150°C (Pursey, 1973), or slightly higher temperatures. This corresponds to burial depths of about 4500 m which would have occurred during the Late Cretaceous (Fig. 4.5).

This brackets the development of thermal cracking to have taken place between burial depths of 3000 and 4500 m during Late Cretaceous. During the initial phases of cracking at around 125°C or depths of about 3500 m, the main increase in pressure would occur after only about 1 to 2.5% of the crude oil had been converted to gas (Barker, 1990, p. 1260), since this would increase the volume by about 431 times. The actual depth and volume increase, will depend on the original composition of the oil, oil/water ratio and the oil/gas conversion factor used, but depths of between 3000 and 4000 m seem reasonable for the Strachan reservoir.

High pore pressures would have induced the formation of the hairline microfractures in the Strachan reservoir if it was well sealed. During overpressuring and microfracturing of the reservoir it is likely that the Ireton seal would also have been fractured and some of the gas and oil leaked off, reducing the pressure. As the reservoir continued to be buried more crude oil would be converted to gas repressurizing the reservoir provided it was effectively sealed. High discovery pressures in the Strachan reservoir suggest that it has been isolated from the main reef trend and that it was initially well sealed. Thus, considerable gas generated near the end of thermal cracking remained in the reservoir.

The information discussed above suggests that cracking of liquid crude oil occurred in the Strachan reservoir at burial depths between 3000 and 4500 m. This process would have generated high pore pressures because the conversion of oil to gas results in a volume increase of more than 400 times (Barker, 1990). The initial stages of thermal cracking and

resulting high pore pressures would have taken place between 3000 and 4000 m of burial, and probably induced the formation of hairline microfractures in the isolated, apparently well sealed Strachan reservoir.

Microfracture orientations

From the preceding discussion it is likely that thermal cracking of crude oil to gas may have altered the local stress state by generating high pore pressures. The orientation of the stresses however may be controlled by external factors. Data on measured in-situ stresses in the Alberta basin show subsurface fractures parallel to present-day maximum horizontal compressive stress (σ_H oriented NE-SW; Bell and Babcock, 1986), suggesting that laterally transmitted horizontal compressive stress from an active thrust belt into the relatively undisturbed strata of the adjacent foreland basin may have created anisotropic horizontal stresses and ultimately fractures (Woodland and Bell, 1988).

The Western Canadian basin lies on the northwestern edge of the Mid-Continent stress province (Zoback and Zoback, 1980) in which maximum horizontal stress is presently oriented in a NE-SW direction. A general NE-SW orientation of the maximum horizontal compressive stress (σ_H), approximately perpendicular to the strike of the Rocky Mountain thrust belt, apparently has been imposed on the Western Canadian basin from the Late Jurassic time until the Paleocene (about 55 Ma ago).

Measurements of current day stresses in the Alberta basin have been reported by Fordjor, et. al. (1983) and Bell and Babcock (1986). It seems that since the Paleocene compression has changed to a current stress condition where

$$\sigma_H \sim \sigma_v > \sigma_h$$

with σ_H oriented perpendicular to the mountain front (NE-SW) and σ_h parallel to the mountain front. However the inferred stress orientation at the time of microfracture

formation (Late Cretaceous) was probably

$$\sigma_H > \sigma_h > \sigma_v$$

where lateral compression led to thrust faulting in the southern Canadian Rockies. Horizontal compressive stresses related to deformation in the thrust and fold belt would have affected the orientation of the principle stress axes around the Strachan buildup. Preferentially, microfractures would propagate horizontally when the maximum compressive stress is horizontal.

More difficult to explain are the radial microfractures. For their formation they would require a pressure distribution which was uniform for all 3 stress axes, which is difficult to achieve in the subsurface. This could happen during overpressuring in conjunction with a compressive horizontal stress. Under these conditions a uniform stress field could be produced at a particular depth during deep burial. These conditions would happen again when the horizontal stress decreased at the end of tectonic compression in the Paleocene.

Distribution of microfractures in the Strachan reservoir

The majority of the studied wells penetrate only the upper part of the reservoirs. However, well 10-31 that penetrated almost the entire reservoir shows the absence of microfracturing 215 m below the top of the reservoir. The reasons for this are not obvious, but as mentioned above failure by hydraulic fracturing in the Strachan reservoir would occur when the total pore pressure equals or exceeds σ_3 . This total pore pressure is composed of the natural aquifer pressure (water pressure) plus the additional hydrocarbon-water capillary pressure. This additional capillary pressure occurs in the hydrocarbon saturated zoned, and is probably responsible for the abundance of microfractures in the upper part of the reservoir. This suggestion needs further testing.

CONCLUSIONS

The characteristics and distribution of late stage hairline microfractures in the Strachan reservoir in the deep Alberta basin indicate:

1) Hairline microfractures in the Strachan reservoir are extensional fractures that always extend away from different pore types in a subhorizontal, radial or random pattern. These microfractures postdate the generation and migration of oil since they are always filled by reservoir bitumen, and crosscut almost all diagenetic features. Hairline microfractures are restricted to reservoirs in the deep basin, below depths of 3800 m that were isolated and inferred to have been well sealed. Their association with pores and their extensional nature suggest that they formed by high pressures that developed within the pores of the reservoir rock.

2) Thermal cracking of crude oil to gas is the most likely mechanism to have developed the necessary high pore pressures to form the hairline microfractures. This is based on the optical textures in reservoir bitumens filling microfractures and pores, and the present gas composition in the Strachan reservoir. The conversion of crude oil to gas would have resulted in a enormous volume increase in an isolated, well sealed reservoir. These high pore pressures would have caused the minimum tangential stresses in the pore walls to become tensile ($\sigma_{\theta\min} < 0$) resulting in microfracturing.

3) The conversion of crude oil to gas would have been initiated at temperatures of about 125°C. Thus high pore pressures would have developed at burial depths between 3000 and 4000 m during the Late Cretaceous. During this time the Strachan reservoir was undergoing continuous burial. Also at this time, laterally transmitted horizontal compressive stresses from the thrust belt to the southwest may have increased the magnitude of horizontal stresses in the Strachan reservoir, thus forming the abundant horizontal fractures.

4) The radial microfractures formed under special conditions of uniform stresses which could happen at a particular depth during overpressuring in conjunction with compressive horizontal stress.

Thus, extensive, hairline microfractures in the Strachan reservoir most likely formed in response to the development of high pore pressures caused by the thermal cracking of crude oil to gas, in conjunction with lateral compression during thrusting in the Late Cretaceous to Paleocene.

CHAPTER 5

GENERAL CONCLUSIONS

The complex reservoir geology of the Leduc buildups in the deep Alberta basin has been determined by a detailed study of the depositional facies and diagenesis of several carbonate buildups and their pore systems. The principal conclusions from each chapter provide new insight about the characterization of carbonate reservoirs.

1) The upper Leduc Formation in the Strachan, Ricinus West and adjacent buildups represent shallow-marine carbonates. High energy, reef margin facies include coral, tabular stromatoporoid and stromatoporoid-coral rudstones. The reef interior is characterized by skeletal packstones/grainstones, skeletal wackestones and microbial laminite facies that indicate shallowing upward peritidal conditions.

2) Textures and compositions of isolated dolomite rhombs and patches in pool D3B of the partially dolomitized Strachan buildup are similar to replacement dolomites in the completely dolomitized Strachan pool D3A. The replacement dolomitization of the Leduc Formation in the study area took place as a major dolomitizing event that occurred in a shallow burial environment at depths of about 500 m based on their crosscutting relationships with early submarine cements, relationships with stylolites, and their occurrence in the overlying Ireton Formation. Dolomitizing fluids were probably modified from Devonian seawater as shown by slight deviations in trace element concentrations and higher $^{87}\text{Sr}/^{86}\text{Sr}$ ratios (0.7083 to 0.7092) than corresponding hypothetical Devonian seawater. These replacement dolomites are similar to replacement dolomites in adjacent buildups (Ricinus West, Ricinus East, Crimson and Chedderville) and in buildups along the Rimbey Meadowbrook reef trend. This suggests that replacement dolomites formed

from the same fluids during a regional to basin-wide event.

3) Migration of crude oil into the reservoir from the adjacent Duvernay Formation took place during the Late Cretaceous (Fig. 2.11). Thermal cracking of crude oil was initiated during rapid burial and increasing temperature at about 125°C and depths most likely between 3000 and 4000 m. Cracking resulted in the formation of gas-condensates and reservoir bitumens. Some of the gas generated dissolved in the crude oil and caused minor deasphalting. The presence of abundant methane together with dissolved sulphate facilitated the onset of thermochemical sulphate reduction (TSR), producing minor amounts of H₂S. TSR reactions thermal cracking and thermochemical sulfate reduction occurred over a long period of geologic time at temperatures in the 110-150°C range during increasing burial.

4) In partly dolomitized rocks of Strachan D3B pool anhydrite, sulphides and native sulfur are absent and the amount of H₂S is low (3.2%). In dolostones of the D3A pool and adjacent dolomitized buildups these cements are common and H₂S concentrations are high (up to 33%). Hairline microfractures are abundant only in the isolated, partially dolomitized Strachan buildup. This can be explained by major differences in diagenesis that took place in the partially dolomitized Strachan buildup compared to completely dolomitized buildups. These differences are best explained if the completely dolomitized buildups were connected, probably since the time of replacement dolomitization, to a regional fluid conduit system along the Cooking Lake platform that underlies the Rimbey Meadowbrook reef trend.

5) The Cooking Lake conduit system provided the flow paths for replacement dolomitization, secondary migration of hydrocarbons and later diagenetic products. On the other hand, the rather unique characteristics of the Strachan buildup (partial dolomitization, different diagenesis, thermal cracking of crude oil, overpressuring and, hairline

microfractures) are explained if it was somewhat isolated from this conduit system. Restriction of fluid flow to the Strachan buildup appears to be related to the underlying Cooking Lake platform being more argillaceous and thinner beneath this buildup.

6) Completely dolomitized Upper Devonian Leduc buildups at depths greater than 4000 m have higher porosities and permeabilities than limestones because dolostones are more resistant to pressure solution.

7) The relationships between the proportion of dolomite and porosity are complex, but a slight increase in porosity with increasing dolomitization occurs, which becomes more pronounced above 80% dolomite. In general porosity and permeability increase with increasing dolomitization, with the highest porosity and permeability occurring in completely dolomitized facies. The highest porosities and permeabilities occur in the completely dolomitized interior of the Strachan buildup. At the reef margin, porous and permeable dolostones are interbedded with nonporous and nonpermeable limestones. These trends are modified by later cements, dissolution and bitumen emplacement.

8) Pore types are grouped into pore systems that closely follow depositional units in the Ricinus West buildup. This buildup is representative of other dolomite reservoirs in the deep basin. At the reservoir scale porosity and permeability are similar throughout. At the next smaller meter scale, pore system I in the upper 131 m of the reservoir is characterized by 1 to 2 m thick, permeable, and laterally continuous, reef interior (lagoonal) zones. Pore system II in the lower 61 m of the reef interior has laterally discontinuous permeable zones. Pore system III is restricted to the 259 m thick reef margin where intervals of fractures and connecting vugs provide vertical permeability. The best lateral permeability occur in pore system I and is related to laterally continuous skeletal wackestone facies that have been dolomitized to a rock with good intercrystalline porosity. The best vertical interconnections are provided by connecting vugs and subvertical fractures in pore system III.

9) At the even smaller pore and mm scale porosity and permeability are controlled

by diagenetic processes. Post-dolomitization processes, such as cementation, dissolution and bitumen plugging, modified porosity and permeability. Anhydrite cementation, minor dolomite, calcite and native sulphur cementation reduced porosity and, more significantly, permeability, producing a high degree of heterogeneity in the lower part of the reservoirs.

10) Reservoir bitumen reduces porosity and permeability by decreasing pore and pore throat sizes mainly in the upper part of the Ricinus West reservoir. Bitumen coating may cause wettability to change from water-wet to intermediate in water/gas systems. Bitumen can only be determined by logging core, petrographic analysis, and core porosity measurements. Errors in reservoir volumetric calculations from well logs can arise because of the lack of significant density contrast between crude oil and bitumen making reservoir bitumen indistinguishable from oil-filled porosity.

11) The characteristics and distribution of late-stage hairline microfractures in the Strachan reservoir in the deep Alberta basin indicate that hairline microfractures in the Strachan reservoir are extensional fractures that always extend away from different pore types in a subhorizontal, radial or random pattern. These microfractures postdate the generation and migration of oil since they are always filled by reservoir bitumen, and crosscut almost all diagenetic features. Hairline microfractures are restricted to reservoirs in the deep basin, below depths of about 3800 m, that were isolated and inferred to have been well sealed. Their association with pores and their extensional nature suggest that they formed by high pressures that developed within the pores of the reservoir rock.

12) Thermal cracking of crude oil to gas is the most likely mechanism to have developed the necessary high pore pressures to form the hairline microfractures. This is based on the optical textures in reservoir bitumens that fill microfractures and pores, and the present gas composition in the Strachan reservoir. The conversion of crude oil to gas would have resulted in a volume increase of about 400 times, in an isolated, inferred to be well sealed reservoir. These high pore pressures would have caused the minimum

tangential stresses in the pore walls to become tensile ($\sigma_{\theta\min} < 0$) resulting in microfracturing.

13) The conversion of crude oil to gas would have been initiated at temperatures of about 125°C. High pore pressures would have developed at burial depths between 3000 and 4000 m during the Late Cretaceous when the Strachan reservoir was undergoing continuous burial. Also at this time, laterally transmitted compressive stresses from the thrust belt to the southwest may have increased the magnitude of horizontal stresses in the Strachan reservoir forming abundant horizontal fractures. The radial microfractures formed under special conditions of uniform stresses during overpressuring in conjunction with compressive horizontal stress. Thus, extensive, hairline microfractures in the Strachan reservoir most likely formed in response to the development of high pore pressures caused by the thermal cracking of crude oil to gas, in conjunction with compression due to thrusting during the Late Cretaceous.

Reconstruction of the depositional and diagenetic history from detailed studies of cores is essential for realistic modelling of reservoirs. Differences in approach in grouping porosity and permeability data in reservoir characterization can lead to major differences in modelling and assessment of a reservoir. Critical to a realistic assessment is to describe the reservoir (depositional facies and sequences and their pore types) as geologically faithful as possible, rather than by means of arbitrary slices or blocks. As shown in this thesis such studies demonstrate that carbonate reservoirs are extremely heterogeneous and that discontinuous relatively nonporous and low permeability zones greatly affect reservoir performance and production.

Future work

This research provides the background and stimulus for future research on the geochemistry of the dolomites (trace elements and fluid inclusions) to determine the presence or lack of geochemical trends and further constrain the origin and timing of dolomites and later diagenetic products. Further research on thermal sulphate reduction (TSR) and its effects on the petrophysical properties of reservoirs in the deep basin is needed.

The Cooking Lake platform that underlies the Rimbey Meadowbrook reef trend appears to have acted as a regional conduit system since the time of dolomitization and controlled the variable dolomitization in the Strachan buildup. A study of the depositional facies and diagenesis of the Cooking Lake Formation in the deep Alberta basin is needed to determine its role as an aquifer.

Reconstruction of the depositional and diagenetic history of the Leduc buildups in the deep Alberta basin serves as a basis for a more detailed study of the smaller scale attributes of carbonate reservoirs. This can be done by studies of matrix pore geometries using SEM microscopy, pore casts, image analyses and capillary pressure curves, determining aspect ratio, spatial distribution, connectivity, roughness of pore walls, and entry pressures. This would increase the ability of reservoir geologists to predict reservoir performance prior to enhanced recovery techniques.

Also needed is a study of the textures and distribution of reservoir bitumen using SEM microscopy, image analysis, point-counting and correlation with well logs in order to better assess the influence of bitumen on reservoir heterogeneity and the use of bitumen textures as paleotemperature indicators.

REFERENCES

- Allan, J. and S. Creaney, 1991, Oil families of the Western Canada Basin. *Bulletin of Canadian Society of Petroleum Geologists*, v. 39, p. 107-122.
- Amthor, J.E., E.W. Mountjoy and H.G. Machel, 1993, Subsurface dolomites in Upper Devonian Leduc Formation buildup, central part of Rimbey-Meadowbrook reef trend, Alberta, Canada. *Bulletin of Canadian Society of Petroleum Geologists*, v. 41, p. 164-185.
- Amthor, J.E., E.W. Mountjoy and H.G. Machel, 1994 in press, Regional-scale porosity and permeability variations in Upper Devonian Leduc buildups: implications for origin and distribution of porosity in carbonates. *American Association of Petroleum Geologists Bulletin*, v. 78
- Anderson, G. M., 1983, Some geochemical aspects of sulphide precipitation in carbonate rocks. *International Conference on M.V.T. deposits, Rolla-Missouri*, p. 61-76.
- Andrichuk, J.M., 1958a, Stratigraphy and facies analysis of Upper Devonian reefs in Leduc, Stettler and Redwater areas, Alberta. *American Association of Petroleum Geologists Bulletin*, v. 42, p. 1-93.
- Andrichuk, J.M., 1958b, Cooking Lake and Duvernay Late Devonian sedimentation in Edmonton area of central Alberta, Canada. *American Association of Petroleum Geologists, Bulletin*, v. 42, p. 2189-2222.
- Archie, G.E., 1952, Classification of carbonate reservoir rocks and petrophysical considerations. *American Association of Petroleum Geologists, Bulletin*, v. 36, p. 278-298.
- Barfoot, G. L. and R. J. Rodgers, 1984, Leduc, A new life at 38. *Journal of Canadian Petroleum Technology*, May-June, p. 41-46.
- Barfoot, G.L. and S.C.M., Ko, 1987, Assessing, and compensating for, the impact of the Leduc D-3A gas cap blowdown on the other Golden Trend pools. *Journal of*

- Canadian Petroleum Technology, July-August, p. 28-36.
- Barker, C., 1972, Aquathermal pressuring-role of temperature in development of abnormal pressure zones. American Association of Petroleum Geologists Bulletin, v. 56, p. 2068 -2071.
- Barker, C., 1979, Organic geochemistry in petroleum exploration. American Association of Petroleum Geologists, Continuing Education Course Note Series 10, 159 p.
- Barker, C., 1988, Generation of anomalous internal pressure in source rocks and its role in driving petroleum migration: Revue de l'Institut Francaise du Petrole, v. 43, p. 349-355.
- Barker, C., 1990, Calculated volume and pressure changes during the thermal cracking of oil to gas in reservoirs. American Association of Petroleum Geologists Bulletin, v. 74, p. 1254-1261.
- Bathurst, R.G.C., 1975, Carbonate sediments and their diagenesis. 2nd ed., Elsevier, New York, p. 658.
- Bell, J.S. and E.A. Babcock, 1986, The stress regime of the Western Canadian Basin and implications for hydrocarbon production. Bulletin of Canadian Society of Petroleum Geologists, v. 34, p. 364-378.
- Bradley, J.S., 1975, Abnormal formation pressure. American Association of Petroleum Geologists Bulletin, v. 59, p. 957-973.
- Burke, W. H., R.E. Denison, E.A. Hetherington, R.B. Koepnick, H.F. Nelson and J.B. Otto, 1982, Variation of seawater $^{87}\text{Sr}/^{86}\text{Sr}$ throughout Phanerozoic time. Geology, v. 10, p. 516-519.
- Burrowes, O.G., 1977, Sedimentation and diagenesis of back-reef deposits, Miette and Golden Spike buildups, Alberta. Unpublished M. Sc. thesis, McGill University, 207 p.
- Burrowes, O.G. and I. Weihmann, 1982, Cambrian and Devonian Geology of the Grassi

- Lake and Big Hill area, Alberta. American Association of Petroleum Geologists Annual Convention, Canadian Society of Petroleum Geologists Field Trip Guide Book no. 5. 46 p.
- Burrowes, O.G. and F.F. Krause, 1987, Overview of the Devonian System: Subsurface Western Canada Basin. *In*: Krause F.F. and O.G. Burrowes eds., Devonian lithofacies and reservoir styles in Alberta, 13th Canadian Society of Petroleum Geologists Core Conference and Display, August 19-21, p. 1-20.
- Carpenter S.J. and K. C. Lohmann, 1989, $\delta^{18}\text{O}$ and $\delta^{13}\text{C}$ variations in Late Devonian marine cements from the Golden Spike and Nevis reefs, Alberta, Canada. *Journal of Sedimentary Petrology*, v. 59, p. 792-814.
- Chilingarian, G.V., S.J. Mazzulo, and H.H. Rieke, 1992, Carbonate reservoir characterization: a geologists - engineering analysis, part I. *Developments in Petroleum Science* 30, Elsevier, 639 p.
- Choquette, P. W. and L. C. Pray, 1970, Geologic nomenclature and classification of porosity in sedimentary carbonates. *American Association of Petroleum Geologists Bulletin*, v. 54, p. 207-250.
- Choquette, P. W., A. Cox and W. J. Meyers, 1992, Characteristics, distribution and origin of porosity in shelf dolostones: Burlington-Keokuk Formation. *Journal of Sedimentary Petrology*, v. 62, p. 167-189.
- Chouinard, H., 1993, Lithofacies and diagenesis of the Cooking Lake platform carbonates, Alberta basin subsurface, Canada. Unpublished M.Sc.thesis, McGill University, 101 p.
- Connolly, C.A., L.M. Walter, H. Baadsgaard and F.J. Longstaffe, 1990a, Origin and evolution of formation waters, Alberta basin, Western Canada Sedimentary basin. Part 1 Chemistry. *Applied Geochemistry*, v. 5, p. 375-395.

- Connolly, C.A., L.M. Walter, H. Baadsgaard and F.J. Longstaffe, 1990b, Origin and evolution of formation waters, Alberta basin, Western Canada Sedimentary basin. Part 2 Isotope systematics and water mixing. *Applied Geochemistry*, v. 5, p. 397-413.
- Cornelius, C.D., 1987, Classification of natural bitumen: A physical and chemical approach. *In*: Meyer, R.F. ed., *Exploration for heavy crude oil and natural bitumens*. American Association of Petroleum Geologists Studies in Geology 25, p. 165-174.
- Creaney, S. and J. Allan, 1992, Petroleum systems in the foreland basin of Western Canada. *in* R.W. Maqueen and D.A. Leckie eds., *Foreland Basins and Fold Belts*, American Association of Petroleum Geologists Memoir 55, p. 279-308.
- Dawans, J. M. and P. K. Swart, 1988, Textural and geochemical alterations in Late Cenozoic Bahamian dolomites. *Sedimentology*, v. 35, p. 385-403.
- Deming, D., 1994, Factors necessary to define a pressure seal. *American Association of Petroleum Geologists Bulletin*, v.78, p.1005-1009.
- Deroo, G., T.G. Powell, T. Tissot, and R.G. McCrossan, 1977, The origin and migration of petroleum in the Western Canadian sedimentary basin, Alberta: A geochemical and thermal maturation study: Geological Survey of Canada, Bulletin 136 p. 262
- Dickinson, G., 1953, Geological aspects of abnormal reservoir pressures in Gulf Coast, Louisiana. *American Association of Petroleum Geologists Bulletin*, v. 37, p.410-432.
- Dix, G. R., 1990, Stages of platform development in the Upper Devonian (Frasnian) Leduc Formation, Peace River arch, Alberta. *Bulletin of Canadian Petroleum Geology*, v. 38A, p. 66-92.
- Dix, G. R., 1993, Patterns of burial and tectonically controlled dolomitization in an Upper

- Devonian fringing-reef complex: Leduc Formation, Peace River arch area, Alberta, Canada. *Journal of Sedimentary Petrology*, v. 63, p. 628-640.
- Domenico, P.A. and F.W.Schwartz, 1990, *Physical and chemical hydrogeology*, John Wiley and Sons, New York, p. 283-315.
- Drivet, E., 1993, Diagenesis and reservoir characterization of Upper Devonian Leduc dolostones, southern Rimbey-Meadowbrook reef trend, central Alberta. Unpublished M. Sc. thesis, McGill University, 115 p.
- Drivet, E. and E. W. Mountjoy, 1993, Porosity variations in Upper Devonian Leduc dolomites, central Rimbey-Meadowbrook reef trend, Alberta. *American Association of Petroleum Geologists Bulletin*, Annual Convention abstracts, p. 93.
- Drivet, E. and E. W. Mountjoy, 1994a, Timing of dolomitization and secondary porosity in Upper Devonian Leduc dolostones, southern Rimbey-Meadowbrook reef trend, Alberta. *Canadian Society of Exploration Geophysicists and Canadian Society of Petroleum Geologists, Joint Annual Convention, Calgary, Alberta Abs.*, 347-348 p.
- Drivet, E. and E. W. Mountjoy, 1994b, submitted, Characterization of Upper Devonian Leduc dolostone reservoir in the Homeglen-Rimbey field, central Alberta. *Bulletin of Canadian Petroleum Geology*,
- Dunham, R.J., 1962, Classification of carbonate rocks according to depositional texture. *In: Ham, W.E. ed., Classification of carbonate rocks. American Association of Petroleum Geologists, Memoir 1*, p. 108-121.
- Dunnington, H.V., 1967, Aspect of diagenesis and shape change in stylolitic limestone reservoirs. *7th World Petroleum Congress Proceedings, Mexico City*, v. 2, p. 339-352.
- Du Rouchet, J., 1981, Stress fields, a key to oil migration. *American Association of Petroleum Geologists Bulletin*, v. 65, p. 74-85.

- Eliuk, L. S., 1984, A hypothesis for the origin of hydrogen sulfide in the Devonian Crossfield member dolomite, Wabamum Formation, Alberta, Canada. *In*: L.S. Eliuk (ed.), Carbonates in subsurface and outcrop, Canadian Society of Petroleum Geologist, Core Conference, Alberta, p. 245-290.
- Embry, A.F. and J.E. Klován, 1971, A late Devonian reef tract on northeastern Banks Island, Northwest Territories. *Bulletin of Canadian Petroleum Geology*, v. 19, p. 730-781.
- Enos, P. and L.H. Sawatsky, 1981, Pore networks in Holocene carbonate sediments. *Journal of Sedimentary Petrology*, v. 51, p. 961-985.
- Evans, C. R. and F. L. Staplin, 1971, Regional facies or organic metamorphism. *In*: R.W. Boyle and J.T. McGerrigle eds, Geochemical exploration, Canadian Institute of Mining and Metallurgy Special volume 11, p. 517-520.
- Fordjor, D.K., J.S. Bell and D.I. Gough, 1983, Breakouts in Alberta and stress in North American Plate. *Canadian Journal of Earth Sciences*, p. 1445-1455.
- Freeze, R.A. and J.A. Cherry, 1979, Groundwater, Englewood Cliffs, New Jersey, Prentice-Hall, 604 p.
- Geldsetzer, H.H. J. and E.W. Mountjoy, 1992, Upper Devonian platform reefs and inter-platform basins, Canmore to Jasper, Alberta. American Association of Petroleum Geologists, annual convention, Calgary, Alberta, Field Trip Guidebook no. 23, 61p.
- Geldsetzer, H.H. J. and M. P. Mallamo, 1993, Upper Devonian reef domain of the Western Canada Sedimentary basin - Banff and Jasper areas. Geological Association of Canada and Mineralogical Association of Canada, Joint Annual Meeting, Field Trip Guidebook, 57 p.
- Ghosh, S. K. and G.M. Friedman, 1989, Petrophysics of a dolostone reservoir: San Andres Formation (Permian), West Texas. *Carbonates and Evaporites*, v. 4,

p.45-119.

- Gonzalez, L.A. and K.C. Lohmann, 1985, Carbon and oxygen isotopic composition of Holocene reefal carbonates. *Geology*, v. 13, p. 811-814.
- Gregg, J.M. and D. F. Sibley, 1984, Epigenetic dolomitization and the origin of xenotopic dolomite texture. *Journal of Sedimentary Petrology*, v. 54, p. 908-931.
- Gregg, J.M. and K.L. Shelton, 1990, Dolomitization and dolomite neomorphism in the back reef facies of the Bonnetterre and Davies formations Cambrian, southeastern Missouri. *Journal of Sedimentary Petrology*, v. 54, p. 908-931.
- Gretener, P.E., and Z-M Feng, 1985, Three decades of geopressures, insights and enigmas. *Bulletin Vereinigung Schweizerischer Petroleum Geologen und Ingenieure*, v. 51, p. 1-34.
- Gretener, P.E., 1976, Pore pressure: Fundamentals, General Ramifications and Implications for Structural Geology. American Association of Petroleum Geologists, Continuing Education Course Notes Series n. 4, 87 p.
- Gretener, P.E., 1983, Remarks by a geologists on the propagation and containment of extension fractures. *Bulletin Vereinigung Schweizerischer Petroleum Geologen und Ingenieure*, v.94, p. 29-35.
- Gretener, P.E., 1986, Microfractures and fluid flow. *Bulletin Swiss Association of Petroleum Geologists and Engineers*, v. 53, p. 59-74
- Gretener, P.E., 1988, More on fractured hydrocarbon reservoirs. 54, p. 61-82
- Grint A. and H. Marsh, 1981, Carbonization of coal blends: Mesophase formation and coke properties. *Fuel*, v. 60, p. 1115-1120.
- Handin, J., R.V. Hager Jr., M. Friedman and J.N. Feather, 1963, Experimental deformation of sedimentary rocks under confining pressure: Pore pressure test. *American Association of Petroleum Geologists Bulletin*, v. 47, p. 717-755.
- Hannon, N., 1987, Subsurface water flow patterns in the Canadian sector of the

- Williston basin. Rocky Mountain Association of Geologists, Symposium, p. 313-321.
- Hawlander, H.M. and H.G. Machel, 1991, Diagenetic and petrophysical types of dolomite, and their relationship to reservoir characteristics of the Grosmont Formation. Canadian Society of Petroleum Geologists Program and Abstracts. p. 71.
- Hesse, R., 1990, Silica Diagenesis: Origin of inorganic and replacement cherts. *In*: I.A. McIlreath and D.W. Morrow eds., Diagenesis, Geoscience Canada, Reprint Series no. 4, p. 253-275
- Hinch, H.H., 1980, The nature of shales and the dynamics of hydrocarbon expulsion in the Gulf Coast Tertiary section. *In*: W.H. Roberts and R.J.Cordell eds., Problems in petroleum migration, American Association of Petroleum Geologists, Studies in Geology no. 10, p. 1-18
- Hollister, L. S., M. L. Crawford, E. Roedder, R. C. Burruss, E. T. C., Spooner, and J. Touret, 1981, Practical aspects of microthermometry. *In*: Hollister, L.S. and M. L. Crawford eds., Fluid inclusions: applications to petrology, Mineralogical Association of Canada, p. 278-304.
- Hriskevich, M.E., J.M. Faber and J.R. Langton, 1980, Strachan and Ricinus West gas fields, Alberta, Canada. *In*: M.T. Halbouty, ed, Giant oil and gas fields of the decade 1968-1978. American Association of Petroleum Geologists, Memoir 30, p. 315-328.
- Hubbert, M.K. and W.W. Rubey, 1959, Role of fluid pressure in mechanics of thrust faulting. Geological Society of America Bulletin, v. 70, p. 115-166.
- Hubbert, M.K. and D.G. Willis, 1957, Mechanics of hydraulic fracturing. AIME Trans., v. 210, p. 153-168.
- Hugo, K., 1990, Mechanisms of groundwater flow and oil migration associated with

- Leduc reefs. Bulletin of Canadian Society of Petroleum Geologists, v. 38, p. 307-319.
- Hunt, J. M., 1978, Characterization of bitumen and coals. American Association of Petroleum Geologists Bulletin, v. 62, p. 301-303.
- Hunt, J. M., 1979, Petroleum geochemistry and geology. San Francisco, W.H. Freeman Publisher, 617 p.
- Illing, L.V., 1959, Deposition and diagenesis of some Upper Paleozoic carbonate sediments in western Canada. Proceedings of the Fifth World Petroleum Congress, New York, Section 1, p. 23-52.
- Jaeger, J.C., 1963, Extension failures in rocks subject to fluid pressure. Journal of Geophysics Research, v. 68, p. 6066-6067.
- Jaeger, J.C. and N.G.W. Cook, 1979, Fundamentals of rock mechanics. London, Chapman and Hall Publisher, 585 p.
- James, A. T., 1990, Correlation of reservoired gases using the carbon isotopic compositions of wet gas components. American Association of Petroleum Geologists Bulletin, v. 74, p. 1441-1458
- James, N. P. and R. N. Ginsburg, 1979, The seaward margin of Belize barrier and atoll reefs. International Association of Sedimentologists Special Publication, no. 3, 196 p.
- James, N. P. and P. W. Choquette, 1990, Limestones - The seafloor diagenetic environment. In: McIlreath, I.A. and D.W. Morrow eds., Diagenesis, Geoscience Canada, Reprint Series 4, p. 13-34.
- Jardine, D., D.P. Andrews, J.W. Wishart and J.W. Young, 1977, Distribution and continuity of carbonate reservoir. Journal of Petroleum Technology, v. 29, p. 873-885.
- Kaufman, J., G.N. Hanson and W.J. Meyers, 1991, Dolomitization of the Swan Hills

- Formation, Rosevear Field, Alberta, Canada. *Journal of Sedimentary Petrology*, v. 60, p. 918-939
- Keith, J.W., 1971, Strachan-Phoenix area, Leduc reef facies and diagenesis. Unpublished Internal Report, 30 p.
- Klovan, J.E., 1964, Facies analysis of the Redwater reef complex, Alberta, Canada. *Bulletin of Canadian Society of Petroleum Geologists*, v. 12, p. 1-100.
- Krebs, W. and R. W. Macqueen, 1984, Sequence of diagenetic and mineralization events: Pine Point lead-zinc property, NWT, Canada. *Bulletin of Canadian Petroleum Geology*, v. 32, p. 434-464.
- Krouse, H.R., C.A. Viau, L.S. Eliuk, A. Ueda and S. Halas, 1988, Chemical and isotopic evidence of thermochemical sulphate reduction by light hydrocarbon gases in deep carbonate reservoirs. *Nature*, v. 333, p. 415-419.
- Kulander, B.R., C.C. Barton and S.L. Dean, 1979, The application of fractography to core and outcrop fracture investigations: Technical Report US Department of Energy Contract EY-77-Y21-1391, METC/SP-79/3, 174 p.
- Kulander, B.R.; S.L. Dean and B.J. Ward Jr., 1990, Fractured core analysis: Interpretation, logging and use of natural and induced fractures in core. *American Association of Petroleum Geologists, Methods in exploration series no. 8*, 88 p.
- Kupecz, J. A., I. P. Montanez and G. Gao, 1992, Recrystallization of dolomite with time. *In: Carbonate Microfacies*. Springer Verlag, p. 187-194.
- Laflamme, A. K., 1990, Replacement dolomitization in the Upper Devonian Leduc and Swan Hills formations, Caroline area, Alberta, Canada. Unpublished M.Sc. thesis, McGill University, 138 p.
- Land, L.S., 1980, The isotopic and trace element geochemistry of dolomite: the state of the art. *In: Zenger, D. H., J. B. Dunham and R.L. Ethington eds., Concepts and models of dolomitization*. Society of Economic Paleontologists and Mineralogists

- Special Publication, no. 28, p. 87-110.
- Land, L.S., 1983, The application of stable isotopes to studies of the origin of dolomite and to the problems of diagenesis of clastic sediments. *In*: Arthur, M. A., T. F., Anderson, I. R. Kaplan, J. Veizer and L.S., Land eds., Stable isotopes in sedimentary geology. Society of Economic Paleontologists and Mineralogists Short Course, no. 10, p. 4-1 to 4-22.
- Land, L.S., 1985, The origin of massive dolomite. *Journal of Geological Education*, v. 33, p. 112-125.
- Langton, R.J. and G.E. Chin, 1968, Rainbow Member facies and related reservoir properties, Rainbow Lake, Alberta. *Bulletin of Canadian Society of Petroleum Geologists*, v. 16, p. 104-143.
- Layer, D.B., 1949, Leduc oil field, Alberta, a Devonian coral reef discovery. *American Association of Petroleum Geologists Bulletin*, v. 33, p. 572-602.
- Lind, I., 1993, Stylolites in chalk from leg 130, Ontong Java Plateau. *In*: Berger, W. H., Kroenke, L.A., Mayer et. al. eds, *Proceedings of the Ocean Drilling Program, Scientific Results*, v. 130, p. 445-451.
- Lippmann, F., 1973, *Sedimentary carbonate minerals*. Springer-Verlag, Berlin, 228 p.
- Lishman, J.R., 1969, Core permeability anisotropy. *Petroleum Society of the Canadian Institute of Mining and Metallurgy, 20th Annual Technical Meeting*, Edmonton, Alberta, paper no. 6920.
- Lomando, A.J., 1992, The influence of solid reservoir bitumen on reservoir quality. *American Association of Petroleum Geologists Bulletin*, v. 76, p. 1137-1152
- Lorenz, J.C., L.W. Teufel and N.R. Warpinski, 1991, Regional fractures I: A mechanism for the formation of regional fractures at depth in flat-lying reservoirs. *American Association of Petroleum Geologists Bulletin*, v. 75, p. 1714-1737.

- Lucia, F.J., 1983, Petrophysical parameters estimated from visual descriptions of carbonate rocks: a field classification of carbonate pore space. *Journal of Petroleum Technology*, v. 35, p. 629-637.
- Machel, H. G., 1985, Facies and diagenesis of the Upper Devonian Nisku Formation in the subsurface of central Alberta. Unpublished Ph.D. thesis, McGill University, Montreal, Canada, 392 p.
- Machel, H. G., 1987a, Saddle dolomite as a by-product of chemical compaction and thermochemical sulphate reduction. *Geology*, v. 15, p. 936-940.
- Machel, H. G., 1987b, Some aspects of diagenetic sulphate - hydrocarbon redox reactions. *In*: Marshall, J. D. ed., *Diagenesis of Sedimentary sequences*, Geological Society of London Special Publication, no. 36, p. 15-28.
- Machel, H. G. and J.H. Anderson, 1989, Pervasive subsurface dolomitization of the Nisku Formation in central Alberta. *Journal of Sedimentary Petrology*, v. 59, p. 891-911.
- Machel, H. G. and E.W. Mountjoy, 1986, Chemistry and environments of dolomitization - A reappraisal. *Earth Science Review*, v. 23, p. 175-222.
- Machel, H. G. and E.W. Mountjoy, 1987, General constraints on extensive pervasive dolomitization - and their application to the Devonian carbonates of western Canada. *Bulletin of Canadian Petroleum Geology*, v. 35, p. 143-158.
- Maddox, D. F., 1984, Reservoir simulation study - Ricinus West D-3A pool, Ricinus West field. Canterra Energy Ltd. internal report, Calgary, Alberta, 90 p.
- Magara, K., 1971, Permeability considerations in generation of abnormal pressures. *Society of Petroleum Engineers Journal*, v. 11, p. 236-242.
- Magara, K., 1975, Importance of aquathermal pressuring effect in Gulf Coast: *American Association of Petroleum Geologists Bulletin*, v. 59, p. 2017-2045
- Marsh, H., 1973, Carbonization and liquid-crystal mesophase development: Part 1. The

- significance of mesophase during carbonization of coking coals. *Fuel*, v. 52, p. 205-212.
- Mattes, B. W. and E.W. Mountjoy, 1980, Burial dolomitization of the Upper Devonian Miette buildup, Jasper National Park, Alberta. *In*: Zenger, D.H.; J.B.Dunham and R.L. Ethington eds., Concepts and models of dolomitization, Society of Economic Paleontologists and Mineralogists Special Publication, no. 28, p. 259-297.
- Mazzullo, S.L., 1992, Geochemical and neomorphic alteration of dolomite, a review. *Carbonate and Evaporites*, v. 7, p. 21-37.
- McCaffery, F.G., 1977, Rock-fluid relationship studies on the Windfall D-3A reservoir and their application in evaluating gas cycling effectiveness. *Journal of Canadian Petroleum Technology*, January-March, p. 55-63.
- McCrossan, R.G., 1961, Resistivity mapping and petrophysical study of Upper Devonian inter-reef calcareous shales of central Alberta, Canada. *American Association of Petroleum Geologists Bulletin*, v. 45, p. 441-470.
- McGillivray, J.G. and E.W. Mountjoy, 1975, Facies and related reservoir characteristics, Golden Spike reef complex, Alberta. *Bulletin of Canadian Society of Petroleum Geologists*, v. 23, p. 753-809.
- McLean, D.J., 1992, Upper Devonian buildup development in the southern Canadian Rocky Mountains: A sequence stratigraphic approach. Unpublished Ph.D. thesis, McGill University, 245 p.
- McLean, D.J. and E.W. Mountjoy, 1993a, Stratigraphy and depositional history of the Burnt Timber Embayment, Fairholme Complex, Alberta. *Bulletin of Canadian Petroleum Geology*, v. 41, p. 290-306.
- McLean, D.J. and E.W. Mountjoy, 1993b, Upper Devonian buildup-margin and slope development in the southern Canadian Rocky Mountains. *Geological Society of*

- America Bulletin, v. 105, p. 1263-1283.
- McLean, D.J. and E.W. Mountjoy, 1994, Allocyclic control on Late Devonian buildup development, Southern Canadian Rocky Mountains. *Journal of Sedimentary Research*, v.B64, p.
- McNamara, L. B. and N.C. Wardlaw, 1991, Geological and statistical description of the Westrose reservoir, Alberta. *Bulletin of Canadian Petroleum Geology*, v. 39, p. 332-351.
- McNamara, L. B., N.C. Wardlaw and M. McKellar, 1991, Assessment of porosity from outcrops of vuggy carbonate and application to cores. *Bulletin of Canadian Petroleum Geology*, v. 39, p. 260-269.
- Meissner, F.F., 1980, Examples of abnormal fluid pressure produced by hydrocarbon generation. *American Association of Petroleum Geologists Bulletin*, abs., v. 64, p. 749.
- Meissner, F.F., 1985, Petroleum geology of the Bakken Formation Williston Basin, North Dakota and Montana. p. 159-179.
- Monger, J.W.H. 1989, Overview of Cordillera Geology. *In*: B.D. Ricketts ed., *Western Canada Sedimentary Basin: A Case history*. Canadian Society of Petroleum Geologists, Calgary, p. 9-32.
- Morrow, D.W. and H.H. J. Geldsetzer, 1988, Devonian of the eastern Canadian Cordillera. *In*: McMillan, N.J., A.F. Embry and D.J. Glass eds., *Devonian of the World*, v. 1. Canadian Society of Petroleum Geologists Memoir 14, p. 85-121.
- Mountjoy, E. W., 1965, Stratigraphy of the Miette reef complex and associated strata, eastern Jasper National Park, Alberta. *Bulletin of the Geological Survey of Canada*, v. 110, 132 p.
- Mountjoy, E. W., 1980, Some questions about the development of Upper Devonian carbonate buildups Reefs, Western Canada. *Bulletin of Canadian Petroleum*

- Geology, v. 28, p. 315-344.
- Mountjoy, E. W., 1987, The Upper Devonian Ancient Wall reef complex, Jasper National Park. Canadian Society of Petroleum Geologists Field trip Guidebook, Excursion A5, 50 p.
- Mountjoy, E. W., 1989, Miette reef complex Frasnian, Jasper National Park. *In*: Geldsetzer, H.H.J., N.P. James and G.E. Tebbutt eds., Reef - Canada and Adjacent Areas. Canadian Society of Petroleum Geologists Memoir 13, p.497-505.
- Mountjoy, E. W. and R.A. Walls, 1977, Some examples of early submarine cements from Devonian buildups of Alberta. Proceedings Third International Symposium on Coral Reefs, v. 2, p. 155-161.
- Mountjoy, E. W., H. Qing and R. H. McNutt, 1992, Strontium isotopic composition of Devonian dolomites, Western Canada Sedimentary Basin: Significant sources of dolomitizing fluids. Applied Geochemistry, v. 7, p. 59-75.
- Mudford, B.S., 1990, A one-dimensional, two phase model of overpressure generation in the Venture gas field, offshore Nova Scotia. Bulletin of Canadian Society of Petroleum Geologists, v. 38, p. 246-258.
- Murray, R. C., 1960, Origin of porosity in carbonate rocks. Journal of Sedimentary Petrology, v. 30, p. 59-84.
- Nelson, R.A., 1985, Geologic analysis of naturally fractured reservoirs. Houston, Gulf Publishing Company, 320 p.
- Oakes, C.S., R. J., Bodnar and J. M. Simonson, 1990, The system NaCl-CaCl₂- H₂O: I. The ice liquidus at 1 atm total pressure. Geochimica et Cosmochimica Acta., v. 54, p. 603-610.
- Orr, W.L., 1974, Changes in sulfur content and isotopic ratios of sulfur during petroleum maturation - Study of Big Horn Basin Paleozoic Oils. American Association of Petroleum Geologists Bulletin, v. 58, p. 2295-2318

- Palciauskas, V.V. and P.A. Domenico, 1980, Microfracture development in compacting sediments: Relation to hydrocarbon-maturation kinetics: American Association of Petroleum Geologists Bulletin, v. 64, p. 927-937.
- Paul, D., 1994, Hydrogeology of the Devonian Rimbey-Meadowbrook reef trend of central, Alberta, Canada. Unpublished M.Sc. thesis, University of Alberta, 152 p.
- Podrusky, J.A., J.E. Barclay, A.P. Hamblin, L.P. Lee, K.G. Osadetz, R.M. Procter and G.C. Taylor, 1987, Conventional oil resources of Western Canada, Part I: Reservoir endowment. Geological Survey of Canada, Paper 87-26, 42 p.
- Porter, J.W., R.A. Price and R.G. McCrossan, 1982, The Western Canada Sedimentary Basin. Phil. Trans. Royal Society of London, v. A305, p. 169-192.
- Powers, R.W., 1962, Arabian Upper Jurassic carbonate reservoir rocks. *In*: Ham E.W. ed., Classification of Carbonate Rocks, American Association of Petroleum Geologists, Memoir 1, p. 122-192.
- Price, N. J., 1974, The development of stress systems and fracture patterns in undeformed sediments. Proceedings of the 3rd Congress of the International Society of Rock Mechanics, v. 1-A, p. 487-496.
- Pursey, W.C., 1973, How to evaluate potential gas and oil source rocks. World Oil, v. 176, April, p. 71-75.
- Radke, B.M. and R.L. Mathis, 1980, On the formation and occurrence of saddle dolomite. Journal of Sedimentary Petrology, v. 50, p. 1149-1168.
- Railsback, L. B., 1993, Lithologic controls on morphology of pressure-dissolution surfaces stylolites and dissolution seams in Paleozoic carbonate rocks from the mideastern United States. Journal of Sedimentary Petrology, v. 63, p. 513-522.
- Reitzel, G.A., G. Davidson, G. O. Callow and D.R. Bates, 1976, Golden Spike D3-A pool oil depletion study, Calgary. Imperial Oil Ltd., Producing Department, Western Region, Report IPRC-5ME-76.

- Reitzel, G.A. and G. O. Callow, 1976, Pool description and performance analysis leads to understanding Golden Spikes's miscible flood. Petroleum Society of CIM, paper no. 7622, 11 p.
- Rogers, M.A., J.D. McAlary and N.J. Bailey, 1974, Significance of reservoir bitumens to thermal maturation studies, Western Canada Basin. American Association of Petroleum Geologists Bulletin, v. 58, p.1806-1824.
- Sassen, R., 1988, Geochemical and carbon isotopic studies of crude oil destruction, bitumen precipitation, and sulphate reduction in the deep Smackover Formation. Organic Geochemistry, v. 12, p. 351-361.
- Secor, D.T., 1965, Role of fluid pressure in jointing. American Journal of Science, v. 263, p. 633-646.
- Secor, D.T., 1969, Mechanics of natural extension fracturing at depth in the earth's crust. *In*: Baer, A.J. and D.K. Norris, eds., Research in tectonics, Geological Survey of Canada, paper 68-52, p. 3-47.
- Seifert, S. R., 1990, Strachan Leduc gas pool. *In*:: M.L. Rose ed., Oil and gas pools of Canada series, Canadian Society of Petroleum Geologists, v.1, variously paginated.
- Schmoker, J.W. and R.B. Halley, 1982, Carbonate porosity versus depth: A predictable relation for South Florida. American Association of Petroleum Geologists Bulletin, v. 66, p. 2561-2570.
- Shi, Y. and C. Wang, 1988, Generation of high pore pressures in accretionary prisms: inferences from the Barbados subduction complex. Journal of Geophysical Research., v. 93, p. 8893-8910.
- Shields, M.J. and Geldsetzer H.H.J., 1992, The MacKenzie margin, Southesk-Cairn carbonate complex: depositional history, stratal geometry and comparison with other Late Devonian platform-margins. Bulletin of Canadian Petroleum Geology v.

40, p. 274-293

Sibley, D. F. and J.M. Gregg, 1987, Classification of dolomite rock textures. *Journal of Sedimentary Petrology*, v. 57, p. 967-975.

Sneider, R.M. 1987, Practical petrophysics for exploration and development. American Association of Petroleum Geologists Education Department Short Course Notes, variously paginated.

Sneider, R.M., K. Stolper and J.S. Sneider, 1991, Petrophysical properties of seals. American Association of Petroleum Geologists, annual convention abstracts, v. 75, p. 673 - 674

Spencer, C.W., 1987, Hydrocarbon generation as a mechanism for overpressuring in Rocky Mountain region. *American Association of Petroleum Geologists Bulletin*, v. 71, p. 368-388.

Stahl, W. 1974, Carbon isotope fractionations in natural gases. *Nature*, v. 251, p.134-135.

Stasiuk, L.D., 1994, submitted, Reflected light optical properties and optical textures of pyrobitumen from Leduc Formation, Strachan and Ricinus West gas fields, Alberta: Preliminary Report. *Fuels*

Stoakes, F. A., 1980, Nature and control of shale basin fill and its effects on reef growth and termination: Upper Devonian Duvernay and Ireton Formations of Alberta, Canada. *Bulletin of Canadian Society of Petroleum Geologists*, v. 28, p. 345-410.

Stoakes, F. A., 1992, Woodbend Megasequence. *In*: J. Wendte, F.A. Stoakes and C.V.Campbell, Devonian-Early Mississippian carbonates of the Western Canada sedimentary basin: A sequence stratigraphic framework. *Society of Economic Paleontologists and Mineralogists, Short Course no. 28, Calgary*, p. 183-206.

Stoakes, F.A. and S. Creaney, 1984, Sedimentology of a carbonate source rock: Duvernay Formation of central Alberta, *in*: Eliuk, L., J. Kaldi, N. Watts and G.

- Harrison, eds, Carbonates in Subsurface and Outcrop: Proceedings of the 1984 Canadian Society of Petroleum Geologists Core Conference, Calgary, p. 132-147.
- Surdam, R.C., Z.S. Jiao and R.S. Martinsen, 1991, The regional pressure regime in Cretaceous sandstones and shales in the Powder Basin. *In*: P.J. Ortoleva and Z. Al-Shaieb, eds., Pressure Compartmentalization in Sedimentary Basins. American Association of Petroleum Geologists Memoir , 62 p.
- Tissot, B. P. and D. H. Welte, 1984, Petroleum formation and occurrence. Second edition, New York, Springer-Verlag, 699 p.
- Toland, W. G., 1960, Oxidation of organic compounds with aqueous sulphate. *Journal of the American Chemical Society*, v. 82, p. 1911-1916.
- Vahrenkamp, V.C. and P.K. Swart, 1990, New distribution coefficient for the incorporation of strontium into dolomite and its implications for the formation of ancient dolomites. *Geology*, v. 18, p. 387-391.
- Van de Graff, W. J. E. and P.J. Ealey, 1989, Geological modelling for simulation studies. *American Association of Petroleum Geologists Bulletin*, v. 73, p. 1436-1444.
- Vavra, C.L., M.H., Scheihing, and J.D. Klein, 1991, Reservoir geology of the Taylor sandstone in the Oak Hill Field, Rusk County, Texas: Integration of petrology, Sedimentology, and log analysis for delineation of reservoir quality in a tight gas sand. *In*: Sneider, R., W. Masssell, R. Mathis, D. Loren and P. Wichmann (eds.), The integration of geology, Geophysics, Petrophysics and petroleum engineering in reservoir delineation, description and management, American Association of Petroleum Geologists, Proceedings of the 1st Archie Conference, Houston, Texas, p.130-158.
- Veizer, 1983, Chemical diagenesis of carbonates: Theory and application of trace element technique. *In*: Stable isotopes in sedimentary geology, Society of Economic

- Paleontologists and Mineralogists Short Course no. 10, Dallas, p.3-1 to 3-100.
- Viau, C., L. Eliuk, K. Aulstead and R. Krouse, 1994, Porosity creation/modification and the origin of H₂S and elemental sulphur in deep carbonate reservoirs. Canadian Society of Exploration Geophysicists and Canadian Society of Petroleum Geologists, Joint Annual Convention, Calgary, Alberta Abs., 193-194 p.
- Walls, R.A., 1977, Cementation history and porosity development, Golden Spike Devonian reef complex, Alberta. Ph.D. Thesis, McGill University, Montreal, 307 p.
- Walls, R.A., 1983, Golden Spike reef complex, Alberta. *In*: Scholle, P.A.; D.G. Bebout and C.H. Moore eds., Carbonate depositional environments. American Association of Petroleum Geologists Memoir 33, p. 445-453.
- Walls, R. A., E. W., Mountjoy and P. Fritz, 1979, Isotopic composition and diagenetic history of carbonate cements in Devonian Golden Spike reef, Alberta. Geological Society of America Bulletin, v. 90, p. 963-982.
- Walls, R.A. and G. Burrowes, 1985, The role of cementation in the diagenetic history of Devonian reefs, western Canada. *In*: Schneidermann N. and P.M. Harris eds., Carbonate Cement, Society of Economic Paleontologists and Mineralogists, Special publication no. 36, p. 185-220.
- Walls, R.A. and G. Burrowes, 1989, Diagenesis and reservoir development in Devonian limestone and dolostone reefs of Western Canada. Canadian Society of Petroleum Geologists, Short Course Notes, Section 5, p. 5-1 to 5-18.
- Wardlaw, N.C., 1980, The effects of pore structure on displacement efficiency in reservoir rocks and in glass micromodel. Society of Petroleum Engineers Bulletin, n. 8843, p. 345-352.
- Wardlaw, N.C., 1990, Characterization of carbonate reservoirs for enhanced oil recovery. Proceedings 1st technical symposium on enhanced oil recovery, Tripoli,

- Libya, paper no. 90-01-05, p. 85-105.
- Wardlaw, N.C., 1992, Effects of carbonate rock-pore systems on oil recovery. *In*: Subsurface dissolution porosity in carbonates: Recognition, causes and implications; American Association of Petroleum Geologists Short Course, Calgary, p.1-28.
- Waring, W.W. and D.B. Layer, 1950, Devonian dolomitized reef, D-3 reservoir, Leduc field, Alberta, Canada. American Association of Petroleum Geologists Bulletin, v. 34, p. 295-312.
- Watts, N.L., 1987, Theoretical aspects of cap-rock and fault seals for single- and two-phase hydrocarbon columns. *Marine and Petroleum Geology*, v. 4, p. 274-307.
- Weber, K.J., 1986, How heterogeneity affects oil recovery. *In*: Lake, L.W. and H.B. Carroll eds., Reservoir characterization, Academic Press, Orlando, Florida, p. 487-544.
- Wendte, J. C., 1992, Platform evolution and its control on reef inception and localization. *In*: J. Wendte, F.A. Stoakes and C.V. Campbell, Devonian-Early Mississippian carbonates of the Western Canada sedimentary basin: A sequence stratigraphic framework. Society of Economic Paleontologists and Mineralogists, Short Course no. 28, Calgary, p. 41-88
- Werre, R.W., Jr.; R.J., Bednar; P.M., Bethke and P.B., Barton, 1979, A novel gas-flow fluid inclusion heating/freezing stage. Geological Society of America, Abstracts with Programs, v. 11, p. 539.
- Weyl, P.K., 1960, Porosity through dolomitization-conservation of mass requirements. *Journal of Sedimentary Petrology*, v. 30, p. 85-90.
- White, J.L., 1976, Mesophase mechanisms in the formation of the microstructure of petroleum coke. *In*: Deviney, M.L. and T.M. O'Grady eds., Petroleum derived carbons. American Chemical Society, Symposium series no. 21, p. 282-314.

Woodland, D.C. and J.S. Bell, 1988, In-situ stress magnitudes from mini-frac records in Western Canada: Paper number 88-39-67, 39th Annual Technical Meeting of the Petroleum Society of the Canadian Institute of Mining and Metallurgy, p. 67-1 to 67-27.

Zoback, M.L. and M. Zoback, 1980, State of stress in the conterminous United States. Journal of Geophysical Research, v. 85, p. 6113-6156.

APPENDIX A
LIST OF WELLS STUDIED

WELL	LOCATION	CORED INTERVAL (ft)	CORED INTERVAL (m)	TOTAL (ft)	TOTAL (m)	FIELD
BANFF AQUITANE	10-31-37-9W5	13442 - 14200	4098.2 - 4329.3	758.0	231.1	STRACHAN
BANFF AQUITANE	12-31-37-9W5	14046 - 14096	4282.3 - 4297.6	50.0	15.2	STRACHAN
AQUITANE	15-2-38-10W5	13485 - 13605	4111.3 - 4147.9	120.0	36.6	STRACHAN
CHEVRON SOBC	14-2-38-10W5	13466 - 13526	4105.5 - 4123.8	60.0	18.3	STRACHAN
AQUIT. SHELL-STRACHAN	5-11-38-10W5	13916 - 13702	4242.7 - 4177.4	245.0	74.7	STRACHAN
BANFF AQUITANE	7-32-37-9W5	13422 - 13494	4092.1 - 4114.0	72.0	22.0	STRACHAN
B.A.et.al.	11-27-37-9W5	13187 - 13197	4020.4 - 4023.5	10.0	3.0	STRACHAN
GULF et.al. STRACHAN	10-24-37-9W5	13322 - 13378	4061.6 - 4078.7	56.0	17.1	STRACHAN
GULF POC et.al.	7-19-37-8W5	13436 - 13493	4096.3 - 4113.7	57.0	17.4	STRACHAN
GULF et.al. STRACHAN	11-22-37-9W5	12970 - 13046	3954.3 - 3997.4	76.0	23.2	STRACHAN
AQUITANE et.al.	10-16-37-10W5	15306 - 15333	4666.5 - 4674.7	27.0	8.2	STRACHAN
ARCO PACIFIC FINA COW Jk	7-33-37-8W5	12133 - 12168	3699.1 - 3709.8	35.0	10.7	CRIMSON
HUSKY et.al.	11-28-37-8W5	12133 - 12178	3699.1 - 3712.8	45.0	13.7	CRIMSON
IMP. CHEDDERVILLE	10-20-37-7W5	11608 - 11687	3539.0 - 3563.1	79.0	24.1	CHEDDERVILLE
PINN.CHEDDERVILLE	16-19-37-7W5	11642 - 11692	3549.4 - 3564.6	50.0	15.2	CHEDDERVILLE
IMP. CHEDDERVILLE	10-29-37-7W5	11991 - 12016	3655.8 - 3663.4	25.0	7.6	CHEDDERVILLE
BP CHEDDERVILLE	6-30-37-7W5	11585 - 11595	3532.0 - 3535.1	9.8	3.0	CHEDDERVILLE
DOME et. al. CHEDDERVILLE	14-9-37-7W5	11634 - 11713	3547.0 - 3571.0	79.0	24.1	CHEDDERVILLE
BANFF et.al.	10-33-36-10W5	14785 - 15319	4507.6 - 4670.4	534.0	162.8	RICINUS
BANFF AQUITANE	11-27-36-10W5	14664 - 14724	4470.7 - 4489.0	60.0	18.3	RICINUS
CHEVRON MOBIL	7-26-36-10W5	14381 - 14434	4384.5 - 4400.6	53.0	16.2	RICINUS
BANFF AQUITANE	15-23-36-10W5	14616 - 15067	4456.1 - 4593.6	451.0	137.5	RICINUS
BANFF et.al.	7-13-36-10W5	14293 - 14865	4357.6 - 4532.0	572.0	174.4	RICINUS
BANFF et.al. RICINUS	6-25-36-10W55	14323 - 14378	4366.8 - 4383.5	55.0	16.8	RICINUS
MOBIL RICINUS	6-10-36-9W5	14240 - 14251	4341.5 - 4344.8	11.0	3.4	RICINUS
ESSO MOBIL RICINUS	10-11-37-8W5	12356 - 12438	3767.1 - 3792.1	82.0	25.0	RICINUS
IMP. HB. RICINUS	12-28-36-7W5	12452 - 12518	3796.3 - 3816.5	66.0	20.1	RICINUS
MOBIL et.al. RICINUS	11-17-35-8W5	13814 - 13921	4211.6 - 4244.2	107.0	32.6	RICINUS
PAN.AMER. RICINUS	6-24-34-8W5	13414 - 13475	4089.6 - 4108.2	61.0	18.6	RICINUS
ALBANY AMOCO RICINUS	6-14-34-8W5	14048 - 14138	4282.9 - 4310.4	90.0	27.4	RICINUS
BANFF AQUIT. RAM RIVER	7-9-37-10W5	15404 - 15510	4696.3 - 4728.7	108.0	32.9	RAM RIVER
HUSKY RAM RIVER	10-16-37-10W5	15306 - 15333	4666.5 - 4674.7	27.0	8.2	RAM RIVER
SHELL CANTERRA RAM R.	5-13-37-12W5	16628 - 16515	5069.5 - 5035.1	113.0	34.5	RAM RIVER
UNO-TEX et.al. PHOENIX	5-4-39-11W5	14220 - 14280	4335.4 - 4353.7	60.0	18.3	PHOENIX
RR AMOCO et.al. ANCONA	7-9-39-12W5	15539 - 15553	4737.5 - 4741.8	14.1	4.3	PHOENIX
C.S.et.al. PHOENIX	6-36-38-11W5	13884 - 13910	4232.9 - 4240.9	26.4	8.0	PHOENIX

APPENDIX B

**DEPOSITIONAL FACIES
STRACHAN AND RICINUS WEST RESERVOIRS**

Facies distribution in partially dolomitized Strachan buildup.

(Depths intervals and total thicknesses in meters)

WELL LOCATION	REEF MARGIN			REEF INTERIOR	
	CORAL RUDSTONE	STROM-CORAL RUDSTONE	TABULAR STROMATOP BOUNDSTONE	STROMATOP. FLOATSTONE	SKELETAL WACKSTONE
5-11-38-10W5				4222-4229 4230-4234 4235-4241 (16m)	4229-4230 4234-4235 (2m)
14-2-38-10W5	4148-4153 4171-4174 (8m)	4105-4116 4119-4123 4153-4171 4174-4180 (39m)	4123-4140 (17m)		4116-4119 4140-4148 (11m)
15-2-38-10W5	4120-4128 (8m)	4110-4120 4133-4138 (15m)	4138-4148 (10m)		4128-4133 (5m)
12-31-37-9W5	4290-4293 (3m)	4282-4290 4293-4298 (13m)			
10-31-37-9W5	4143-4162 (19m)	4098-4115 4119-4134 4256-4275 4277-4293 4300-4311 (81m)	4181-4195 4221-4228 4238-4251 (34m)	4293-4300 (7m)	4115-4119 4134-4143 4162-4181 4195-4221 4228-4238 4251-4256 4275-4277 (93 m) 4311-4329

(Depth intervals in meters)

GSh: Green shales

APPENDIX C**DIAGENETIC FEATURES POTENTIALLY RELATED TO THERMAL
SULPHATE REDUCTION REACTIONS**

According to: Machel, (1987b); Krouse et. al., (1988); Sassen, (1988)

Legend**SULPHATES**

An: Anhydrite
Gp: Gypsum

SULPHIDES

Sp: Sphalerite
Py: Pyrite

S: Free sulphur

CARBONATES

L Cal: Late calcite cement

BRECCIAS:

Crackle: Initial breaking up of rock, no clast rotation
Mosaic: Initial clast rotation
Rubble: Total clast rotation and mixture

LITHOLOGY

Ls: Limestone
Dol: Dolomite

TABLE TS PRODUCTS

WELL LOCATION	DEPTH (m)	SULPHATES	CARBONATES	SULPHIDES	FREE SULPHUR	DISSOLUTION	H ₂ S (%)	LITHOLOGY
10-31-37-9W5	4103.6		L Cal				8.90	
	4110.9			Sp, Py				
	4112.8			Sp, Py				
	4125.0		L Cal					
	4128.0		L Cal					
	4167.6		L Cal					
	4175.6		L Cal					
	4213.4		L Cal					
	4251.2	An						
	4258.5	An						Ls, Dol
	4284.1	Gp						
	4292.6	An	L Cal	Py				
	4300.6			Py				
	4304.8		L Cal					
	4321.3	An						
12-31-37-9W5	4282.3		L Cal					
	4285.0					Rubble breccia		
	4288.1		L Cal					
	4296.9		L Cal					
15-2-38-10W5								
14-2-38-10W5	4149.2		L Cal				4.28	
	4172.2		L Cal					
	4175.3		L Cal					
	4178.6		L Cal					
5-11-38-10W5	4227.7					Crack breccia		
	4228.6		L Cal	Py				
	4232.9		L Cal					
	4234.4		L Cal					
	4235.6	An						
7-32-37-9W5	4239.0		L Cal			Along stylolites		
	4085.6	An					8.85	Dol
	4088.1	An						
	4089.9	An						
	4098.7	An						
11-27-37-9W5	4099.0	Gp						
	4099.3	An						
	3933.5	Gp					9.08	
	3937.5	Gp						
10-24-37-9W5	3940.0	Gp						
	3825.6	An	L Cal		S		47.35	
	3832.3	An	L Cal		S			
	3837.8	An	L Cal		S			

TABLE TSF PRODUCTS

WELL LOCATION	DEPTH (m)	SULPHATES	CARBONATES	SULPHIDES	FREE SULPHUR	DISSOLUTION	H ₂ S (%)	LITHOLOGY
	4034.7					Crack breccia		
	4044.2	An		Py				
	4045.4	An		Py				
7-19-37-8W5	4099.3			Py				Ls, Dol
	4110.6			Py				
	4112.8			Py				
7-33-37-8W5	3702.7					Rubble breccia	9.95	Dol
11-28-37-8W5	3703.0	An					9.09	
	3710.3	An	L Cal					
	3710.9	An	L Cal					
11-22-37-9W5	3955.7		L Cal				23.48	
	3960.9	An						
10-33-36-10W5	4512.7			Py			33.60	
	4416.7			Sp				
	4530.7		L Cal					
	4546.7			Py				
	4554.7			Py				
	4576.7		L Cal					
	4610.7	An	L Cal					
	4626.7	An	L Cal					
	4636.7	An	L Cal					
11-27-36-10W5	4489.7			Py				
	4500.7		L Cal	Py				
7-26-36-10W5	4391.4				S		32.16	
	4394.4		L Cal					
	4399.4		L Cal					
7-13-36-10W5	4357.9					Rubble breccias	33.48	
15-23-36-10W5	4457.0			Py				
	4461.0			Sp				
	4464.0	An						
	4467.0	An						
	4470.0	An						
	4495.0		L Cal					
	4520.0	An						
	4525.0	An						
	4534.0	An						
	4538.0	An						
	4549.0	An						
	4552.0	An						
	4564.0			Py				
	4576.0	An						
	4582.0	An	L Cal					

TABLE TS PRODUCTS

WELL LOCATION	DEPTH (m)	SULPHATES	CARBONATES	SULPHIDES	FREE SULPHUR	DISSOLUTION	H2S (%)	LITHOLOGY
	4585.0	An	L Cal					
	4590.0	An						
10-16-37-10W5								
10-20-37-7W5	3539.6			Py, Py			6.91	
	3540.8	An				Large vugs		
	3542.6	An		Py				
	3548.7					Rubble breccia		
	3554.8					Rubble breccia		
	3559.5	An						
	3563.4	An						
16-19-37-7W5	3550.0	An					8.61	
	3552.4	An						
	3554.2	An						
	3560.9	An						
10-29-37-7W5	3660.3				S			
	3661.5	An						
	3663.4				S			
6-30-37-7W5	3534.0					Rubble breccia		
14-9-37-7W5	3548.0	An					7.47	
	3566.0	An				Rubble breccia		
10-11-37-8W5	3780.0	An						
	3788.0	An						
15-27-37-7W5							4.91	
12-28-36-7W5	3800.3	An				Crack breccias		
	3803.3				S			
	3806.4					Mosaic breccia		
	3811.8				S	Rubble breccia		
	3813.4				S	Rubble breccia		
7-9-37-10W5	4711.8		L Cal					Ls
11-17-35-8W5	4237.8		L Cal					
	4243.2	An						
	4242.3					Mosaic breccias		
10-16-37-10W5	4674.6	An						
6-24-34-8W5	4089.9	An		Py				Sh, Ls
	4371.9				S			
	4380.1	An						
	4385.3				S			
	4385.9				S			
6-14-34-8W5	4283.2				S	Rubble breccias		Dol
	4288.1				S	Rubble breccias		
	4309.4	An	L Cal					
5-4-39-11W5	4341.4	An	L Cal					Ls

TABLE TSP PRODUCTS

WELL LOCATION	DEPTH (m)	SULPHATES	CARBONATES	SULPHIDES	FREE SULPHUR	DISSOLUTION	H ₂ S (%)	LITHOLOGY
7-9-39-12W5	4738.0	An						
	4741.0			Py				
6-36-38-11W5	4238.0			Py, Py				Sh, Ls
5-13-37-12W5	5052.2				S			
	5068.5		L Cal	Py	S	Along stylolites		Ls, Dol

APPENDIX D

**CHARACTERISTICS OF RESERVOIR BITUMENS FROM STRACHAN
AND
RICINUS WEST RESERVOIRS**

RESERVOIR BITUMEN

Optical texture analyses and quantitative reflectance microscopy of reservoir bitumen provide information about their source and origin. Hairline microfractures are always filled with reservoir bitumen, therefore an attempt have been made below to determine the relationship between solid reservoir bitumen and hairline microfractures.

Reservoir bitumen is a black precipitate that lines and fills pore spaces. Reservoir bitumen (Rogers et. al., 1974) is used as a descriptive term to avoid genetic implications and confusion with source rock bitumen and in situ kerogen. In the Strachan buildup reservoir bitumen is uniformly distributed from the top of the reservoir to 4313.7 m below the initial gas/water contact (4251 m; Seifert, 1990). In pool D3B it occurs as dull, black, continuous to discontinuous thin coatings on both primary (intrasketal) and secondary pores (microfractures). In pool D3A reservoir bitumen is dull to bright, black, sometimes vitreous and occurs in three morphotypes: droplets, carpets and peanut brittle (Lomando, 1992). Droplets are rounded, individual particles scattered or clotted mostly on intercrystalline pore walls. Carpets are continuous coatings with a smooth surface lining vug walls. Peanut brittle ranges from continuous to discontinuous thin coatings with random rounded lumps in intercrystalline pores, vugs and microfractures. To investigate the origin and nature of the source material optical textural analyses and quantitative reflectance microscopy were performed on reservoir bitumens from wells 10-31 and 15-2 in the Strachan buildup (Stasiuk, 1994). These analyses show that reservoir bitumens from the Strachan buildup are characterized by anisotropic bitumens having only very minor amounts of isotropic bitumens. Their characteristics and distribution are presented below.

Optical textures in reservoir bitumens

Optical textures in the reservoir bitumen were characterized using the classification schemes developed for coke textures produced during carbonization experiments (e.g.

Marsh, 1973; Grint and Marsh, 1980) and for industrial scale oil-refining by White (1976).

Strachan Pool D3A (Well: 10-31)

Reservoir bitumens in the upper part of this well (4141 - 4137 m) differ from bitumens in the lower part (4321 - 4308 m). In the upper part reservoir bitumens are fine (average mosaic unit size $<2.0\ \mu\text{m}$) to medium grained (average mosaic unit size of $5\ \mu\text{m}$) mosaics that partially fill fractures, intraskeletal pores and hairline microfractures. The bitumen filling the hairline microfractures is very fine-grained (commonly $<1.25\ \mu\text{m}$) and increases in size towards the intraskeletal pores where it is medium-grained (Plate D1a). Reservoir bitumen is also present along some stylolites (stylo-bitumen, Stasiuk, 1994) with a much finer mosaic grain size than the bitumen in the microfractures.

In the lower part, reservoir bitumens exhibit significantly coarser-grained mosaics and complex and heterogeneous textures. Pore lining bitumen (carpets) less than 1 to $4\ \mu\text{m}$ thick shows alternating dark and light anisotropic lamellae oriented perpendicular to the face of the enclosing carbonate (Plate D1c). Commonly semi-globular, globular (droplets, up to $10\ \mu\text{m}$) or agglomerations of individual spheres (up to $500\ \mu\text{m}$) of bitumen show coarse flow to flow domain textures in optical continuity that are attached to the thin pore-lining phase (Plate D1d). Some of the spheres with coarse flow to flow domain textures have been fractured, brecciated and bound together by an isotropic to fine-grained bitumen. In unbrecciated spheres the isotropic to fine-grained bitumen coats and/or infills the intersphere areas (peanut brittle).

Reservoir bitumen from a sample at 4311.5 m shows fine-deformed and coarse-deformed lamellar textures (Plate D1e) that, as will be discussed later, form through the nucleation, growth and percolation of gas bubbles during the gasification of carbons (e.g. White, 1976). Minor multilayered pyrolytic carbon textures (precipitation of carbon from a hot gas phase; Stasiuk, 1994) separated by a layer of fine-grained mosaic bitumen were noted at 4314 m depth. A rare accumulation of isotropic bitumen globules along a stylolites plane shows devolatilization vacuoles (4317.6 m).

Strachan Pool D3B (Well: 15-2)

Reservoir bitumens from well 15-2 (4144 - 4114 m) show identical textures (Stasiuk, 1994) to bitumens from the upper part of well 10-31. The bitumens have very fine, fine to medium-grained size mosaic textures and also fill fractures, stylolites, intraskeletal pores and microfractures (Plate D1b). In areas where stylolites are crosscut by a network of microfractures (mostly perpendicular to the stylolite surface), bitumen along the stylolites appears to have been forced apart and subsequently infilled with a relatively coarse crystalline calcite cement (e.g. 4124 m).

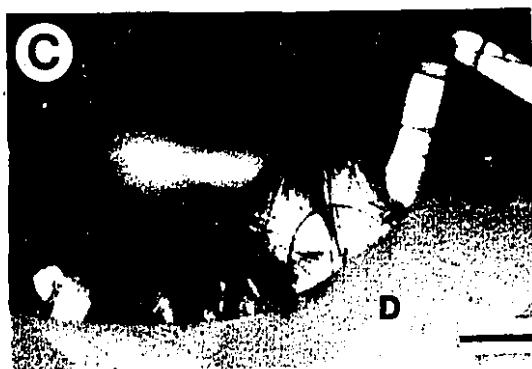
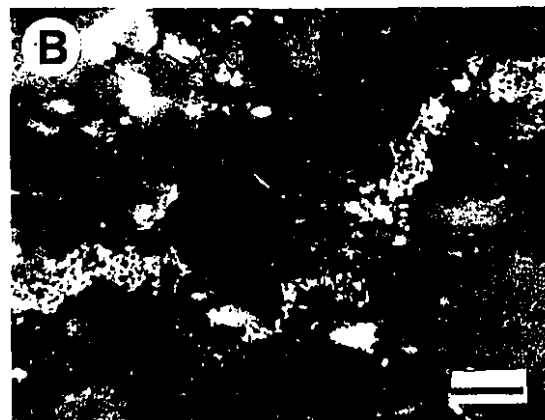
Reflectance Microscopy

Quantitative reflectance microscopy measures the percentage of polarized light reflected from polished surfaces of carbon, both in the direction parallel ($\%Ro_{max}$) and perpendicular ($\%Ro_{min}$) to the layer planes or lamellae, and indicates the degree of anisotropy in the carbon. It is used in conjunction with optical textures to investigate the nature of the source material.

Fine to medium-grained reservoir bitumens in hairline microfractures show a $\%Ro_{max}$ range from 4.5 to 5.5 %. Coarse flow to flow domain textures in bitumen spheres are characterized by $\%Ro_{max}$ greater than 6.0. Non-granular isotopic bitumen filling fracture and interparticle areas in brecciated spheres and stylolites surfaces exhibit $\%Ro_{max}$ range between 2.2 and 2.4. This suggest that reservoir bitumens in the Strachan buildup can be separated into two different types: 1) isotropic, very fine and fine-grained mosaic ($< 2 \mu m$) with $\%Ro_{max}$ generally < 3.5 , and 2) coarser grained mosaics (5 to 100 μm) associated with flow and domain textures with $\%Ro_{max} > 4.5$. No textural evidence for a transitional stage or direct link between these two types have been observed (Stasiuk, 1994).

Plate D1: OPTICAL TEXTURES IN RESERVOIR BITUMENS FROM THE STRACHAN BUILDUP

- A) Very fine-grained to fine-grained mosaic texture (arrow) in bitumen filling hairline microfractures extending away from late calcite-filled (Ca) pore. 10-31-37-9W5, 4137.9 m. Scale bar 100 μm
- B) Fine-grained mosaic bitumen along stylolite surface (arrow). 15-2-38-10W5, 4118.9 m. Scale bar 100 μm
- C) Thin pore lining bitumen (carpets) showing dark and light anisotropic lamellae (arrow) oriented perpendicular to the dolomite crystal surface (D). Note semi-globular spheres of bitumen with rotating cross. 10-31-37-9W5, 4313.7 m. Scale bar 50 μm
- D) Coarse flow anisotropy in bitumen filling an intercrystalline pore. 10-31-37-9W5, 4313.7 m. Scale bar 100 μm
- E) Fine to coarse, lamellar, deformed microstructure with regions illustrating a buckled lamellar texture (arrow) produced by collapse of gas bubbles during the plastic state. 10-31-37-9W5, 4311.5 m. Scale bar 100 μm
- F) Close-up of area indicated in Plate D1E. Note the lamellae deformation around gas bubbles (arrow). 10-31-37-9W5, 4311.5 m. Scale bar 50 μm



APPENDIX E

GEOCHEMISTRY DATA

1) MAJOR AND TRACE ELEMENTS - STRACHAN RESERVOIR

For each analysis, oxide totals measured 100 \pm 0.7 wt % with a 2σ < 0.4%.
 Sr and Na concentrations are not reliable since their values of < 0.02 wt%
 carry a 2σ of 95%.

Legend

R₂, R₃: Replacement dolomite

C₁, C₂: Dolomite cements

SMC: Early calcite cements

2) ISOTOPE DATA AND TEMPERATURE CALCULATIONS FROM OXYGEN ISOTOPE DATA

Carbon and oxygen isotopic values are reported relative to the PDB scale,
 and have a precision of \pm 0.05‰.

Precision for the ⁸⁷Sr/⁸⁶Sr range between \pm 0.000010 and \pm 0.000045

3) MICROTHERMOMETRIC DATA FROM FLUID INCLUSIONS

The fluid inclusions are primary, liquid-vapour inclusions in dolomite cements C₁ and C₂ and late calcite cements from Ricinus West and Crimson buildups and late calcites from Strachan buildup. The melting temperature of ice was converted into weight percent NaCl equivalent using equations in Oakes et al. (1990). Reported temperatures are accurate to \pm 0.3°C in the subzero range and \pm 2°C for the highest temperatures measured.

Legend

Freezing:

T_f: Freezing temperature

Melting data:

T_e: eutectic

T_{mice}: Ice last melt temperature

Heating:

T_h: Homogenization temperature

Appendix Microprobe Analyses

LOCATION	DEPTH (m)	POINT	CaCO ₃ (%)	MgCO ₃ (%)	Fe (ppm)	Mn (ppm)	Sr (ppm)	Na (ppm)	TYPE	COMMENTS
10-31-37-9W5	4300	1	50.90	49.60	570	120	40	10	C2	Pyrite (TSR?)
		2	49.40	50.40	1000	160	0	30	C2	C2 single crystal
			49.65	50.02	785	140	20	20	Average	
		3	50.00	50.30	1190	50	430	0	R2	
		4	50.20	50.20	960	40	180	120	R2	
		5	49.20	50.70	800	320	70	40	R2	
			49.80	50.40	983	137	227	53	Average	
10-31-37-9W5	4287.8	1	49.80	50.90	500	150	0	80	R2	
		2	48.70	48.70	440	100	90	330	R2	
		3	49.95	50.75	600	240	0	590	R2	
		4	50.15	49.85	680	100	40	10	R2	
			49.65	50.05	555	173	33	253	Average	
		5	49.55	49.95	2380	220	250	10	C1	Rim 1
		6	49.80	50.30	1880	240	240	100	C1	Rim 1
		7	50.15	50.00	600	20	0	40	C1	Rim 2
			49.80	50.08	1620	120	123	38	Average	
		8	50.50	50.50	60	270	0	60		
		9	50.10	50.45	460	140	90	10		
		10	50.20	50.70	450	160	310	10		
			50.30	50.50	323	190	133	27	Average	
10-31-37-9W5	4311.5	1	49.50	50.80	2280	340	50	150	R2	
		2	49.60	51.50	450	250	70	50	R2	
		3	50.00	52.00	120	220	90	70	R2	
		6	50.80	50.00	2690	160	0	30	R2	
			49.90	51.10	1385	243	53	75	Average	
		4	49.50	51.30	1970	290	0	0	C1	
		5	50.60	49.80	1270	250	0	40	C1	
		7	50.20	50.90	1610	180	170	0	C1	
			50.10	50.60	1616	240	57	13	Average	
		8	100.00	0.00	0	230	200	20	L. Calcite	
		9	49.30	51.00	2190	300	80	40	C2	
		10	50.20	51.10	1010	320	0	140	C2	
			49.75	51.10	1600	310	40	90	Average	
10-31-37-9W5	4177.1	1	98.00	0.00	70	250	70	260	SMC	Mg=1310 ppm
		2	99.10	0.00	80	0	100	50	SMC	Mg= 2130 ppm
		4	95.80	4.60	0	10	0	30	SMC	Mg= 11210 ppm
			98.00	2.50	50	87	57	113	Average	
		3	50.40	50.80	770	90	0	80	R2	

Appendix E1Microprobe Analyses

LOCATION	DEPTH (m)	POINT	CaCO3 (%)	MgCO3 (%)	Fe (ppm)	Mn (ppm)	Sr (ppm)	Na (ppm)	TYPE	COMMENTS
		5	50.60	50.60	950	140	40	30	R2	
		6	49.80	49.40	1040	220	0	280	R2	
		7	50.00	50.70	1460	320	50	240	R2	
		8	49.30	51.30	1480	450	0	110	R2	
			50.00	50.60	1140	244	18	148	Average	
10-11-37-8W5	3769.5	1	49.50	51.15	1910	160	0	10	R3	Ricinus East
		2	50.00	51.70	0	20	180	10	R3	
		3	49.80	52.00	20	0	0	200	R3	
		4	49.70	51.00	3050	80	50	220	R3	
		5	49.70	51.60	1020	60	190	190	R3	
		6	49.45	51.90	70	180	0	160	R3	
			49.69	51.50	1012	83	70	132	Average	

Approximate equilibrium concentrations of trace elements (ppm) for marine dolomites

Trace element	Veizer (1983)	Vahrenkamp and Swart (1990)	Machel and Anderson (1989)	Amthor et. al. (1993)
	Seawater			UpperDevonianSeawater
Mg	130400			
Fe	3 - 50			3 - 50
Mn	1			1
Sr	470 - 550	50 - 70	128 - 155	128 - 155
Na	110 - 160			

Appendix E2 Isotopes

FIELD	LOCATION	DEPTH (m)	TYPE	$\delta^{13}\text{C}$	$\delta^{18}\text{O}$	$^{87}\text{Sr}/^{86}\text{Sr}$
STRACHAN	15-2-38-10W5	4145.1	SMC1	1.97	-6.46	
STRACHAN	15-2-38-10W5	4145.1	SMC2	1.94	-6.59	
STRACHAN	15-2-38-10W5	4145.1	SMC3	1.56	-5.86	
STRACHAN	15-2-38-10W5	4145.1	SMC4	1.82	-5.87	
STRACHAN	15-2-38-10W5	4145.1	SMC5	1.72	-5.55	
STRACHAN	15-2-38-10W5	4145.1	SMC6	2.09	-6.54	
STRACHAN	15-2-38-10W5	4145.1	SMC7	2.43	-6.07	
STRACHAN	15-2-38-10W5	4144.7	SMC1	1.55	-6.88	
STRACHAN	15-2-38-10W5	4144.7	SMC2	1.67	-7.87	
STRACHAN	15-2-38-10W5	4144.7	SMC3	2.14	-5.51	
STRACHAN	15-2-38-10W5	4144.7	SMC4	1.62	-7.44	
STRACHAN	15-2-38-10W5	4144.7	SMC5	1.73	-7.59	
STRACHAN	10-31-37-9W5	4156.0	SMC	1.90	-8.78	
STRACHAN	10-31-37-9W5	4156.0	Matrix	1.71	-5.71	
STRACHAN	10-31-37-9W5	4156.0	Corals	1.91	-8.67	
STRACHAN	10-31-37-9W5	4276.5	Matrix	2.24	-6.65	
STRACHAN	10-31-37-9W5	4276.5	Corals	2.63	-7.38	
STRACHAN	10-31-37-9W5	4226.2	Matrix	3.73	-5.46	
STRACHAN	10-31-37-9W5	4226.2	Corals	3.25	-6.22	
STRACHAN	10-31-37-9W5	4226.2	Corals	3.44	-6.47	
STRACHAN	10-31-37-9W5	4182.6	Corals	1.89	-7.87	
RAM RIVER	5-13-37-12W5	5067.4	Matrix	3.15	-6.42	0.70837 +/- 4
STRACHAN	10-31-37-9W5	4156.0	Patch	3.07	-8.31	0.70861 +/- 1
STRACHAN	10-31-37-9W5	4276.5	Patch	2.51	-7.45	0.70840 +/- 1
STRACHAN	10-31-37-9W5	4226.2	Patch	3.40	-8.53	0.70822 +/- 1
STRACHAN	10-31-37-9W5	4182.6	Patch	3.17	-7.85	0.70827 +/- 1
STRACHAN	10-31-37-9W5	4182.6	Patch	3.22	-7.50	
STRACHAN	10-31-37-9W5	4325.6	R2	3.57	-4.50	
STRACHAN	10-31-37-9W5	4318.3	R2	3.54	-4.57	0.70825 +/- 1
STRACHAN	10-31-37-9W5	4300.3	R2			0.70968 +/- 1
STRACHAN	10-24-37-9W5	3828.0	R2 (TSR)	1.94	-4.23	
STRACHAN	10-24-37-9W5	3827.7	R2 (TSR)	2.20	-5.38	
STRACHAN	12-31-37-9W5	4295.4	R2	2.30	-6.58	
CRIMSON	11-28-37-8W5	3699.7	R2A	2.03	-3.84	0.70854 +/- 1
	11-28-37-8W5	3699.7	R2B	2.00	-3.67	
RICINUS W.	10-33-36-10W5	4661.0	R2	1.94	-4.90	0.70865 +/- 1
	10-33-36-10W5	4629.9	R2	1.79	-4.70	0.70833 +/- 1

Appendix E2 Isotopes

FIELD	LOCATION	DEPTH (m)	TYPE	$\delta^{13}\text{C}$	$\delta^{18}\text{O}$	$^{87}\text{Sr}/^{86}\text{Sr}$
	11-27-36-10W5	4476.2	R2	2.39	-4.43	
RICINUS E.	6-14-34-8W5	4286.9	R2	2.26	-4.55	
CHEDDERVILLE	10-29-37-7W5	3656.1	R2	2.37	-4.47	
RAM RIVER	5-13-37-12W5	5047.3	R2	1.43	-7.19	
STRACHAN	7-32-37-9W5	4113.9	R1	3.19	-5.34	
STRACHAN	7-32-37-9W5	4085.4	R1	3.14	-4.28	
RICINUS W.	15-23-36-10W5	4593.0	R1			0.70830 +/- 1
RICINUS W.	10-33-36-10W5	4577.4	R1	2.58	-4.85	0.70860 +/- 1
RICINUS W.	15-23-36-10W5	4592.4	R1	5.11	-4.65	0.70841 +/- 2
RICINUS E.	7-26-36-10W5	4397.9	R1	2.34	-4.52	
RICINUS E.	6-24-34-8W5	4386.0	R1	1.83	-5.32	0.71000 +/- 1
RICINUS E.	6-24-34-8W5	4380.2	R1	2.44	-4.91	0.70831 +/- 1
RICINUS E.	6-14-34-8W5	4285.3	R1	1.99	-4.64	0.70865 +/- 3
STRACHAN	11-27-37-9W5	3937.5	R3	2.56	-5.32	
STRACHAN	11-27-37-9W5	4022.3	R3	3.52	-4.51	
RICINUS W.	10-33-36-10W5	4564.0	R3	2.42	-4.61	0.70923 +/- 1
RICINUS W.	10-33-36-10W5	4633.8	R3	1.81	-4.58	0.70866 +/- 3
RICINUS E.	10-11-37-8W5	3797.9	R3	1.35	-4.03	
CHEDDERVILLE	10-20-37-7W5	3541.2	R3	1.74	-4.06	
CHEDDERVILLE	6-30-37-7W5	3532.0	R3	2.28	-4.89	
STRACHAN	10-31-37-9W5	4276.5	C2	2.47	-6.84	
STRACHAN	10-31-37-9W5	4276.5	C2	2.63	-7.84	
STRACHAN	10-31-37-9W5	4276.5	C2	2.57	-7.01	
STRACHAN	10-31-37-9W5	4276.5	C2	2.57	-7.65	
STRACHAN	10-31-37-9W5	4226.2	C2/frac.	3.31	-8.28	
STRACHAN	10-31-37-9W5	4226.2	C2	3.23	-5.97	
CRIMSON	11-28-37-8W5	3699.7	C2A	-4.83	-5.95	0.71045 +/- 1
CRIMSON	11-28-37-8W5	3699.7	C2B	-4.07	-5.63	
RAM RIVER	5-13-37-12W5	5067.4	C2	2.09	-7.38	
RAM RIVER	5-13-37-12W5	5067.4	C2	2.79	-7.84	
RICINUS E.	6-24-34-8W5	4386.0	C2	1.37	-6.85	
RICINUS E.	6-24-34-8W5	4380.2	C2	1.61	-7.26	0.70920 +/- 1
RICINUS W.	15-23-36-10W5	4592.4	C2			0.70882 +/- 2
STRACHAN	10-31-37-9W5	4325.6	Cal. Cem.	-3.65	-6.62	
STRACHAN	5-11-38-10W5	4228.0	Cal. Cem.	0.08	-6.60	0.70930 +/- 3
STRACHAN	10-31-37-9W5	4318.3	Cal. Cem (TSR)	-10.29	-7.47	0.70960 +/- 1
RICINUS W.	10-33-36-10W5	4577.4	Cal. Cem.	-2.49	-8.95	0.70854 +/- 1

Appendix E2 Isotopes

FIELD	LOCATION	DEPTH (m)	TYPE	$\delta^{13}\text{C}$	$\delta^{18}\text{O}$	$^{87}\text{Sr}/^{86}\text{Sr}$
RICINUS W.	10-33-36-10W5	4633.8	Cal. Cem (TSR)	-25.77	-8.07	0.70861 +/- 1
RICINUS W.	10-33-36-10W5	4661.0	Cal. Cem (TSR)	-19.01	-9.01	0.70850 +/- 1
RICINUS W.	15-23-36-10W5	4593.0	Cal. Cem.			0.70901 +/- 4
RICINUS E.	6-14-34-8W5	4285.3	Cal. Cem (TSR)	-8.61	-8.77	0.70944 +/- 1
RAM RIVER	5-13-37-12W5	5047.3	Cal. Cem (TSR)	-17.15	-7.48	

Calculations of paleotemperatures for precipitation of replacement dolomites

Assuming temperature of Devonian seawater of 25 °C and $\delta^{18}\text{O}_{\text{water}} = -2.5\text{‰ SMOW}$ and isotopic equilibrium between calcite and sea water (following Amthor, et. al., 1993)

For replacement dolomite R_1

$$\delta^{18}\text{O}_{\text{dolomite}} = -4.87\text{‰ PDB} = 27\text{‰ SMOW}$$

$$1.1 \quad 10^3 \ln \alpha = 2.78 \times 10^6 (T (^{\circ}\text{K}))^{-2} + 0.91 \quad (\text{Land, 1985})$$

$$1.2 \quad \alpha \equiv \delta^{18}\text{O}_{\text{dolomite}} + 1000 / \delta^{18}\text{O}_{\text{water}} + 1000 = 0.9754$$

$$1.3 \quad T = (2.78 \times 10^6 / (10^3 \ln \alpha) - 0.91)^{1/2} = 328.44\text{ °K} = 55.29\text{ °C}$$

$$T = 55.29\text{ °C}$$

Appendix E Fluid Inclusion

WELL LOCATION	DEPTH (m)	CHIP	HOST	TYPE	Tf	Te	Tmice	Th	S	COMMENTS
10-33-36-10W5	4577	1-1	Dol-C1	L-V	-51	-30	-11.2	114	15.1	
		1-2	Dol-C1	L-V				140		
		1-3	Dol-C1	L-V	-55	-30	-10.7	87	14.7	
		1-4	Dol-C1	L-V				126		
		1-5	Dol-C1	L-V				149		
		1-6	Dol-C1	L-V				147		
		1-7	Dol-C1	L-V				153		
		Mean							131	14.9
11-28-37-8W5	3700	1-1	Dol-C2	L-V				125		
		1-2	Dol-C2	L-V				160		
		1-3	Dol-C2	L-V				157		
		1-4	Dol-C2	L-V				155		
		1-5	Dol-C2	L-V				157		
		1-6	Dol-C2	L-V				114		
		1-7	Dol-C2	L-V				159		
		1-8	Dol-C2	L-V				163		
		1-9	Dol-C2	L-V				145		
		1-10	Dol-C2	L-V				156		
		1-11	Dol-C2	L-V				160		
		1-12	Dol-C2	L-V				154		
		1-13	Dol-C2	L-V				153		
		1-14	Dol-C2	L-V				155		
		1-15	Dol-C2	L-V				130		
		1-16	Dol-C2	L-V				153		
		2-1	Dol-C2	L-V				154		Quartz
		2-2	Dol-C2	L-V				156		
		2-3	Dol-C2	L-V				154		
		2-4	Dol-C2	L-V				157		
		2-5	Dol-C2	L-V	-69	-29	-18.0	154	20.2	
		2-6	Dol-C2	L-V	-70	-29	-18.5	156	20.5	
		2-7	Dol-C2	L-V	-71	-30	18.8	173	20.6	
		2-8	Dol-C2	L-V	-69			154		
		2-9	Dol-C2	L-V	-70		-18.5	157	20.5	
		2-10	Dol-C2	L-V	-69		-18.4	169	20.4	
		2-11	Dol-C2	L-V	-67	-30	-18.3	161	20.4	
Mean								159	20.4	
10-33-36-10W5	4577	1-1	Calcite	L-V	-55	-30	-16.4	156	19.1	
		1-2	Calcite	L-V	-57	-32	15.3	154	18.4	

Appendix E Fluid Inclusion

WELL LOCATION	DEPTH (m)	CHIP	HOST	TYPE	Tf	Te	Tmice	Th	S	COMMENTS
		1-3	Calcite	L-V	-57	-32	-15.4	149	18.5	
		1-4	Calcite	L-V	-60	-37	-16.0	152	18.9	
		1-5	Calcite	L-V	-57	-34	-15.8	144	18.7	
		1-6	Calcite	L-V	-54	-40	-16.2	151	19.0	
		1-7	Calcite	L-V	-55	-41	15.9	156	18.8	
		1-8	Calcite	L-V	-60	-33	-12.8	152	16.5	
		1-9	Calcite	L-V	-62	-36	-15.1	147	18.2	
		1-10	Calcite	L-V	-58	-34	-15.0	139	18.2	
		1-11	Calcite	L-V	-58	-32	-14.6	141	17.9	
		1-12	Calcite	L-V	-60	-34	-11.8	138	15.6	
		2-1	Calcite	L-V	-61	-43		156	12.6	
		2-2	Calcite	L-V	-58	-33	-10.2	166	14.2	
		2-3	Calcite	L-V	-60	-39	-13.9	154	17.3	
		2-4	Calcite	L-V				163		
		2-5	Calcite	L-V	-58	-30	-15.8	169	18.7	
		3-1	Calcite	L-V	-58	-35	-14.1	132	17.5	Methane
		3-2	Calcite	L-V	-62	-35	-14.9	152	18.1	
		3-3	Calcite	L-V	-65	-34	-14.3	147	17.6	
		3-4	Calcite	L-V	-60	-32	-15.8	156	18.7	
		3-5	Calcite	L-V	-57	-38	-14.7	154	17.9	
		3-6	Calcite	L-V	-55	-31	-14.2	157	18.1	
		3-7	Calcite	L-V	-61	-33	-14.4	161	17.5	
	Mean							152	17.6	
10-33-36-10W5	4628	1-1	Calcite	L-V	-59	-48	-12.4	176	16.1	Along same plane
		1-2	Calcite	L-V	-60	-43	-12.8	177	16.5	
		1-3	Calcite	L-V	-66	-44	-12.6	177	16.1	
		1-4	Calcite	L-V	-62		-14.2	177	17.6	
		1-5	Calcite	L-V	-54		-11.9	169	15.6	
		1-6	Calcite	L-V	-56	-49	-12.1	170	15.9	
		1-7	Calcite	L-V		-42	-15.2	158	18.3	Along same plane
		1-8	Calcite	L-V	-59	-42	-15.5	154	18.5	
		1-9	Calcite	L-V	-57	-42	-15.3	156	18.4	
		1-10	Calcite	L-V	-58	-45	-15.3	160	18.4	
		1-11	Calcite	L-V	-65		-15.2	158	18.3	
		1-12	Calcite	L-V		-44	-15.1	159	18.2	Isolated
		1-13	Calcite	L-V	-59	-43	-15.3	158	18.4	Isolated
		1-14	Calcite	L-V		-37	-12.5	168	16.2	Along same plane
		1-15	Calcite	L-V		-37	-14.5	170	17.8	

Appendix E Fluid Inclusion

WELL LOCATION	DEPTH (m)	CHIP	HOST	TYPE	Tf	Te	Tmice	Th	S	COMMENTS
		1-16	Calcite	L-V		-37	-13.8	171	16.3	
		1-17	Calcite	L-V		-37	-12.6	167	17.3	
		1-18	Calcite	L-V		-37	-12.0	165	15.8	
	Mean							166	17.3	
5-11-38-10W5	4228	1-1	Calcite	L-V			-19.1	148	22.0	
		1-2	Calcite	L-V			-18.3	147	21.4	
		1-3	Calcite	L-V			-19.2	148	22.1	
		1-4	Calcite	L-V			-19.0	146	21.9	
		1-5	Calcite	L-V			-19.1	146	22.0	
		1-6	Calcite	L-V			-18.9	147	21.9	
		1-7	Calcite	L-V			-18.7	147	21.7	
		1-8	Calcite	L-V			-19.0	147	21.9	
	Mean							147	21.8	
10-31-37-9W5	4300	1-1	Calcite	L-V	-70	-44	-19.0	154	20.8	
		1-2	Calcite	L-V	-71		-19.0	155	20.8	
		1-3	Calcite	L-V	-68		-19.3	142	21.0	
		1-4	Calcite	L-V	-73	-34	-20.5	161	21.7	
		1-5	Calcite	L-V		-39	-18.0	161	20.2	
		1-6	Calcite	L-V		-34	-20.5	147	21.7	
		1-7	Calcite	L-V		-31	-18.5	155	20.5	
		1-8	Calcite	L-V	-66		-20.3	148	21.6	
		1-9	Calcite	L-V	-64	-31	-20.2	155	21.5	
		1-10	Calcite	L-V	-64		-19.4	162	20.8	
		1-11	Calcite	L-V		-38	-19.0	162	20.8	
		1-12	Calcite	L-V				145		
		1-13	Calcite	L-V				163		
		1-14	Calcite	L-V				138		
	Mean						-19.5	153	21.0	

APPENDIX F

**GAS COMPOSITION FROM STRACHAN, RICINUS WEST AND
CHEDDERVILLE RESERVOIRS**

From files of Energy Resources Conservation Board (ERCB), Calgary, Alberta

GAS ANALYSIS - STRACHAN

WELL:	14-2-38-10W5	6-1-38-10-W5	10-31-37-9W5	7-32-37-9W5	6-33-37-9W5	11-28-37-9W5	11-27-37-9W5
SAMPLE FROM:	Gas separator	HP separator	HP separator	HP separator	Drill pipe	Wellhead gas	HP separator
TEMPERATURE (oC):	49	65	25	55	36	20	45.5
PRESSURE (Kpa/m):	247	20,453	904	22,600	10,622	109,169	22,826
DEPTH INTERVAL (m):	4035.0-4179.5	4039.3-4082.3	4490.0-4498.3	4146.9-4156.0	4205.7-4219.5	4066.4-4107.6	3935.9-3945.1
POOL:	D-3B	D-3B	D-3A	D-3A	D-3A	D-3A	D-3A
NATURAL GAS (Vol. %):							
Hydrogen	0.00	0.00	0.00	0.00	0.00	0.00	0.00
Methane	91.71	88.62	84.93	80.08	85.69	82.57	80.73
Ethane	0.80	1.31	2.15	4.06	4.04	3.96	4.03
Propane	0.32	0.42	0.53	1.50	1.37	1.43	1.46
Isobutane	0.12	0.15	0.20	0.45	0.36	0.44	0.42
n-Butane	0.13	0.15	0.19	0.60	0.43	0.43	0.64
i-Pentane	0.07	0.08	0.08	0.24	0.13	0.12	0.16
n-Pentane	0.05	0.06	0.06	0.24	0.10	0.09	0.14
Hexanes	0.13	0.08	0.05	0.29	0.05	0.05	0.10
Heptanes	0.49	0.18	0.02	0.73	0.07	0.06	0.25
Octanes							
Nitrogen	1.27	0.45	0.49	0.73	0.50	0.44	0.32
Helium	0.02	0.02		0.01			
Carbon Dioxide	1.66	2.06	2.12	2.22	2.22	1.90	2.67
Hydrogen Sulphide	3.23	6.42	8.94	8.85	5.04	8.51	9.08
TOTAL:	100.00	100.00	100.00	100.00	100.00	100.00	100.00

GAS ANALYSIS - RICINUS

GAS ANALYSIS - CHEDDERVILLE

WELL:	10-33-36-10W5	7-26-36-10W5	6-25-36-10W5	7-13-36-10W5	16-19-37-7W5
SAMPLE FROM:	Gas separator	HP separator	HP separator	HP separator	Wellhead
TEMPERATURE (oC):	62	66.5	70	76.5	
PRESSURE (Kpa/m):	18,306	29,945	22,035,000.00	28,476,000.00	
DEPTH INTERVAL:	4504.8-45917.6	4384.1-4460.3	4404.8-4417.6	4385.6-4399.0	3545.7-5348.7
POOL:	D-3A	D-3A	D-3A	D-3A	D-3A
NATURAL GAS (Vol. %)					
Hydrogen	0.00	Tr	0.00	Tr	0.00
Methane	60.72	60.31	60.35	58.86	79.86
Ethane	0.55	0.58	0.57	0.52	4.38
Propane	0.05	0.06	0.05	0.07	1.89
Isobutane	Tr	Tr	Tr	0.01	0.73
n-Butane	0.01	0.00	0.01	0.02	1.00
i-Pentane	Tr	0.00	0.00	0.01	0.42
n-Pentane	Tr	0.00	0.00	0.01	0.40
Hexanes	Tr	0.00	Tr	0.04	0.21
Heptanes	0.03	0.00	Tr	0.06	0.50
Octanes					
Nitrogen	0.50	0.27	0.24	0.31	
Helium	0.00	0.01	Tr	Tr	0.80
Carbon Dioxide	6.84	6.61	5.98	6.61	1.20
Hydrogen Sulphide	31.30	32.16	32.8	33.48	8.61
					100.00
TOTAL:	100.00	100.00	100.00	100.00	

H2S CONTENT

WELL	H2S (%)	FIELD
14-9-37-7W5	7.47	
16-19-37-7W5	8.61	
10-20-37-7W5	6.91	
15-27-37-7W5	4.93	CHEDDERVILLE
11-28-37-8W5	9.09	
7-33-37-8W5	9.95	CRIMSON
10-24-37-9W5	47.35	
11-27-37-9W5	9.08	
12-27-37-9W5	9.50	
6-28-37-9W5	9.50	
11-28-37-9W5	8.51	
10-31-37-9W5	8.94	
7-32-37-9W5	8.85	
8-32-37-9W5	9.90	
6-33-37-9W5	5.04	
6-1-38-10W5	6.42	
14-2-38-10W5	3.23	STRACHAN
7-13-36-10W5	33.48	
6-25-36-10W5	32.80	
7-26-36-10W5	32.16	
10-33-36-10W5	31.30	RICINUS

APPENDIX G

WELLS THAT PENETRATE THE COOKING LAKE FORMATION

Wells with information on the Cooking Lake Formation

LOCATION	SOURCE	TOP (ft)	BOTTOM (ft)	THICKNESS (ft/m)	CORED (ft)	LITHOLOGY	** Ø (%)	Km (md)	Kv (md)
7-19-37-8W5	Core	13340	13460	120/36 *	26	Dolostones/Mudstones	4.7	21	1.3
7-28-36-8W5	GR Log	13787	13927	140/43		?			
6-24-34-8W5	Core	?	?	?	60 ?	Dolostones			
10-31-37-9W5	GR Log	14186	14306	120/36 ?	13	Dolostones			
10-30-37-9W5	GR Log	14490	14560	70/21 * ?		?			
6-34-37-9W5	GR Log	14225	14300	75/23 * ?		?			
10-33-36-10W5	GR Log	15470	15611	141/43		?			
11-27-36-10W5	GR Log			70/21 * ?		?			
15-23-36-10W5	Core			140/43		Dolostones			
10-16-37-10W5	Core	15306	15333	156/47	27	Dolostones	4.5	32	.69
7-9-37-10W5	Core	15282	15490	208/63 *	96	Partly dolomitized			
5-4-39-11W5	GR Log	15040	15110	70/21		?			
7-9-39-12W5	Ticket			60/18		?			
5-13-37-12W5	Core	16678	16800	122/37		Partly dolomitized			

* Offreef well

** from ERCB files

APPENDIX H

VERTICAL PROFILES OF POROSITY AND PERMEABILITY OF DEPOSITIONAL FACIES IN THE RICINUS WEST BUILDUP SHOWING THE MAIN PORE TYPE AND PERMEABLE ZONES

Skeletal packstone/grainstones

- a) well:10-33
- b) well:11-27
- c) well:7-26
- d) well:15-23

Skeletal wackestones

- e) well: 10-33
- f) well:11-27
- g) well:15-23

Laminites

- h) well: 10-33
- i) well: 11-27
- j) well: 7-26
- k) well:15-23

Stromatoporoid floatstone/rudstone

- l) well: 10-33
- m) well: 15-23

Coral rudstones

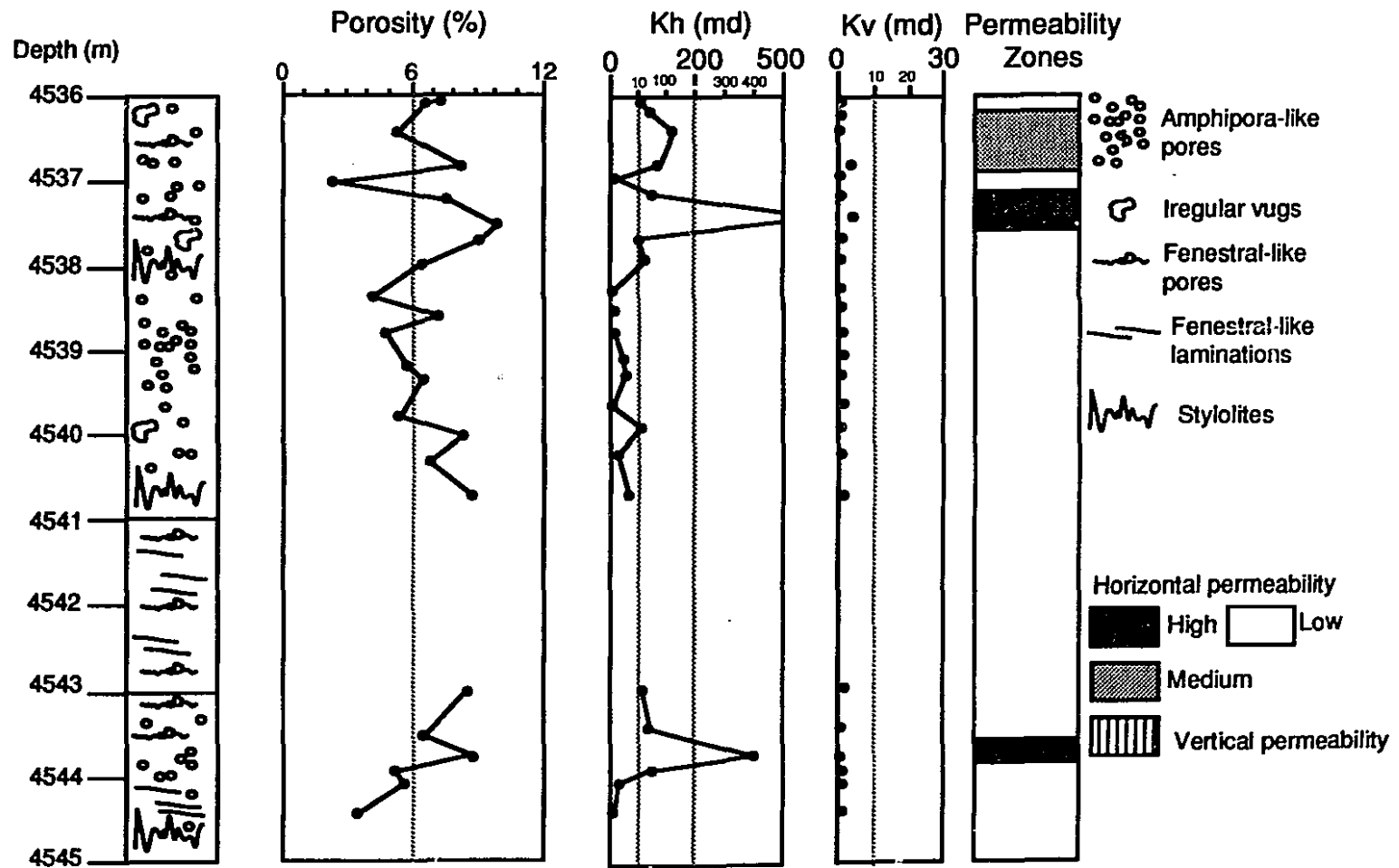
- n) well: 10-33
- o) well: 15-23

Tabular stromatoporoid boundstones

- p) well: 7-13

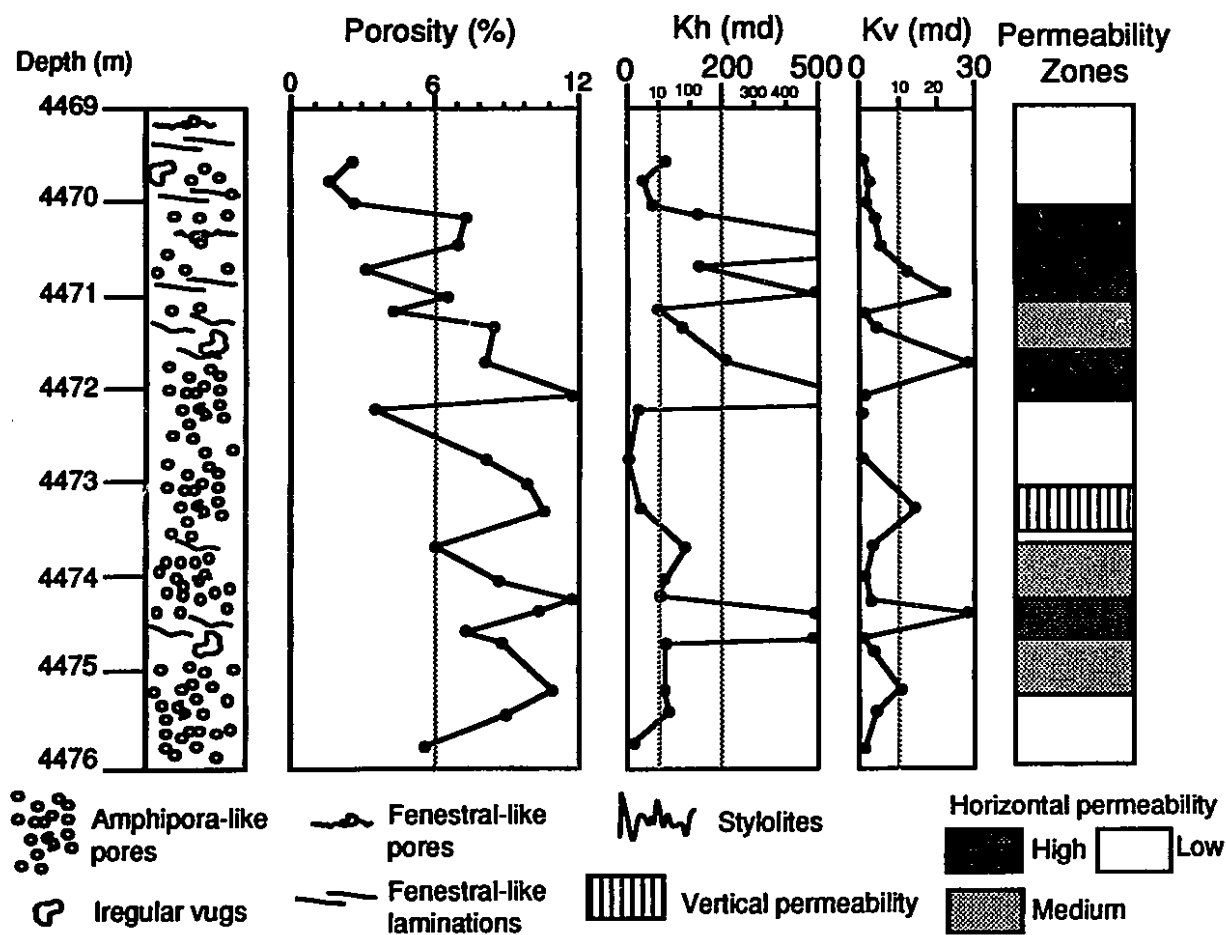
Depositional Facies: SKELETAL PACKSTONES/GRAINSTONES

Well: 10-33



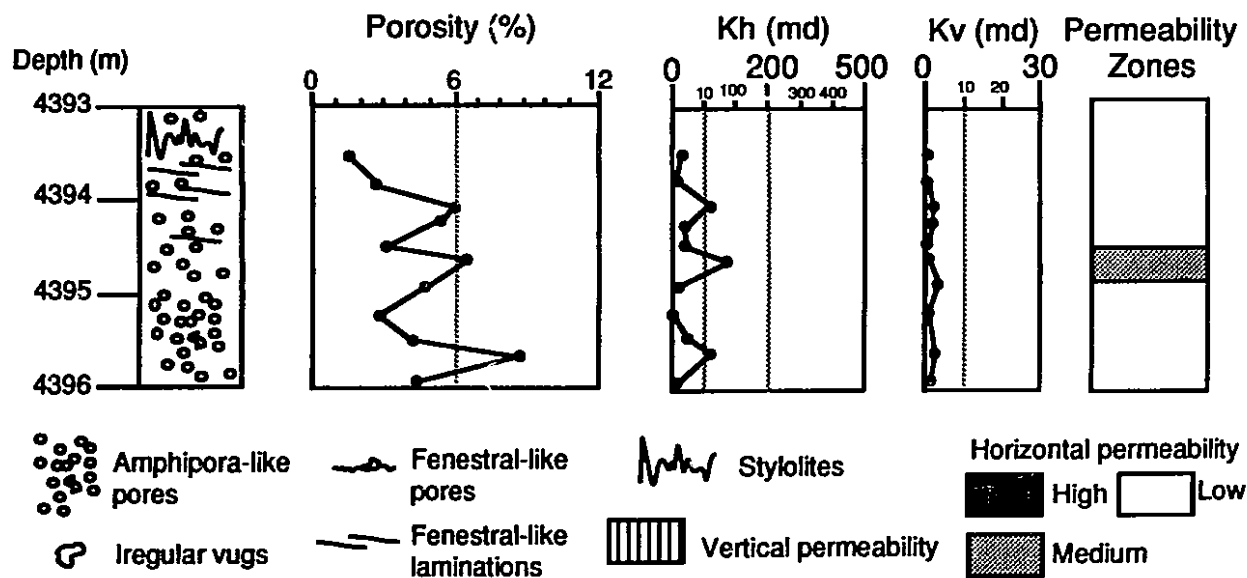
Depositional Facies: SKELETAL PACKSTONES/GRAINSTONES

Well: 11-27



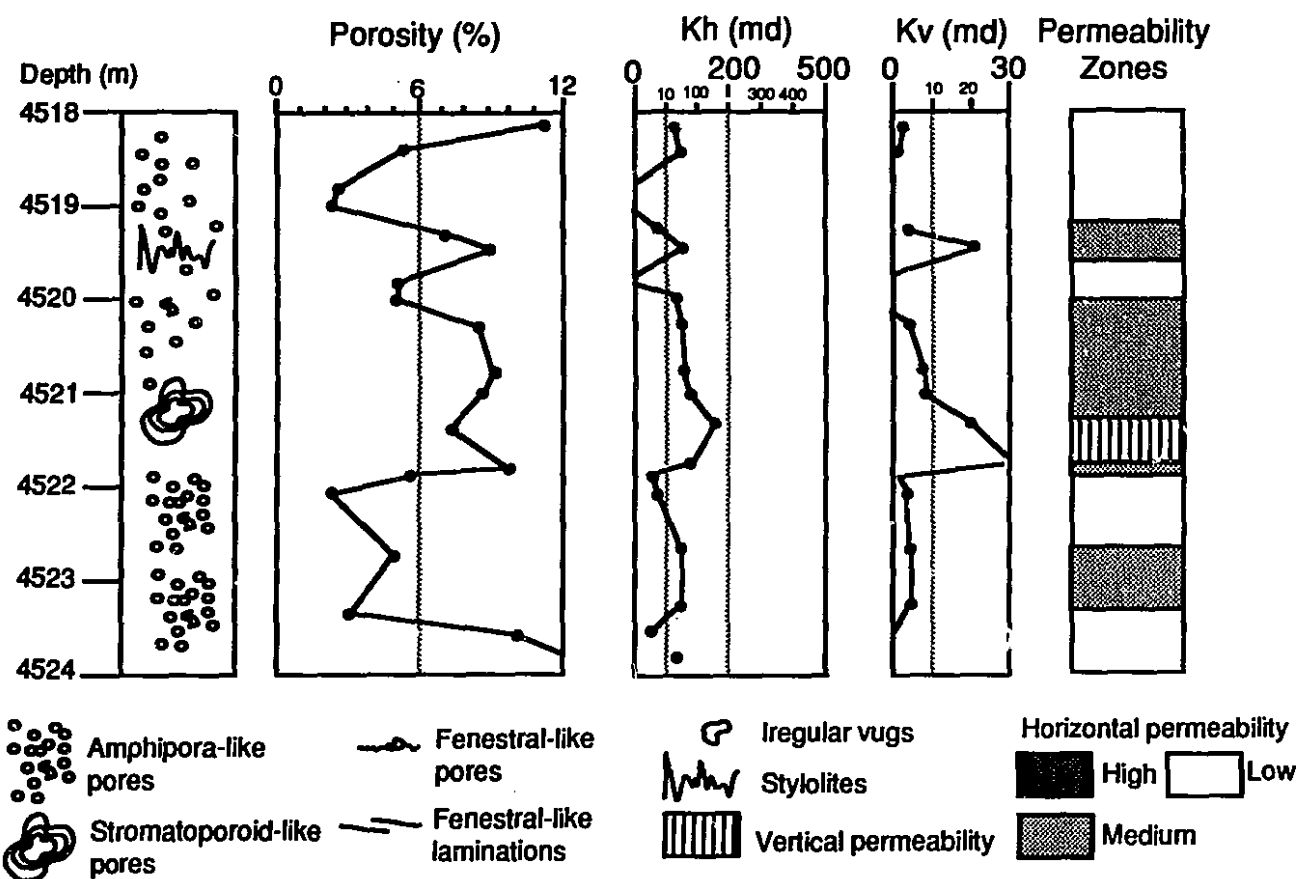
Depositional Facies: SKELETAL PACKSTONES/GRAINSTONES

Well: 7-26



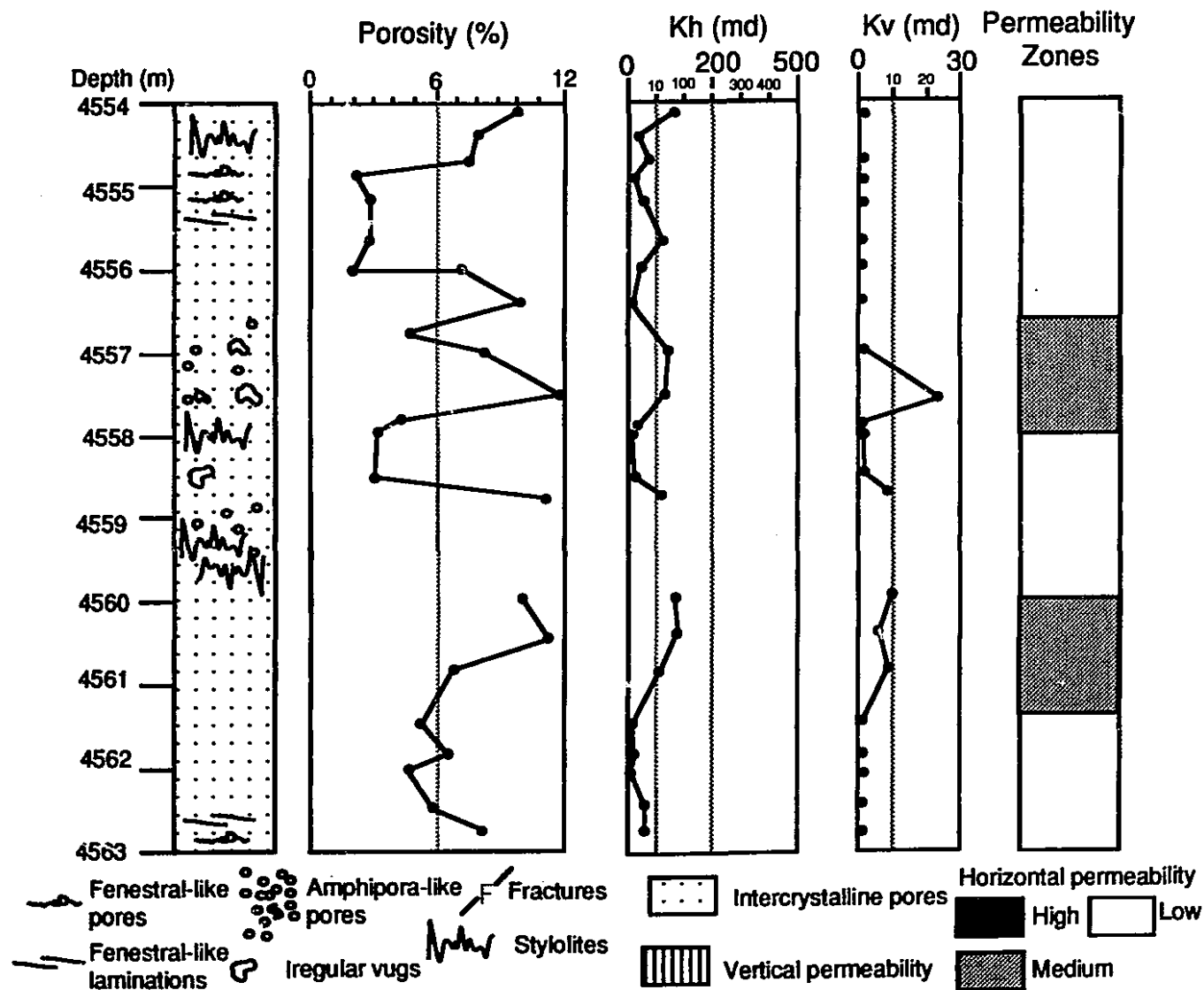
Depositional Facies: SKELETAL PACKSTONES/GRAINSTONES

Well: 15-23



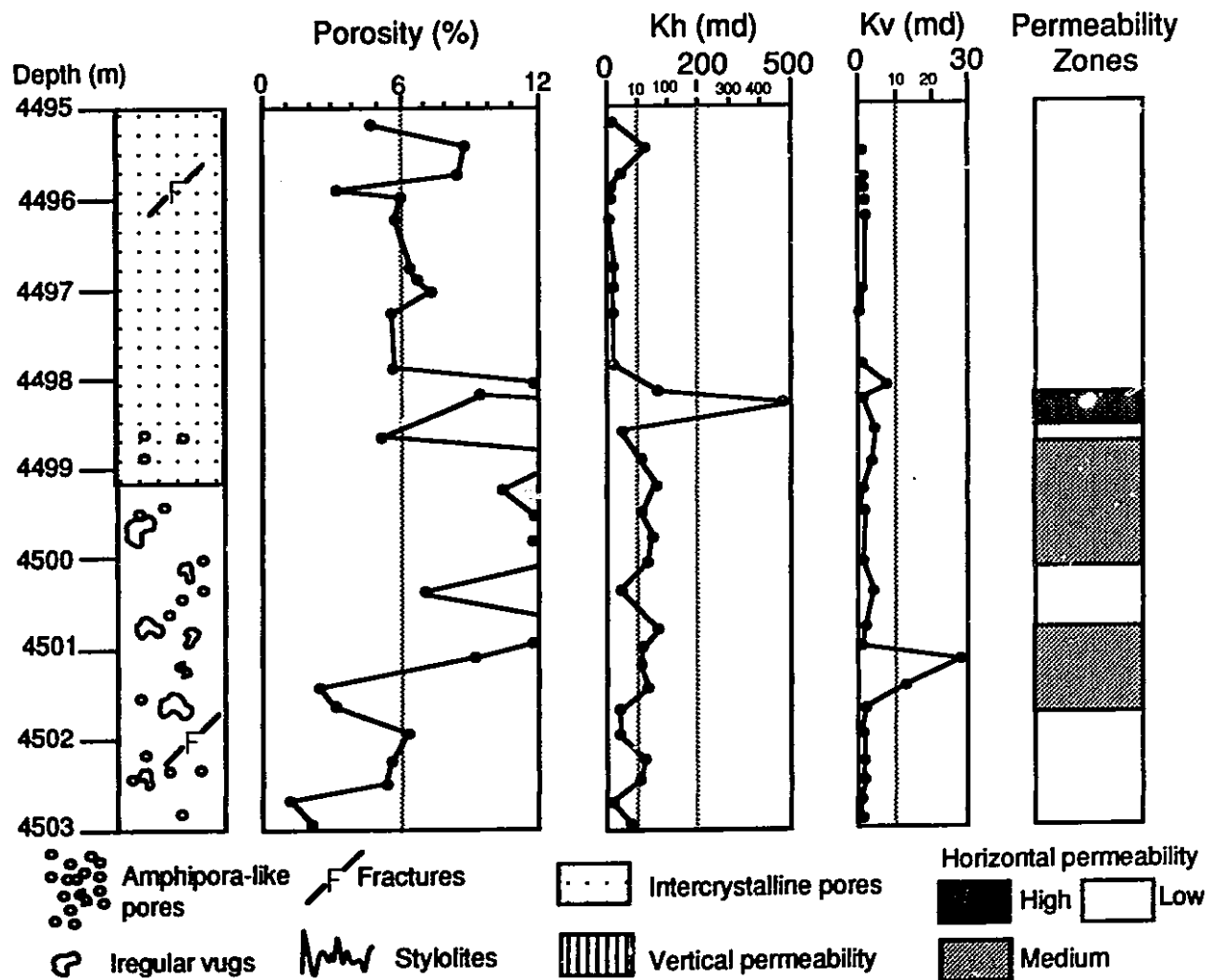
Depositional Facies: SKELETAL WACKESTONES

Well: 10-33



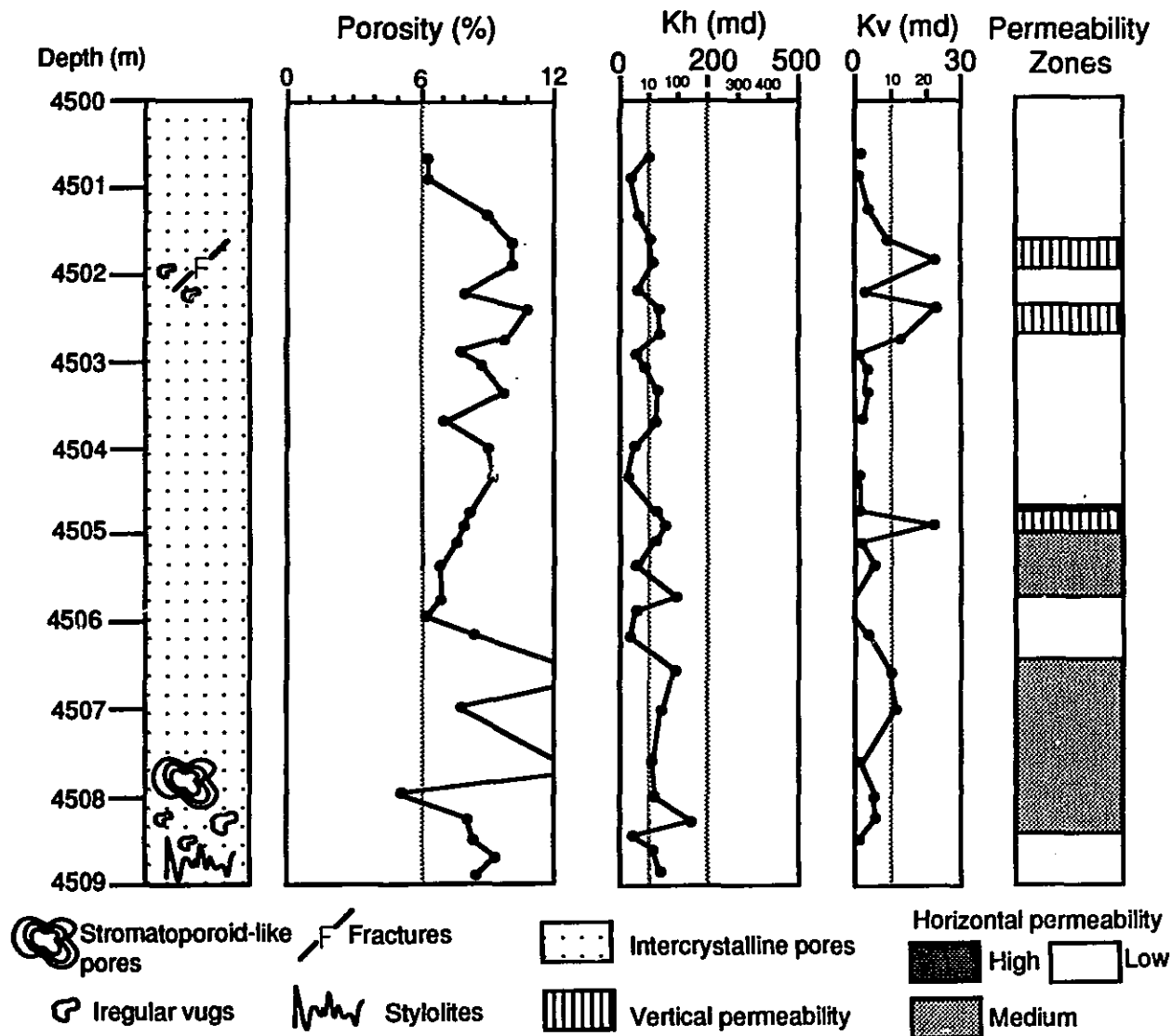
Depositional Facies: SKELETAL WACKESTONES

Well: 11-27



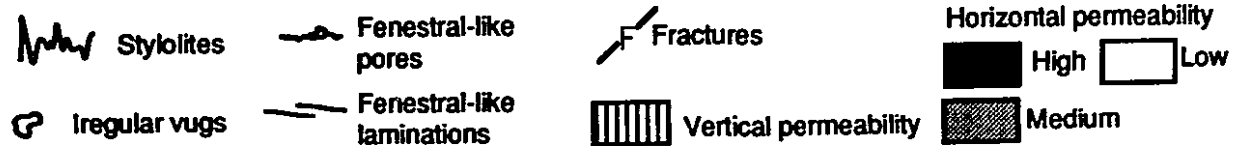
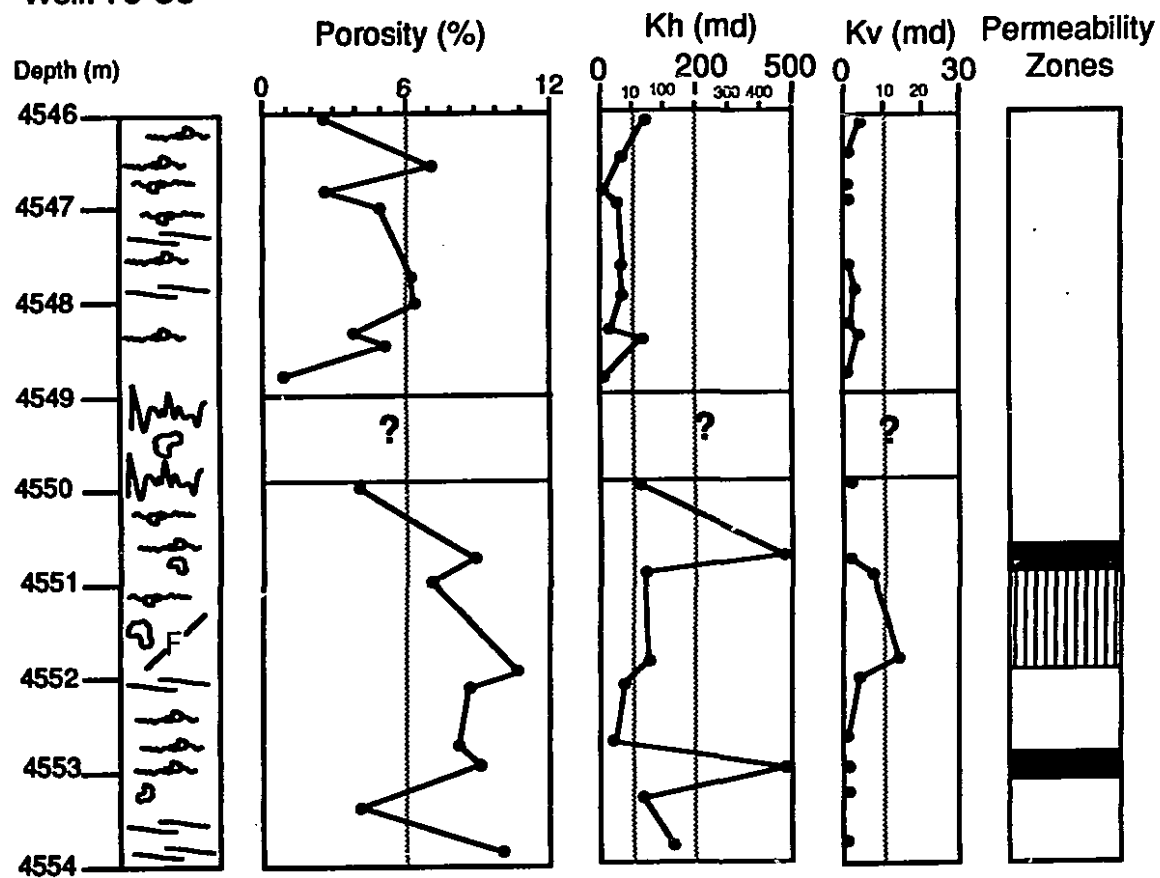
Depositional Facies: SKELETAL WACKESTONES

Well: 15-23



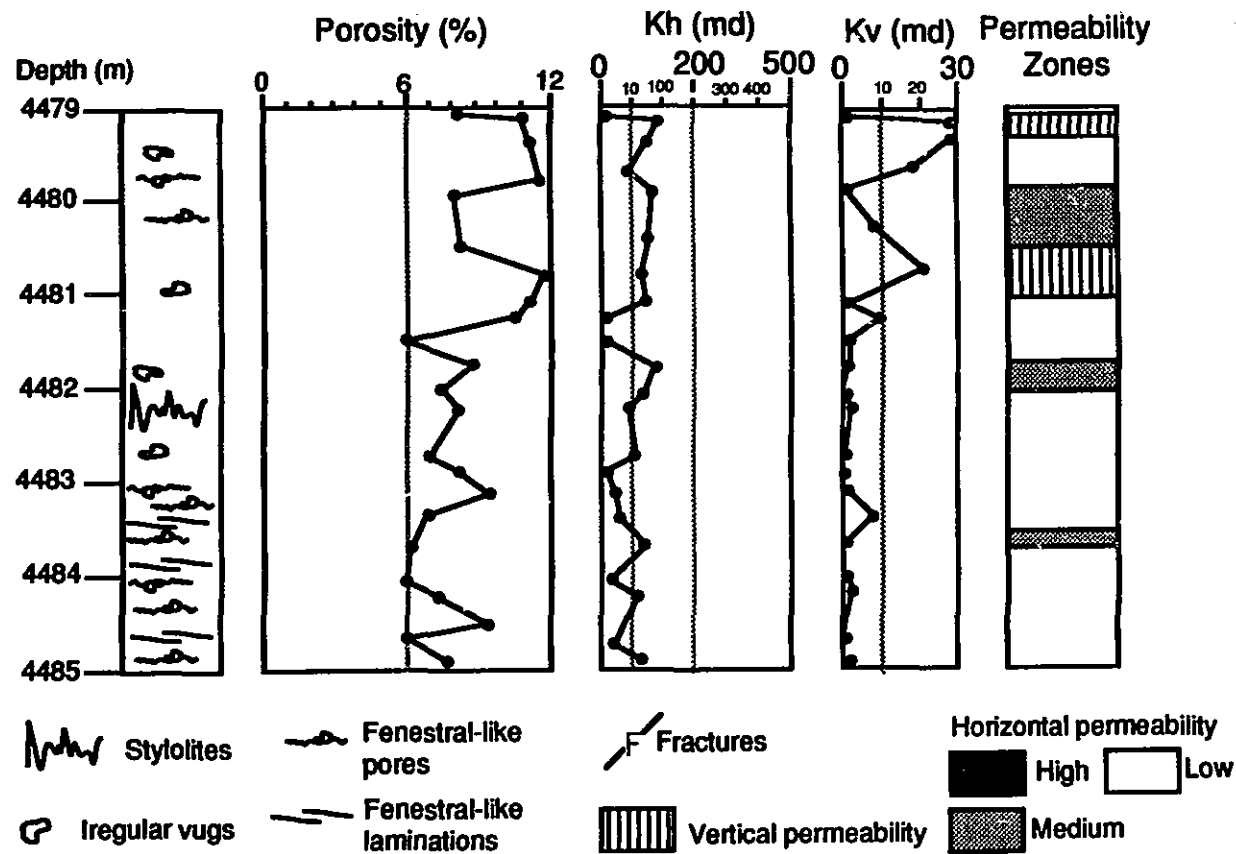
Depositional Facies: LAMINITES

Well: 10-33



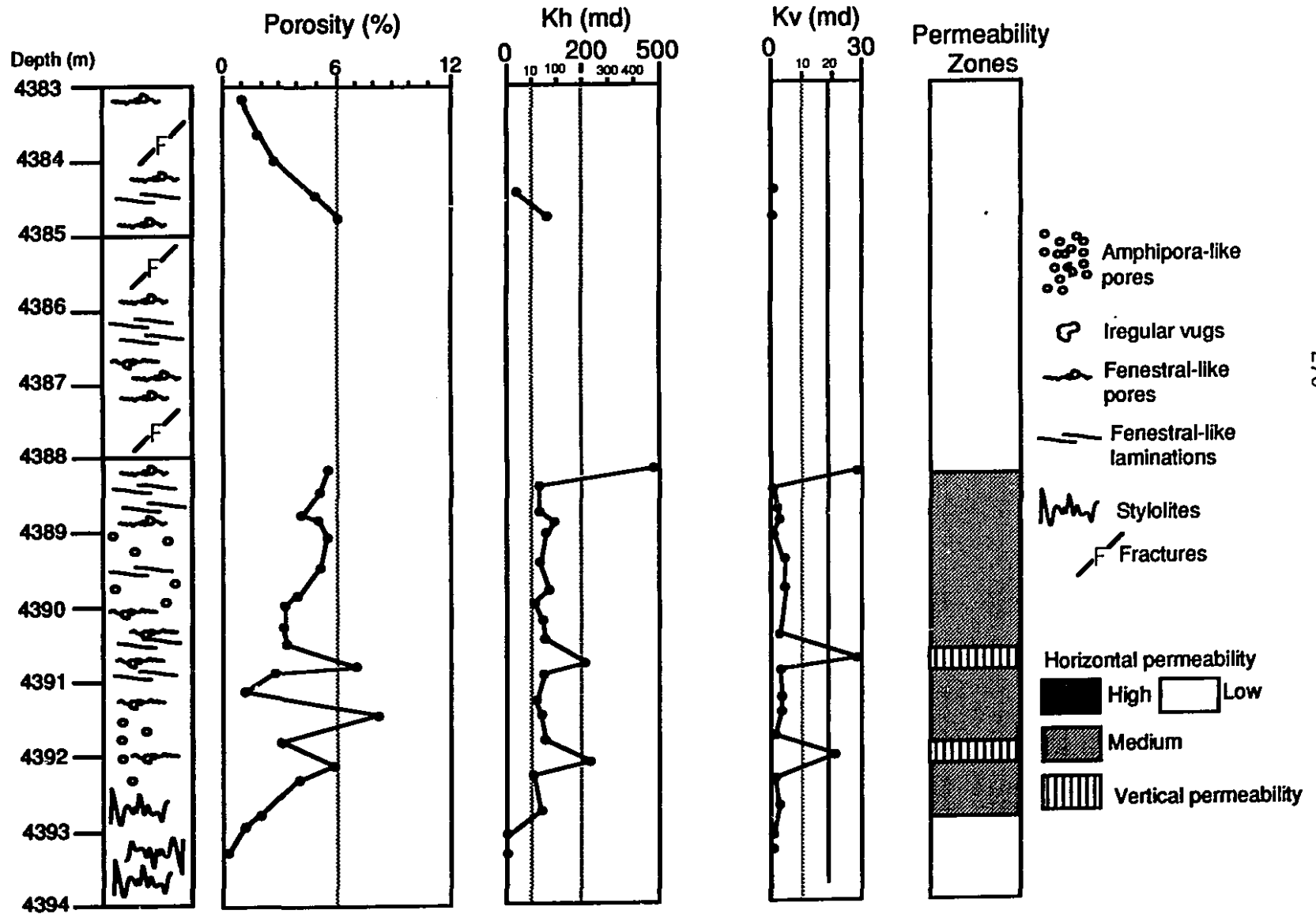
Depositional Facies: LAMINITES

Well: 11-27



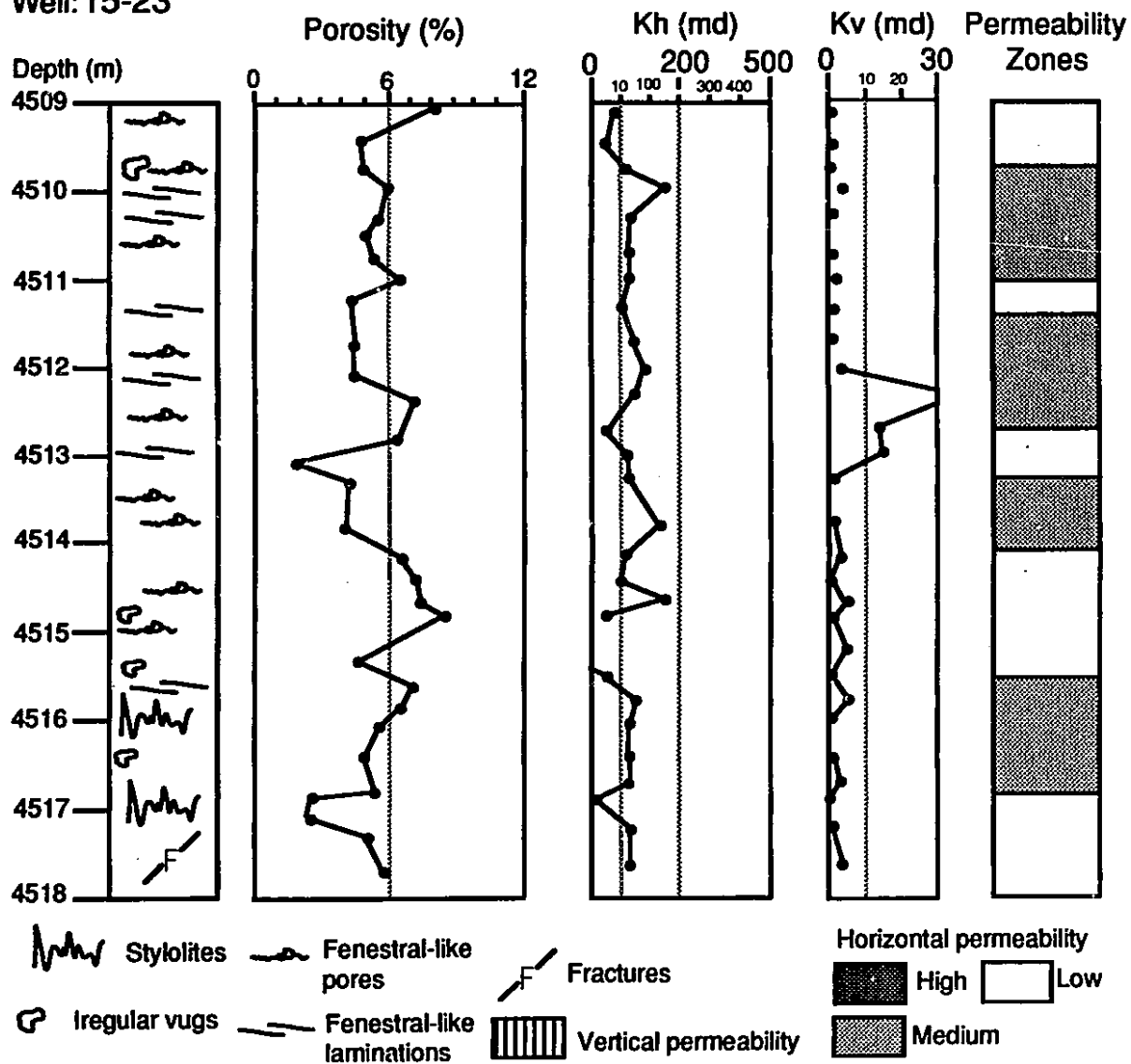
Depositional Facies: LAMINITES

Well: 7-26



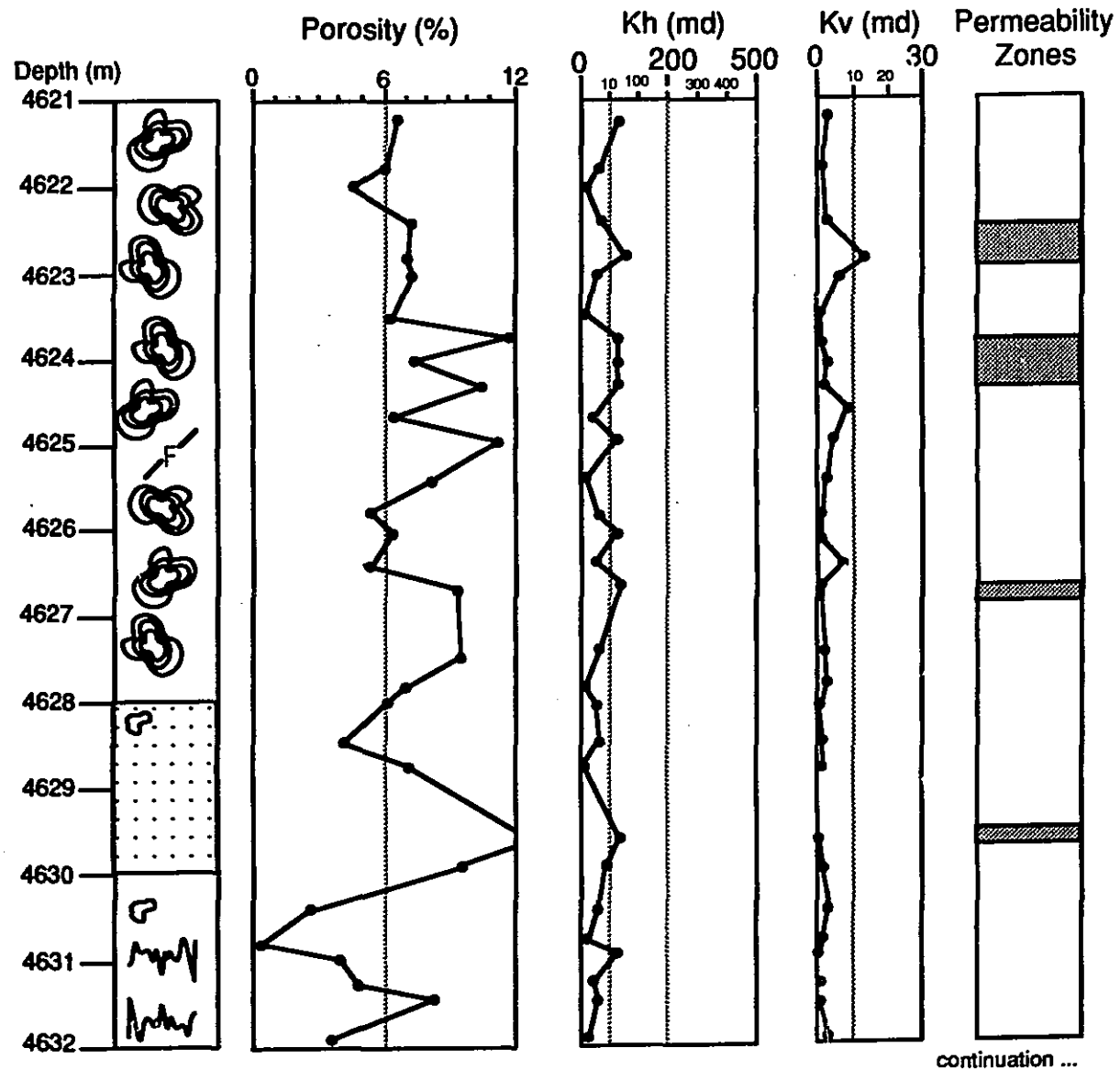
Depositional Facies: LAMINITES

Well: 15-23



Depositional Facies: STROMATOPOROID FLOATSTONES/RUDSTONES

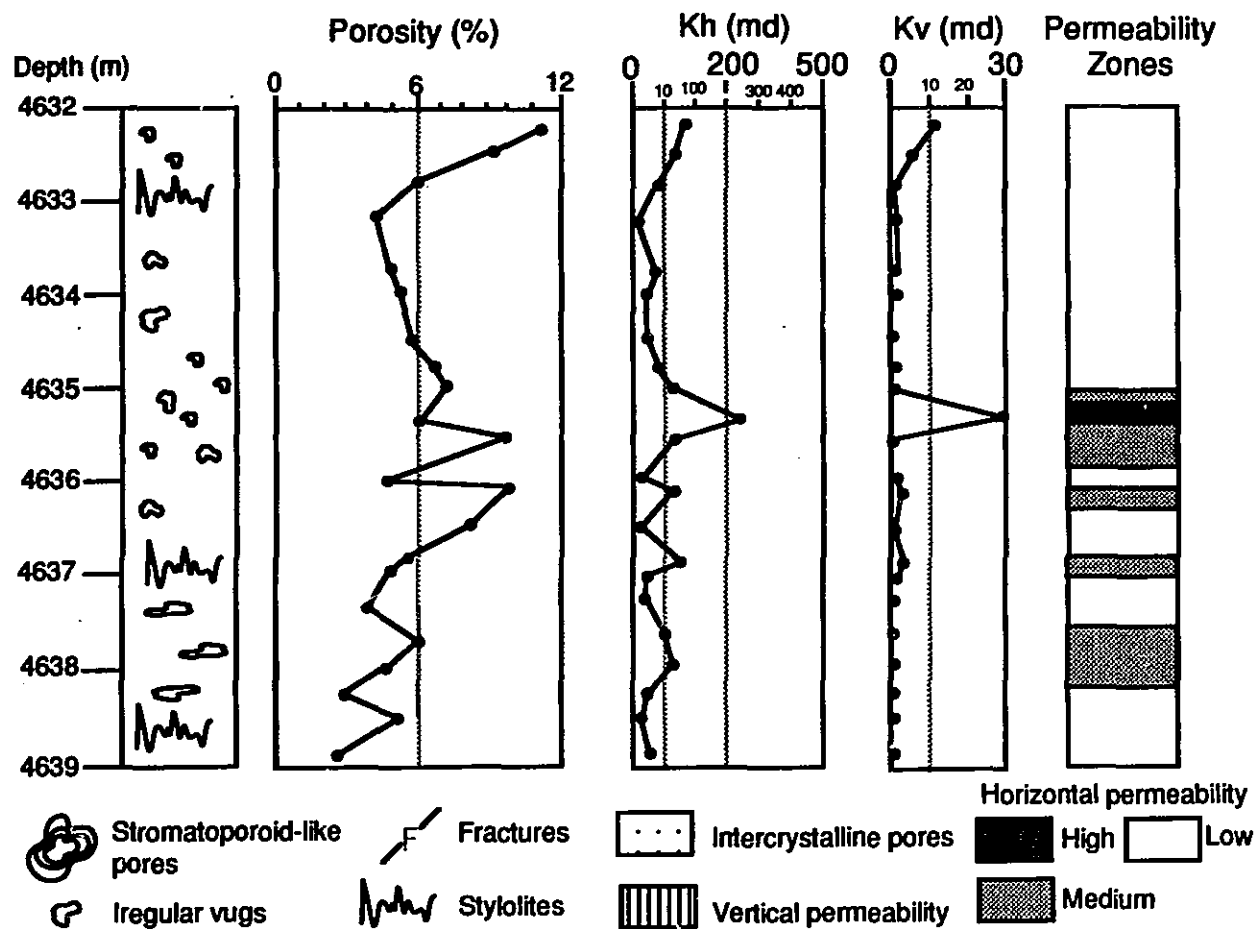
Well:10-33



continuation ...

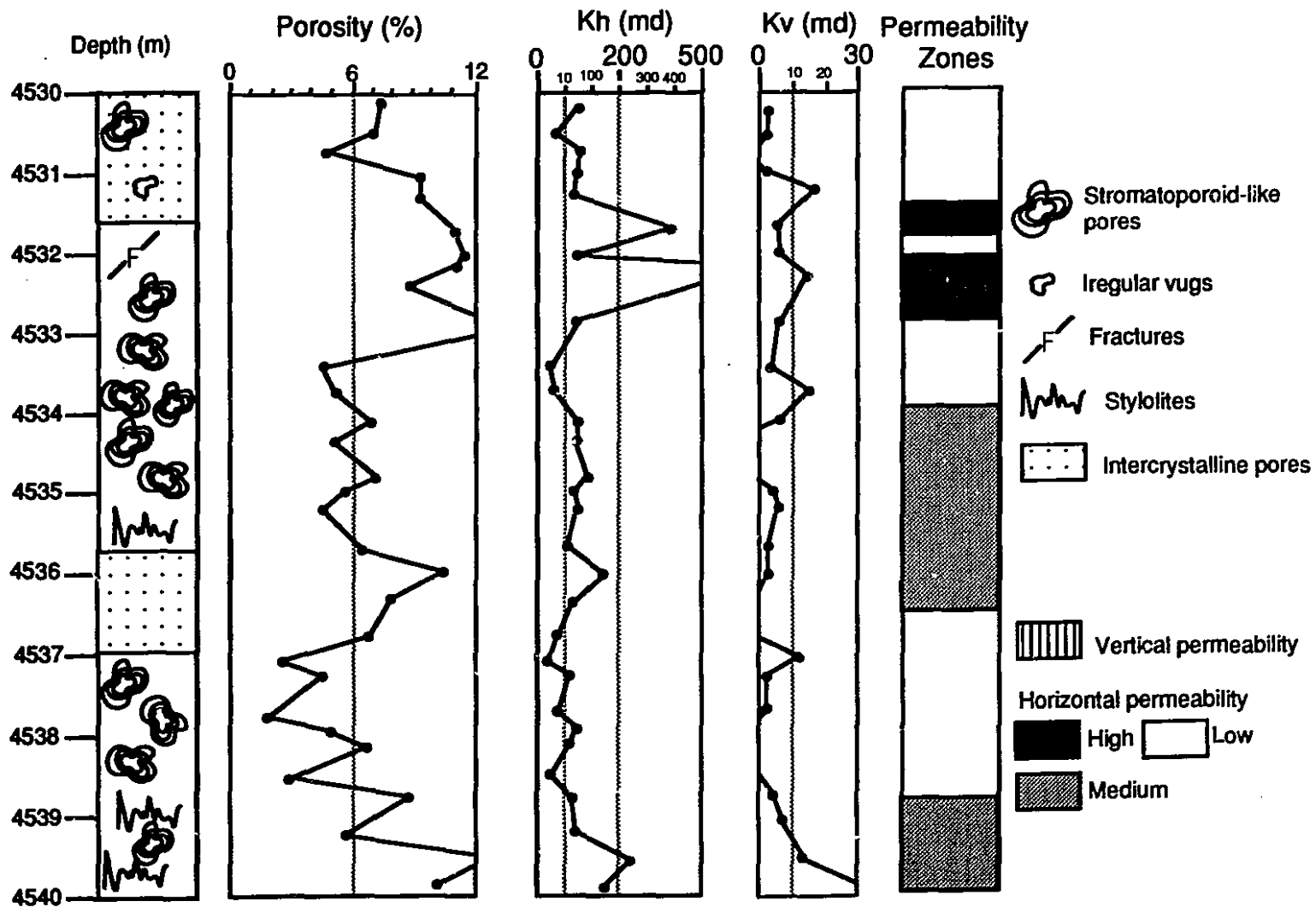
Depositional Facies: STROMATOPOROID FLOATSTONES/RUDSTONES

Well: 10-33



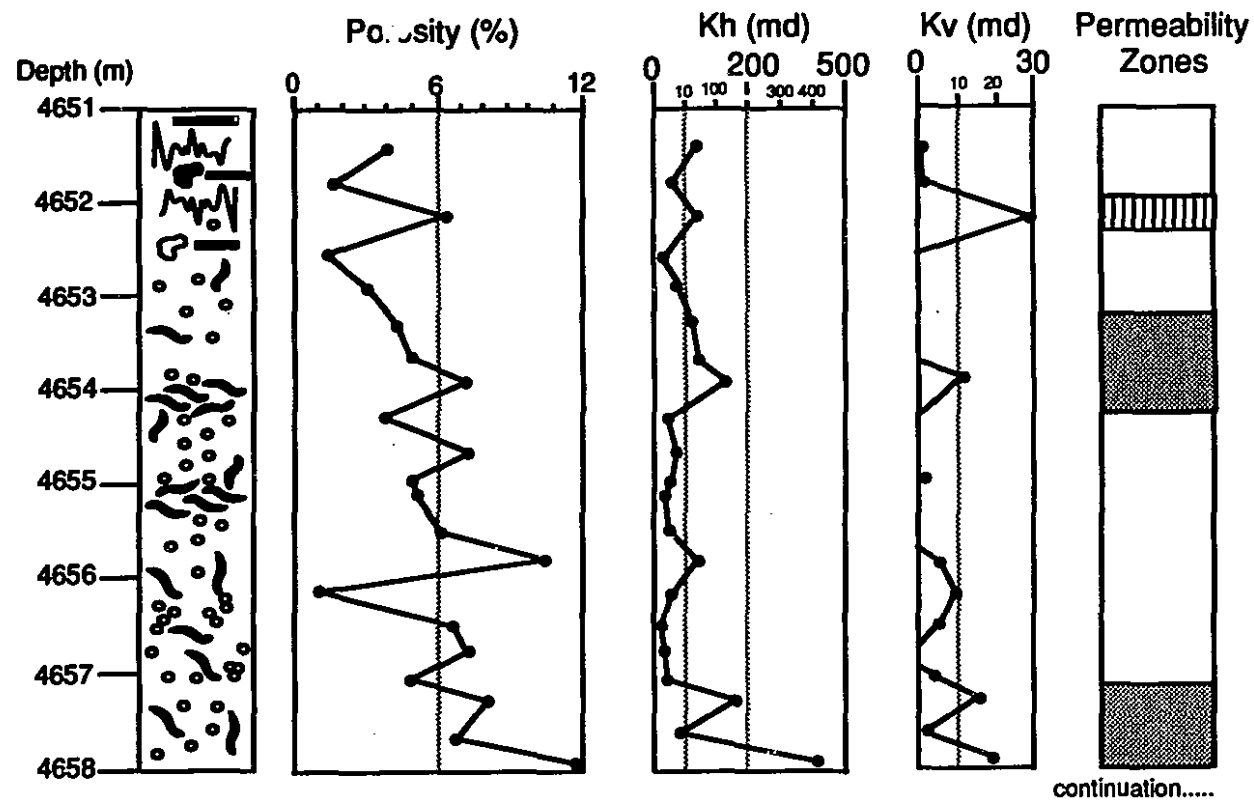
Depositional Facies: STROMATOPOROID FLOATSTONE/RUDSTONE

Well: 15-23



Depositional facies: CORAL RUDSTONES

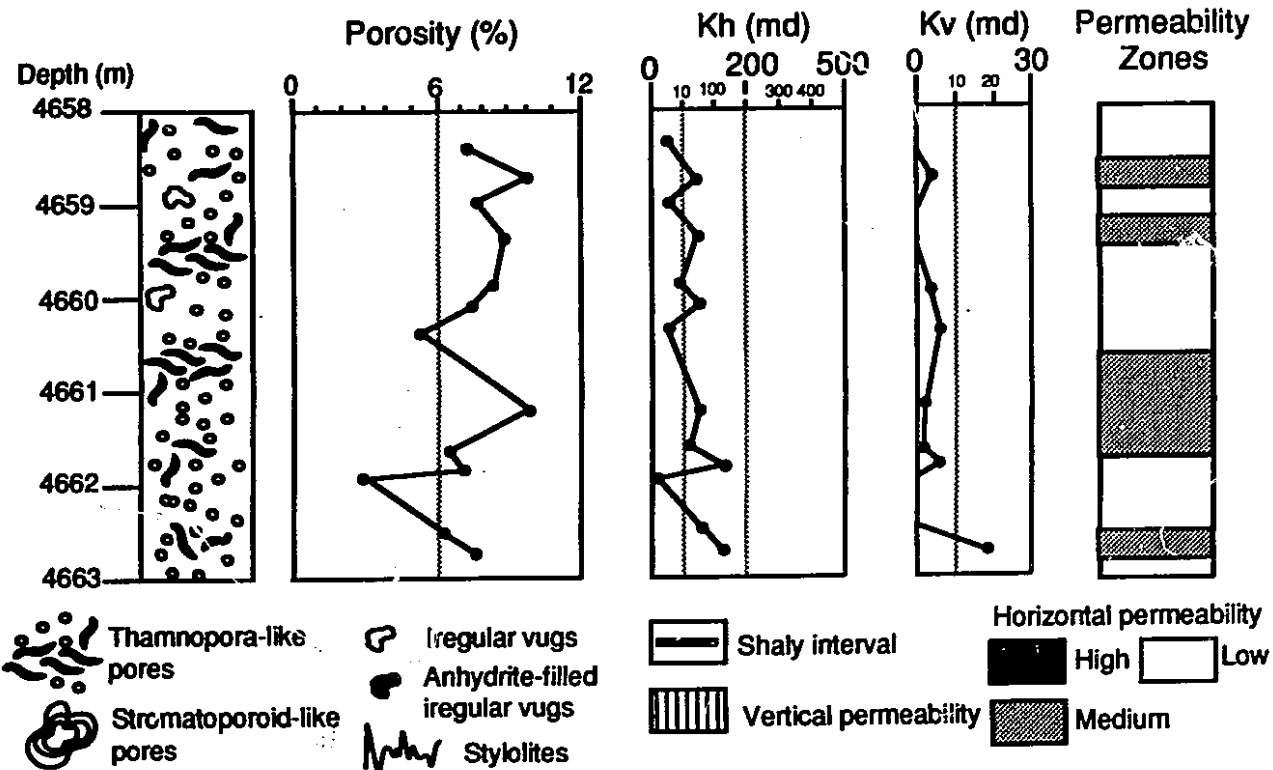
Well:10-33



continuation.....

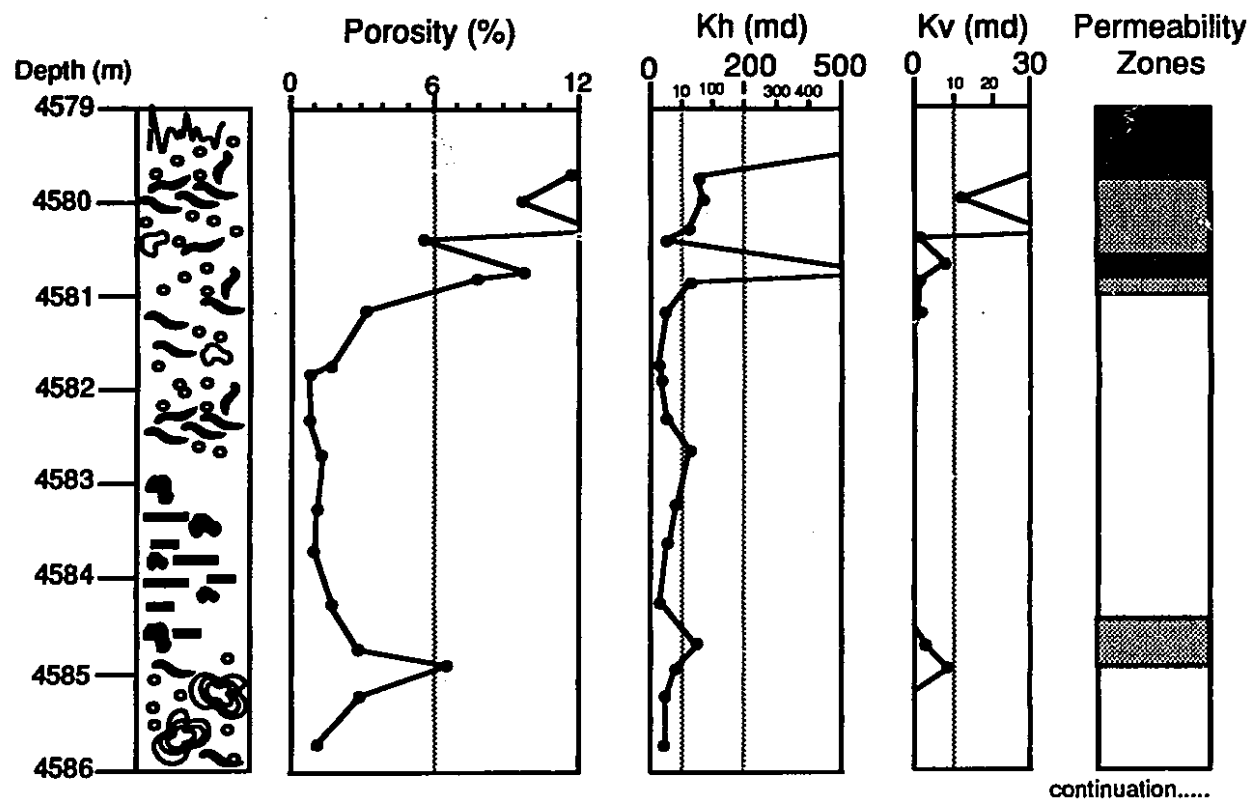
Depositional facies: CORAL RUDSTONES

Well:10-33



Depositional facies: CORAL RUDSTONES

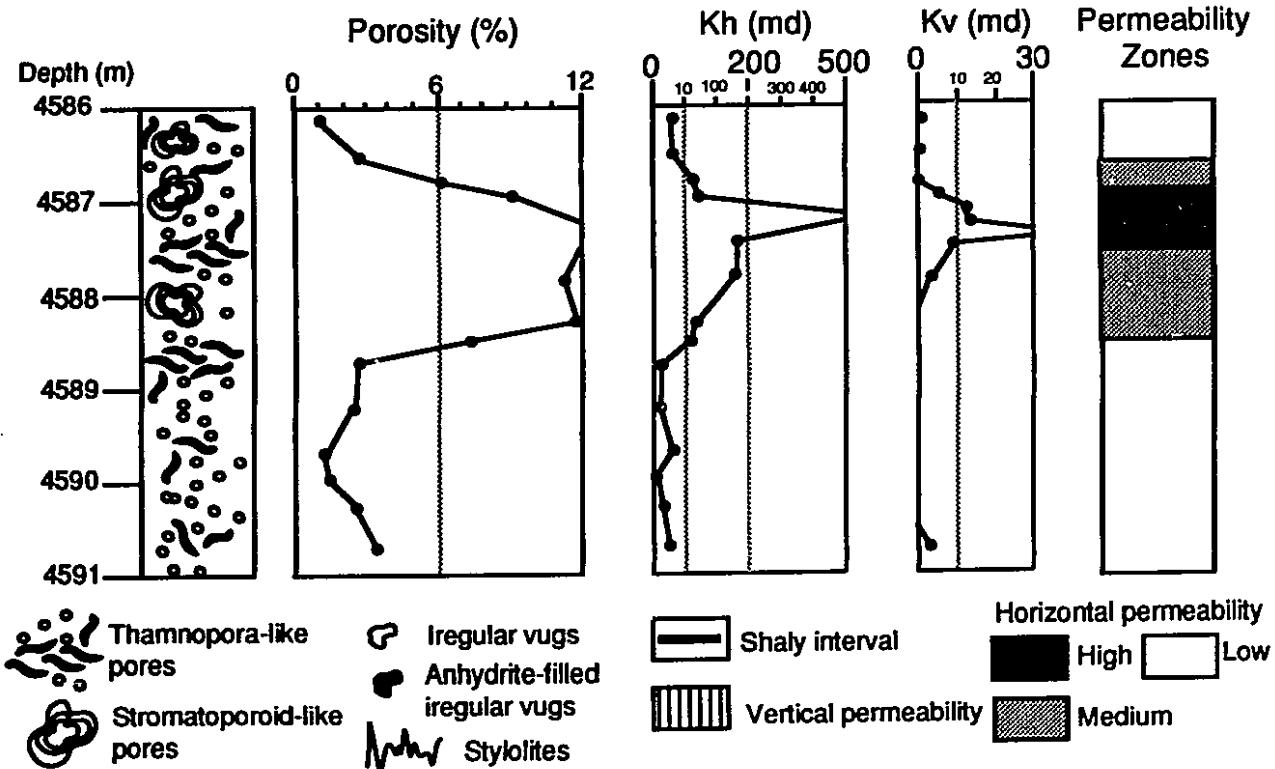
Well:15-23



continuation.....

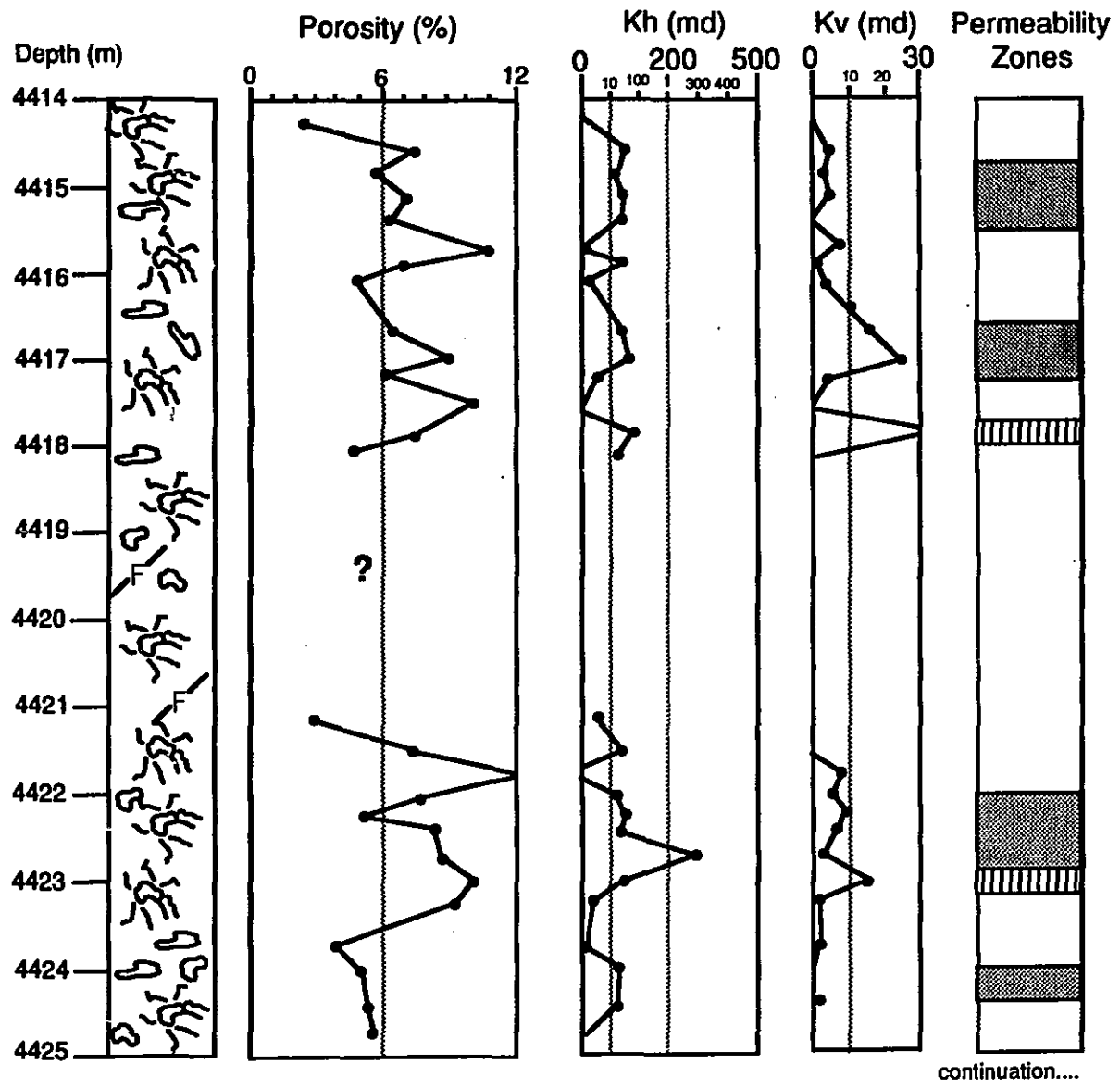
Depositional facies: CORAL RUDSTONES

Well:15-23



Depositional Facies: TABULAR STROMATOPOROID BOUNDSTONES

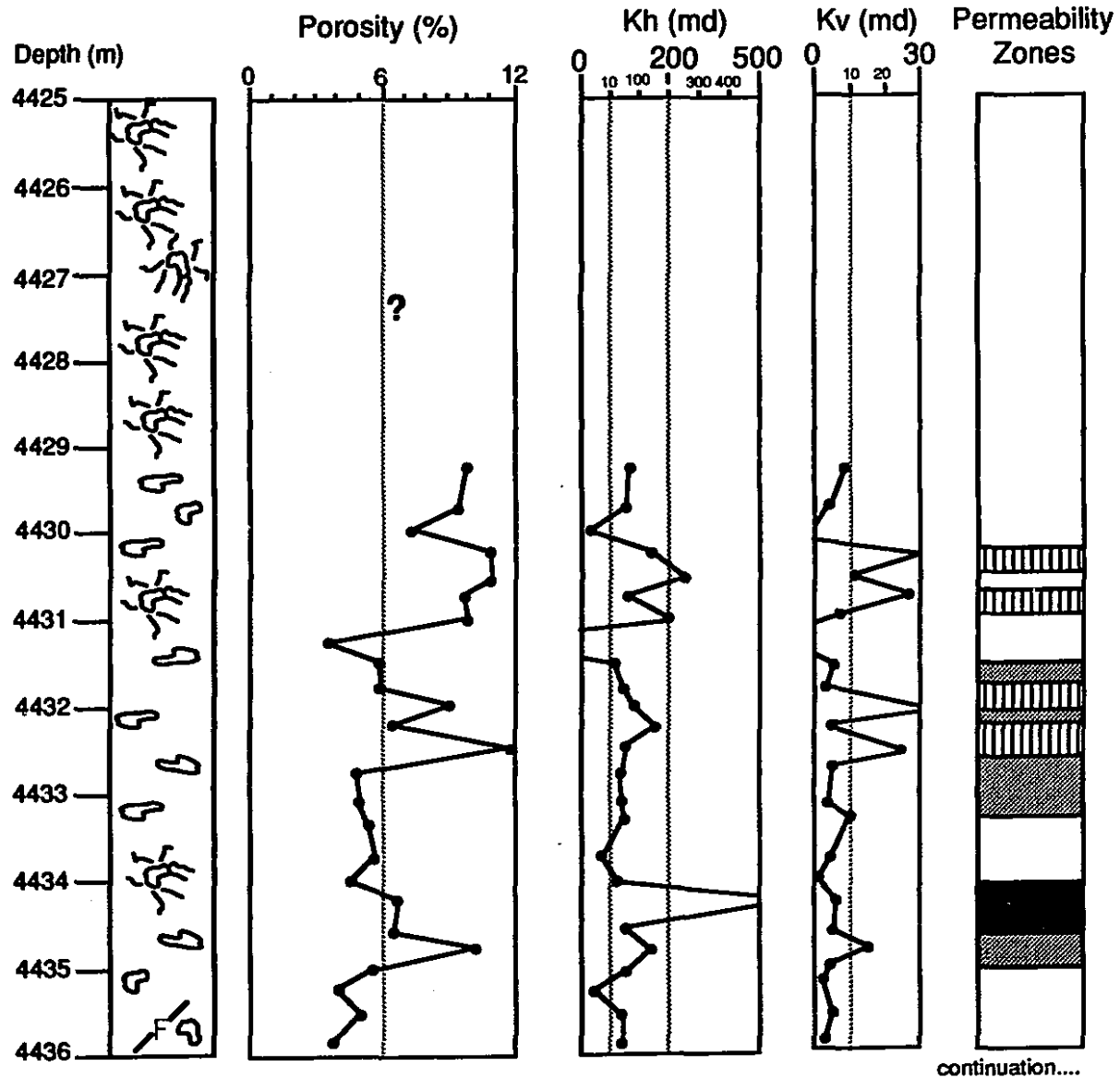
Well: 7-13



continuation....

Depositional Facies: TABULAR STROMATOPOROID BOUNDSTONES

Well: 7-13



continuation....

Depositional Facies: TABULAR STROMATOPOROID BOUNDSTONES

Well: 7-13

